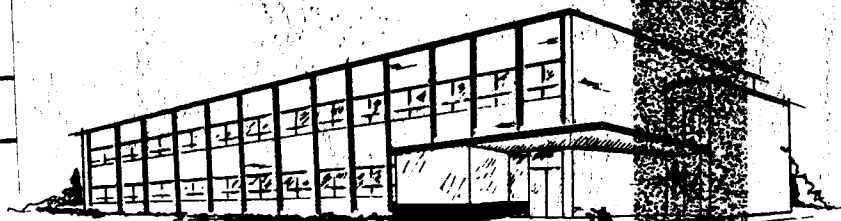Copy No. _____

GPO PRICE $ _____

CFSTI PRICE(S) $ _____

Hard copy (HC) ___6.00___

Microfiche (MF) ___1.50___

ff 653 July 65

THE *Bendix* CORPORATION

BENDIX SYSTEMS DIVISION · ANN ARBOR, MICHIGAN

N 66-16387
(ACCESSION NUMBER)

(THRU)

299
(PAGES)

1
(CODE)

CR-69859
(NASA CR OR TMX OR AD NUMBER)

30
(CATEGORY)

FACILITY FORM 602

LUNAR NAVIGATION STUDY
FINAL REPORT
(June 1964 to May 1965)

BSR 1134

June 1965

Sections 1 through 7

Prepared for:

George C. Marshall Space Flight Center
Huntsville, Alabama
under
Contract No. NAS8-11292

Authors:

L. J. Abbeduto   W. G. Green
M. E. Amdursky   T. F. King
D. K. Breseke   R. B. Odden
J. T. Broadbent   P. I. Pressel
R. A. Gill   T. T. Trexler
H. C. Graboske   C. Waite

BENDIX SYSTEMS DIVISION
OF
THE BENDIX CORPORATION
Ann Arbor, Michigan

CONTENTS

CONTENTS (CONT.)

CONTENTS (CONT.)

CONTENTS (CONT.)

ILLUSTRATIONS

ILLUSTRATIONS (CONT.)

ILLUSTRATIONS (CONT.)

ILLUSTRATIONS (CONT.)

TABLES

SECTION 1

INTRODUCTION

The objective of the lunar exploration programs in general has been defined as increasing knowledge of the moon (i. e. , to gather significant scientific data). This objective will be accomplished by both manned and unmanned surface vehicles. Regardless of the tasks assigned during the different phases of the programs, some means of surface navigation is required if the vehicle position must be measured. This navigation function is derived from the necessity of astronaut return to a lunar shelter, LEM, or other return vehicle. To determine the feasibility of fulfilling the mission navigation requirements, a study of the problem was undertaken.

The Lunar Surface Navigation Study was directed toward the determination of technological areas in which research and development would be required to implement typical navigation requirements into the late 1980s. This required the development of error models that could be utilized for parametric evaluation of component and navigation concept performances.

Error models were purposely developed in a modular form during the study. This assures a maximum flexibility in their possible applications to subsequent evaluations of other potentially feasible navigation components and concepts. This capability will be of great importance during trade-off studies required to optimize a complete vehicle design.

To establish typical navigation objectives and feasible concept configurations, it was necessary to review the proposed lunar exploration plans. This also afforded an insight into other potential vehicle systems that would interface with the navigation equipment and might have common performance requirements.

A number of ground rules applicable to the study were established at an initial coordination meeting between the contractor's representatives and the NASA program monitors. The more important ones are:

1. All errors used in the study will be 3σ values; e.g., a
    100-m probable error will be converted to an error
    of approximately 450 m.

2. Errors will be combined in a root-sum-square (RSS)
    manner.

3. Astronaut safety is of primary importance, and a navigation
    capability independent of earth support is desirable.

4. Weight, volume, and power constraints should not be
    emphasized.

For the purposes of the study and this report, the following definitions,
derived from American Practical Navigator by N. Bowditch, are applicable:

1. Position fixing is the navigation process of determining a
    position (and a heading reference) in either a relative or
    absolute coordinate system. Initial position and heading
    reference data are required to implement the dead-reckoning
    function.

2. Dead reckoning is the navigation process of determining
    position by advancing a known position for both course and
    distance. Displays of dead-reckoning system data are used
    to implement the piloting function.

3. Piloting is navigation involving frequency reference to
    objective range and direction and requires good judgment
    and almost constant attention and alertness on the part
    of the navigator.

The foregoing definitions encompass the three subconcepts or functions
that must be fulfilled by virtually all navigation concepts. However,
the requirement for remote control of navigation functions was not a
part of the contract effort; although it is an important factor, it is be-
lieved that adequate command and data link capabilities will be included
during mission systems designs. The piloting function, whether on-board
or remote, was considered only briefly, because it was outside the scope
of the contract except for potential interface considerations.

This report represents the results of a 12-month study program.

SECTION 2

PROBLEM DEFINITION AND STUDY APPROACH

The problem of the lunar navigation analysis was to establish parametric performance capabilities of navigation system models to be used for future lunar surface exploration missions. Specific areas of investigation were described in the contract scope of work as navigation references, techniques, environmental problems, accuracy requirements, and mission dependent problems. The three navigation systems designated for analysis (passive nongyro; inertial; and RF technology) were considered as generalized system models for reference point evaluation. (These systems are represented in the functional diagrams of Figures 2-1, 2-2, and 2-3.)

The investigation did not place heavy emphasis on weight, volume, and power constraints associated with any specific lunar exploration system design but rather on hardware component parametric accuracies, the resultant navigation system error, and the recommendations of R&D needed to provide improvements in component parameters. Environmental constraints were considered only at the problem statement level; physical references were considered at a level to define the dependent systems' accuracies. Navigation system requirements were defined only to permit technique and component evaluation.

The study approach used is illustrated in Figure 2-4, where the ideal approach is indicated by solid lines and the approach used is shown by the dotted lines. During the study, the translation of mission objectives directly to navigation requirements neglected vehicle constraints because of time and manpower limitations. The state of the art was assessed for various navigation components and techniques and applied to the navigation system concepts so that appropriate error models could be developed for evaluation of performance as a function of parameter variation. Areas in which technology improvements are desirable were thus made evident. By comparison of concepts, recommendations for additional research and development in support of lunar exploration programs can be derived.
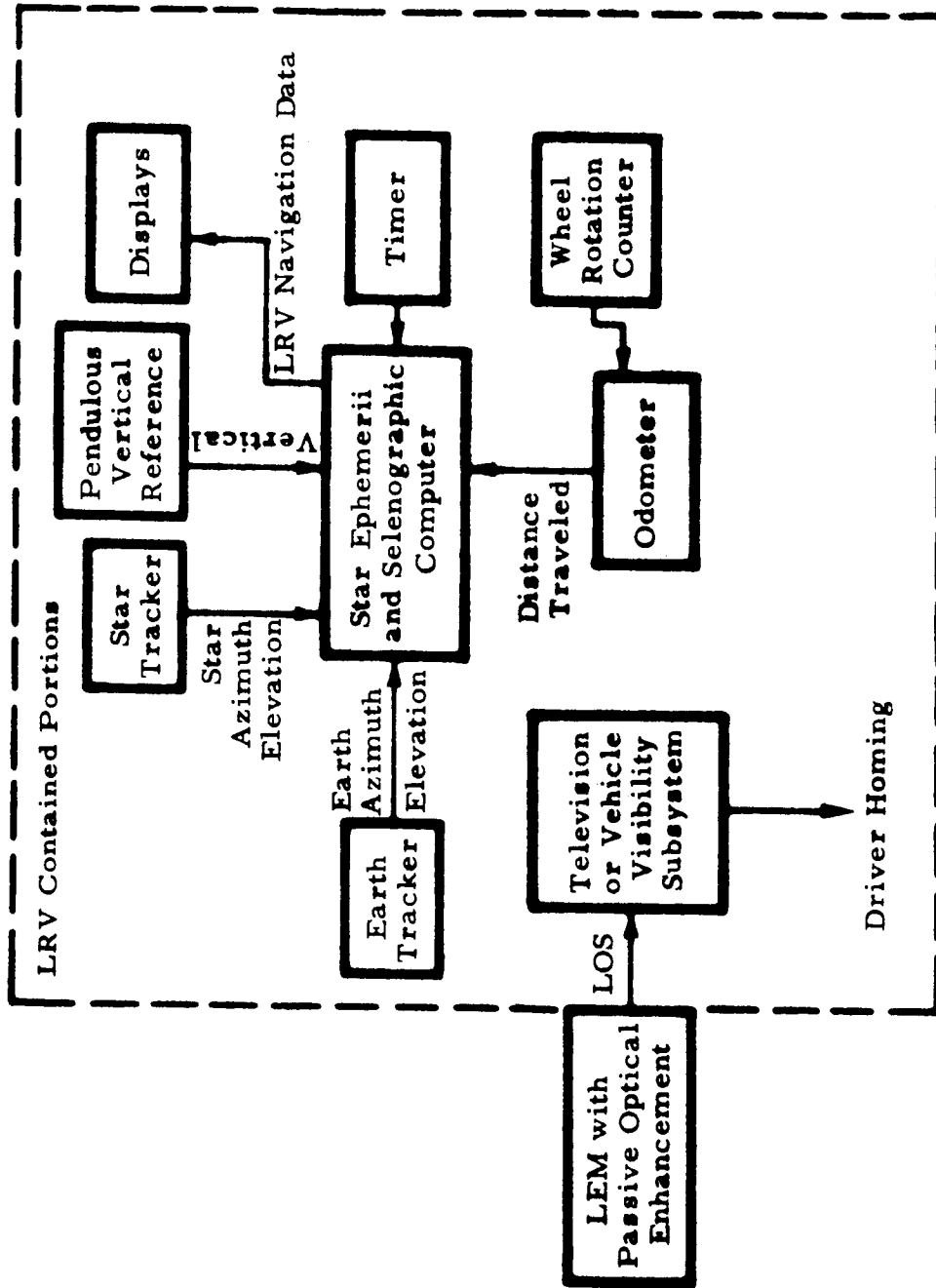
Figure 2-1 Concept 1-Passive, Nongyro System Block Diagram
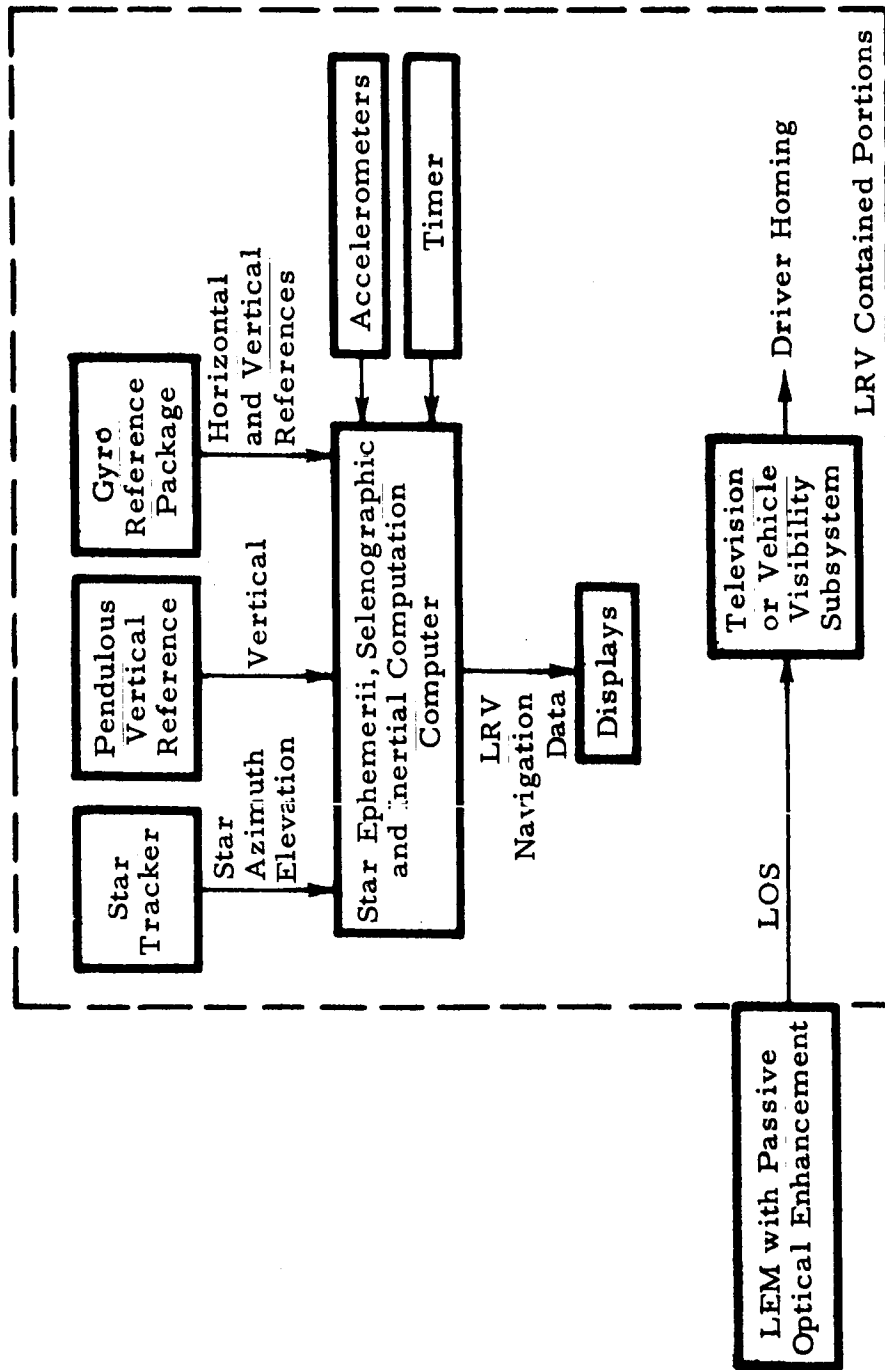
Figure 2-2 Concept 2-Inertial System Block Diagram
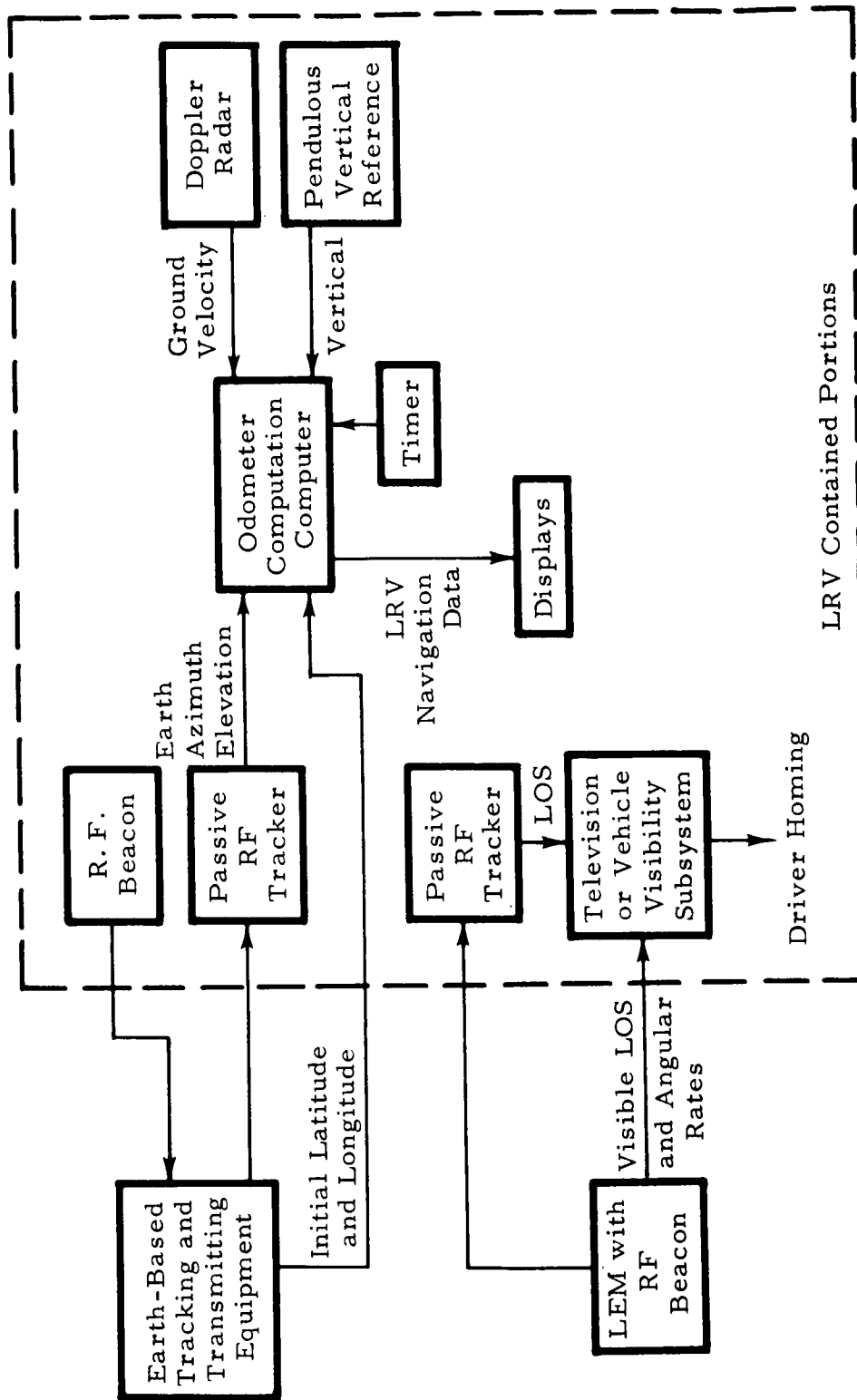
Figure 2-3 Concept 3–RF Technology System Block Diagram
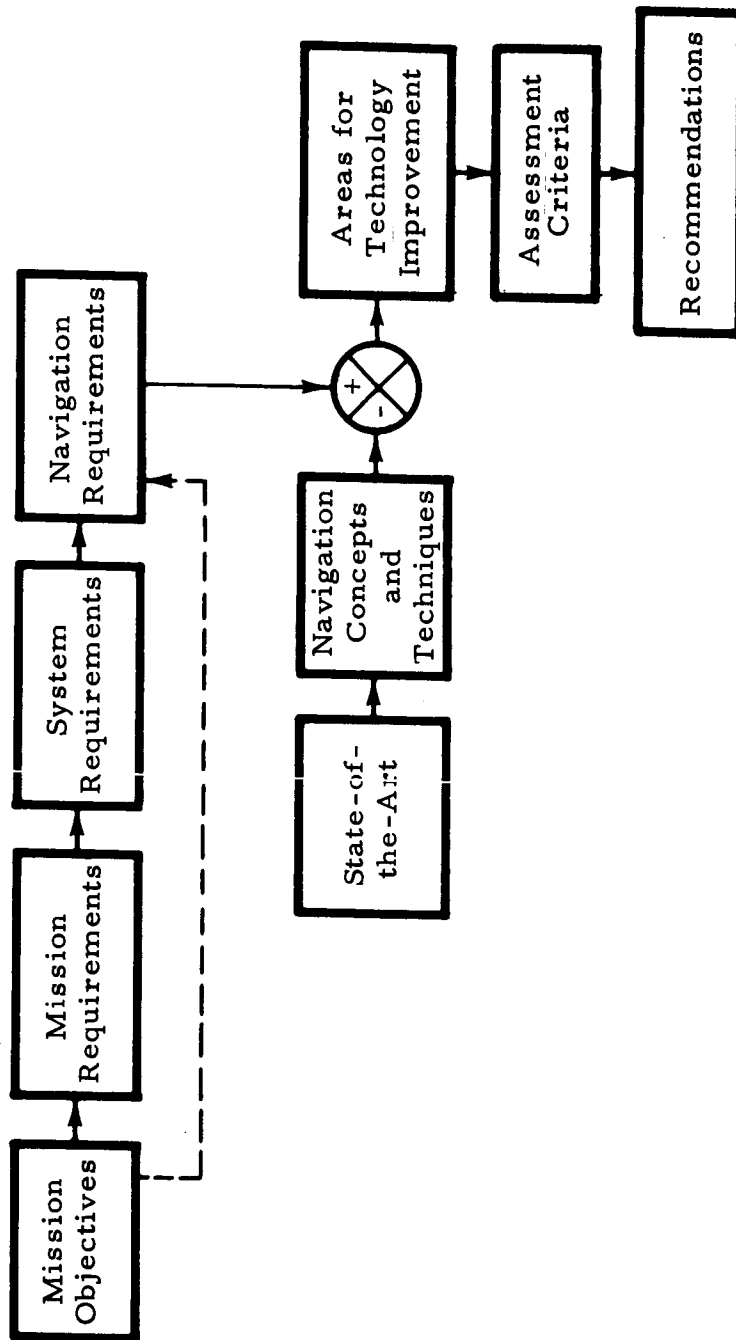
Figure 2-4 Block Diagram of Study Approach

As a basis for the navigation studies, guidelines for four mission types were identified to cover the planned lunar exploration programs.[19] The mission types were: (1) unmanned LRV operations; (2) early manned reconnaissance operations; (3) intermediate reconnaissance and exploration missions; and (4) extended vehicular reconnaissance expeditions. These missions included objectives ranging from landing site selection to dark side expeditions that extend for a period up through the 1980s. As a part of the study program, these mission types were expanded to six missions for use in deriving typical navigation system functions and accuracy requirements with which to perform the component evaluation.

The degree of mission detail developed was dictated by the problem completeness required in performing the system analysis. Unless such a multi-mission lunar exploration program is assumed, no basis exists for surface navigation requirements.

The missions must be defined only generally in order to develop over-all traverse navigation requirements. The definition of scientific experiments to be performed on the mission must be considered to determine the navigation requirements in support of specific experiments.

The six evaluation missions are described in Figure 2-5 with respect to location on the surface, range to be covered, and time of first occurrence (which sets the time at which navigation capabilities matching the mission requirements must be available). Research and development must provide, if they do not presently exist, components with capabilities matching a mission at its first inception. The program outlined does not limit the total number of missions or probes since each of the missions could occur many times in many locations, it simply defines the time at which requirements first arise.

Although the actual time of occurrence of these missions may vary greatly from that shown, the relative phasing of the missions should remain fairly constant, assuming that explorations beyond initial fixed-point investigations are carried through. If missions are delayed or altered, it should be no problem to define the corresponding effect on the results shown by this study.

The first mission corresponds to one concept within the Apollo Experiment Support Program and utilizes an intermediate weight roving vehicle. The second and third missions correspond roughly to MOLAB-type missions

N 90°

55°

40°

25°

10°

0°

10°

25°

40°

55°

S 90°

Lunar Latitude

(1) Mission Paths (2)

(3)

(4)

(5)

(6)

1972   1974   1976   1978   1980   1982   1984

Time that Mission Type First Occurs
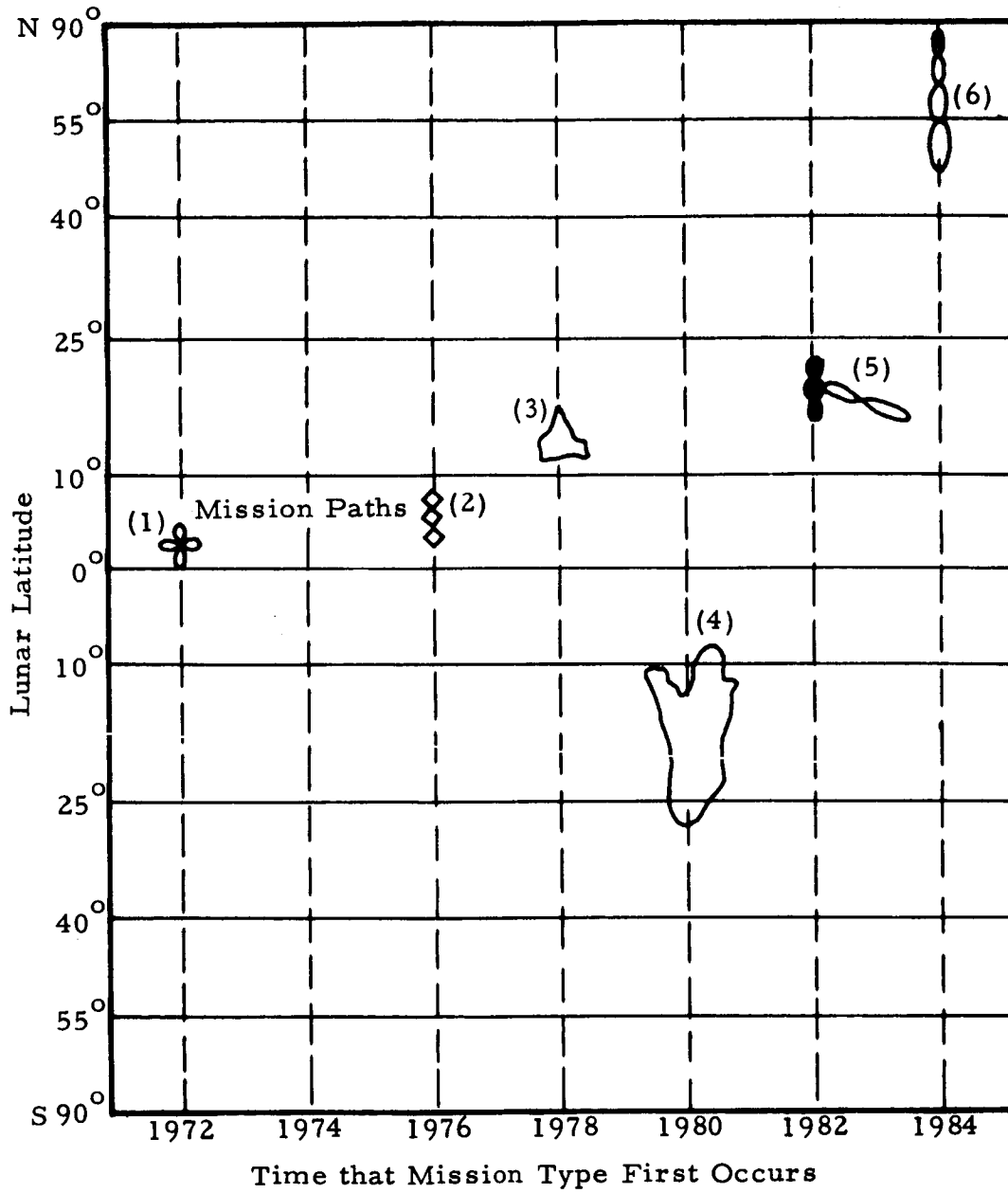
Note: Far side mission is shown solid

Figure 2-5 Total Exploration Program

with surface ranges up to 500 km. The fourth mission extends the mission
length (up to 1500 km) and enters the lunar highlands.

A final element which governed the selection of missions to be em-
ployed in the study was obtaining as complete coverage of the lunar surface
as was reasonable by 1985. Thus Mission 5 was selected for far-side
operations, while polar operations are covered by Mission 6. Marial travel
is employed almost exclusively in all missions, although provision has
been made to include highland-type areas in Missions 4 and 6.

Details of each mission follow.

Mission 1 - 1972

Mission 1 (Figure 2-6) is the first mission after successful Apollo touchdowns. Its role is to extend the range of exploration out to the maximum provided by astronaut-carried life support equipment. Each mission consists of two launches: a LEM shelter with on-board vehicle, and a manned LEM with two astronauts aboard. A key phase of this mission is the surface rendezvous in which the vehicle is driven unmanned from the shelter to the manned LEM. Following this rendezvous the astronauts board the vehicle and drive to the shelter. Thereafter, operations originate from the shelter, the vehicle being driven about the shelter either in a manned or unmanned mode. The final mission phase is the return of the astronauts to the LEM for earth return.

Terrain is roughly categorized as one of three types: smooth mare, rough mare, or gentle highlands. These descriptions correspond to particular analysis parameters required such as:

1. Acceleration distribution applied to vehicle

2. Azimuthal distribution

3. Gravitational anomaly directional distribution

4. Terrain slope distribution.

Mission Duration

Fourteen days.

Mission Objectives

1. Landing site selection and verification for future missions

2. Surface exploration

3. Preliminary scientific experiments.

Mission Location:

4°N / 48°W / 46°W / 44°W / 2°N / 0°N

h = Altitude above datum

Site Location 2.267°N
46°W
h = 0

Mission Details:

Note: Solid paths indicate unique mission tasks.

Dotted paths are repetitions and will be omitted from analysis

LEM Shelter (h = 0)

Selenographic Location
2°N, 46.267°W
h = 0

LEM Location
(2 men)
2°N, 45.733°W
h = 0

≈ 8 km
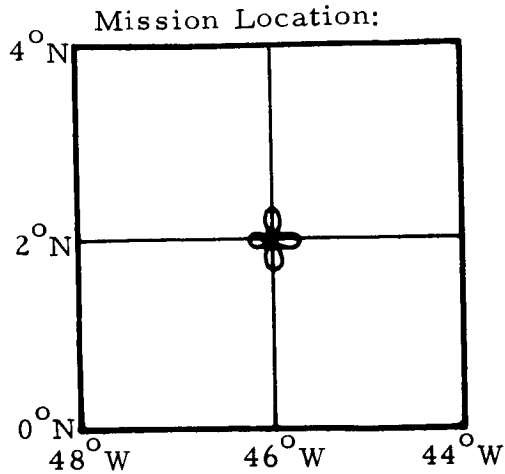
Relative Location
1.733°N, 46° W h = 0
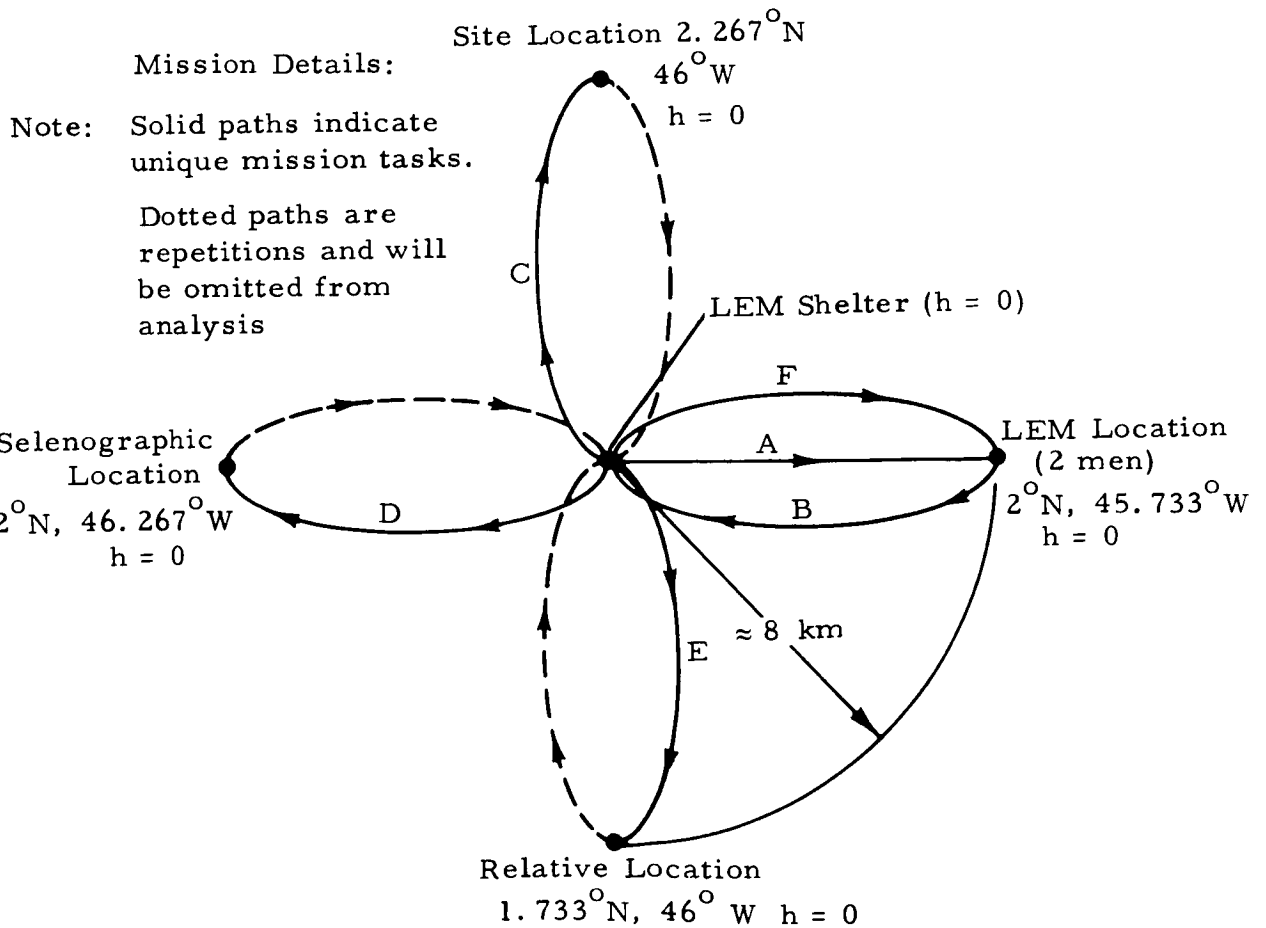
Figure 2-6 Mission 1—1972

Navigation Functions to be Performed

A. Unmanned travel from LEM shelter to manned LEM

B. Manned travel from LEM to LEM shelter (Retrace)

C. Determine location of point of interest relative to LEM shelter

D. Determine selenographic coordinates of a point of interest

E. Determine selenographic coordinates of an acceptable landing site and relative locations of significant points within the landing site.

F. Manned travel from LEM shelter to LEM

G. Support preliminary scientific experiment.

Typical Mission Leg Descriptions

Mission Leg	Origin	Destination	Approx. Range (km)	Terrain Type	Travel Type*	Avg. Speed** (km/hr)
A	LEM Shelter	LEM	8	Smooth Mare	U	3
B	LEM	LEM Shelter	8	Smooth Mare	M	4
C	LEM Shelter	Site	8	Smooth Mare	U	3
D	LEM Shelter	Selenographic Location	8	Smooth Mare	U	3
E	LEM Shelter	Relative Location	8	Smooth Mare	U	3
F	LEM Shelter	LEM	8	Smooth Mare	M	4

* U = Unmanned, M = Manned
** Vehicle parameters are: a. Earth weight - 1000 lb
                                        b. Marial speed - Manned 4 km/hr
                                                                   Unmanned 3 km/hr
                                        c. Total available range - 200 km

Mission 2 - 1976

Mission 2 (Figure 2-7) marks the beginning of long-range travel over the lunar surface and corresponds to early MOLAB missions. Although operations are still confined to the equatorial region of the near side, the range of travel is increased beyond 100 km by reason of a vehicle with on-board life support. Straight-line distance from the return LEM, however, is limited to 80 km. Each mission, as in Mission 1, involves two launches, a LEM truck-vehicle combination, and a two-astronaut-return LEM combination. Rendezvous between vehicle and astronauts still is required.

Mission Duration

Fourteen days.

Mission Objectives

1. Reconnaissance and mapping of both preselected features and features of opportunity

2. Verification and mapping of areas as landing sites or operational sites for future missions

3. Scientific experimentations.

Navigation Functions to be Performed

A. Unmanned travel from LEM truck to manned LEM

B. Manned travel from LEM to LEM truck

C. Determine location of point of interest relative to LEM truck

D. Determine selenographic coordinates of a point of interest

E. Determine selenographic coordinates of an acceptable site and relative locations of significant points within the landing site

F. Travel to equipment/data pickup point

G. Travel back to LEM for earth return.
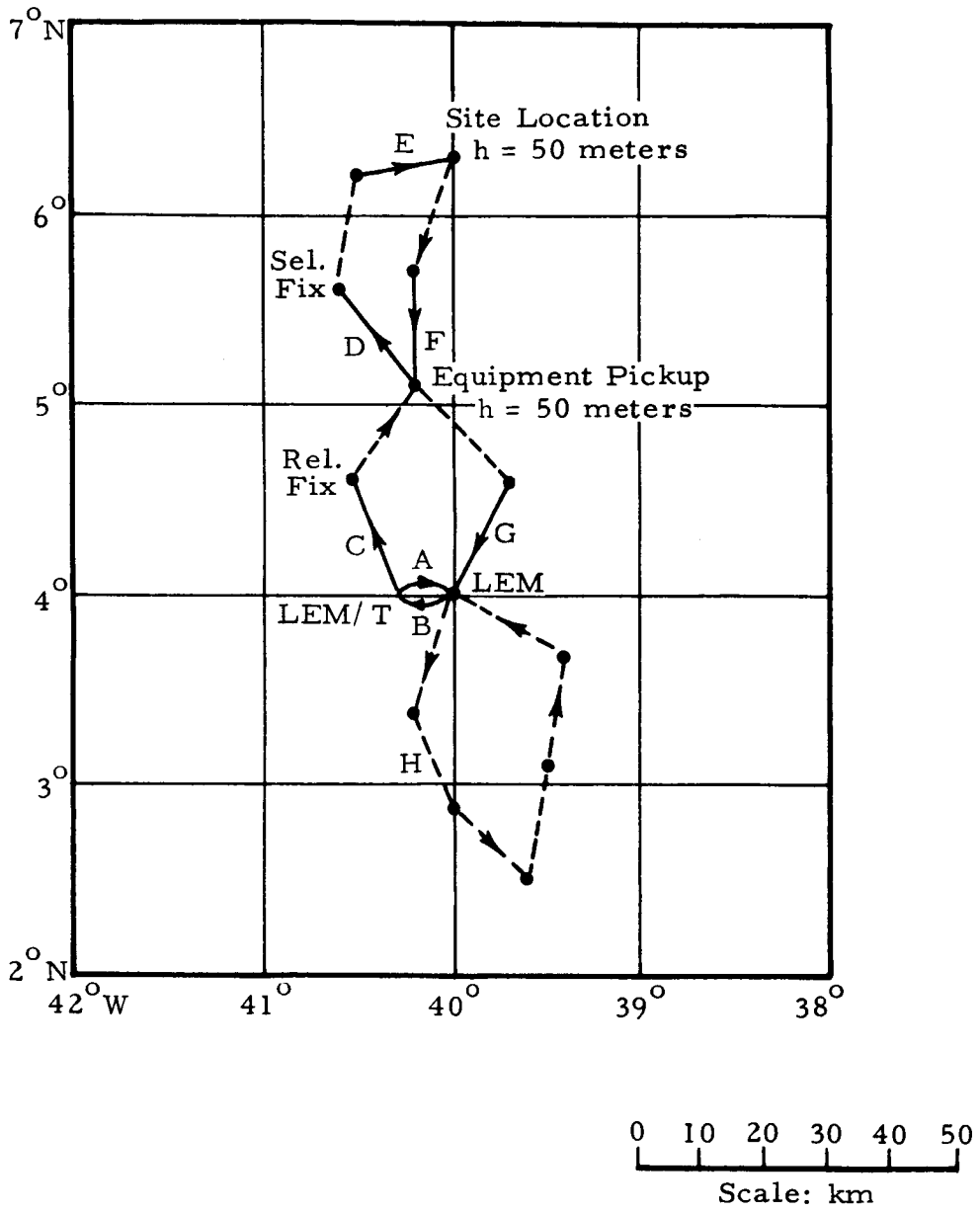
Note: All end-point elevations = 0 except as noted.

Figure 2-7 Mission 2 — 1976

Typical Mission Leg Descriptions

Mission Leg	Origin	Destination	Approx. Range (km)	Terrain Type	Travel Type	Avg. Speed (km/hr)
A	LEM Truck	LEM	8	Smooth Mare	U	3
B	LEM	LEM/T	8	Smooth Mare	M	5
C	LEM Truck	Relative Location	18	Smooth Mare	M	5
D	Selenographic Location	Selenographic Location	18	Rough Mare	M	5
E	Selenographic Location	Site Location	18	Rough Mare	M	5
F	Selenographic Location	Equipment Location	18	Rough Mare	M	5
G	Selenographic Location	LEM	18	Smooth Mare	M	5

Mission 3 - 1978

Mission 3 (Figure 2-8) is an advanced MOLAB mission, with specific plans as to features to be investigated. Travel extends somewhat beyond the early Apollo landing areas of ±10° in latitude. The principal distinguishing characteristic is the achievable length of travel (and, hence, time on the surface) of well over 200 km. Travel during both lunar day and night is expected. Mission 3 no longer has site verification as an objective. It is assumed that landing sites can now be found with confidence with a combination of orbital data, unmanned surface probes, and acquired general knowledge of the surface characteristics.

Mission Duration

Thirty days.

Mission Objectives

1. Scientific experimentation

2. Observation of changes over a complete lunar day

3. Advanced mapping/surveying.

Navigation Functions to be Performed

A. Unmanned travel from LEM/T to LEM

B. Manned travel from LEM to LEM/T

C. Manned travel to lunar surface feature

D. Determine selenographic coordinates of point of interest

E. Determine location of one point of interest relative to another

F. Manned travel back to LEM for earth return.

Typical Mission Leg Descriptions

Mission Leg	Origin	Destination	Approx. Range (km)	Terrain Type	Travel Type	Avg. Speed (km/hr)
A	Selenographic Location	Surface Feature	83	Smooth Mare	M	8
B	Selenographic Location	Selenographic Location	62	Rough Mare	M	8
C	Selenographic Location	Relative Location	69	Rough Mare	M	8
D	Selenographic Location	LEM	50	Smooth Mare	M	8

Note: All end-point elevations = 0 except as noted.
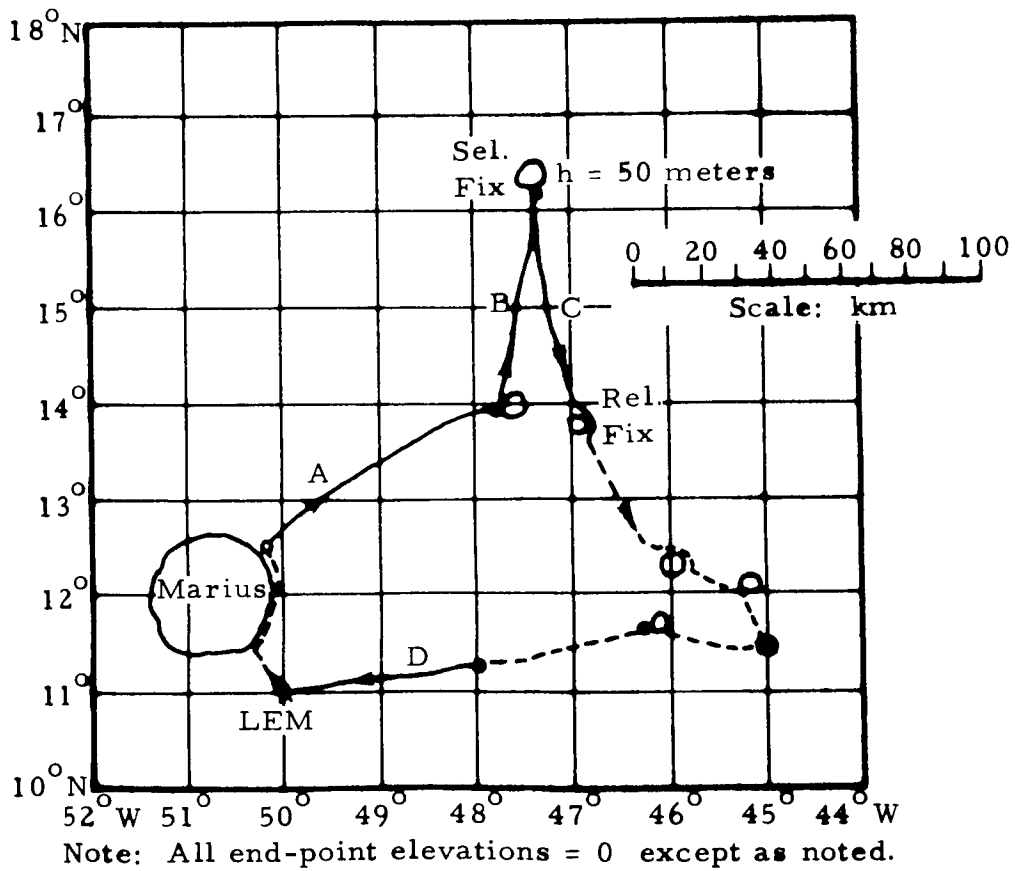
Figure 2-8 Mission 3 — 1978

Mission 4 - 1980

Missions to the highland areas appear both attractive and difficult. Initial mission legs (Figure 2-9) are over relatively smooth terrain. The travel in highland regions, occurring midway in the mission, may actually prove too difficult, but is assumed feasible in order to thoroughly study navigation requirements.

Mission Duration

Fifty days.

Mission Objectives

1. Reconnaissance and mapping

2. Comparison of highland and marial areas.

Navigation Functions to be Performed

A. Unmanned travel from LEM truck to manned LEM

B. Manned travel from LEM to LEM truck

C. Manned travel to lunar surface feature

D. Determine selenographic coordinates of point of interest

E. Determine location of one point of interest relative to another

F. Manned travel back to LEM for earth return.

Typical Mission Leg Descriptions

Mission Leg	Origin	Destination	Approx Range (km)	Terrain Type	Travel Type	Avg. Speed (km/hr)
A	LEM/Truck	LEM	8	Smooth Mare	U	3
B	LEM	LEM Truck	8	Smooth Mare	M	5
C	LEM Truck	Selenographic Location	100	Smooth Mare	M	10
D	Selenographic Location	Selenographic Location	50	Gentle Highlands	M	8
E	Selenographic Location	Selenographic Location	50	Rough Highlands	M	5
F	Selenographic Location	LEM	50	Smooth Mare	M	10
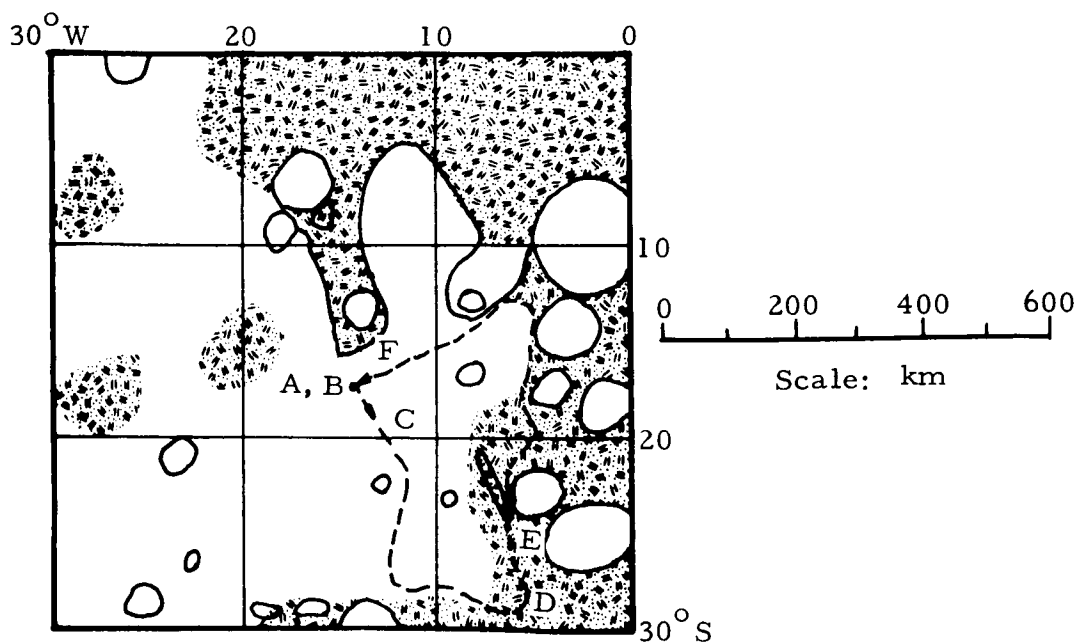
Figure 2-9 Mission 4 — 1980

Mission 5 - 1980

Mission 5 (Figure 2-10) is a traverse to the far side of the moon and a repeat of Mission 2. Mission duration for these initial far-side operations is limited to 90 days. The distinguishing characteristic of this mission from a navigation standpoint is the complete independence of the mission from direct earth observation/communication while on the back side of the moon. Orbital communications relay will be used in all probability, but navigation information must be generated at the vehicle independent of earth.

The objective of landing site location has been deleted from this mission in accordance with the comments made under Mission 3.

Mission Duration

Ninety days.

Mission Objectives

1. Reconnaissance and mapping

2. Scientific experimentation and investigation

3. Geological surveys.

Navigation Functions to be Performed

A. Determine location of point of interest relative to LEM truck

B. Determine selenographic coordinates of a point of interest

C. Travel to equipment/data pickup point (including enroute logistic resupply)

D. Travel back to LEM for earth return.
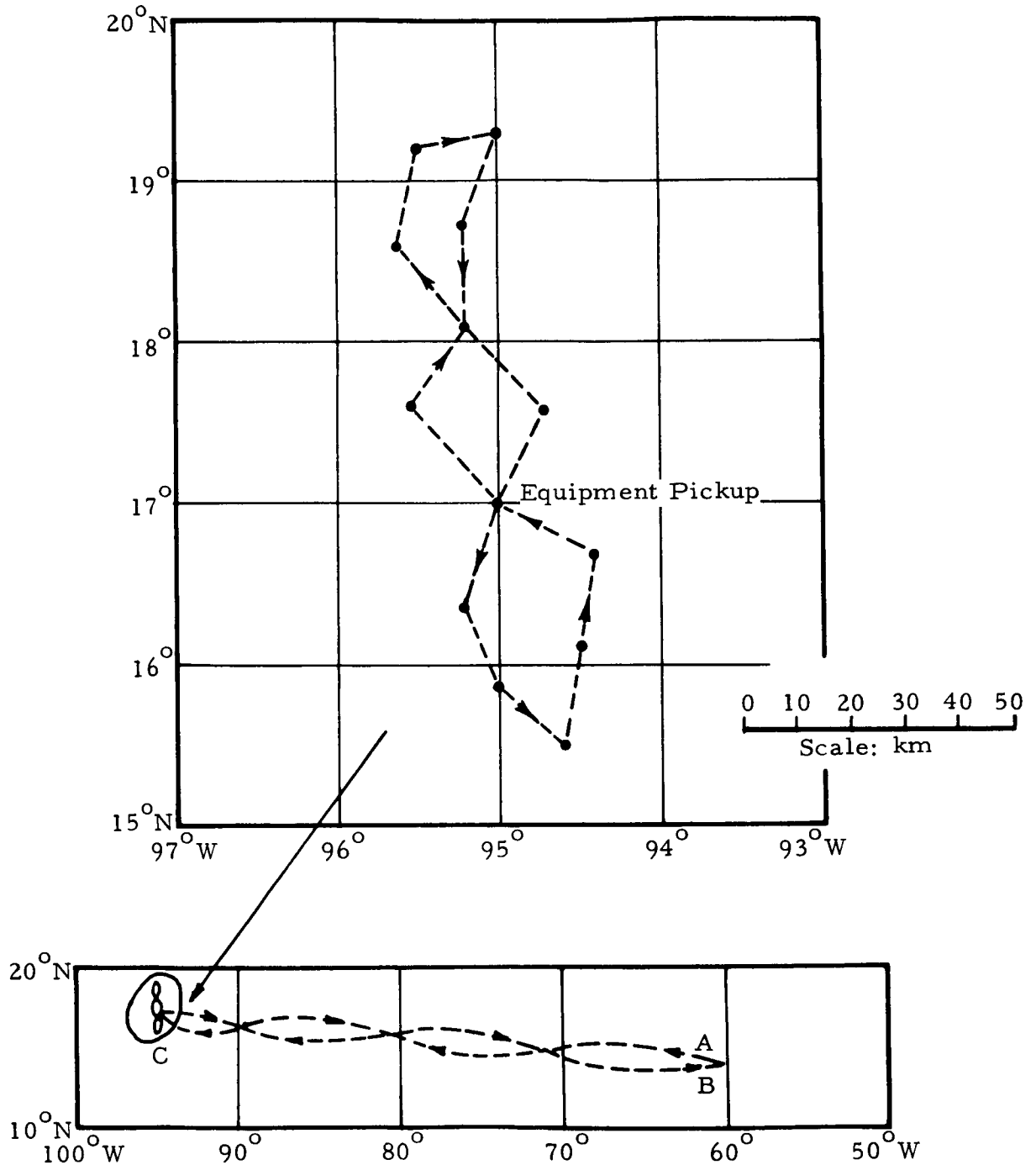
Figure 2-10 Mission 5—1980

Typical Mission Leg Descriptions*

Mission Leg	Origin	Destination	Approx. Range (km)	Terrain Type	Travel Type	Avg. Speed (km/hr)
A	LEM Truck	Surface Feature	100	Smooth Mare	M	8
B	Selenographic Location	Equipment Location	50	Rough Mare	M	5
C	Selenographic Location	Selenographic Location	50	Unknown	M	5
D	Selenographic Location	LEM	100	Smooth Mare	M	8

*Refer to Mission 2 for typical mission legs at
95°W and 15.5° to 19.5° North

Mission 6 - 1984

Mission 6 (Figure 2-11) is a polar mission into the highlands of the North Pole. The northern polar region has been selected not because of any known surface features, but merely to serve to uncover any difficulties associated with navigation in this area. The navigation function of this mission is distinguished from the others by the peculiarities of the polar position.

Mission Duration
_____

Ninety days.

Mission Objectives
_____

1. Reconnaissance and mapping

2. Comparison of highland and marial areas

3. Prospecting.

Navigation Functions
_____

A. Determine location of point of interest relative to LEM truck

B. Determine selenographic coordinates of point of interest

C. Travel to equipment/data pickup point (including enroute logistic supplies)

D. Manned travel back to LEM for earth return.

Typical Mission Leg Descriptions

Mission Leg	Origin	Destination	Approx. Range (km)	Terrain Type	Travel Type	Avg. Speed (km/hr)
A	LEM Truck	Selenographic Location	100	Smooth Mare	M	10
B	Selenographic Location	Selenographic Location	50	Rough Highlands	M	5
C	Selenographic Location	Selenographic Location	50	Rough Highlands	M	5
D	Selenographic Location	LEM	100	Smooth Mare	M	10
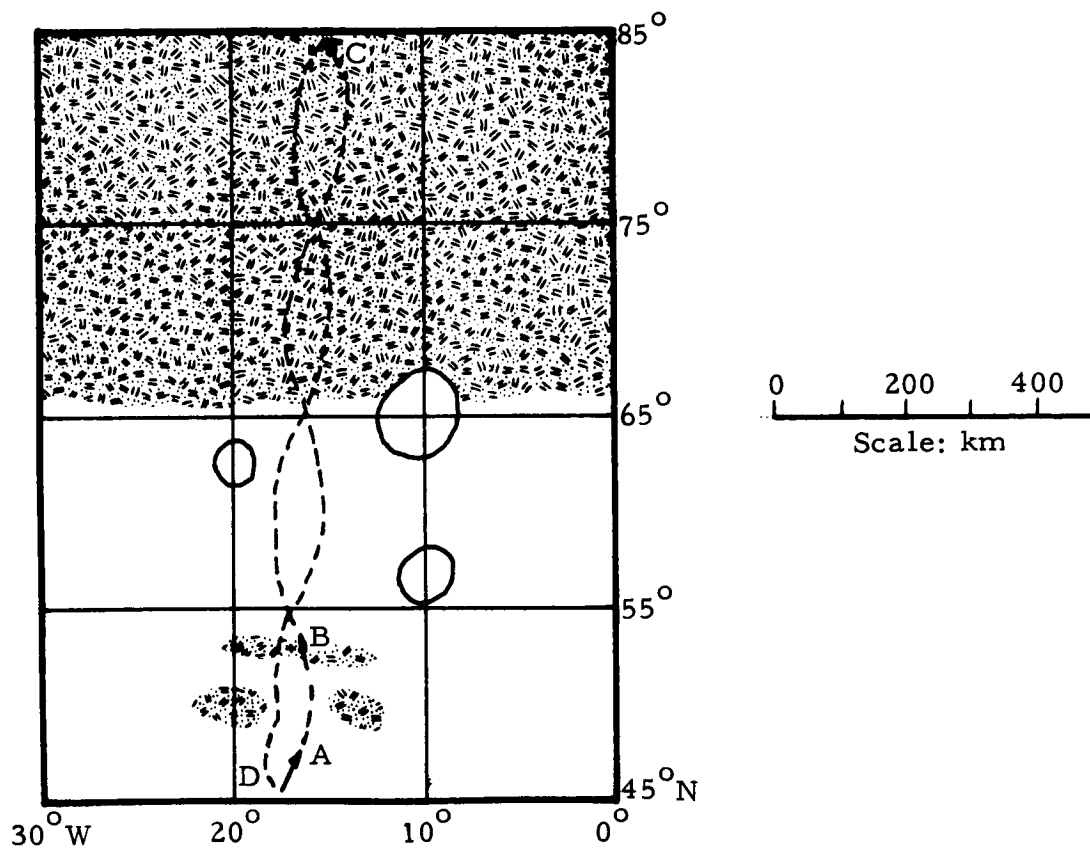
Figure 2-11 Mission 6 — 1984

SECTION 3

PRELIMINARY ANALYSIS OF NAVIGATION SYSTEM CONCEPTS

Three distinct system concepts were defined for detailed navigation component analysis: the passive nongyro, inertial, and RF technology systems. In order to obtain an early estimate of the magnitude of the navigation system errors associated with the ALSS MOLAB vehicle, a preliminary analysis of the concepts was performed before detailed requirements, computer error models, and component data were available. This section presents, for each system concept, navigation requirements, a preliminary error analysis, an error allocation, and a comparison of these error allocations with initially available state-of-the-art component data.

3.1   NAVIGATION FUNCTIONS AND REQUIREMENTS

Establishment of navigation functions and requirements is necessary to define the parameter ranges (order of magnitude) and to provide a basis for navigation subsystem and component evaluation. The definition of navigation subsystem requirements is ideally derived from total system requirements. In the absence of such requirements, however, the navigation subsystem needs may be defined directly from mission objectives. First, the mission objectives may be interpreted in terms of specific navigation functions which may then be examined individually to derive navigation requirements. It is this direct approach which is used here. The obvious drawback of this approach is the total neglect of system integration problems such as blockage of field of view, thermal control, etc. However, the basic feasibility of various concepts may still be examined without considering such constraints. The detail design of a particular system, however, would necessarily be made within whatever system constraints are necessary.

Attention during the preliminary survey was limited to considering Mission Type II alone. Consideration will be given to other mission types in subsequent portions of the study. For Mission Type II, then, the navigation functions are first enumerated and the navigation requirements resulting are then identified.

3.1.1 Mission Type II

A MOLAB-type mission description is typical of this mission type and defines six possible mission tasks which require navigation functions. These are:

1. Navigation of LRV from the LEM truck (LEM/T) landing point to LEM landing point

2. Navigation for LRV steering from the LEM to the first lunar point of interest, from the first lunar point to the second, etc., and from the last lunar point of interest to the LEM. This is called "Closed Path Excursion"

3. High precision retrace of path to recover scientific equipments positioned during outgoing journey.

4. Emergency navigation for rapid retrace of path from any point back to the LEM.

5. High precision mapping of specific area relative to a lunar landmark, the LEM/T, the LEM or other benchmark for scientific experimental purposes

6. Selenographic position fixes at LEM landing point, LEM/T landing point, and at various other lunar locations.

Each of these functions is discussed in detail in the following subsections.

3.1.1.1 LRV From LEM/T to LEM

The LEM is expected to land within 10 km of the LEM/T landing point, and the location of the LEM landing point is expected to be known to a 3 sigma accuracy of 0.455 km in moon coordinates per NASA estimates of a 100 m probable error. Navigation information must be supplied to allow driving the LRV (by remote control) from the LEM/T to the LEM. It will be assumed that the terminal navigation requirement will always be accomplished by visual observation (and crew control) of the relative positions and orientations of the LRV and the LEM. Reference 6 indicates that either the LEM or LRV (with passive optical enhancement) is visible against

the lunar background for distances of about one km. The LOS between LRV and LEM, assuming 6 meter heights for each, is about 9 km.

If an active optical beacon or an RF beacon is placed upon the LEM and elevated approximately an additional 4 meters, LOS is 10 km and it would be possible to "pilot" the LRV from the LEM/T to the LEM. The homing or heading indication would need be no better than ±8 degrees, based upon the criteria of Reference 6 that heading errors should not provide more than a one per cent increase in distance traveled over the ideal condition.

A selenographic system providing LRV latitude and longitude, plus an azimuth heading reference, would require that the RSS (root sum squared) value of the LEM map coordinate uncertainty and the LRV map coordinate uncertainty be less than or equal to the terminal homing range. Thus,

$$(E_{LEM})_S^2 + (E_{LRV})_S^2 \leq (H_R)^2 \tag{3-1}$$

where

$$(E_{LEM})_S = \text{error in LEM selenographic coordinates}$$

$$(E_{LRV})_S = \text{error in LRV selenographic coordinates}$$

$$H_R = \text{homing range.}$$

For the nonbeacon homing case, the LRV map coordinate requirement $(E_{LRV})_S$ is 0.89 km. For the beacon cases, the LRV map coordinate requirement is essentially equal to the LOS distance of 10 km. The azimuth and homing heading references would require a directional accuracy of ±8 degrees.

A navigation system providing x, y, and z coordinates relative to a lunar landmark, plus an azimuth reference, would require that the RSS value of the uncertainty in LEM location relative to the benchmark and the LRV location uncertainty be less than the terminal homing.

Thus,

$$(E_{LEM})_R^2 + (E_{LRV})_R^2 \leq (H_R)^2 \qquad (3-2)$$

where

$(E_{LEM})_R$ = error in LEM position relative to benchmark

$(E_{LRV})_R$ = error in LRV position relative to benchmark.

Assuming that the uncertainty of LEM location relative to the lunar bench-
mark is equal to the uncertainty in LEM position in map coordinates, then,
for Equations 3-1 and 3-2, $(E_{LRV})_S = (E_{LRV})_R$ or the accuracy require-
ments for the relative coordinate system are the same as for the seleno-
graphic system. It should be noted that relative coordinate systems are
generally limited to LOS operations, and for this mission task, homing
would be less complex and equally feasible for operations within LOS.

A dead-reckoning navigation system with azimuth reference
would require the addition of some means of locating the LEM/T relative
to the LEM or a lunar benchmark as initial conditions. Feasible perform-
ance would require that the RSS value of the uncertainty in LEM/T location,
the uncertainty in LEM location, and the total dead-reckoning error con-
tribution be less than the homing range or

$$(E_{LEM/T})^2 + (E_{LEM})^2 + (E_{DR})^2 \leq (H_R)^2 \qquad (3-3a)$$

Assuming $E_{LEM/T} = E_{LEM}$, then

$$2(E_{LEM})^2 + E_{DR}^2 \leq (H_R)^2 \qquad (3-3b)$$

Inserting E_{LEM} = 0.455 km, then E_{DR} = 0.77 km. Since most of a dead-
reckoning system's errors are a function of the distance traveled (approxi-
mately 10 km minus the homing range of 1 km), linear error rates allowable

would be about 0.77/9 = 0.086 km/km for the nonbeacon homing case. After the LRV leaves the LEM/T, the following equation applies:

$$E_{LRV}^2 + E_{LEM}^2 + E_{DR}^2 \leq (H_R)^2 \qquad (3-3c)$$

Assuming $E_{LRV} = E_{DR}$, then $E_{LRV} = 0.63$ km.

For the beacon homing cases, the dead-reckoning total error contributions are approximately equal to LOS distance of 10 km. Azimuth and homing heading tolerances would again be ±8 degrees.

The discussion above is summarized below.

Navigation Requirements

	With No Beacon	With 4-meter Beacon Atop LEM
Homing Range	1 km (visibility)	10 km
Heading Error	±8 deg	±8 deg
Selenographic and Relative Position Fix Error	0.63 km	10 km (LOS)
Dead-Reckoning Total Error	0.77 km	10 km
Dead-Reckoning Error Rate	0.086 km/km	1.0 km/km

3.1.1.2   Closed Path Excursions

Closed path excursions involve navigation and guidance information to allow visiting a series of lunar surface objective points, spaced 30 to 60 km apart, and returning to the point of origin (the LEM). Navigation and guidance requirements differ for each leg of the path according to the terminal conditions. There are three different terminal conditions:

1.   The last leg, which involves returning to the LEM such that the crew can be transferred from the LRV to the LEM

2. Those legs of the path whose objective is a set of map coordinates

3. Those legs of the path whose objective is a lunar landmark.

Each of these is discussed in the following paragraphs.

Final Leg Back to LEM

The requirements for this task are similar to the LRV-to-LEM task except that the total distance is increased to 50 km. Thus, homing all the way does not appear feasible since a beacon height on the LEM of 625 meters would be required to extend the LOS.

The selenographic system would require a position fix accuracy, E_{LRV}, of 0.89 km for the nonbeacon homing case. For the beacon homing cases, assuming a four meter extension to the LEM height, the accuracy requirement would be relaxed to 10 km (a 100-meter LEM extension would relax accuracy to 23 km).

Equation 3-3c may then be employed, recognizing that $(E_{LEM/T})$ of Equation 3-3a is now replaced by (E_{LRV}). Thus, repeating Equation 3-3c.

$$(E_{LRV})^2 + (E_{LEM})^2 + (E_{DR})^2 \leq H_R^2 \qquad (3-4)$$

Substituting $E_{LEM} = 0.455$ km, the dead-reckoning and position fix errors are related by

$$E_{LRV}^2 + E_{DR}^2 \leq H_R^2 - (0.455)^2 \qquad (3-5)$$

Map Coordinate Objectives

Homing is not involved in this mission task, which is to navigate to a preselected set of map coordinates (a given lunar latitude and longitude).

A selenographic system should have a position fix accuracy requirement, E_{LRV}, equivalent to the best accuracy expected of lunar maps of that era (ACIC estimates give 3.56 km for this value). A relative

coordinate system would have the same requirement assuming that the
lunar benchmark uncertainty in map coordinates is 3.56 km. Then,

$$E_{LRV}^2 + E_{DR}^2 \leq E_M^2 \qquad (3\text{-}6)$$

where E_M is mapping error.

Inserting $E_M = 3.56$ km,

$$E_{LRV}^2 + E_{DR}^2 \leq (3.56)^2 \qquad (3\text{-}7)$$

Lunar Landmark Objectives

These objectives are lunar phenomena like craters, rills, rays,
walls, etc. which are generally several kilometers in extent and many
meters high. They cannot be considered as point sources for homing; how-
ever, their large size and adjacent identifiable features provide a "piloting"
range in itself. It will be assumed that this piloting range is at least equal
to 5.0 km.

Navigation requirements are the same as for the map coordinate
objective:

$$E_{LRV}^2 + E_{DR}^2 \leq (3.56)^2 \qquad (3\text{-}8)$$

3.1.1.3   Nominal Retrace

This mission task involves retracing the original closed path to
collect scientific data and instrumentation which was left on the original
journey. There is no need for a precision retracing of the original path;
all that is required is a precision return to the exact location of the instru-
ments. These instruments will, generally, not be left at every outgoing
objective, such that the distances between objectives (or legs of the path)
will increase to about 100 km. It will be assumed that the location of the
instrument package is marked in map or relative coordinates, its location
relative to various observable lunar features is indicated, and if necessary
a beacon or other marker will be used to produce a homing range of at
least 5.0 km.

Based upon previous assumptions for other mission tasks (RSS errors less than homing range, etc.) and the assumption that the same navigation system is used for both the original path and the retrace (uncertainty in objective location equals uncertainty in returning to it), navigation system accuracy is given by:

$$2 (E_{LRV}^2 + E_{DR}^2) \leq H_R^2 \qquad (3\text{-}9)$$

or

$$E_{DR}^2 \leq \frac{(5.0)^2}{2} - E_{LRV}^2 \qquad (3\text{-}10)$$

3.1.1.4 Emergency Retrace

This mission task provides for an emergency return to the LEM and an abort of the closed-path excursion. The original path must be retraced for two reasons:

1. If the LRV attempted (during the emergency) to continue the closed-path excursion or to go directly to the LEM, it may enter a cul-de-sac, encounter terrain too rough to be negotiated, or encounter other unknown hazards

2. The original path offers a certain route to the LEM that is hazard free and of proven sufficient smoothness.

It will be assumed that the original path's location is known in map or relative coordinates, and its location relative to various observable lunar features is indicated. Critical portions, turns, passes, etc. on the route will be assumed marked (actively or passively), and the retrace is only required to be precise during the critical junctures. The navigation system must only "find" the beginnings of these critical portions of the route. It will be assumed that the effective homing range to the markers is 5.0 km and that the LRV distance of travel to that marker is 100 km. Assuming that the uncertainty in marker location equals the uncertainty in returning to it, and using the assumptions made earlier for other mission tasks, navigation accuracy requirements are given by:

$$E_{DR}^2 = \frac{(5.0)^2}{2} - E_{LRV}^2 \qquad (3\text{-}11)$$

3.1.1.5 Benchmark Mapping

This mission task involves locating the position of lunar features and phenomena relative to a lunar benchmark as a necessary support for scientific experimentation. Early MOLAB missions would require accuracies of about 600 meters in horizontal and one part in 500 for the vertical dimension. Later missions accuracy requirements may approach 60 meters in horizontal dimensions and one part in 5000 for the vertical. Since the LEM will be a principal benchmark, and the maximum distance between LEM (straight-line) and the LRV is 80 to 100 km, the distance for the relative measurements will be taken as 100 km.

Thus, a dead-reckoning system would require error rates of:

	Horizontal	Vertical
Early Missions	0.006 km/km	0.002 km/km
Later Missions	6×10^{-4} km/km	2×10^{-4} km/km

For a relative position system, the position fix requirements may be computed from

$$(E_{LEM})^2 + (E_{LRV})^2 \leq (0.6)^2 \qquad (3\text{-}12)$$

Assuming $E_{LEM} = 0.455$ km, then $E_{LRV} = 0.39$ km.

For later missions, with horizontal errors of only 60 meters,

$$(E_{LEM})^2 + (E_{LRV})^2 \leq (0.06)^2 \qquad (3\text{-}13)$$

Assuming $E_{LEM} = E_{LRV}$, then $E_{LRV} = 42$ meters.

3.1.1.6 Selenographic Mapping

This mission task involves locating the position of lunar features and phenomena in map coordinates as a necessary support for scientific experimentation. For the early MOLAB mission, the navigation accuracy

requirement should be equivalent to the best maps of that era: 3.56 km. Later missions would require higher accuracies for map improvements, etc. which should approach 60 meters.

Homing is not applicable to this mission task. A relative coordinate position fix system could be utilized, assuming that the lunar benchmark location is known in selenographic coordinates. Since the principal lunar benchmark will be the LEM, and the MOLAB will always be within 100 km of the LEM (straight line distance), the relative coordinate system must operate over a distance of 100 km.

The position fix accuracy is given by

$$(E_{LRV})^2 + (E_{LEM})^2 \leq E_M^{\ 2} \qquad (3-14)$$

Using E_M = 3.56 and E_{LEM} = 0.455, then E_{LRV} = 3.54 km for early missions.

For later missions, assuming E_M = 0.06 and $E_{LRV} = E_{LEM}$, then E_{LRV} = 42 meters.

The dead-reckoning error is then given by

$$E_{DR}^{\ 2} + E_{LRV}^{\ 2} \leq E_M^{\ 2} \qquad (3-15)$$

which yields

$$E_{DR} = \left[(3.56)^2 - (3.54)^2 \right]^{1/2} = 0.37 \text{ km} \quad \text{Early Missions}$$

$$E_{DR} = \left[(0.06)^2 - (0.042)^2 \right]^{1/2} = 0.042 \text{ km} \quad \text{Later Missions}$$

Dead-reckoning error rates over 100km then become

Early Missions $\qquad 3.7 \times 10^{-3}$ km/km

Later Missions $\qquad 4.2 \times 10^{-4}$ km/km

3.2 PASSIVE NONGYRO CONCEPT

3.2.1 Concept Definition

The passive nongyro system utilizes a star tracker, local vertical reference, timer, computer, and ephemeris to obtain a position fix. Azimuth reference is provided by a vertical reference, earth tracker, timer, and ephemeris. Distance travelled is measured with a wheel rotation odometer. Homing is accomplished by TV or direct viewing using passive optical enhancement on the LEM.

3.2.2 Navigation Requirements—Mission Type II

The requirements to be met by this navigation system concept may be derived from the general expressions contained in Section 3.1. It will be assumed that the LRV position fix error and dead-reckoning error are equal, i.e. $E_{LRV} = E_{DR}$, in Equations 3-4, 3-8, 3-9, 3-10 and 3-11 and that $H_R = 1.0$ km. The requirements for this system concept then become:

Mission Task	Azimuth Reference	Position Fix (km)	Dead Reckoning (km/km)
LEM/ T-to-LEM	$\pm 8^{\circ}$	0.63	0.086
Final leg back to LEM	$\pm 8^{\circ}$	0.63	0.013
Map position objective	N/A	2.50	0.050
Landmark objective	$\pm 8^{\circ}$	2.50	0.050
Nominal retrace	$\pm 8^{\circ}$	2.50	0.025
Emergency retrace	$\pm 8^{\circ}$	2.50	0.025
Benchmark mapping	N/A	0.060 to 0.60*	6×10^{-4} to 6×10^{-3}
Selenographic mapping	N/A	0.060 to 2.5	4.2×10^{-4} to 0.025

*Benchmark mapping also requires vertical accuracy of 1:5000 to 1:500 with dead-reckoning error rate of 2×10^{-4} to 2×10^{-3} km/km.

It is seen from the preceding table that all mission tasks except mapping may be accomplished with a system with

Position Fix Accuracy = 0.63 km

Dead-Reckoning Error Rate = 0.013 km/km

3.2.3 Error Allocation—Mission Type II

3.2.3.1 Position Fix Without Benchmark Mapping

The primary sources of error in the position fix capability of this system concept are considered to be: star-tracker equipment errors in measuring azimuth and elevation of the celestial bodies; local vertical reference equipment errors; timer equipment errors; uncertainties in the correlation of local vertical with the gravity vector, and uncertainties in the ephemeris (computational and reading errors are included here). The relationship of these errors to the uncertainty of the position fix has been derived in Reference 18.

$$E_{LRV} = \left[(C_1 E_1)^2 + (C_2 E_2)^2 + (C_3 E_3)^2 + (C_4 E_4)^2 + (C_1 E_5) \right]^{1/2} \quad (3-16)$$

where:

E_1	is local vertical sensor error
E_2	is star-tracker sensor error (azimuth and elevation error assumed equal)
E_3	is timer error
E_4	is ephemeris uncertainty
E_5	is gravity-local vertical correlation uncertainty
C_1 to C_4	are partial derivatives.

The coefficients of Equation 3-16 are a function of the geometrical relationships between the star-positions and the vehicle position. These

coefficients can be varied as discussed in Reference 18, but a set has been selected for preliminary analysis purposes. If:

Vehicle Position: 5° Latitude 30° Longitude

1st Stellar Subposition: 20° Latitude, -14° Longitude

2nd Stellar Subposition: 42° Latitude, 60° Longitude

1st Star Sighting: 51° Azimuth, 45° Elevation

2nd Star Sighting: -51° Azimuth, 45° Elevation

then:

$$C_1 = 3.7 \times 10^{-3} \text{ km/arc second}$$

$$C_2 = 1.9 \times 10^{-2} \text{ km/arc second}$$

$$C_3 = 6.6 \times 10^{-3} \text{ km/second}$$

$$C_4 = 1.2 \times 10^{-2} \text{ km/arc second.}$$

The allowable position fix error E_{LRV} is 0.63 km. Assuming that all errors contribute equally to the total error (each error can contribute 0.28 km), then the following requirements exist:

Local Vertical Sensor Accuracy: 76 arc seconds (E_1)

Star Tracker Accuracy: 15 arc seconds (E_2)

Timer Accuracy: 42 seconds (E_3)

Ephemeris Uncertainty: 23 arc seconds (E_4)

Local Vertical Deflection: 76 arc seconds (E_5)

Reference 4 indicates the following accuracies are achievable within the state of the art:

Star Tracker Accuracy: 45 arc seconds

Timer Accuracy: 0.3 seconds

Ephemeris Uncertainty (with computation and heading): 108 arc sec

Gravity-local Vertical Uncertainty: 180 arc seconds.

Several sources have indicated local vertical sensor accuracies varying from 2 arc seconds to 6 arc minutes without defining whether these values are probable, one sigma etc.; the sources also fail to signify whether the accuracies given are for the earth or lunar gravitational fields. Clarification of these deficiencies will be undertaken. In any case, it appears that the position fix requirements of a passive nongyro system concept may be difficult to meet with the present state of the art.

3.2.3.2   Dead-Reckoning Without Benchmark Mapping

A preliminary dead-reckoning error model was developed to relate the pitching motion of the vehicle relative to the vertical reference, the heading motion of the vehicle relative to the azimuth reference, and the distance traveled to the vector position of the vehicle relative to its starting point. An error model as derived in Appendix A relates errors in azimuth, pitch, and distance traveled to the positional uncertainty during dead-reckoning. The error, E_{DR}, can be expressed as follows:

$$(E_{DR})^2 = (C_5 E_6)^2 + (C_6 E_7)^2 + (C_7 E_8)^2 \qquad (3-17)$$

where:

E_6 is vehicle pitch error

E_7 is vehicle azimuth error

E_8 is error in distance traveled

C_5 to C_7 are partial derivatives.

The coefficients of Equation 3-17 are a function of the geometry of the path traversed. A path chosen for preliminary purposes is:

Path length: 100 km

Desired azimuth (a constant): 45°

Differential altitude between starting and end points: 0.1 km.

Then:

$$C_5 = 0.00175 \text{ km/deg}$$

$$C_6 = 1.75 \text{ km/degree}$$

$$C_7 = 1.0 \text{ (unitless)}$$

and:

$$(E_{DR})^2 = (0.00175 E_6)^2 + (1.75 E_7)^2 + (E_8)^2$$

The allowable dead-reckoning error is 0.63 km. Assuming that pitch, azimuth and distance errors contribute equally to the total error (each error can contribute 0.36 km) then:

Distance error: 0.36 km (E_8)

Azimuth error: 12.0 arc minutes (E_7)

Pitch error: can be ignored (E_6).

Primary error sources in the measurement of vehicle azimuth motion are: earth-tracker equipment errors, timer equipment errors, ephemeris uncertainties, local vertical sensor errors, and the uncertainty in the correlation of gravity and geometric vertical. Reference 18 provides an error model relating these errors to the total azimuth error.

$$\text{Azimuth error} (E_7) = \left[(C_8 E_9)^2 + (C_9 E_3)^2 + (C_{10} E_4)^2 + C_{11}^2 (E_1 + E_5)^2 \right]^{1/2}$$

(3-18)

where

E_9 is earth-tracker equipment error

C_8 to C_{11} are partial derivatives.

The coefficients of Equation 3-18 are a function of the geometrical relationships between the earth position and the vehicle position. Assuming:

Vehicle position: 5° latitude, 30° longitude

Earth sub-point: 0° latitude, 0° longitude

then

C_8 = 1.0 unitless

C_9 = 3.2 x 10^{-2} arc minutes/hour

C_{10} = 4.8 x 10^{-2} unitless

C_{11} = 1.25 unitless.

The allowable azimuth error is 12.0 arc minutes. Assuming that all errors contribute equally to the total error (each error can contribute 6.0 arc minutes), then the following requirements exist:

Earth Tracker Equipment Error: 6.0 arc minutes

Ephemeris Uncertainty: 125 arc minutes

Local Vertical Deflection Uncertainty: 4.8 arc minutes

Timer Error: 190 hours

Wheel Slippage: 0.36%.

The timing error was calculated upon the basis of the "optical librations" which produce oscillations of the moon to an earth observer of about ±8 degrees, with a period of approximately twenty-eight days. The physical librations were not included since their angular motion per unit time is about 10^{-5} less than the optical librations.

The primary error source in the measurement of vehicle distance of travel is wheel slippage.

3.2.3.3   Dead-Reckoning With Benchmark Mapping

Benchmark mapping requirements must be met by the dead-reckoning portions of the system.   The requirement for early missions is 600 meters in the horizontal plane and one part in 500 in the vertical plane. Distributed equally, the horizontal requirement defines:

Distance error: 350 meters or .35%

Azimuth error: 12 arc minutes

Pitch error: can be ignored.

Distributed equally, the vertical requirement defines:

Distance error: 140 meters or 0.14%

Pitch error: 0.61 arc seconds.

The vertical requirement has been derived from Appendix A on the basis of the error equation:

$$(\Delta_h)^2 = (C_{12}E_8)^2 + (C_{13}E_6)^2 \qquad (3-19)$$

where

$$C_{12} = 10^{-3} \text{ m/m}$$

$$C_{13} = 0.23 \text{ m/arc second.}$$

The requirements for the benchmark mapping dead-reckoning can be summarized as:

Distance error: 140 meters or 0.14%

Azimuth error: 12 arc minutes

Pitch error: 0.61 arc seconds.

Using Equation 3-18 and the above distance, azimuth, and pitch requirements, individual error source requirements were derived as:

Earth Tracker Equipment Error: 6.0 arc minutes

Ephemeris Uncertainty: 125 arc minutes

Local Vertical Deflection: 0.43 arc second

Local Vertical Sensor Error: 0.43 arc seconds

Time Error: 190 hours

Wheel Slippage: 0.14%.

A summary of system performance is given in Table 3-1.

3.3 INERTIAL SYSTEM CONCEPT

3.3.1 Concept Definition

The inertial system concept utilizes the same items as the passive nongyro concept to obtain a position fix. Directional references, vertical and horizontal, are provided by a gyro-accelerometer platform. Initial azimuth is provided by the position fix elements. The accelerometer output is doubly integrated to distance traveled. Homing is accomplished by TV or direct viewing, using passive optical enhancement on LEM.

3.3.2 Navigation Requirements—Mission Type II

The specific requirements for the inertial concept may again be computed from Section 3.1. Assuming that a 4-meter beacon is employed

TABLE 3-1

PASSIVE NON-GYRO SYSTEM

$R_H = 1km$

Error Sources	Requirements (without benchmark mapping)	State of Art	Requirements (with benchmark mapping)
Position Fix			
L.V. Sensor	76 arc seconds	30 arc seconds	None
Star Tracker	15 arc seconds	45 arc seconds	None
Timer	42 seconds	0.3 seconds	None
Ephemeris	23 arc seconds	108 arc seconds	None
Gravity Uncertainty	76 arc seconds	180 arc seconds	None
Dead-Reckoning			
Earth Tracker	6.0 arc minutes	6 arc minutes	6.0 arc minutes
Ephemeris	125 arc minutes	1.8 arc minutes	125 arc minutes
Gravity Uncertainty	4.8 arc minutes	3 arc minutes	0.43 arc seconds
L.V. Sensor	4.8 arc minutes	0.5 arc minutes	0.43 arc seconds
Timer	190 hours	0.3 sec	190 hours
Wheel Slippage	0.36%	To be defined	0.14%

atop LEM, homing may be accomplished all the way from the LEM/ T to LEM. Thus the position fix and dead-reckoning requirements are trivial for this mission task. For the final leg back to LEM, H_R = 10 km for a beacon 4 meters above LEM, and 23 km for a 100-meter beacon. Requirements on all other mission tasks are identical to those for the passive nongyro system.

Mission Task	Azimuth Reference	Position Fix (km)	Dead Reckoning (km/km)
LEM/ T-to-LEM	$\pm 8^\circ$	-	-
Final leg back to LEM	$\pm 8^\circ$	7.10	0.144
Map position objective	N/A	2.50	0.050
Landmark objective	$\pm 8^\circ$	2.50	0.050
Nominal retrace	$\pm 8^\circ$	2.50	0.025
Emergency retrace	$\pm 8^\circ$	2.50	0.025
Benchmark mapping	N/A	.060 to 0.60*	6×10^{-4} to 6×10^{-3}
Selenographic mapping	N/A	.060 to 2.5	4.2×10^{-4} to 0.025

From the above, the requirements on the inertial system are (without mapping tasks):

    Position Fix Accuracy - 2.50 km

    Dead-reckoning Error Rate = 0.025 km/km.

3.3.3 Error Allocation—Mission Type II

3.3.3.1 Position Fix Without Benchmark Mapping

The error sources in the inertial system are the same as those for the passive nongyro system which are detailed in Section 3.2.3.1.

---

* Benchmark mapping also requires vertical accuracy of 1:5000 to 1:500 with dead-reckoning error rate of 2×10^{-4} to 2×10^{-4} km/km.

The allowable position fix error is 2.50 km. Using the same sensitivity coefficients as for the first system concept in Equation 3-16, the following requirements are defined:

Local Vertical Sensor Accuracy: 300 arc seconds (E_1)

Star Tracker Accuracy: 60 arc seconds (E_2)

Timer Accuracy: 170 seconds (E_3)

Ephemeris Uncertainty: 93 arc seconds (E_4)

Gravity-Local Vertical Uncertainty: 300 arc seconds (E_5).

It appears that these requirements can be met by the state of art except for the ephemeris uncertainty (which could be met by a slightly different error assignment).

3.3.3.2 Dead-Reckoning Without Benchmark Mapping

The allowable dead-reckoning error is 2.5 km for the inertial system. Assuming that pitch, azimuth and distance errors contribute equally to the total error (each error can contribute 1.75 km) then:

Distance error: 1.75 km

Azimuth error: 60 arc minutes

Pitch error: can be ignored.

Primary error sources in the measurement of vehicle azimuth motion are: initial directional errors from position fix elements, gyro-acceleration platform nulling accuracies, linear time growth errors due to gyro drift rates, and extraneous acceleration inputs to the accelerometers caused by vehicle structural dynamics interacting with surface roughness.

$$\text{Azimuth error} = \left[E_{10}^2 + E_{11}^2 + E_{12}^2 t^2 \right]^{1/2} \tag{3-20}$$

where

E_{10} is initial directional error due to position fix elements

E_{11} is gyro platform nulling accuracies

E_{12} is gyro drift rate

t   is time of travel (12.5 hours)

V   is average vehicle speed (8 km/hr).

The initial directional error from the position fix elements
(E_{10}) can be found from the requirements for position fix elements as
8.8 arc minutes. Assuming an equivalent error assignment for the remain-
ing error sources (each error can contribute 42 arc minutes), then the
requirements are:

Gyro platform nulling error: 42 arc minutes

Gyro drift rate: 0.056 degress/hour.

The primary error source in the measurement of distance
traveled is extraneous acceleration inputs which are doubly integrated
into position errors and are thus:

$$E_{DR} = 0.5t^2 E_{13}$$

where

E_{13} are the extraneous inputs.

The requirement is that E_{13} be less than 1.8×10^{-6} meters/second
squared.

3.3.3.3   Dead-Reckoning With Benchmark Mapping

Using Equation 3-20 and the distance, azimuth, and pitch errors
of Section 3.2.3.3, the following requirements may be computed:

Initial Directional Fix: 7 arc minutes

Local Vertical Sensor: 0.43 arc seconds

Star Tracker: 48 arc seconds

Timer: 140 seconds

Ephemeris: 74 arc seconds

Gravity-Local Vertical Correlation: 0.43 arc seconds

Gyro Platform Nulling Error: 7 arc minutes

Gyro Drift Rate: 0.01 degrees/hour

Extraneous Acceleration Inputs: $<1.35 \times 10^{-7}$ meters/$\sec^2$.

It would be necessary that the position fix elements of the inertial system be improved to provide a more accurate initial directional fix than the 8.8 arc minutes derived from Equation 3-18. (Assuming that the initial error contributes the same as the nulling and drift errors, then the initial error is as given above (7 arc minutes)). A summary of performance and requirements is given in Table 3-2.

3.4 RF TECHNOLOGY CONCEPT

3.4.1 Concept Definition

The RF technology system utilizes driver visual and RF homing (LEM contains an RF beacon; LRV contains receiver and antennas) to perform the LEM/T-to-LEM and emergency functions. Position fixes are obtained by earth-based tracking of a beacon on the LRV. Directional reference is provided by a vertical sensor, timer, ephemeris, and an RF earth tracker. Doppler radar provides vehicle velocity which is integrated to provide distance traveled.

3.4.2 Navigation Requirements—Mission Type II

Assuming a 40-meter extended beacon atop the LEM, the LOS to LEM is 10 km. Thus the LRV can home all the way from LEM/T to LEM

TABLE 3-2

INERTIAL SYSTEM SUMMARY

$R_H = 10$ km

Error Sources	Requirements (without benchmark mapping)	State of Art	Requirements (with benchmark mapping)
Position Fix			
L.V. Sensor	5 arc minutes	30 arc seconds	0.43 arc seconds
Star Tracker	1 arc minute	45 arc seconds	48 arc seconds
Timer	2.8 minutes	0.3 seconds	140 seconds
Ephemeris	93 arc seconds	108 arc seconds	74 arc seconds
Gravity Uncertainty	5 arc minutes	3 arc minutes	0.43 arc seconds
Dead-Reckoning			
Platform Null	42 arc minutes	To be defined	7 arc minutes
Gyro Drift Rate	0.056 deg/hour	0.005 to 4 deg/hr	0.01 deg/hour
Extraneous Acceleration	$<1.8 \times 10^{-6}$ m/sec^2	To be defined	$<1.3 \times 10^{-7}$ m/sec^2

and the position fix and dead-reckoning requirements are not needed. The requirements on individual mission tasks are identical to those of the inertial system concept and will not be repeated here. The position and dead-reckoning requirements are therefore:

Position Fix Accuracy = 2.50 km

Dead-Reckoning Error Rate = 0.025 km/km.

3.4.3 Error Allocation—Mission Type II

3.4.3.1 Position Fix Without Benchmark Mapping

The RF technology system concept utilizes an RF beacon on the vehicle and the DSIF tracking network to obtain position fixes. The allowable position fix requirement is 2.5 km.

3.4.3.2 Dead-Reckoning Without Benchmark Mapping

This system concept utilizes a local vertical sensor, timer, ephemeris, and an RF earth tracker to determine directional references. A doppler radar provides vehicle velocity. The doppler velocities are integrated to provide the distance of travel. The allowable distance, azimuth, and pitch errors are the same as for the inertial concepts dead-reckoning system.

Primary sources of error in the measurement of vehicle azimuth motion are: local vertical sensor errors, uncertainties in correlation of acceleration vector and geometric vertical, timer errors, ephemeris uncertainties and RF tracker equipment errors.

Thus

$$\text{Azimuth Error} = \left[(C_8 E_9)^2 + (C_9 E_3)^2 + (C_{10} E_4)^2 + C_{11}^2 (E_1 + E_5)^2 \right]^{1/2} \quad (3\text{-}21)$$

where all parameters are as defined previously,

The allowable azimuth error is 60 arc minutes. Assuming that all errors contribute equally (each error contributes 26 arc minutes), then the following requirements exist:

Earth Tracker Equipment Error: 26 arc minutes

Ephemeris Uncertainty: 540 arc minutes

Acceleration-Local Vertical Correlation
Uncertainty: 21 arc minutes

Local Vertical Sensor Error: 21 arc minutes

Timer Error: 810 hours.

The primary error source in the measurement of distance traveled is doppler equipment errors which are integrated to form position errors. Thus,

$$E_{DR} = E_{14}t$$

where

E_{14} is the doppler equipment errors.

The requirement is that E_{14} be less than 0.04 meters/second or 1.6% of the 8 km/hour vehicle velocity.

3.4.3.3   Dead-Reckoning With Benchmark Mapping

Using Equation 3-21 and the distance, azimuth, and pitch errors of Section 3.2.3.3, the following requirements may be derived:

Earth Tracker Equipment Error: 5.4 arc minutes

Ephemeris Uncertainty: 110 arc minutes

Acceleration-Local Vertical Correlation
Uncertainty: 0.43 arc sec

Local Vertical Sensor Error: 0.43 arc second

Timer Error: 170 hours

Doppler Equipment Errors: 0.08% of vehicle velocity.

A summary of system requirements is presented in Table 3-3.

3.5 CONCEPT TOTAL ACCURACY

The selected system concept total accuracy as a result of preliminary state of the art and nominal component accuracies can be calculated using basic Equations 3-16 and 3-17. The azimuthal error terms for Equations 3-16 and 3-17 are calculated, where applicable, from Equations 3-18, 3-20, and 3-21. In all cases component or subelement error contributions used in calculations were the state-of-the-art figures in Tables 3-1, 3-2, and 3-3. Nominal uncertainty values for platform null (.1°), extraneous acceleration (10^{-6} m/sec^2), and doppler equipment (5%/degree of tilt) were assumed. The error sensitivity coefficients used were those defined by the assumed celestial and mission geometry as stated in Sections 3.2.3.1 and 3.2.3.2.

Table 3-4 presents summarized accuracy requirements and the calculated attainable accuracies. The results indicate a method of analysis rather than conclusive answers due to the constraints of the single assumed geometrical point or error sensitivity coefficients. However, within the restrictions stated, no system concept total attainable accuracy satisfies all the stipulated position fix and dead-reckoning uncertainty requirements.

3.6 CONCLUSIONS

The results of the preliminary error analysis have been summarized primarily in Tables 3-1, 3-2, and 3-3. These results could be changed somewhat by different error assignments. However, the results as presented are representative of requirements under the guidelines laid forth, and a large mismatch in state of the art and requirements presently exists.

It should be noted that the dead-reckoning requirements could be materially reduced by requiring more frequent stops to make more

accurate position fixes. It is also worthy of mention that the passive non-gyro system concept requirements could be considerably relaxed by the addition of a longer range homing capability.

Attention should be paid to the difficulty of performing angular measurements to a celestial body from a moving vehicle under the extreme dynamic vehicle attitude changes produced by terrain traverse. This also applies to local vertical sensors. The remedy will probably be a gyro system to either maintain a reference or stabilize the tracker.

TABLE 3-3

RF SYSTEM SUMMARY

$$R_H = 10 \text{ Km}$$

Error Sources	Requirements (without benchmark mapping)	State-of-Art	Requirements (with benchmark mapping)
Position Fix			
DSIF Tracking	2.5 km	4.5 km*	None
Dead-Reckoning			
Earth Tracker	26 arc minutes	6 arc minutes	5.4 arc minutes
Ephemeris	9.0 degrees	1.8 arc minutes	1.8 degree
Gravity Uncertainty	21 arc minutes	3 arc minutes	0.43 arc seconds
L.V. Sensor	21 arc minutes	30 arc seconds	0.43 arc seconds
Timer	810 hours	yes	170 hours
Doppler Equipment	1.6% of velocity	To be determined	0.08% of velocity

* Latest DSIF/MSFN Estimate

TABLE 3-4

SYSTEM ERRORS

System Concept	Passive Non-Gyro		Inertial		RF	
	Pos. Fix km	D.R. km	Pos. Fix km	D.R. km	Pos. Fix km	D.R. km
Requirements w/o Benchmark Mapping	.63	1.3	2.5	2.5	2.5	2.5
Requirements w/Benchmark Mapping (Horizontal)	-	0.60	-	0.60	-	0.60
Concept Total Accuracy	1.7	0.60	1.7	1.5	0.455 km 4.5 DSIF	0.60

SECTION 4

NAVIGATION REQUIREMENTS

4.1 NAVIGATION SYSTEM REQUIREMENTS

Navigation system configurations proposed for use on the lunar surface are generally derived from techniques and instruments used for navigation on the earth. Hence, it is reasonable to assume that many of the parameters and associated weighting functions used to evaluate the performance of an earth surface system are equally applicable to a lunar surface system. Lunar surface navigation system concepts will, at various times, be evaluated using parameters such as accuracy, reliability, weight, power, cost, and the mission task time chargeable to the navigation function. The accuracy of the navigation data is the most significant parameter if the system is available and functional. The navigation function is assumed to be required for all missions even if a mission is within line of sight of the LEM. Broadly stated, any requirement for vehicle location and/or heading in either relative or absolute terms is a requirement for navigation data.

As a preliminary task in the analysis of navigation implementation, typical system accuracy requirements were defined. These requirements were used to:

1. Limit the scope of the study to the area of applicable techniques and sensors

2. Form a basis in performing a meaningful evaluation of techniques and components as applied to the three systems defined for this study

3. Derive component R&D recommendations following comparison of requirements and state-of-the-art performance.

These requirements, as described in the following text, are based on specific navigation tasks associated with scientific experiments and also general navigation functions related to the previously discussed typical mission types.

4.1.1   LEM Landing Site Surveys

Mission tasks of site selection and verification necessitate bearing strength and slope (and possible gravity) measurements in accordance with planned traverse patterns in order to establish confidence that site surfaces will be qualified for LEM landing areas. Assuming that a position fix benchmark(s) can be accurately established, an exploration search pattern relative to the benchmark is then required. Other position fixes in addition to returns to the original benchmark can be made to verify dead-reckoning performance. (Consideration must also be given to trilateration and/or triangulation techniques for verification.) Gravity measurements were included, because this may be the best means for initial determination of the presence of subsurface caves hazardous to LEM landing impacts. In addition, these caves and/or high density subsurface volumes can cause deflections in the gravity vector that can result in navigational errors.

Preliminary calculations of survey requirements applicable to Apollo landing areas indicate that the following might be required:

1.   Nineteen landing sites spaced approximately 400-m apart, center to center, in a hexagonal pattern

2.   Landing site diameter of 40 m.

For each landing site, it is necessary to measure and map slopes, protuberances, depressions, and soil bearing strengths. Site acceptability is dependent upon satisfactory measurements.

Navigational requirements applicable to the site survey tasks include the following measurements: (1) locations of the landing areas in selenocentric coordinates, (2) locations of the sites within the landing area, and (3) vehicle traverses and test point locations within the sites. From the standpoint of remote control operations, it will be assumed that laser ranging and the placement of optical markers will not be utilized. This

leads to requirements for a position-fix capability to locate areas and a dead-reckoning capability for the location of the sites and test points. To fulfill the site survey requirements, a procedure using the TV system and surface features for reference will also be required.

System requirements applicable to the earth independent site survey tasks are as follows:

1. Area Location

    Assume:

    $$E_S^2 + E_N^2 \leq (0.5 D_A + R_{LEM})^2$$

    where

    E_S = area location error

    E_N = LEM navigation error

    D_A = area diameter = 1500 m

    R_{LEM} = LEM translational range = 350 m

    or

    $$E_S^2 + E_N^2 \leq (750 + 350)^2$$

    For the condition $E_S = E_N$, $E_N = 777$ m.

    For near-side sites where earth-based tracking of the vehicle can reduce the site location error (E_S) over an extended time period to 100 m then:

    $$E_N^2 \leq (750 + 350)^2 - (100)^2$$

    $$E_N \leq 1093 \text{ m}$$

It is also apparent that possible increases in LEM translational ranges and hover times will also reduce the position accuracy requirement.

2. Site Locations (relative to area position reference)

Latitude and Longitude: ± 50 m

Elevation: not critical.

4.1.2 Gravity Surveys

Gravity surveys are important in the scientific mission planning, because it is believed that gravity measurements are the only geophysical technique that is certain to obtain usable subsurface data on the moon. In addition to the detection of anomalies, the data aid in defining the moon's geometric shape (lunar geoid) and provide rough elevation ties between the explored areas.

Requirements imposed upon the navigation system for location of gravity stations are not too well defined for two reasons. First of all, the data needed to establish the basic lunar geometry do not impose requirements for accuracy better than ±1° in the locations of the stations. Secondly, the detection and mapping of anomalies is dependent upon the width, depth, density, and size of the anomaly. In general, it is necessary to space the stations at a distance that is half the width of density anomalies such as caves and lava tubes of interest. Also, the gravity anomaly is always wider than the mass anomaly that produces it, and a wide but shallow anomaly can have the same measured effect as one that is narrow and deep. For the latter case, the station spacing should be no less than the depth of the mass anomaly. Hence, station spacing, S, can be defined as:

1. $S \leq \dfrac{w}{2}$ (w = width)

2. $S \leq d$ (d = depth).

The selection of either 1 or 2, above, is subject to on-the-spot decisions. For the lunar survey, the smallest spacing would be desirable for initial operations.

4-4

Locational accuracy and fine grain gravity surveys will be important during later phases of the lunar exploration program when it may be desirable to construct subsurface lunar base facilities in natural caves for environmental protection. During that time, requirements for the more important lunar scientific mission tasks will have been fulfilled to an extent that will permit the allocation of more time to the fine grain and more precise survey tasks.

During the early mission phases, it is believed that the vehicle exploration area will be such that a difference in elevation of 600 m will not be exceeded. As a result, a surveying accuracy of about 1:500 will allow gravity corrections for elevation to within 0.1 milligal. This value approaches the current limit of feasible data interpretation.

Standard earth gravity survey techniques utilize station spacings of various dimensions from 100 ft or less up to many miles. However, measurements or computations of vertical deflections are not as well defined in literature surveyed to date. Where specific data for the deflection of the local vertical have been of interest, the procedure for making measurements has involved both precision surface surveys and celestial position measurements. The survey accuracies, from the standpoint of fine grain data needed for navigation, are appreciably greater than those utilized to define the earth's geoid. In any event, the smallest "area" utilized in gravity survey data analysis (Ref. 155) has been a 1° square. If the same requirement is utilized for the lunar surveys, a position-fix accuracy of 0.5° or better is required to position the measurement in the central region of the area; this is equivalent to errors of about 0.11° in both latitude and longitude. The required location accuracy, relative to the central fixed point, of the survey measurements is 2 m (Ref. 107).

4.1.3 Seismic Surveys

Seismic velocities between 90 and 6100 m/sec are encountered on earth for surface dust and granite, respectively, and it is expected that lunar materials will be within that range. Except for surface materials, it is believed that the velocities will range from 200 to 5500 m/sec for lunar materials.

A preliminary estimate of a seismic survey installation would place the geophones approximately 1 km from the shot hole. The geophones would then be implanted at approximately 30-m intervals on a common radial line from the shot hole.

Position accuracy requirements imposed by the seismic survey system can only be estimated at the present time, and these requirements may change appreciably as soon as initial data have been evaluated. For the present time, it has been assumed that the distance between the shot hole and the first geophone will be 1000 ± 2 m. The geophone spacings would then be held to ± 0. 3 m. This places rather stringent requirements on the LRV systems, but it may be feasible to use laser ranging and precut cable lengths to relieve the navigation system of the requirements. After an initial measurement has been accomplished on the lunar surface. it will obviously be easier to specify requirements for a seismic survey. Hence, it may be more advantageous to specify maximum sensitivity and resolution for the initial equipment and reduce the location accuracy requirement (i. e. , seismic instrumentation size and weight will not be traded off against navigation and survey instruments).

4. 1. 4 Magnetic Surveys

Magnetic surveys are performed to measure both the intensity and direction of a magnetic field. On the earth, measurement points may be spaced at grid intervals of 25 to 50 km (Ref. 156) for standard surveys and at more frequent intervals for the detection and location of magnetic material deposits. Locational accuracies required for the standard survey would be from 4. 4 to 9 km in each coordinate to place the measurement point in the central portion of each area. Better accuracies may be required for the location and mapping of magnetic anomalies, but the effects of and the requirements imposed by the assumed absence of a lunar magnetic field have not been available in literature surveyed to date.

Insofar as the lunar magnetic field is concerned, it is believed that it will be about 0. 001 of that on the earth. As a result, modifications of earth magnetic field equipment will probably be inadequate for the lunar surveys and new developments will be required. Some probes have indicated that a dipole characteristic does not exist; due to probe velocities and the low frequency response of the magnetometers, it is possible that the dipole field would not have been detected.

Magnetic field measurements include both the horizontal and vertical components of the fields. Thus, a requirement for a horizontal reference exists. This requirement in addition to location data might be fulfilled by navigation system components. The use of navigation components should be

considered even though the accuracy requirements for magnetic survey pur-
poses are not too demanding. In the event that better accuracy or resolution
is required after an initial coarse survey, the requirements will probably
be less than those imposed by other tasks.

4.1.5 Path Retrace

The lunar surface mission traverses include requirements for path
retrace during emergencies, emplacement of scientific instruments, and
recovery of scientific instruments. During an emergency, the path re-
trace operation assures a pre-established, safe route back to the exploration
base point (such as the LEM). The requirement imposed on the navigation
system is that it shall provide the guidance data necessary to maintain the
vehicle on the safe route and to position the vehicle within either optical or
RF beacon homing range of the base point.

To minimize the time required to retrace the outgoing path, some
form of path marking, a combination of passive optical beacons and im-
prints of the prior track, might be required. The nature of the lunar sur-
face, the illumination conditions, and astronaut time allowed for the function
of hazard detection will establish the accuracy required for the return path.
That is, the path retrace accuracy requirements are relaxed to a relatively
wide (approximately 6-km) safe return channel. (1) if the lunar surface is
relatively flat (permitting a long line of sight) and relatively free of hazards
such that each may be easily detected, (2) if the illumination is such that a
hazard can be easily distinguished at either side of the vehicle, and (3) if
the astronaut is free to observe and record vehicle hazards continually.
However, a limitation on any of the above three assumptions can reduce
the safe return channel to the width of the outgoing vehicle path and place
an extremely restrictive accuracy requirement on the navigation system.

Path retrace to implant or recover scientific instruments will re-
quire precision at the specific points of interest rather than the 100% re-
trace of the emergency mode. It is planned that passive optical marking
will be provided at each point to obtain a minimum homing range of 1 km.
In addition to the navigation data derived by the components of the three
navigation systems used in this study, relative position fixes using terrain
features and/or path markers (placed on the outbound leg) will aid in the
return to the desired points. This procedure can be implemented using the
TV system and/or a periscopic theodolite for remote and/or on-board po-
sition measurements relative to identifiable features. (Results of a pre-
liminary study of reflective materials suitable for use in the lunar environ-
ment on markers are presented in Section 6.2.3.)

4.1.6 Selenodetic Mapping

Predictions of lunar map accuracies have been obtained from a number of sources (Ref. 119) that include MSC, ACIC, AFCRL and Army Map Service. Nominal values for lunar landmarks relative to the absolute selenocentric coordinate system are as follows:

Time Period	Departure from 0° Long 0° Lat (Deg)	Horiz 3 σ (m)	Vert 3 σ (m)
1965	0	750	2400
	30	2000	2700
	60	3900	2700
Predicted (Lunar Orbiter Successful)	0	675	1800
	30	1050	1700
	60	2550	1700
Predicted (After Manned Lunar Survey)	0	37 to 700	150 to 400
	30	375 to 700	150 to 400
	60	375 to 700	150 to 400

It is obvious that a navigation and/or surveying system or technique must be more accurate than the maps in order to update them. However, one consideration regarding the predicted map accuracies after a manned lunar survey concerns the technique used in deriving the corrections. The 125 (1σ) meter horizontal accuracy is close to the predicted accuracy (100 m) attainable with DSIF and MSFN tracking of a cooperative target on the lunar surface, and this may be the technique that was considered when the prediction was made.

If it is assumed that lunar orbiter is successful and that the succeeding surface missions originate from the Kepler-Encke region during the first decade of lunar surface exploration, some preliminary accuracy requirement estimates can be made. Since the area will be in the vicinity of 45° from $0^\circ/0^\circ$, a 3-σ map error of 1.5 km may prevail.

A 375-m (3-σ value to be consistent with the remainder of the study) error in either latitude of longitude can be converted to a local vertical error of 44 arc sec. If the error components are equal on orthogonal axes, the errors would be 31 arc sec. Some of the navigation system components are sufficiently accurate to meet the instrument requirements, but errors in local vertical and ephemeris data are such that surface survey techniques may not provide sufficient accuracy during the first decade of lunar exploration.

4.1.7 LEM/T to LEM Traverse

The initial lunar surface navigation requirement is encountered when the LRV is maneuvered from the LEM/T landing site to the LEM. To accomplish this task, one or more of a combination of the following conditions must prevail:

1. The LRV is within optical (TV) homing range of the LEM by remote control.

2. The LRV is within RFDF homing range of the LEM, and this technique can be used to reduce the range to the optical (TV) homing range by remote control.

3. The LRV has an earth-dependent capability of measuring its surface position and heading using lunar vertical and celestial references (surface features may be useful for direction and location via TV); from that and destination data, it is capable of being remotely operated to bring it within either RFDF or optical homing range. (Landing of an LRV or supplies on the far side of the moon is not being considered at this time.)

In the event that the third condition prevails, the position-fix components must be operable either automatically or by remote control in order to derive data for transmission to earth-based stations for position and heading computation. The mechanization of a complete navigation system is not important at this point, but instantaneous heading, distance traveled or velocity, altitude, and TV data must also be transmitted to implement the remote control of the vehicle.

Homing range calculations have been based on the assumption that elevated antennas on the LEM or LEM site and the LRV would provide a 10-km RFDF homing range on a spherical surface (20 arc min great circle path). Investigations of propagation conditions on the moon have indicated that knowledge of conductivity and dielectric constant are such that propagation beyond line of sight is still questionable. Therefore, it is desirable to investigate lunar surface characteristics to determine the probability of encountering an obstruction on any 10-km range that would interfere with RF propagation. In the event that the probability is low, then it is desirable to determine a 3-σ limit range for the RFDF homing capability (preferably independent of earth support for safety and backup). The position-fix accuracy can then be set at the 3-σ limit of the extended homing range, or transmitter power can be increased.

4.1.8 Typical Navigation Requirements

For each leg of the previously discussed six missions (Section 2), a general navigation accuracy requirement (hereafter referred to as terminal requirement) may be established. The navigation system, whatever its makeup, must provide this degree of accuracy to successfully accomplish the mission leg.

There are two types of terminal requirements which should be differentiated. The first type is a requirement (of which Mission 1, Leg A is an example) to arrive at a particular destination. For this type of leg, the terminal navigation requirement is computed from

$$(TR)^2 = R_D^2 - E_{DR}^2 \qquad (4\text{-}1)$$

where

TR = terminal navigation requirement [km]

R_D = detection radius [km]

E_{DR} = uncertainty in knowledge of position of the destination [km].

The detection radius is defined as that radius at which contact (whether visual, RF, or other) can be achieved between vehicle and destination.

The second type of requirement is set, not by any particular destination, but by the wishes of the scientific experimenters. Thus, it may be desired to map the location of a surface feature or data point to a given accuracy. This accuracy then becomes the terminal requirement for the mapping leg.

Table 4-1 summarizes the terminal requirements for the six typical missions of Section 2.

4. 2 INTERFACES WITH OTHER VEHICLE SYSTEMS

The selection of a functional group of components to meet vehicle navigation requirements may depend upon factors other than those associated with navigation. In fact, navigation requirements may have to change during the final mission planning and vehicle system optimization phases. It is the purpose of this section to outline areas in which navigation components may either affect or be affected by other vehicle systems or their functional components.

4. 2. 1 Communications System

The areas include:

1. Navigation data formatting for transmission to earth and/or lunar bases

2. Remote command control of navigation sensors and operating modes

3. RF tracking of earth to provide an azimuth reference

4. Pointing and stabilization of a nontracking type of communications antenna

5. RF direction finding for extending homing range to LEM or lunar base.

4.2..2 Vehicle Mobility and Remote Control Systems

The areas include:

1. Directional reference for use in control of vehicle heading

2. Vehicle attitude and acceleration sensors for vehicle maneuver limiting and other safety purposes

3. Pointing and dynamic stabilization of TV camera

4. Use of TV camera to aid in star acquisition and also as a backup for celestial tracker

5. Drive wheel odometers or tachometers.

4.2.3 Scientific Mission Instrumentation System

The areas include:

1. Precise measurement of static surface positions in selenodetic coordinates

2. Intermittent or continuous measurement of surface position during traverse on scientific surveys

3. Reference coordinate system for pointing of scientific instruments

4. Intermittent or continuous measurement of sun position relative to vehicle or other reference coordinate system

5. Dynamic stabilization of scientific sensors during traverse

6. Optical or laser system measurement of ranges and angles for navigation relative to either man-made or natural surface objects.

TABLE 4-1

TERMINAL REQUIREMENTS*

Mission	Leg	Range (km)	Terrain Type	Destination	R_D (km)	E_{DR} (km)	TR (km)
1	A	8	SM	LEM	2.5(1a)	1.0(4)	2.29
	B	8	SM	LEM Shelter	2.5(1a)	1.0(4)	2.29
	C	8	SM	Landing Site			0.4(5)
	D	8	SM	Sel Location			0.45(6)
	E	8	SM	Rel Location			0.08(7)
	F	8	SM	LEM	2.5(1a)	1.0(4)	2.29
2	A	8	SM	LEM	4.0(1b)	1.0(4)	3.87
	B	8	SM	LEM Truck	4.0(1b)	1.0(4)	3.87
	C	18	SM	Rel Location			0.18(7)
	D	18	RM	Sel Location			0.45(6)
	E	18	RM	Site Location			0.4(5)
	F	18	RM	Equip Location	1.5(2)	0.45(6)	1.43
	G	18	SM	LEM	4.0(1b)		
3	A	83	SM	Surface Feature	3.0(3a)	1.0(8)	2.83
	B	62	RM	Sel Location			0.45(6)
	C	69	RM	Rel Location			0.7(7)
	D	50	SM	LEM	4.0(1b)	0.45(6)	3.97
4	A	8	SM	LEM	4.0(1b)	1.0(4)	3.87
	B	8	SM	LEM Truck	4.0(1b)	1.0(4)	3.87
	C	100	SM	Sel Location			0.45(6)
	D	50	GH	Sel Location			0.45(6)
	E	50	RH	Sel Location			0.45(6)
	F	50	SM	LEM	4.0(1b)	1.0(4)	3.87
5	A	100	SM	Surface Feature	2.5(3b)	1.0(10)	2.29
	B	50	RM	Equip Location	1.5(2)	0.45(6)	1.43
	C	50	Unknown	Sel Location			0.45(9)
	D	100	SM	LEM	4.0(1b)	1.0(4)	3.87

6	A	100	SM	Sel Location			0.45(6)
	B	50	RH	Sel Location			0.45(6)
	C	50	RH	Surface Feature	2.5(3b)	1.0(10)	2.29
	D	100	SM	LEM	4.0(1b)	1.0(4)	3.87

*Explanations of values in last three columns are contained in the following notes: Numbers in parentheses following parameter value refer to note number.

Terrain Types:
M = Smooth Mare; RM = Rough Mare; GH = Gentle Highlands;
RH = Rough Highland
Destination Types:
Rel = Relative; Sel = Selenographic

Notes:

1. (a) Viewing height of 2 m on one vehicle and 4 m on the other (LEM max height = 7 m) results in line of sight (LOS) of 6 km for smooth moon. This is reduced to about 2.5 km for smooth maria where terrain undulation amplitude is assumed as 3 m.

   (b) Viewing height of 4 m on each vehicle (LEM = 7 m, LEM/T = 3.3 m, LRV = 4 m) gives LOS of 7 km for smooth moon. This is reduced to about 4.0 km for smooth maria where terrain undulation amplitude is assumed as 3 m.

2. Viewing height of 4 m on vehicle and 4 or 5 m on equipment (height of optical marker for example) gives LOS of 7 km on smooth moon. This is reduced to about 1.5 km on rough maria where terrain undulation amplitude is assumed as 4 m.

3. (a) Viewing height of 4 m on vehicle and 10 m as height of feature gives LOS of 9 km on smooth moon. This is reduced to about 6 km over smooth maria where terrain undulation is assumed as 3 m in amplitude. This 6-km figure has been halved to 3 km to allow for recognition of the feature as distinct from adjacent and similar features.

   (b) From 3(a) the LOS was 9.0 km for smooth moon. Approaching rough maria this is reduced to about 5 km which has been reduced further to 2.5 km for feature recognition as in 3(a).

4. Bendix estimate based upon NASA data (Ref. 125 and 126).

5. Per location error as stated in Bendix IDM "Primary Mission Definition - Apollo - LEM Landing Surface Requirements" (63-261-778, p. 3).

6. Required absolute accuracy for scientific experiments (Ref. 107).

7. 1% of range traveled.

8. MSC mapping accuracy estimate at 40° longitude with improvement because of later operational date (Ref. 119).

9. Assumed comparable to (6) even though for far-side operation.

10. Equal to map accuracy at 60° (2550 m) but reduced for later operational date.

SECTION 5

LUNAR PHYSICAL AND ENVIRONMENTAL PARAMETERS

Many physical and environmental parameters of the moon are of importance to lunar surface navigation studies. Among them are gravity, illumination, surface photometric characteristics, surface electrical conductivity, dielectric constant of surface materials, the surface physical relief characteristics, temperature, vacuum, and radiation. The parameters of particular interest here are those that influence navigation accuracies such as deflections of the vertical and those that affect a homing range capability such as either RF or optical/visual lines of sight.

5.1 GRAVITY AND DEFLECTIONS OF VERTICAL

Most methods of navigation depend upon the use of the direction of the gravity vector as a reference axis for position measurements. This is especially true of systems that are independent of other support facilities such as LORAN, DSIF, etc. The primary exception would be the piloting type of navigation where readily indentifiable map landmarks would be used to establish and follow a desired route to a particular destination.

The magnitude of the gravity vector is important to the navigation system and the scientific mission planners. On the moon where gravitational acceleration is about 1/6 that of the earth, local vertical sensors must have better sensitivity and repeatability to provide angular accuracies comparable to those attained on the earth. The scientific mission planner is interested in accurate measurements of lunar gravity, because it is believed that these measurements, as compared to other parameter measurements, will provide the maximum information on the moon's subsurface structure. However, this latter requirement is important to navigation only from the standpoint of the location accuracy requirements imposed on the navigation system.

5.1.1 Deflections of Lunar Vertical

Some insight into the behavior of the deflections of lunar local vertical may be gained through comparisons with the deflections of earth's vertical. This is desirable because navigation and mapping accuracies may be affected and these in turn may affect the safety of astronauts on surface vehicle missions. Differences and similarities must be recognized and considered in establishing parameter range for concept analyses. They must also be considered for possible mechanization of vehicle systems.

The gross behavior of the vertical is determined of course by the size and shape of the moon (mass magnitude and distribution). Since the lunar radius is only 0.273 times that of the earth, one minute of arc at the lunar center subtends only about 1/4 nautical mile (n. mi) rather than 1.0 n. mi as on the earth. Thus, for vehicles with equal velocities and neglecting rotational rates the vertical direction on the moon will change at 4 times the rate of the earth vertical.

Since the local vertical is made up of two components of acceleration, mass attraction and centripetal, the vertical does not pass through the mass center of the earth or moon, but is deflected slightly toward the equatorial plane. For the earth, this deflection has a maximum value of 11.5 min of arc at a latitude of 45° (Ref. 111) which corresponds to a positional error of 11.5 n. mi or 21.3 km. This value is computed from the approximation

$$\delta = e \sin 2\theta$$

where

$$\theta = \text{latitude}$$

$$e = \text{ellipticity} = \frac{1}{297.0} \text{ for earth}$$

$$e = 1 - \frac{R_{pole}}{R_{equator}}$$

For the moon, the values shown in Figure 5-1 are given by Ref. 112.

c = 1737.49 km

b = 1738.21 km

a = 1738.57 km

Toward
Earth
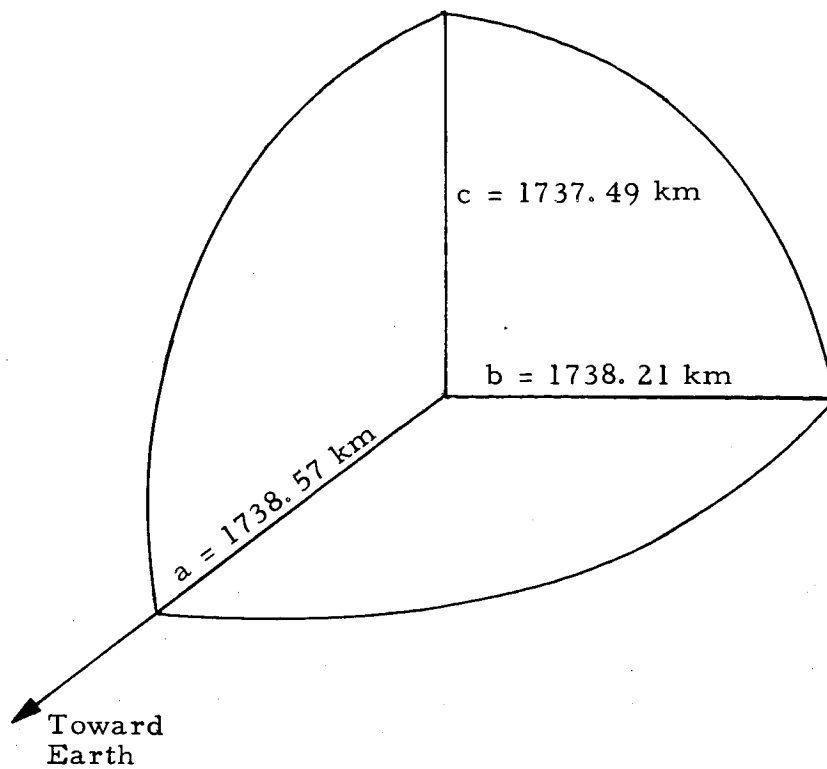
Figure 5-1 Definition of Lunar Radii

Thus, the maximum deviation for the moon would be approximately:

$$e \approx 1 - \frac{1737.5}{1738.2} = 1 - 0.9996 = 0.0004$$

$$\delta \approx e \sin 2\theta = 0.0004 \text{ rad at } 45° \text{ latitude}$$

$$= 0.0229°$$

$$= 1.37 \text{ min of arc}$$

Thus, the deflection is 1.37/11.5 = 0.119 ≈ an order of magnitude less
on the moon as compared to earth. Since this is so low, it is worthwhile
to compare it with the magnitude of gravitational anomalies which might
be expected on the moon. On the earth, the gravity anomalies may reach
1.1 min (Ref. 4), of arc, although Ref. 113 states that 30 arc sec is the
upper limit in the US.   The value of 1.1 min is still an order of magnitude
less than the 11.5 min of arc from centripetal acceleration. However,
since the deflection because of centripetal acceleration is only on the order
of 1 min of arc on the moon, the effect of anomalies may be actually
greater than the centripetal acceleration effect. The mission profile
should be kept in mind, however, when considering the anomalistic

maximums expected. Since the earlier and intermediate missions will undoubtedly be located in primarily marial regions, the anomalies to be experienced are probably not the maximums. It is most likely that the maximum anomalies, assuming some degree of homogeneity of the sub-surface volume, will occur in the highland regions or perhaps at the junction of marial and highland regions. The maximum elevation of a visible feature has been estimated as about 8.8 km, this being from the floor of Newton to a peak on its wall (Ref. 114). This compares approximately with the highest elevations on the earth. Of course it is not the elevation alone, but also the total mass of an anomaly-generating feature, that are the determinants of the anomaly magnitude. Yet, it appears conservative to assume that the anomalies are caused by features of the same order magnitude in size. The mass involved might be considerably less, since the moon's mean density is only 0.6043 times that of the earth (Ref. 114).

To get a feeling for the effect (which results from equal-sized features) on the local verticals of the two bodies, a rather simplified case has been worked out. Assume a granite pyramid on earth with dimensions of 9.2 km on a side and 9.2 km in altitude. This feature would have a mass of 5.26×10^{17} gm, producing a deflection on earth at the base of about 0.58 min of arc, about half the expected earth maximum. The point at the base was selected for the computation, since this represents a reasonable surface vehicle location. This same size feature on the moon might have a mass of $0.6043 (5.2 \times 10^{17}) = 3.18 \times 10^{17}$ gm and would result in a gravitational anamoly of 2.14 minutes of arc. The ratio of increase is then $2.14/0.58 = 3.7$. This is significantly below the 6:1 predicted by Ref. 4 (because of the density difference). For flat-appearing marial areas, the maximum anomaly should be below this value, since a pyramid of this size would be visible from earth. This assumes of course no extreme departures in homogeneity exist below the surface.

For the MOLAB mission, in which the largest crater approached closely is Maestlin or Encke G, both being approximately 9.2 km in diameter but of relatively low height (500 m), the anomalies experienced might be as much as an order of magnitude less than 2.14 min, or on the order of 20 sec of arc ($\cong 0.3$ min). For other missions involving approaches to large features, the anomalies might exceed 2 min.

Without any correction for gravity anomalies, the navigation system will exhibit an error in position as a result of the anomaly. A vertical indicator based on this erroneous vertical will then exhibit a total error of

$$\epsilon_T = \left[\epsilon_A^2 + \epsilon_I^2 \right]^{1/2}$$

where

ϵ_A = gravitational anomaly (min)

ϵ_I = vertical instrument error (min)

Using the figure mentioned above, the following expressions apply:

1. For marial areas:

$$\epsilon_T = \left[(0.3)^2 + \epsilon_I^2 \right]^{1/2} \text{ min}$$

2. For highland areas or close approach to earth-visible features:

$$\epsilon_T = \left[(2)^2 + \epsilon_I^2 \right]^{1/2} \text{ min}$$

The sensitivity of position error to vertical error for the moon is approximately 8.43 m/arc-sec or roughly 0.5 km/arc-min for a lunar radius of 1738 km.

Publications by Messrs. Heiskanen, [108] Kaula [109] and Bowditch, [116] were reviewed to obtain more information relative to the nature of the deflections of earth verticals. This was done in an attempt to find vertical deflection contour maps, because it is believed that the gradient is an important factor for a lunar surface system where position is determined by star sightings. In addition, the US Coast and Geodetic Survey was contacted; the data received from them included plots of the gravity contours along a path between Canaveral and a downrange target in the Atlantic Missile Range and USGS Special Publication No. 229 on deflections of vertical in the US.

Maximum vertical deflections in the US were found to be approximately 30 arc sec and they are generally found in the vicinity of mountain ranges, especially where there is a land-water boundary. However, data in the form of contour maps were not found, although it was learned that a

gradient of 1 arc min in 30 miles (30 arc min) did exist in the vicinity of an island. This has been tentatively accepted as a maximum condition.

Ref. 109 states that, based upon present knowledge and parameter estimates, lunar vertical deflections could be expected to be from 12 to 36 times as large as those on the earth (5.7 arc sec rms). This results in deflections of 70 to 200 arc sec (rms) on the moon. The ratio between peak and rms values published for the earth is approximately 10. If this is applied to the lunar estimates, peak values of 700 to 2000 arc sec might be encountered. This would be a surface position error of 6 to 17 km and may indicate the need for an extended homing range capability that would help prevent ambiguities in surface position and reduce the requirements imposed on navigation sensors.

5.2   LUNAR SURFACE AND ITS PHOTOMETRIC CHARACTERISTICS

5.2.1   Relief Characteristics

At present, the small-scale relief characteristics that will be encountered in a lunar mare are not accurately defined. By extrapolating from observed large-scale features and using Ranger 7 data, the basic mare structure is defined as a gently undulating flow plain with a shallow dust layer of unknown bearing strength. The undulating surface contains, as a dominant feature, craters (both observed, which range from 1 meter to kilometers in diameter, and unobserved, presumably of even smaller size). Larger craters appear to contain central peaks, and some contain blocks or ejecta from distant impacts. Small craters occur both in "soft" and "hard" forms, which means some have smooth rounded edges with very gradual slopes, while others are sharp edged like the large impact craters. Crater walls are very small in relation to their diameter, and outside slopes are relatively shallow, in the range 0° to 30°. Inner slopes may be somewhat steeper, ranging from 10° to 45°. Because of the moon's radius of curvature and the small crater height-to-diameter ratio, only the craters of very pronounced type will stand out above the surrounding terrain. A second feature of the mare is the dome. This smooth symmetrical protuberance occurs only in maria, often has a central crater, and has more gradual slopes than craters, without any discontinuities such as the crater lip. Domes tend to be large, some being tens of kilometers in diameter, but with gradual slopes usually not exceeding 20°. Other protuberance features are the blocks which are ejected by impact

at distant points. The one observed in the Ranger 7 data has dimensions of 90 m, and slopes in excess of 23°. These blocks may be quite irregular in shape and have slopes up to 90°, with dimensions of less than 1 m to 300 m. They occur in association with craters.

Three large-scale features which may be encountered are ridges, rays, and rilles or faults. The latter two are the most difficult types of terrain to negotiate in the lunar maria and may be purposely avoided for this reason. The wrinkle ridges present in the maria are long ridges which wind across the surface. They have slopes ranging up to 30°, and can be hundreds of kilometers in length. These features will appear as a gradual slope in the terrain with no sharp discontinuities. They are not uncommon in large-scale photographs, but small-scale ridges were not present in much of the Ranger data. Rays are composed of large numbers of small craters which are related to the more massive craters. They exhibit unusual photometric and polarimetric properties, are the most reflective feature on the lunar surface, and have over-all dimensions of kilometers. Rilles and faults are large-scale features observed primarily around the boundaries of the dark circular maria. Rilles are valley formations from 0.5 to 4.0 km in width, 30 to 150 km in length, and 100 to 600 m in depth with bottoms somewhat depressed below mean mare level. Some rilles have small nonmeteoritic craters along the length. Again because of their large width-to-depth ratio, slopes are shallow. Faults are step-like formations, exhibiting the largest slopes measured on the lunar mare, up to 45° to 60°. They are 15 to 150 km in length, and Ranger data did not indicate their presence in small scale on the maria.

The actual appearance of the surface layer can only be inferred from large-scale observations. It is believed to be smooth in the maria down to a scale of centimeters, and fairly uniform over large areas. The data obtained by Ranger 7 show a basic surface material that is uniform and smooth on a 40-cm scale, but smaller resolution features can still only be inferred.

5.2.2 Photometric Characteristics

The appearance of a lunar landscape depends strongly on the photometric characteristics of the environment. These characteristics include the various illuminating sources, their illuminance levels, their time variation, collimation and color, the albedo of the surface, its

directional reflectance, color, polarization properties, texture, the shadow-casting features, seeing conditions, and contrast range. These can be divided into three categories: illumination, surface optical properties, and environmental conditions.

Illumination is produced by the sun, the earth, the stellar-planetary background, and by surface-scattering by nearby terrain features. The primary source during the lunar day is the sun, the secondary source being earth-reflected sunlight (earthlight). During the lunar night, the primary source is earthlight; the secondary source is the stellar-planetary background. The illuminance values produced at the moon's surface by these sources are listed in Table 5-1. Assuming the surface reflectance of a mare to be 0.073 phi (where phi is the directional reflectance factor, called the photometric function), the resultant surface luminances are also given in Table 5-1, in foot-lamberts (ft-L). Because of the low albedo (0.073), the surface luminances will be smaller than those for a terrestrial scene under a clear sky. The lunar terrain features will be similar in brightness to a rocky earth terrain on an overcast day. The earthlight (lunar night) luminances are over 10 times brighter than the luminances of a terrestrial landscape under a full moon. Thus, a lunar landscape under earthlight illumination will have luminances similar to terrestrial twilight. In the absence of sunlight and earthlight (in shadowed region or on far side of moon) lunar night luminances are 10^{-6} ft-L, too faint to use unaided vision.

The sources of illumination vary because of positional changes of the bodies involved. The sun moves from horizon to horizon in about 14 days, which causes the illumination incident on a horizontal unit area of the moon's surface to vary as the cosine of the sun's zenith angle. If the lunar surface were composed primarily of diffuse materials as is the earth's surface, this would not cause a variation in the apparent luminance of the surface. But since the reflectance of the lunar surface is strongly direction-dependent, incident radiation with a back-scattering peak toward the source of the luminance of an area, viewed from the same direction, will change with time as the sun moves across the sky. This is a complicated variation because of the complex nature of the lunar directional reflectance pattern (photometric function), but it amounts to this: the apparent luminance of a lunar surface element viewed from the same position during the lunar day will vary in brightness as the sun moves across the sky, having a peak luminance when the sun comes closest to

TABLE 5-1

ILLUMINANCE VALUES AT MOON'S SURFACE

Source	Illuminance (lumen/ft^2)	Surface Luminance (ft-L)	Variation for Horizontal Surface of Unit Area	Collimation	Color Temperature
Sun	1.3×10^{4}	$960\ \phi$	varies with time	$1/2^{\circ}$	$\sim6000^{\circ}$
Maximum Earth-light (lunar day)	6.7×10^{-1}	$0.05\ \phi$	varies with time lunar location	$\sim2^{\circ}$	$\sim5500^{\circ}$
Maximum Earth-light (lunar night)	1.33	$0.096\ \phi$	varies with time lunar location	$\sim2^{\circ}$	
Maximum Planetary	9.2×10^{-6}	$6.7 \times 10^{-7}\ \phi$	varies with time		$\sim5500^{\circ}$
Average Planetary	1.9×10^{-6}	$1.4 \times 10^{-7}\ \phi$		diffuse	
Starlight	2.3×10^{-5}	$1.66 \times 10^{-6}\ \phi$	constant		$\sim6000^{\circ}$

the observer's line of sight. Conversely, if the observer is moving rela-
tive to a given lunar surface element with the sun essentially motionless
(1/2 degree per hour), the apparent luminance of that element will vary
with the view angle, peak luminance occurring when the observer's line
of sight comes closest to the sun direction (factor of 10).

The variation of earthlight-produced luminances is more complicated.
The variation due to observer motion is the same as for sunlight, with a
maximum variation of about 10, and a peak value when the direction if in-
cidence of the earthlight is coincident with the line of sight. But the earth
varies only slightly in position, appearing to stand almost motionless in
the sky, its zenith angle dependent on the observer's selenographic latitude
and longitude. However, the intensity of the earthlight varies with time,
corresponding to the phase changes as the earth goes from new phase to
full earth, and then back. This intensity variation is monotonic, reaching
a peak at lunar local midnight and approaching zero at lunar local noon.
This is fortunate in that the minimum phases of earthlight occur during
the lunar day, while the maximum phases are available during the lunar
night. An approximate formula expressing the earthlight illuminance on
a horizontal surface of unit area is

$$E_e = 1.3 \cos \lambda \, \cos \beta \, \frac{|g'|}{\pi} \text{ lumens/ft}^2$$

$$g' = \begin{cases} g + \lambda_W \\ g - \lambda_E \end{cases}$$

where

λ = selenographic longitude

β = selenographic latitude

g = lunar phase angle.

Due to the earth zenith angle being greater as the observer's lati-
tude is increased, there is a spatial dependence of earthlight. For an
observer in the western (lunar) hemisphere, the sun sets later than for
an observer at the center of the visible lunar disc. Hence, the earthlight
just at sunset that is incident on a horizontal unit area surface will be

higher at the western position, since the earth will be closer to full phase. Further, the earthlight just prior to sunrise will be lower than at the central position, since the earth is closer to new phase. The converse is true for an observer in the eastern hemisphere, and the effect is a function of lunar latitude.

A summary of approximate earthlight maxima and minima are given in Table 5-2.

In general, the farther west in longitude the observer is, the lower peak earthlight incident on a horizontal surface will be, and the lower the minimum earthlight will be. This applies to the eastern hemisphere as well, but here minimum earth light occurs at sunset rather than at sunrise.

TABLE 5-2

EARTHLIGHT MAXIMA AND MINIMA SUMMARY

Longitude West	Minimum Illuminance (lu/ft^2)	Maximum Illuminance (lu/ft^2)
0°	0.65	1.33
30°	0.28	1.13
45°	0.18	0.93

The collimation of the various sources is quite different. The sunlight can be considered collimated to about $1/2^{\circ}$ which is the same as at the earth's surface. This well-collimated source produces fairly sharp shadows and gives the lunar photometric function its sharply peaked form. Earthlight is collimated to 2° or more at best, due to the relatively large angular subtense of the earth as viewed from the lunar surface. This source produces fairly well defined shadows (comparable to those produced by moonlight on the earth) with larger penumbral regions than sun-produced shadows. The photometric response of the lunar surface under earthlight illumination has never been measured; it should be quite similar to that produced by sunlight, but with the curve broadened slightly.

Starlight and planetary light are the only sources of illumination which are always present, and vary only slightly (about ±25%), but are so weak that unaided human vision will not be able to utilize them. Starlight is a completely diffuse source, however, distributed over the entire visible hemisphere. This will give the lunar surface a completely different photometric response, making it appear as a diffusely reflecting surface rather than a strongly back-scattering surface as it appears under sunlight and earthlight. There will be no shadowing under starlight, except the cave-like structures which are cut off from all but a tiny part of the sky hemisphere.

The second set of factors involved in the photometric characteristics of a lunar scene is the surface reflectance properties. The normal albedo or reflecting power of the lunar surface is everywhere quite low. The brightest features, the rays, have albedos approaching 0.30 to 0.40 (30 to 40% reflecting), but the maria, the most likely landing areas, are quite dark, average maria albedo being 0.07, with a range from 0.055 to 0.10 (5 1/2 to 10%). Thus, for the same solar illuminance as on the earth, the lunar scene luminances will be several times lower (typical earth scene albedos are in the 10 to 40% range).

The most unusual photometric characteristic of the lunar surface is its photometric function, or directional reflectance. Although almost all terrestrial surfaces are fairly diffuse reflectors (Lambertian), the entire lunar surface exhibits a strong optical back-scattering reflectance with little or no diffuse component. This strongly back-scattering surface property has been demonstrated to belong only to very porous materials with interconnected cavities and a very high void volume. Knowing this photometric function allows one to **predict** certain characteristics of the lunar scene. The photometric function was derived from very poor resolution photos, but extrapolation to centimeter resolution is felt to be quite valid in view of radar scattering studies and the recent Ranger photographic data, both of which indicate 20 surface structure elements of 10-cm size or larger are involved in the photometric response—i.e., the photometric surface is a microstructure, smaller than the centimeter scale. The predictions which can be made are: peak surface luminances occur when the observer is viewing almost along the source-to-surface line; minimum surface luminances occur when the observer's line of sight approaches 180° from the source-to-surface line; variations in view angle or in source angle can produce surface luminance variations of at least 10:1. All this

5-12

is true for partially collimated light sources such as the sun, the earth, or artificial sources. For a completely diffuse light such as starlight, a back-scattering surface will appear to be quite Lambertian so that the same surface viewed from the same angles may have different relative luminances under starlight than they did under sunlight or earthlight.

As for surface colors, only large-scale data are available so that small local color concentrations may exist without appearing on present photographs. In general, the maria are a reddish brown in color, although their very low albedo will tend to neutralize any color present. Some younger continental features seem to have greenish hues, but the maria are all red-hued. In addition to natural colors, certain regions of the lunar surface luminesce so that very strong surface color in red to green regions of the spectrum may occur locally.

The third factor in photometric characteristics comprises general features such as contrast ranges, seeing effects, and shadowing. As the lunar atmosphere is known to be extremely tenuous, there should be no seeing effects comparable to terrestrial effects, even though surface temperatures will be much higher. There is some speculation about an electron-ion cloud in the meter above the surface, which might cause some optical effect, but this is not proved. Shadows are a problem, especially during the pre-sunset and post-sunrise periods, just before and after terminator passage. Here the sun's zenith angle (Z) is approaching 90°, and the shadow lengths are functions of tan Z. Shadows of distant large-scale features can envelope a region of hundreds of square kilometers. The shadowing of earthlight is less serious in that for lunar longitudes within 45°E or W, the earth's zenith angle is less than 45°, so the shadow's length will be less than the shadow-casting object's height. However, one drawback is that the shadowed areas will be always shadowed, since the earth's position is fairly constant in the sky, changing by only some $\pm 8^{\circ}$. Thus, an earth-shadowed area during the lunar night must either be viewed with a special sensor or artificially illuminated.

The contrast range present in a lunar scene will be quite similar to that of a terrestrial scene, although for different reasons. The lunar scene luminance differences are produced by the photometric function, with albedo fairly uniform, while a terrestrial scene has different luminances due to albedo differences, with fairly uniform directional properties. The one additional factor in the lunar scene is the presence of extremely

dark shadows. Due to the lack of atmospheric scattering, the ratio of unshadowed-to-shadowed surface luminances is about equal to the ratio of the primary-to-secondary sources of illuminance. During the lunar day when the sun is primary and the earth secondary, their ratio is about 10^4. Thus, shadows will be some 10^4 times dimmer than sunlit areas. This will be partially reduced by the scattering of sunlight by nearby sunlit surface elements. The magnitude of this "surface scattered" illuminance depends on scene geometry and thus cannot be generally estimated, but it will only reduce the ratio by perhaps 10. Thus, shadows will be some 1000 to 10,000 times darker than sunlit areas, requiring sensors with extremely large dynamic range or artificial illumination. It should be kept in mind that a daytime shadow is an earth-illuminated surface, so that an observer who could dark-acclimate his eyes could easily see in such a zone. During the lunar night when earthlight is primary and star plus planetary light is secondary, their ratio is coincidentally also about 10^4. Therefore, contrast ranges, shadow contrast, and relative scene luminances will be about the same during the lunar night as during the lunar day. The only difference will be the lower light levels and the diffuse, very weak character of the secondary source (starlight).

5.2.3 Feature Recognition and Definition

The recognition and identification of features for mapping or guidance purposes during remote control operations require the use of some type of stereo sensor system. Monoptic TV presentations have been demonstrated to have insufficient information content to uniquely define or identify surface characteristics resembling the lunar case. Under collimated light, with surface photometric properties matching the lunar properties, monoptic TV cannot resolve 90° differences in slopes with complicated non-real-time photometric procedures. Although the complex photometric nature of the lunar surface will render stereo representations somewhat more difficult to interpret, stereo is capable of defining lunar scene structure.

Certain mapping aids such as landmarks may be required. If photometric methods are to be used in addition to the standard photogrammetric methods, some type of sensor calibration will be needed. Operation in shadowed regions and possibly under the most severe earthlight conditions may require some working lights to provide artificial illumination. Extreme contrast ranges may require the use of spectral filters to provide contrast reduction to aid recognition. Conversely, in very uniform regions

where luminance variations are especially small, higher contrast may be desired. Present investigations indicate that near-infrared regions may provide higher contrast than visual regions, which could lead to the use of IR sensors.

For the purposes of mapping and piloting, certain observing conditions will prove optimum. Choosing certain ranges of source angle and/or viewing angle will allow the observer to optimize contrast range, level of illumination, and shadow effects to provide the best combination of photometric and relief characteristics for the job at hand. For example, the very low sun condition (solar zenith angle approaching 90°) will give a low illuminance on a horizontal unit area, which may be desirable to discern fine surface structure that is washed out at high sun position, but at the same time, low sun gives relatively large shadows, thus obscuring much of the surface and causing very high contrast range. Similarly, high sun minimizes shadow, but also minimizes contrast range so that very uniform luminances result. Careful planning will therefore be required to optimize viewing conditions for mapping and piloting during a mission.

Studies pertaining to the recognition of various man-made and natural features on the lunar surface were performed because of the importance of the function to piloting and terrain mapping. Results of these studies are included under navigation techniques, part of Section 6, in this report.

5.3 OPTICAL LINE OF SIGHT ON LUNAR SURFACE

The usual chart showing line-of-sight (LOS) distances on the moon accounts for only the curvature effect. Of equal importance in arriving at realistic values of LOS are the effects of surface obstacles and undulations. In the absence of actual data on obstacle size and distributions and undulation amplitude and period, only estimates of these parameters can be made. However, even allowing for some error in the estimates, it is felt that LOS calculations based on a terrain model including such estimates are more realistic than those based on the academic smooth moon.

Several different approaches were tried in attempting to arrive at the magnitude of LOS reduction caused by terrain characteristics. Attempts to define LOS in probabilistic terms were rather disappointing, inasmuch as the cases that were easily handled were all of extremely short range (up to 100 m approximately). It became apparent that distinguishing between undulations and obstacles was rather unimportant until data are available on

the existence of each. Rather, the problem reduced to determining only the curtailment in LOS because of an intervening general terrain anomaly of a given size. Interpretation of the anomaly, whether it be a terrain undulation, a rock, or combination of the two, was left open. Thus, in Figure 5-2 LOS between two vehicles, for example, of heights h_1 and h_2 depends upon the terrain height h_t which is simply an undefined positive departure from the smooth moon datum.

For the simplest case, letting $h_1 = h_2 = h$, Figure 5-3 shows the reduction in LOS caused by terrain anomalies of amplitude h_t. The smooth moon values ($h_t = 0$) show sharp reductions for even minor terrain anomalies when the viewing heights h correspond to reasonable vehicle heights.

It may be argued that the results shown in Figure 5-3 are also not too realistic, since the obstacle or terrain undulation would not necessarily appear at the horizon as shown in Figure 5-2. However, this contention would be disputed on the basis that Figure 5-3 shows 3-σ values of LOS availability for terrains which are characterized as having the anomaly present throughout. Were the anomaly a singularity within a terrain area, the LOS probability would of course be almost unaffected by the presence of the anomaly. As the number of anomalies increases to the point where they characterize the terrain, Figure 5-2 becomes more realistic.

At the present time, there is no reason to believe that a TV camera can or would be operated at a height appreciably greater than normal viewing height. As a result, the television LOS is not expected to vary appreciably from the optical/visual LOS.

5.4 RADIO FREQUENCY LINE OF SIGHT

The radio frequency LOS is a function of lunar physical parameters such as terrain contours, terrain conductivity, and material dielectric constants. Other parameters such as frequency, power, antenna height, etc, can be controlled to optimize a system. An extended LOS range is desirable to provide a large homing range both for safety and, if practical, to reduce the accuracy requirements imposed on the navigation system.

Computations of surface RF propagation have been done primarily by Vogeler.[100] These computations used terrain dielectric constant and conductivity parameter values that were derived from studies of radar scattering by the moon.[104] Although work is still being continued in these areas,
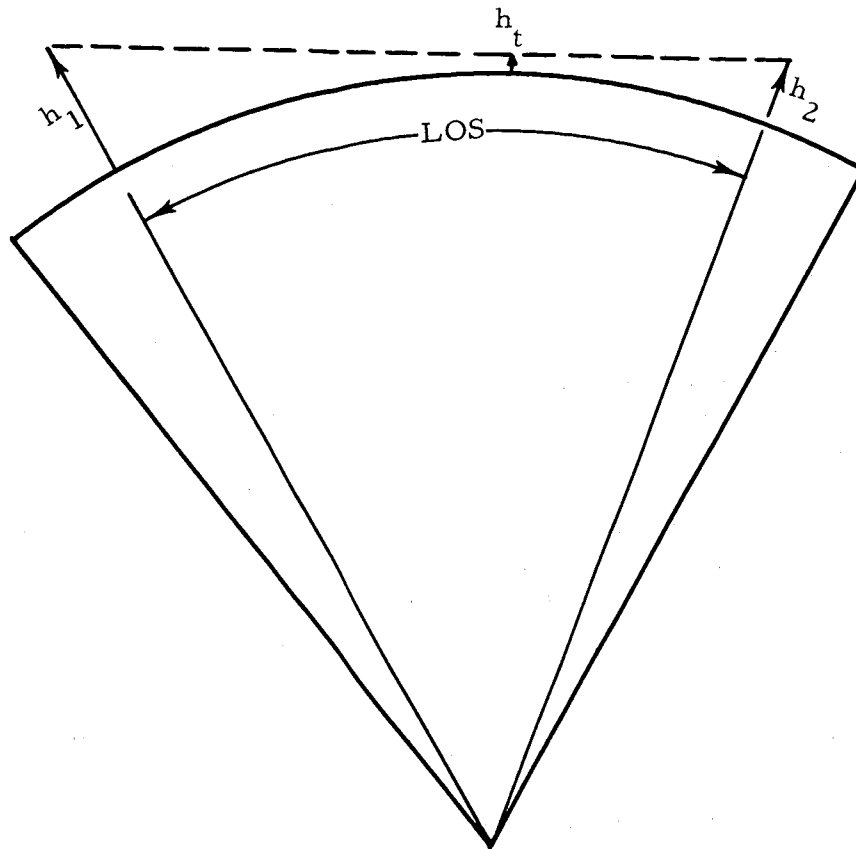
Figure 5-2 Line of Sight Geometry
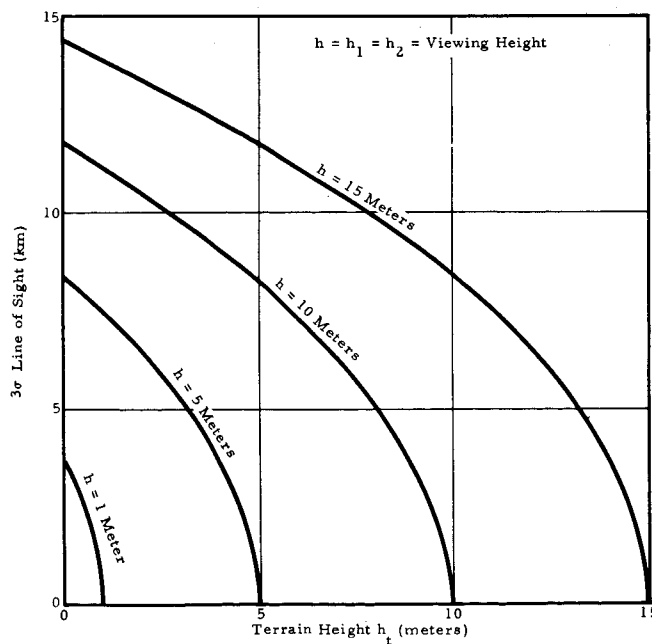
Figure 5-3 Line of Sight vs Terrain Height

measurements of the critical parameters might well be priority items for scientific investigation during early missions (see Appendix D).

The use of lunar ionosphere for lunar surface communications[72] has also been studied and the results are interesting. However, as pointed out in the referenced report, the assumptions regarding the lunar ionosphere impose rather stringent conditions. To verify the assumptions and establish parameter limits, low frequency radio propagation experiments at a lunar-based station are desirable.

Studies of lunar surface radio propagation are being continued by others and the associated assumptions and results are being presented and discussed at technical conferences.[99] Insofar as lunar surface navigation studies have been concerned, a range of values (including optical LOS) was assigned for use in evaluating applicable concepts.

5.5 PHYSICAL AND ENVIRONMENTAL PARAMETER VALUES

A range of values for the physical and environmental parameters was necessary for use in the analysis of the system concepts. The results of studies and inquiries were compiled and are in Table 5-3, which lists the parameters, suggested 3σ parameter range, nominal values and references. Also included are other parameters associated with programs such as LEM, Lunar Orbiter, DSIF and MSFN tracking, and lunar surface exploration.

1

TABLE 5-3

PHYSICAL AND ENVIRONMENTAL PARAMETERS

Parameter	Suggested Parameter Range (3σ)	Nominal Values	References
LEM Location	0. 5 km to 5 km		0. 455 km (0. 1 km probable error), Coordination Mtg., 26 June 1964, DSIF Tracking; NASA Memorandum, MT-1, dated 22 Sept. 1964. 100 m. probable converted to 3 974 meters (3σ). 63-261-778, "Primary Mission Definition Apollo-LEM Landing Surface Requirements" - 10 Dec. 1963. 2 km Lunar Logistic System, Vol. VI-Tracking & Mission Control, MTQ-M-6-1, March 15, 1963 MSFC CEP of 800 meter radius - MOLAB RFQ Question & Answer #62.
Map Accuracy		0. 91 km	LEM-Landing Accuracy Objective CEP
Horizontal	0. 5 km to 10 km	1 km	3. 56 km and 1 km to 2. 5 km per MSC as of 4 Aug 64 1. 2 km per ACIC as of 28 Aug 64
Vertical	0. 3 km to 3 km	NA	1 km in "Considerations on Lunar Surface Vehicle Navigation" Harden & Doyle from NSL E30-8 references.
LEM/ LRV Landing Separation	1 km to 10 km	5 km	10 km - ALSS 402, Trip Report, NASA (CEP for each is 0. 91 km. See first parameter)
Scientific Instr. Homing Range	1 km to 10 km	2 km	Bendix estimate
Surface Position Markers	Active - 2 km to 10 km Passive - (0. 5 km to 2 km)	2 km	Bendix estimate
LRV to LEM or Base	5 km to 3000 km		"Post-Apollo Lunar Program Phases & Possible Exploration Mission Sequence" by David Paul III, MSFC.
Deflection of Vertical	0 to 600 arc sec		(1) "Working Paper" NSL E30-8, June 1964 on Task Order N-21; (2) Bendix Report BSR 1016, 17 Sept. 1964 (3) Bowditch, American Practical Navigator (4) W. Kaula - letter to F. Digesu - Max. of 180 to 600 arc sec RMS
Visual TV Homing Range	0. 5 km to 5 km	2 km	1 km (Bendix estimate and (1) above)
RFDF Homing Range	5 km to 50 km	10 km	(Bendix estimate)
Vehicle Velocity (Avg.)	1 km/hr to 15 km/hr	10 km/hr	Bendix estimate; Post Apollo Lunar Program Phases etc., by D. Paul III, MSFC
Traverse Day	2 hr to 24 hr		Bendix estimate based upon "Post Apollo Lunar Program Phases, etc." by D. Paul MSFC
DFIF & MSFN Position Measurement	3. 3 km to 185 m (2 days to 2 weeks tracking time)	2 km	JPL IOM 312. 7-93 dated 3 March 1965 by T. H. Elconin
Relative Map Accuracy	0. 01% to 1% of future separation distance		Ref 152

SECTION 6

NAVIGATION TECHNIQUES AND COMPONENTS

This section discusses directly applicable navigational techniques
and components which apply to the lunar surface navigation problem. The
techniques are classified as those of position fix, piloting, and dead-
reckoning; included are celestial, command service module observation,
earth-based tracking, surface feature recognition, RF homing, and
distance traveled (directly sensed distance or integrated velocities and
accelerations) techniques. The results of a navigation component survey
are presented. Navigation component performance data, component
characteristics and the manufacturers are tabulated.

6.1 NAVIGATION TECHNIQUES

6.1.1 Position Fix Techniques

6.1.1.1 Celestial Tracking

A star tracker was evaluated as an integral component of the
passive nongyro and the inertial system concepts. The star tracker pro-
vides angular information as celestial body altitude, and azimuth relative to
some coordinate system—body fixed or inertial. Associated with a celestial
tracker as a navigational system subelement are:

1. Parameters of celestial observables

2. Acquisition of the selected observables.

6.1.1.1.1 Parameters of Celestial Observables

To establish the requirements for selecting an observable as
a reference, the basic considerations which affect the selection must be
understood. That is, the inherent celestial target parameters which qualify
an observable as a reference to a navigational system must be defined as a

function of celestial tracker properties. The following factors should be considered:

1. Magnitude

2. Spatial distribution

3. Spectral radiance

4. Planets as acceptable targets

5. Centroid-center of radiance errors

6. Background illumination

7. Relative spatial position for minimum error sensitivity

8. Occultations of observables

9. Parallax

10. Ephemeris data errors.

Magnitude

One relative measuring scale of the brightness of a celestial body is the visual magnitude. The visual magnitude scale is adjusted arbitrarily so a zero order magnitude star has an irradiance, measured outside the earth's atmosphere, of 2.1×10^{-10} lumens per cm^2. The general expression relating luminous flux density and visual magnitude is:

$$\frac{\ell_m}{\ell_o} = 2.51^{-m_v}$$

where ℓ_m = luminous flux density (lumens/cm^2, or watts/cm^2) from a body of visual magnitude m_v

ℓ_o = 2.1×10^{-10} lumens/cm^2 (or 3.1×10^{-13} watts/cm^2) flux density for a star of $m_v = 0$.

6-2

The larger the visual magnitude, the dimmer the star. Presently it appears that state-of-the-art dynamically tested equipments detect and track observables of visual magnitude $\leq$ 2.5. Of the 57 selected navigational stars, 52 of them have magnitudes $\leq$ 2.5.

Spatial Distribution

The navigational stars are distributed uniformly in sidereal hour angle, 3 stars/20°, about the celestial sphere and should provide continual reference to a lunar observer except for occultation by the earth, sun, planets, and lunar surface features. The 52 navigational stars are positioned approximately in $\pm 75°$ declination of the celestial equator. Within $\pm 60°$ declination there are approximately 7 stars/10° declination. However, difficulty might occur if a bright target star is required at the celestial poles. Figure 6-1 shows the number of target stars available for a star tracker ephemeris. A conclusion drawn from investigation of star tables is that a uniform distribution of observables of visual magnitude $\leq$ 2.5 is available for a star tracker window limiting field of 25° (Ref. 14).

Spectral Radiance

A parameter which affects the ability of a star tracker to detect and track a selected observable is the frequency or wavelength of the observable spectral emission. Approximately 95% of the navigational stars lie in the spectral classes B, A, F, G, K, and M, with extremes in effective temperature ranging from BO (22,000°K) to M5 (2800°K). A relative spectral distribution is shown in Figure 6-2. Peak efficiency of star tracker detection is obtained for tracker response functions compatible with star irradiance wave lengths. Figure 6-3 is a plot of normalized response functions for four classes of detectors. Since the brighter stars are generally selected as navigational stars, and since the hotter-type stars dominate the distributions, the detector can be assured of response compatibility. Table 6-1 contains response bandwidths and sensitivities for four specific detectors.

Planets as Acceptable Observables

Planets as selected observables can be used for: (1) observation for position fixing, and (2) reference body from which angular reference is taken to point and acquire a second observable. Following is a listing and presentation of particular polar system observables and their associated parameters (Ref. 117, 118, 14, 120):
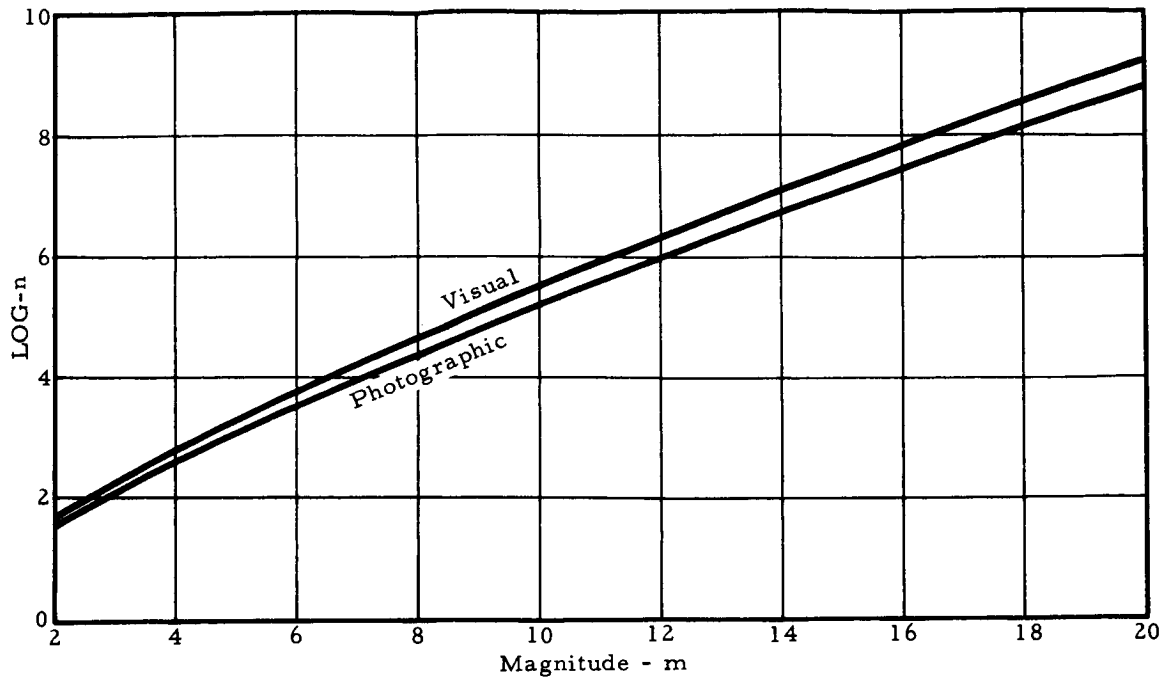
Figure 6-1 Number of Stars, n, Brighter Than Magnitude, m
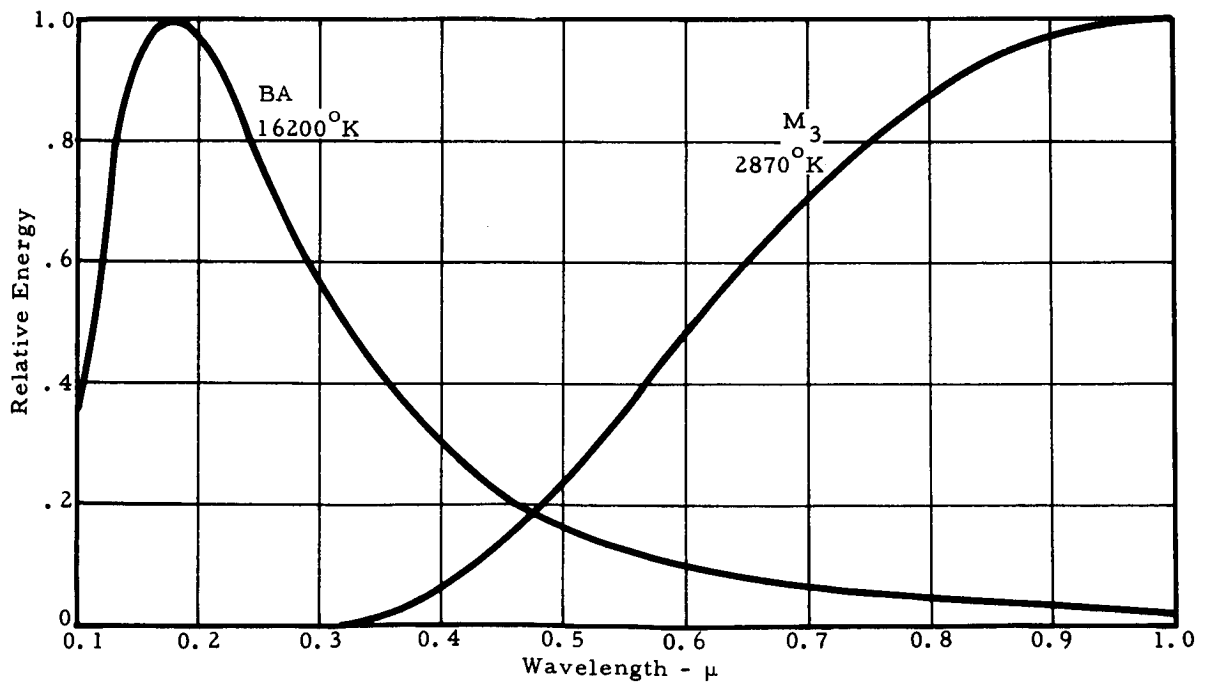
Figure 6-2 Spectral Distribution Range of Stars

6-4
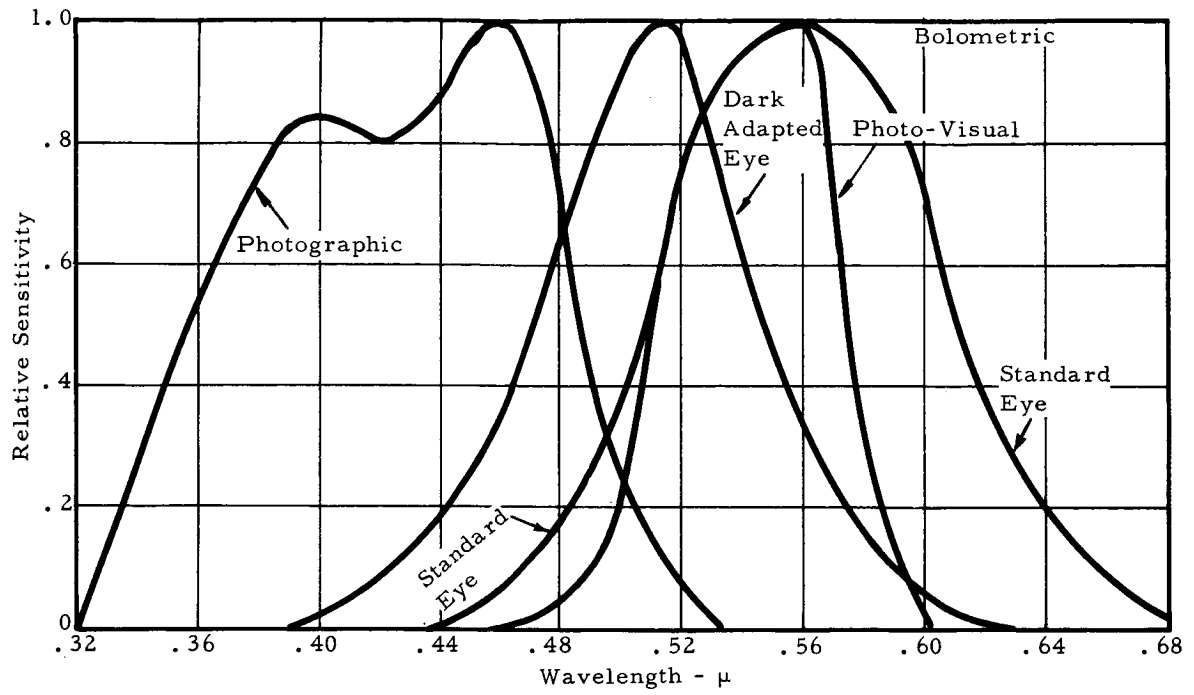
Figure 6-3 Relative Optical Sensitivity
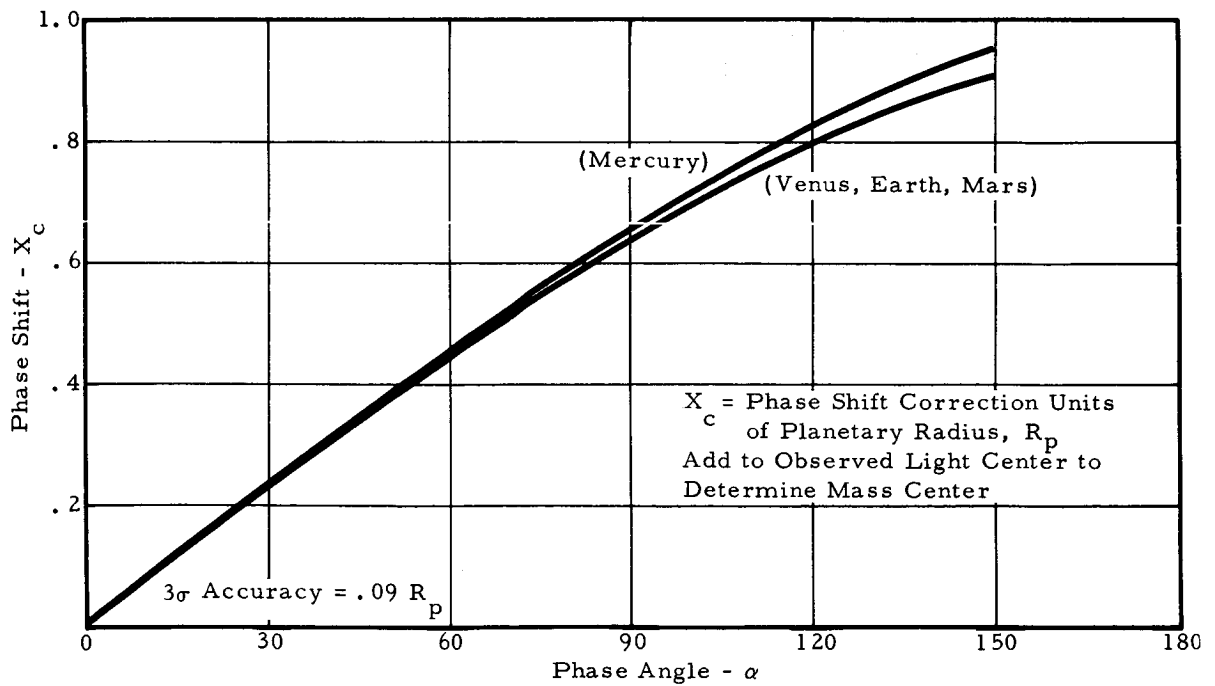
Figure 6-4 Mass Center and Illumination Center Correction

TABLE 6-1

DETECTOR CHARACTERISTICS

Typical Detectors	Gain	Sensitivity	Noise	Spectral Sensitivity Bandwidth Microns
		μ a/lumen	Dark Current μa (at photo surface)	
Photomultiplier	0.32×10^6 @ 1250v	125	10^{-6}	0.32 - 0.65
Vidicon	3.1×10^4 for 176 line raster	650	0.02	0.45 - 0.60
Orthicon	500	60	?	0.30 - 0.70
Image Dissector	10^7 A 1800v	40	3×10^{-7}	0.32 - 0.70

6-6

Sun: $m_V \cong -26.9$; average horizontal parallax value 2.2 arc minutes from moon

Mercury:

Albedo 0.07; phase illumination; variable visual magnitude $m_V \cong -0.20$; disc phase illumination error of 15 arc sec if used as point source; slight error in polar direction; estimated position error 440km

Venus:

Albedo 0.61; phase illumination; $-4.3 \leq m_V \leq -3.3$; significant predictable . bias error due to phase illumination; estimated position error 670 km; maximum horizontal parallax value from moon is 9.0 arc sec

Earth:

Albedo 0.29; phase illumination; $m_V \cong -3.8$; reflectance difference between surface and clouds causes large random errors in centroid tracker; infrared radiation peaks at 12 μ, absorption and scattering by atmosphere attenuates blue end of spectrum; position error 440km; 14.6 arc min to 16.7 arc min extreme horizontal parallax values from the moon

Mars:

Albedo 0.15; phase illumination; $-2.8 \leq m_V \leq 1.6$ useful for a tracking, maximum phase illumination error is 6 arc sec; position error 670km; 7 arc sec maximum value horizontal parallax from moon

Asteroids:

To eliminate occultation and phase illumination problems, the asteroids may serve partially as a source of position information. Ceres, the largest asteroid, subtends 1 arc sec at 1 astronomical unit; and since all but three asteroids subtend less than 0.5 arc sec in diameter, phase illumination problems are negligible. However, limiting magnitudes of 7.7 to 9.9 would represent difficult identification and acquisition. Position error for Ceres, Pallas, Juno, Vesta is 9 arc sec.

Jupiter:
       Albedo 0.44; $-2.5 \le m_V \le -1.4$; brightness change of 12% due to phase illumination; error due to phase illumination negligible; position error 2670km

Saturn:
       Albedo 0.42; $m_V \cong .8$; reflected light at yellow end of spectrum; no phase illumination error, can be tracked accurately; position error 2670km

Uranus:
       Albedo 0.45: $m_V \cong 5.8$; too dim for acquisition confidence; position error 4400km

Neptune:
       Albedo 0.52; $m_V \cong 7.7$; acquisition and tracking too difficult; position error 6700km

Pluto:
       Albedo 0.04; $m_V \cong 14.5$; acquisition and tracking uncertain; probable position error 1340km

The variation of visual magnitude of the planets may be calculated as:

$$v(\alpha) = V_1(0) + 5 \log r\Delta + a\left(\frac{\alpha}{100^{\circ}}\right) + b\left(\frac{\alpha}{100^{\circ}}\right)^2 + c\left(\frac{\alpha}{100^{\circ}}\right)^3 .$$

where

    a, b, c, $V_1(0)$ are tabulated constants (Ref. 118).

    α = phase angle

    r = distance planet to sun, au

    Δ = distance planet to observer, au

  1AU = 149,598,650±450km

Centroid-Center of Radiance Errors

When tracking a star, the static image is a point image since the stars are effectively located on the celestial sphere at infinite radius. However, the planets are not energy sources and are seen only through reflected sun light. Thus the brightness of the planets is continually varying with distance from the sun and tracker. Therefore, varying visual magnitudes, non-uniformity in surface brightness, and phase illumination offset the light center or radiation center from the mass center. The curves in Figure 6-4 show correction in abscissa position relative to planetary radius to compensate for phase illumination mass centroid shift. No shift occurs in ordinate direction. Curves pertain to Mercury, Earth, Venus and Mars.

Background Illumination

As a means of lowering star tracker detector and therefore probable system noise errors, it is advantageous for the selected observable to possess a low background radiation. A brightness ratio of 10:1 requires a limiting optical field of view of approximately 10 degrees. In some areas of the celestial sphere, star density would limit the field of view to approximately one degree. The twenty brightest stars possess, within a 1 degree radial field, an average of 1.2 background stars with m_V of +6.6. The number of background stars should be minimized.

Relative Spatial Position for Minimum Error Sensitivity

A particularly important parameter involved in the selection of a celestial observable is the minimization of the sensitivity of errors in true azimuth and elevation as a function of relative pointing angles. Certain errors such as local vertical errors cannot be minimized by selecting particular pointing angles. However, minimization of declination, right ascension, and tracking error is achieved for the two reference bodies separated 90° in azimuthal direction and low altitudes to the local horizontal plane.

Iterative sightings on one observable as a means of navigation is inaccurate due to negligibly small angular displacements during the elapsed time, but alternate sightings on two references appear feasible.

Occultations of Observables

The primary interference body will be the earth. A calculation could be made expressing the locus for occulted position on the celestial sphere due to interference of earth, planets, and sun, thereby providing a reference of eclipsed stars, as a function of mission time. A typical technique of eliminating intensive solar energy is to automatically interrupt optical path of tracker when the sun line is within 30° of optical axis.

Also a statistical study of occultations by selenographic features could be considered.

Parallax

Parallax is the angular change in a star's position when observed from two separate points or the angular change in position during an elapsed time interval of celestial measurement. The parallax problems encountered with planet sightings are given above. For star tracker accuracies of 30 arc sec, parallax of stars is no problem. When 3 arc sec accuracies are required, selected stars for the emphemeris must have small parallax correction values.

Ephemeris Data

The positional accuracy of star spatial position is not the same for all catalogued stars. Generally the positional accuracy is less for fainter stars, and also for stars in the southern celestial hemisphere, with accuracy decreasing toward the south celestial pole. For stars less than visual magnitude of 2.5, the error in position is 0.36 arc sec (RMS combination of right ascension and declination). Figure 6-5 shows the error in position for stars catalogued in 1960. For a lunar referenced emphemeris, an additional inaccuracy contribution of 20 arc sec is approximated based upon lack of knowledge of moon motion due to physical librations (Ref. 127).

Appendix C discusses the ephemeris data transformation from the earth referenced coordinate system to the lunar referenced coordinate system.

Figure 6-5 3σ Errors of Catalog Star Position

6.1.1.1.2   Acquisition of Selected Observable

Acquiring and tracking a selected observable involves the following steps:

1.   Pointing telescope boresight axis

2.   Scanning optical field of view

3.   Detecting and tracking the selected observable.

Pointing

The single important factor in tracking an observable is the initial positioning of the telescope boresight axis to a command spatial position.   The first requirement for pointing is angular reference alignment. This might be accomplished through reference to:

1.   Earth and/or sun trackers

2.   Automatic star tracker slaved to manual sextant or TV camera

3.   Celestial comparator

4.   Inertial platform or a body fixed reference

The first system considered, the passive nongyro concept, utilizes an IR earth tracker for azimuthal reference information; a condensed listing of appropriate horizon sensors and available data and accuracies is given in Table 6-2. Assuming the star tracker base is accurately positioned and referenced through any of the above methods, the pointing accuracy limitations are contained in inaccuracies of positioning of telescope boresight axis to an input axis command, and also in uncertainties of transducer outputs of telescope boresight axis position. Present data indicate a state-of-the-art axial positioning capability of 19 arc sec. The contribution of angular position transducers errors increases the total axial uncertainty to 30 arc sec. Orthogonal combination of the two axes results in an accuracy of 42 arc sec. Thus it sometimes occurs that telescope positional uncertainties are larger than the optical field of view.

TABLE 6-2

HORIZON SENSORS

Program	Supplier	Altitude Capability	Scan Pattern	Accuracy
Advent	General Electric Missiles & Space Vehicles Dept.	Synchronous Design but applicable over a large range	Rectilinear generated by 360° rotation of a parabolic mirror in each of two scanning heads. Mirror focuses 12-30 micron radiation on a single thermistor Bolometer.	1.7° is claimed to have been achieved
Nimbus	GE/MSVD	No Data	Scanning optics are refractive. A conical 90° scan is generated by a prism-lens. A thermistor bolometer detector is operated in the 12-18 micron region. Unit is hermetically sealed.	No Data
OGO	Advanced Technology Laboratories	A search & track capability over a 90° range in the scan plane is claimed. This indicated practically all altitude capability	Four tracker rectilinear scan tracker servo circuitry performs search & track control functions	No Data
Agena A	ATL	No Data	Little data except that a mirror scan of some type was employed	No Data
Agena B & C	General Electric Light Military Electronics Dept.	No Data	Conical 75° included angle, with centerlines separated nominally 95°, variable for mission altitude profile.	0.1° claimed. No distribution available
Agena B & C	Barnes Engineering Co.	No Data	No data except that it is "very similar" to the Mercury system also produced by Barnes	No Data
Agena D	ATL	No Data	Dual azimuth and dither scan of a single detector, a separate search mode causes an 85° scan dither amplitude	"More accurate than gemini scanner". No further data
Mercury	Barnes	No Data	Conical, 110° included angle, with center lines separated by 90°. Scan rate 30 Rps	$<1.0^\circ$ excluding cloud disturbances
Mariner M (Mars probe)	Barnes	322,000 km	A rosette search pattern is generated by a pair of contra-rotating prisms. Following acquisition, the scan is stopped and roll & pitch error signals point the vehicle	No Data
Mariner 2 (Venus probe)	JPL Design Nortronics Production	The sensor is designed to operate in a region between 1.6×10^6 km and 58.1×10^6 km from earth	A three section photomultiplier-tube operated earth sensor mounted on and aligned with the high gain antenna. Field of view varies between 0.5° and 20°	Resolution 10 arc sec; accuracy $4.45 \rightarrow 9.0$ arc min; linear to $\pm 1^\circ$
Johns Hopkins U. Applied Physics Lab.	Minneapolis Honeywell Aero Division, Boston	The field of view is greater than 2π steradians	Radiation from hemisphere is collected by a reflective cone which reverses the image (earth outside, space inside). Single thermistor detector measures IR alternated from quadrants. Either mechanical or germanium choppers used.	0.257°, 3σ RSS is claimed which includes instrument errors, solar radiation & source errors
Ranger	JPL Design No production data	Lunar	The short range earth sensor (SRES) operates on a shadow-box principle with photomultiplier tube detection. Field of view is $40^\circ - 60^\circ$	No Data

Scanning and Detecting

Scanner and detector requirements and salient features for space navigation are:

1. Search through largest field of view in minimum time with maximum detection reliability

2. Sensitivity

3. High signal-to-noise ratio

4. Signal gain through storage or photo multiplication

5. Dark current

6. Type of scan pattern.

The four basic types of detectors (Ref. 118, 17) are presented in Table 6-1.

Of these, the photomultiplier and vidicon are the most promising for high performance applications. A vidicon is desirable due to high scanning and acquisition rates of less than 1 second. However, using criteria 2, 4, and 5 above, the detector types rank in the order of image dissector, photomultiplier, image orthicon, and vidicon.

Assuming a properly pointed telescope, two means of acquiring a star are characteristic recognition and pattern recognition. Characteristic recognition requires a specific search field of view in which the target star characteristics are unique. Two means of target star recognition are star discrimination through magnitude level and star discrimination through wavelength of spectral emission. However if no initial alignment is available (no platform), the condition of star uniqueness in a search field is difficult to meet.

Pattern recognition requires some type of memory system in which angular differences between stars are stored. The tracker then operates through the error signal comparison between stored and measured angular differences. An inertial platform is required if one star tracker is used to measure angular differences: Two trackers are necessary to determine

a coordinate system in the absence of short term stability. Pattern recognition fixes a coordinate system, whereas characteristic recognition determines a line of sight. A typical type of pattern recognition device, using 10° zenith star maps displayed on a tracker reticle, provides an accuracy of 0.01 degrees of arc. This celestial correlator is fixed to an interial platform. The platform has static accuracies of 45 arc sec and dynamic accuracies of 4.4 degrees.

A pattern recognition feasibility model tested indicates pointing accuracy of 33 arc sec using a vidicon detector and optical field of view of 7.8^o, with an acquisition angle of 36 arc minutes. Nominal star field illumination was 0.5×10^{-13} watts/cm^2 ($m_v \cong 2$). However, the pattern recognition technique development is hindered by the more precise positioning information requirement, slow acquisition, unless a principal star is identified through characteristic recognition, and a larger signal-to-noise ratio.

The type of search pattern to be used depends on the type of tracker and noise level. For high signal-to-noise ratios and high probability of target detection, normal or weighted scanning about an assumed position is unnecessary, and scanning equal areas in equal times suffices. However, to decrease scanning time, programmed scanning of most probable areas is practical. For example, the spiral search starting from the center of the field spends more time scanning elements closer to the center.

For low signal-to-noise ratio searching conditions, a program search technique should include provisions for a continuing search pattern if interruption occurs due to false alarm stars.

The electronic imaging detectors include the programmed scan as one package. Scans include the typical raster scan, spiral, or rosette. The raster scan can contain both fine scan and coarse scan, with typical accuracies of 27 arc sec in 30 arc min field of view. A typical figure for star location accuracy is within 0.5% of instantaneous field of view, or that portion of detector beam which scans the optical field of view of the telescope. Search is generally performed over $\pm 1^o$ of commanded pointing angle.

Tracking

Various state of art figures on trackers indicate:

1.. Telescope boresight to star LOS accuracy of 45 arc seconds

2. Tracking acquisition for target star within 30 arc minute of telescope boresight

3. Maximum nulling error of 9 arc sec for star tracker stationary relative to star line of sight.

A preliminary comparison of compiled tracker systems with the above detectors follows:

1. Photoelectric Tracking System (Contract W33-038-ac-14175)

   Over 250 flight tests; a basic system of three star tracking telescopes on a gyro-stabilized instrument.

   a. Instantaneous field of view is limited to 40 arc sec

   b. Search field of 30 arc minutes

   c. Tracking field of 2 arc minutes

   d. Scanning time search field is 10 minutes

   e. Scanning time of tracking field is 2 seconds

   f. Tracks stars of $m_V \leq 3.0$.

2. Photomultiplier Tracking System

   Celestial tracker as an astrocompass (MD-1 Kollsman)

   a. Stabilized telescope utilizing a photomultiplier tube as as sensor

   b. Photomultiplier with peak response in 0.4 to 0.5 μ region

   c. Total telescope pitch and roll freedom of $\pm 15^\circ$

d. Tracks stars of $m_v \leq 2.1$

e. Tracking accuracy of 45 arc sec

f. Spiral scan covering $0^{\circ} - 4^{\circ}$

g. Over-all accuracy of 18 arc min dynamically

h. 6 arc min accuracy statically including tracker angular transducers.

3. Vidicon Tracking System (Contract AF 33(616)-5954) Experimental tracking system; flight tested.

a. FOV adjustable from 1° square to $1/4^{\circ}$ square

b. Overall accuracy claimed is 30 arc sec in both coordinate axes

c. Tracks stars of $m_v \leq 2$.

4. Image Orthicon Tracking System

Theoretical calculations show

a. Optical FOV is 13 arc sec

b. Tracks stars of $m_v \leq 6.4$ with no background illumination.

Theory indicates that with a stabilized platform mounted star tracker, and with tracker errors fed into stabilization gyros, the tracker frequency response is limited to 2 or 3 cps, resulting in favorable signal-to-noise characteristic discrimination capabilities.

6.1.1.2   Command Service Module (CSM) Reference

The feasibility of this concept as a means of position fixes lies in the accuracy of the CSM orbit determination and the errors in measurements relative to the CSM. The limitation of the use of the method only

during the orbital pass, while being an important consideration in actual implementation, is not as fundamental a limitation as the accuracy of the method. It has been shown[4] that the effect of errors in measuring range from the LRV to the CSM is less critical in determining LRV position than is the effect of CSM position errors. In particular, the ratio of LRV position error to range error may be as low as 6:1. The ratio of LRV position error to CSM position error, however, is more like 25:1. It appears then that the basic feasibility lies in whether CSM position can be known accurately enough so that the LRV position errors, being a factor of 25 greater, will still be competitive with other concepts.

The accuracy of lunar orbit determination has been treated by Gunckel[121]. In his discussion it is assumed that an on-board navigation system is being used for orbit determination, with either a radar or a horizon-scanner as primary sensor. Other equipment includes an inertial platform for attitude reference and a computer for data processing. Dr. Gunckel presents an error analysis of the orbit determination process, accounting for uncertainties in the lunar gravitational field (which includes uncertainties in the mass and shape of the moon) and sensor errors (which also include the uncertainties in the mean radius, location of center-of-mass, and ellipsoidal shape of the moon). From his analysis it is concluded that the primary error sources are not the sensor errors but the uncertainties in

1. Lunar mass

2. Mean size of the moon

3. Location of center-of-mass relative to the mean lunar surface.

4. Effects of local variations of altitude and shape of the surface.

Based upon the uncertainties assumed in this paper, an orbit determination accuracy of about 2 km is presently feasible.

Applying the 25:1 magnification factor of Thomas,[4] it appears that the LRV position error would be on the order of 50 km, neglecting the contribution of errors in ranging.

The concept of LRV position determination from CSM ranging does not presently appear feasible based upon the above error contributions.

A subsequent section of this report contains the derivation of an error model for the CSM position fix technique.

6.1.1.3 Deep Space Instrumentation Facility (DSIF) and Manned Space Flight Network (MSFN) tracking

The capabilities of the DSIF are outlined in Reference 122. The S-band system, with two-way precision, will measure range rate to accuracies of $\pm$ 0.2 m/sec. Angle tracking accuracy is quoted as 0.01 to 0.02 deg (1.7×10^{-4} rad). With precision ranging, range should be determined to approximately $\pm$ 15 meters.

Reference 123 lists the following accuracy capabilities and quotes them as 1 σ values.

Angles $\pm$ 0.4 deg $= 7 \times 10^{-4}$ rad

Range rate $\pm$ 0.2 m/s

Range $\pm$ 15m.

A third reference [150] presents a curve of position error on the lunar surface as a function of DSIF tracking time. The curve is based on angular errors of 3×10^{-4} rad and gives a minimum position error of 5.5km. Other figures presented in the reference quote range accuracy as $\pm$ 15 meters and velocity as $\pm$ 0.03 and $\pm$ 0.1 m/s, with angular errors of $\pm 2 \times 10^{-4}$ radians and $\pm 6 \times 10^{-4}$ radians also appearing. The inconsistency of these values throughout the curves presented reduces the confidence in accepting any figure such as 5.5km as 3 σ, especially when Reference 123 quotes similar figures as 1 σ.

Reference 124 maintains that the MOLAB with beacon can be located within 120km. Reference 6 states the position uncertainty as a 19km diameter circle. A final reference [151] states a 1km accuracy may be assumed based on a Bissett-Berman report entitled "Capabilities of MSFN for Apollo Navigation and Guidance".

It can be stated, however, that doppler information from a beacon on the lunar surface appears to offer little in the way of position location information. Gabbard and Baker[1] have shown that although the total maximum doppler velocity is on the order of 1500 fps, only a small portion of this, a few feet per second, is location-dependent. With the uncertainty in DSIF velocity being on the order of 0.5 fps, the possibility of using doppler shift appears remote. (See Table 8-18 for revised data.)

6.1.2 Piloting

Piloting, the recognition and identification of features for guidance purposes, requires the use of some type of stereo sensor system. This system can simply be the human visual system during manned operations or a TV system during remote operations (it may be found desirable to use the TV system with an onboard monitor during manned operations because of the illumination and contrast conditions). Monoptic TV presentations have been demonstrated to have insufficient information content to uniquely define or identify surface characteristics resembling the lunar case. Under collimated light, with surface photometric properties matching the lunar properties, monoptic TV can not resolve 90° differences in slopes with complicated non-real-time photometric procedures. Although the complex photometric nature of the lunar surface will render stereo representations somewhat more difficult to interpret, stereo is capable of defining lunar scene structure.

Certain mapping aids may be required, such as landmarks. If photometric methods are to be used in addition to the standard photogrammetric methods, some type of sensor calibration is needed. Operation in shadowed regions and possibly under the most severe earthlight conditions may require some working lights to provide artificial illumination. Extreme contrast ranges may require the use of spectral filters to provide contrast reduction to aid recognition. Conversely, in very uniform regions where luminance variations are especially small, higher contrast is desired. Present investigations indicate that near infrared regions provide higher contrast than visual light regions, which could lead to the use of IR sensors.

For the purposes of mapping and navigation, certain observing conditions will prove optimum. Choosing certain ranges of source angle and/or viewing angle allows the observer to optimize contrast range, level of illumination, and shadow effects to provide the best combination of photometric and relief characteristics for a particular job. For example, the

very low sun condition (solar zenith angle approaching 90°) gives a low illuminance on a horizontal unit area, which is desirable to discern fine surface structure that is washed out at high sun position, but at the same time, a low sun angle gives relatively large shadows, thus obscuring much of the surface and causing a very high contrast range. Careful planning is therefore required to optimize viewing conditions for mapping and navigation during a mission.

6.1.2.1   Visibility of Man-Made Objects on the Lunar Surface

For purposes of navigation on the lunar surface, it is necessary to know the maximum range at which certain objects are visible. The possible combinations of targets and sensors include either man-made reflecting objects or lunar terrain targets, and either visual search or use of a television sensor.

The maximum range at which a target can be detected (not identified) depends on seven parameters: target-to-background contrast, the required probability of detection, the transmittance of the light path (expressed as meteorological range), the absolute background luminance, the uniformity of the background luminance distribution, the target area and the target shape.

Of these, the three most significant parameters are absolute background luminance, contrast, and target area. The effect of target shape is believed to be least significant, as long as the target shape is not a long extended narrow one. For this analysis a hemispherical target has been assumed. Background uniformity should be as high as possible to maximize sighting range (the lunar surface has been assumed to be fairly uniform). The required probability of detection can be empirically related to the contrast. For man-made targets an 80% reflectance has been assumed; a lunar maria albedo of 0.073 was assumed. A 99% probability of detection was obtained by multiplying the contrast required for a 90% detection probability (the measured case) by an empirically determined factor. Finally, on the lunar surface it is highly likely that atmospheric attenuation will be quite small, hence a meteorological range of infinity was used.

Based on the above assumptions and parametric values of absolute background luminance and target area, visibility nomograms for visual sighting range were developed. These nomograms are presented in Figures 6-6 through 6-9.
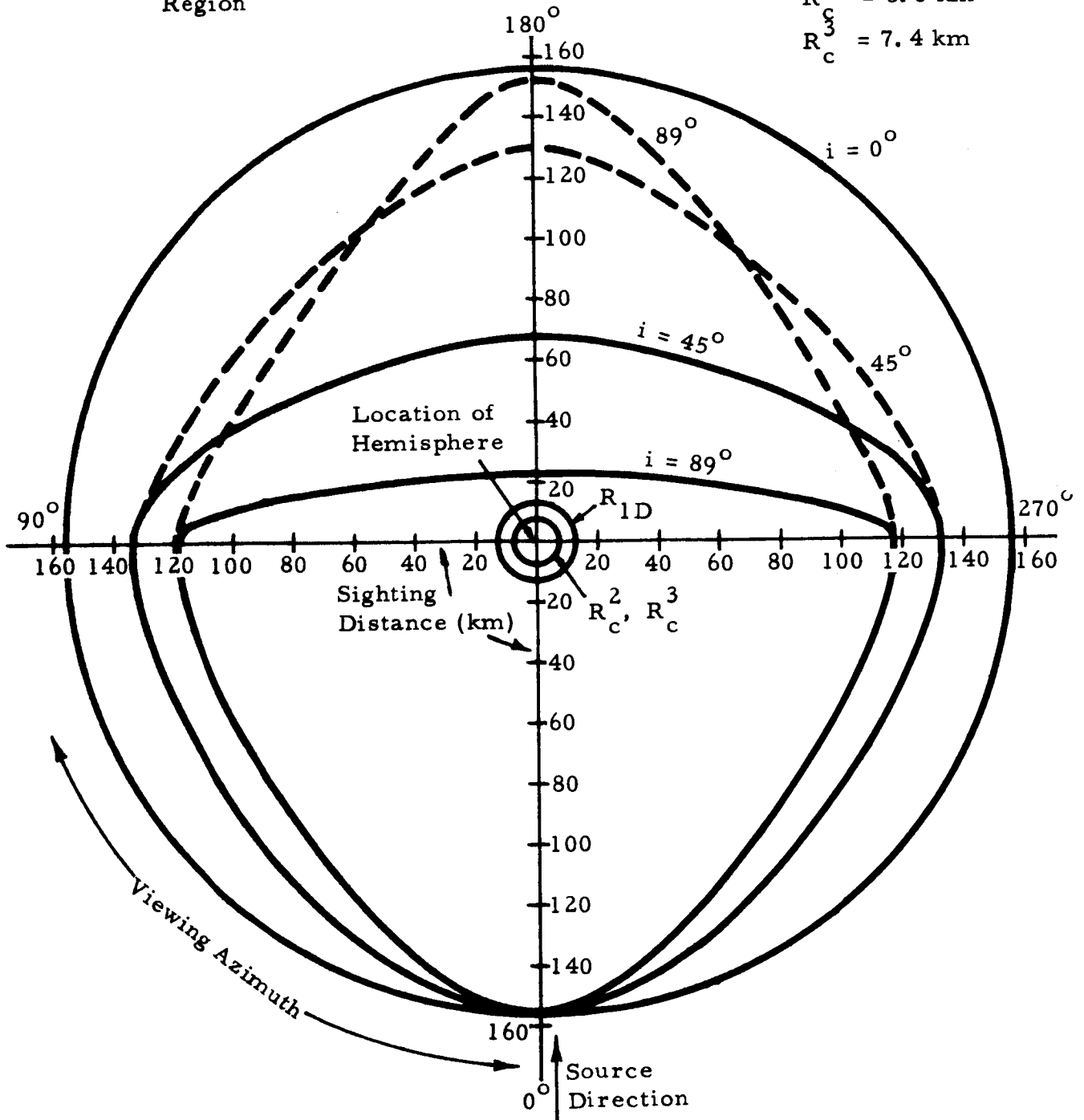
Figure 6-6 Visual Sighting Distance vs Viewing Azimuth;
5-Meter Hemisphere, Lunar Day

6-22
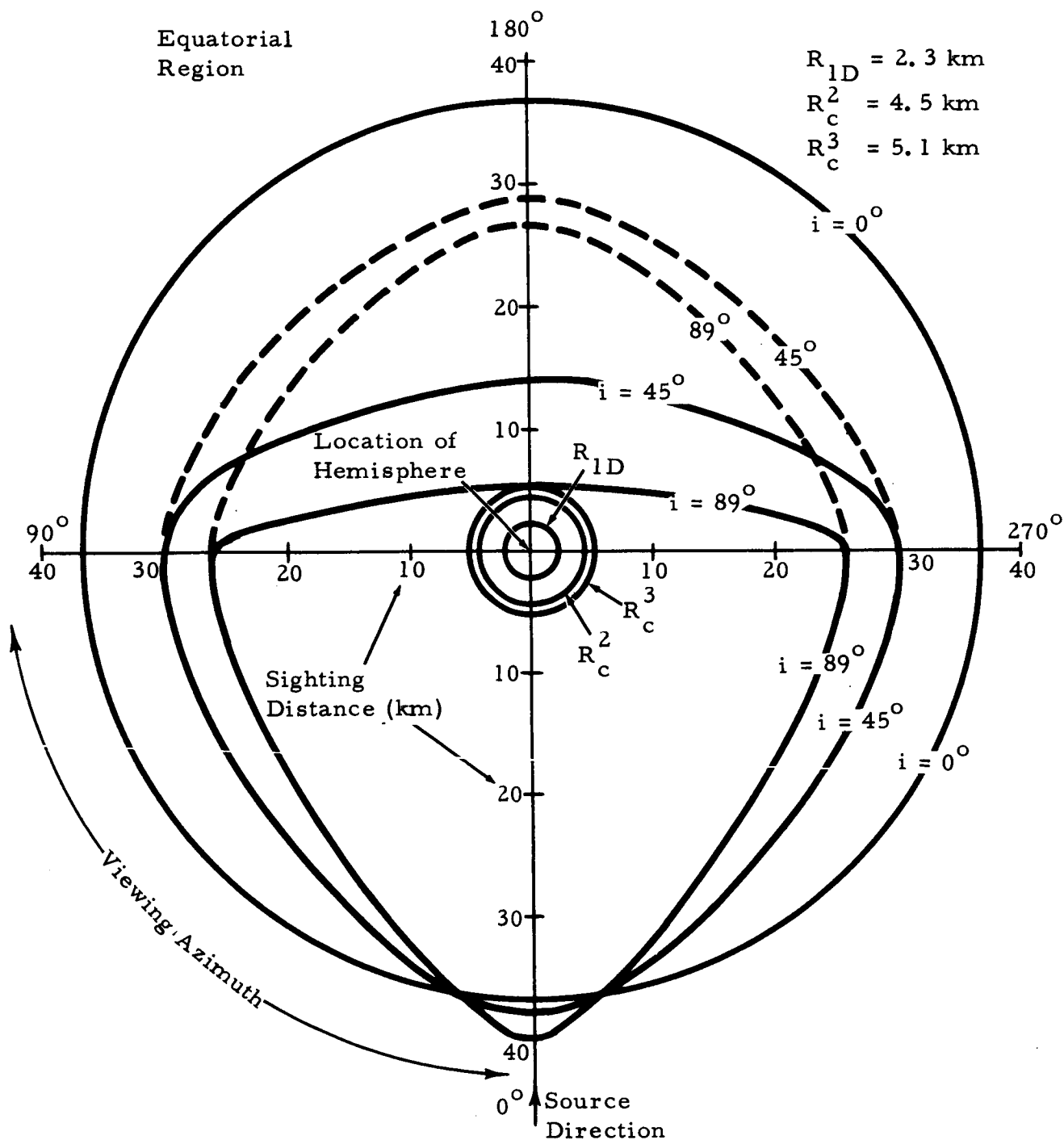
Figure 6-7 Visual Sighting Distance vs Viewing Azimuth;
1-Meter Hemisphere, Lunar Day
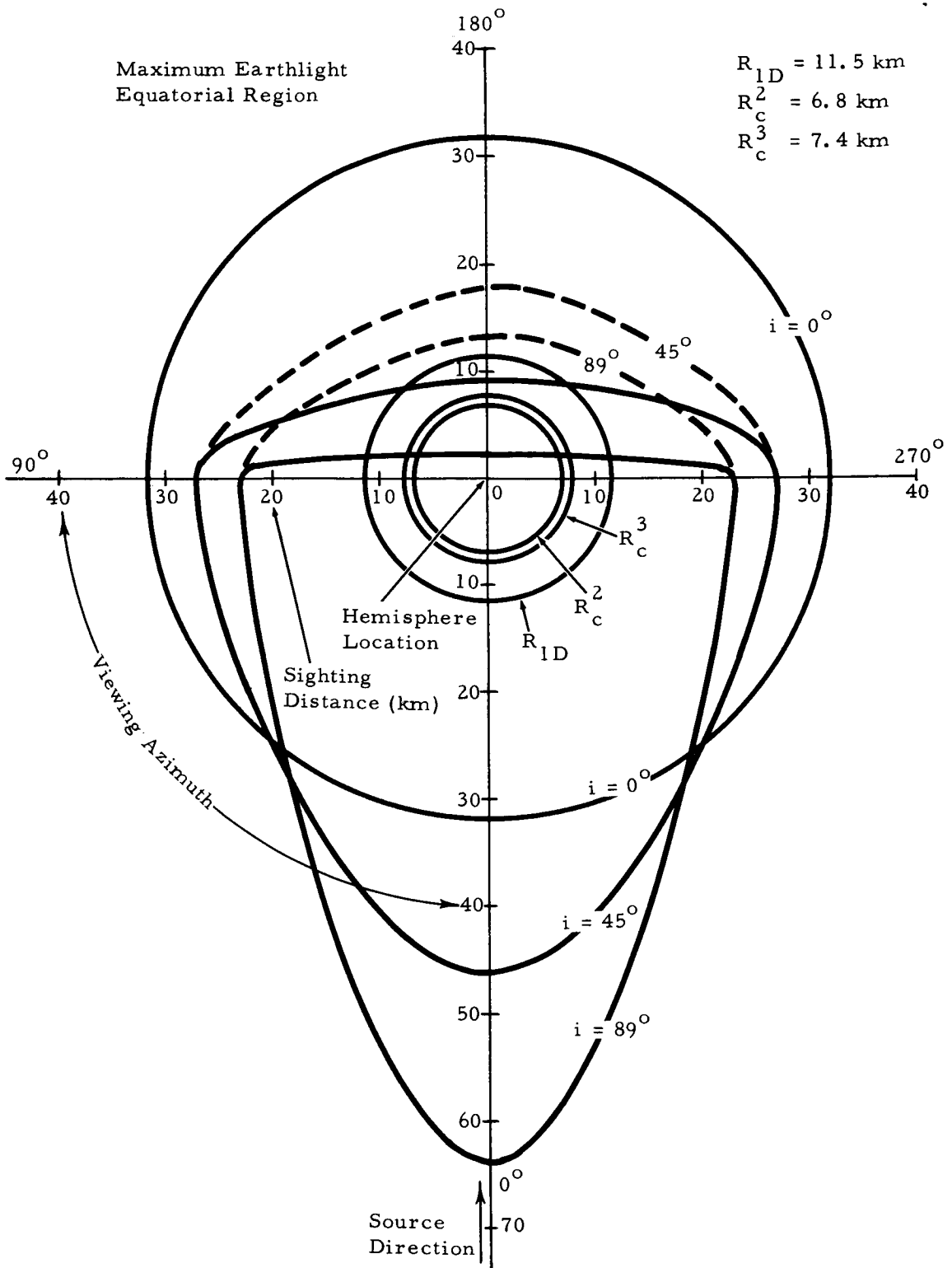
Figure 6-8 Visual Sighting Distance vs Viewing Azimuth;
5-Meter Hemisphere, Lunar Night
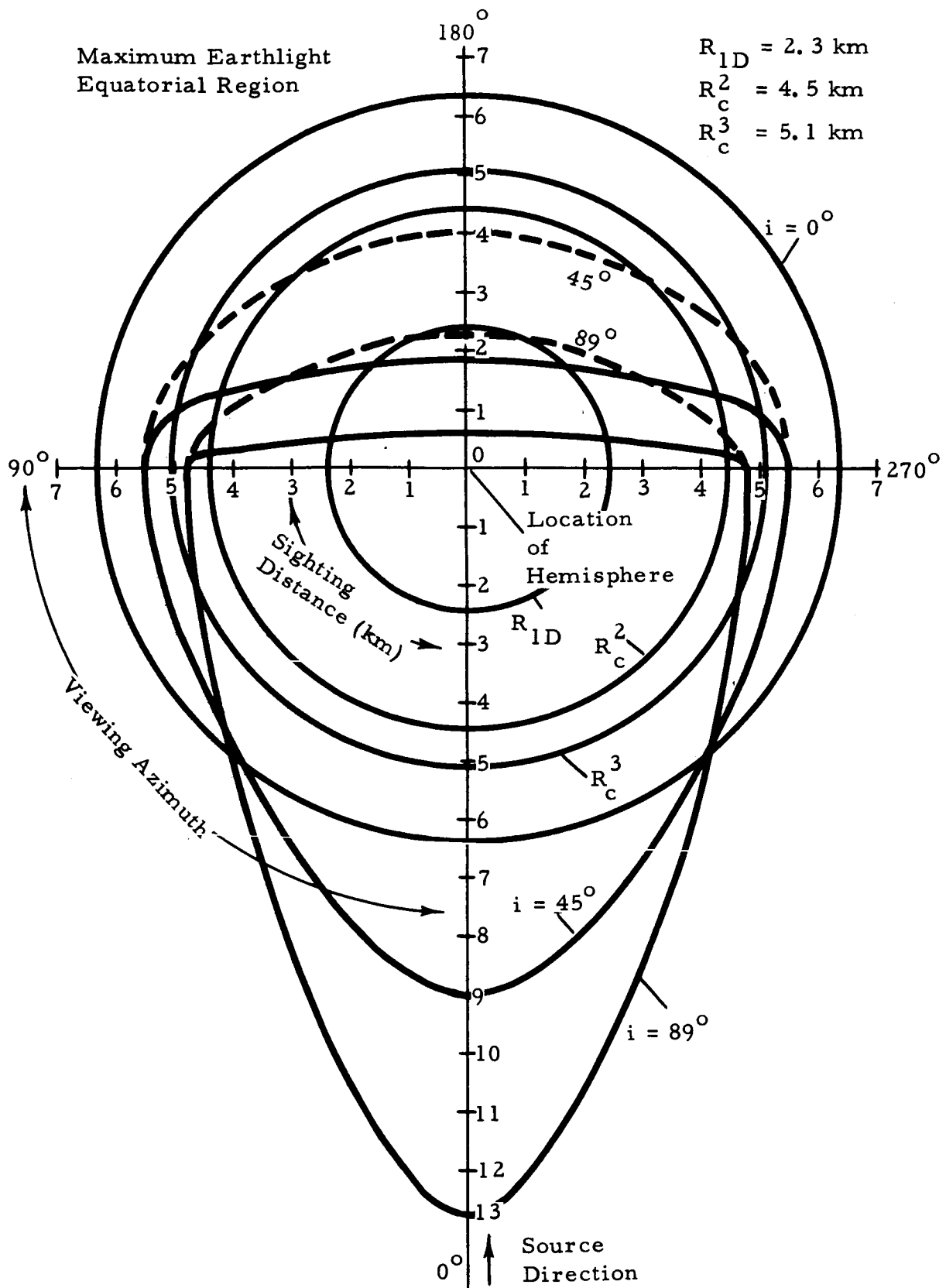
Figure 6-9 Visual Sighting Distance vs Viewing Azimuth;
1-Meter Hemisphere, Lunar Night

Figure 6-6 gives the visual sighting range for a five-meter radius hemispherical target, in the equatorial region of the moon, under sunlight (i.e., lunar daytime), as a function of viewing azimuth. The target is at the center, and the curves labelled $0°$, $45°$, $89°$ give the visual sighting range in kilometers versus sensor azimuth with respect to source direction. The four $90°$ points are the calculated points, and the curves connecting them are merely reasonable interpolations. The true curves may vary considerably from these estimates. The $0°$, $45°$, $89°$ values indicate the elevation angle of the sun, corresponding to noon, mid-afternoon, or mid-morning, and sunrise or sunset (a total span of 14 earth-days). The circular curve marked R_{ID} represents the approximate range at which the target can be visually resolved as a hemisphere. The curves $R_c^{(2)}$, $R_c^{(3)}$ represent the range at which the top of a five-meter hemisphere just appears above the lunar horizon to a sensor two or three meters above the surface (this assumes a smooth curved surface). This is called the curvature limit and it is an absolute limit, since the lunar curvature does not permit viewing of targets at any larger range regardless of how large the visual detection range may be.

It can be seen that the visual detection ranges near azimuths of $180°$ are quite small because the part of the hemispheric target that is illuminated by the sun is a very small crescent-shaped segment. The dotted lines labelled $45°$, $89°$ represent the visual sighting range for that part of the hemisphere which is not sun-illuminated, but is illuminated by sunlight backscattered by the surrounding lunar surface. This part of the hemisphere is also visible at large ranges, as shown, so that the true visual sighting range near $180°$ azimuth is greatly extended over the range for the small sunlit crescent target.

The ranges shown in Figures 6-6 to 6-9 are conservative; a target-to-background contrast of 10 was used from the true contrast range of a minimum of 11 to over 100.

Figure 6-7 represents the same conditions as Figure 6-6, for a 1-meter radius hemisphere. Figure 6-8 and 6-9 represent the approximate visual sighting ranges in lunar equatorial regions under maximum earthlight illumination (lunar night) for five and one meter hemispheres, respectively. The $0°$, $45°$, $89°$ angles represent the earth zenith angles, which are equivalent to lunar longitudes, east or west of the central meridian. For the minimum earthlight illuminance condition these values are reduced by about a factor of less than 2.

On the backside of the moon, the lunar day curves are represented by Figures 6-6 and 6-7. During the lunar night, since earthlight is absent, the surface luminances are so low that artificial illumination is required for a visual search, which is an entirely different problem.

For the case of the lunar polar regions, the sighting ranges are of the same order of magnitude as for the equatorial regions but the shapes of the curves are different.

In summary, Figures 6-6 and 6-7 show that during the lunar day, the curvature of the moon is the limiting factor for both the one-and five-meter target cases. This means that as long as part of the target is above the horizon, it can be visually detected with 99% probability. Figure 6-8 shows that the same holds for a five-meter radius hemisphere during earthlight. Figure 6-9 indicates that the sighting range is the limiting factor for a one-meter hemisphere during parts of the lunar night, for all but the central portion of the visible hemisphere of the moon, where curvature is again the limiting factor.

6.1.2.2   Comparative Visibility of Man-Made and Natural Objects on the Lunar Surface

This section defines the relative visibility between man-made objects (described in Section 6.1.2.1) and natural terrain features of comparable size. The visibility of natural features is of course basic to any navigation scheme depending on landmark recognition.

The problem of estimating visual sighting ranges for targets which are elements of the lunar terrain is much more difficult than for an artificial target. This is because the reflectance of most artificial targets is essentially Lambertian, while the reflectance of the lunar surface has a complex directional form, depending on the orientation of the target, the sensor, and the source. This makes it difficult to calculate the variation of surface luminance with sensor azimuth for even a flat surface, as was done in Section 6.1.2.1 to determine the background luminance. When a target even as simple in shape as a hemisphere is added having this complex directional reflectance, the calculation is greatly complicated.

A very rough estimate was made for the visual sighting range of a lunar block, for comparison with the values derived for the 5-meter

hemisphere man-made target. The seven parameters defining maximum detection range (discussed in Section 6.1.2.1) were considered identical to the man-made target case except for the target reflectance. Thus, for the condition of a 99% detection probability, an infinite meteorological range, the background luminance used previously with uniform distribution, and a hemispherical lunar block with 5-meter radius target, the only difference is the target-to-background contrast due to different target luminances.

The mean albedo for the lunar maria was again assumed as 0.073, defining a maximum target reflectance that is 11 times lower than for the 0.80 reflectance hemisphere. It is obvious that with the resulting much lower contrast, the sighting range for these targets is much smaller. From the lunar photometric function (the directional factor in the high value of reflectance, which varies from about 0.01 to 1.0), a high value of contrast is 1.0. The resultant visual sighting ranges for a lunar block are shown in Figure 6-10. For comparison purposes, the values for the 5-meter artificial hemisphere are also included, as are the LOS and curvature distances.

The sighting ranges for a 5-meter hemispherical lunar block, under the same conditions as stipulated for the 5-meter hemisphere case, are about 3 to 5 times smaller. And this is a maximum case, since the artificial target curves represent a minimum range, while the lunar block curves represent a maximum range. However, for this maximum case, the curvature range is again the limiting factor at most sensor positions. This is not true for smaller terrain features. Further, under many conditions the target-to-background contrast may be much smaller than 1.0, so that very small sighting ranges will result.

In summary, the sighting ranges for a lunar block, under identical conditions to that of a similarly shaped and sized artificial target, are much lower than the sighting ranges for the highly reflecting artificial target. Actual calculations of the sighting range depend completely on the lunar photometric function, and are too time consuming to be included in this study.

Some preliminary work has been done at BSD to determine experimentally the sighting and recognition ranges for lunar features such as craters, crevices, and cones, using a simulated lunar photometric material to provide a proper surface response. This work has shown that under certain illumination conditions, targets can blend completely into the background and crevices can not be differentiated from fault faces (cliffs), using monoptic systems.

A second beacon should then be dropped at point B, corresponding to the LOS limit relative to beacon A. Thus, the beacon spacing will be equal to the LOS distance. Ideally, however, if one neglects the practical matter of placing the beacons during the mission, the first beacon could be placed at B, thus utilizing LOS on both sides of a beacon. The problem of course is that the beacon B must be emplaced prior to the mission.

The feasibility of employing beacons rests on two considerations:

1.   The degree of assistance to the navigation task

2.   The penalty (weight, etc.) paid to gain this assistance.

It was assumed in the following analysis that a mission could be separated into a number of closed-loop excursions. Thus, a figure eight mission with LEM at the center would comprise two excursions or loops. The number of beacons required to give various degrees of LOS coverage was investigated therefore on a per/loop basis. Figure 6-12 shows a typical loop, assumed circular. The LOS from LRV to LEM is shown, as well as the coverage attained with a single beacon. Figure 6-13 shows the number of beacons required for a given loop coverage. For a loop diameter of only 10 km, LOS exists to LEM 73% of the time even without a beacon. The addition of one beacon at ground level in the region of maximum LRV-LEM separation will afford complete coverage.

If the loop diameter is extended to 100 km, the coverage with no beacons drops from 73% to about 6%. Each ground-level beacon will cover 10 degrees of the loop. Complete coverage of the loop requires 34 beacons.

For a 10 meter tower-mounted beacon, complete coverage requires 15 towers per loop. Even if the tower height is extended to 100 meters, complete coverage requires 7 towers, representing considerable mass regardless of tower design.

From Figure 6-13 it appears that the use of towers offers an impractical solution to the problem of short LOS. The contribution to the navigation problem is minor except for a large number of towers. Also, the penalty paid for this contribution would be severe in terms of weight and erection time. The feasibility of designing a tower of great height, light weight, and with ease of erection by a space-suit clad astronaut has not been investigated.
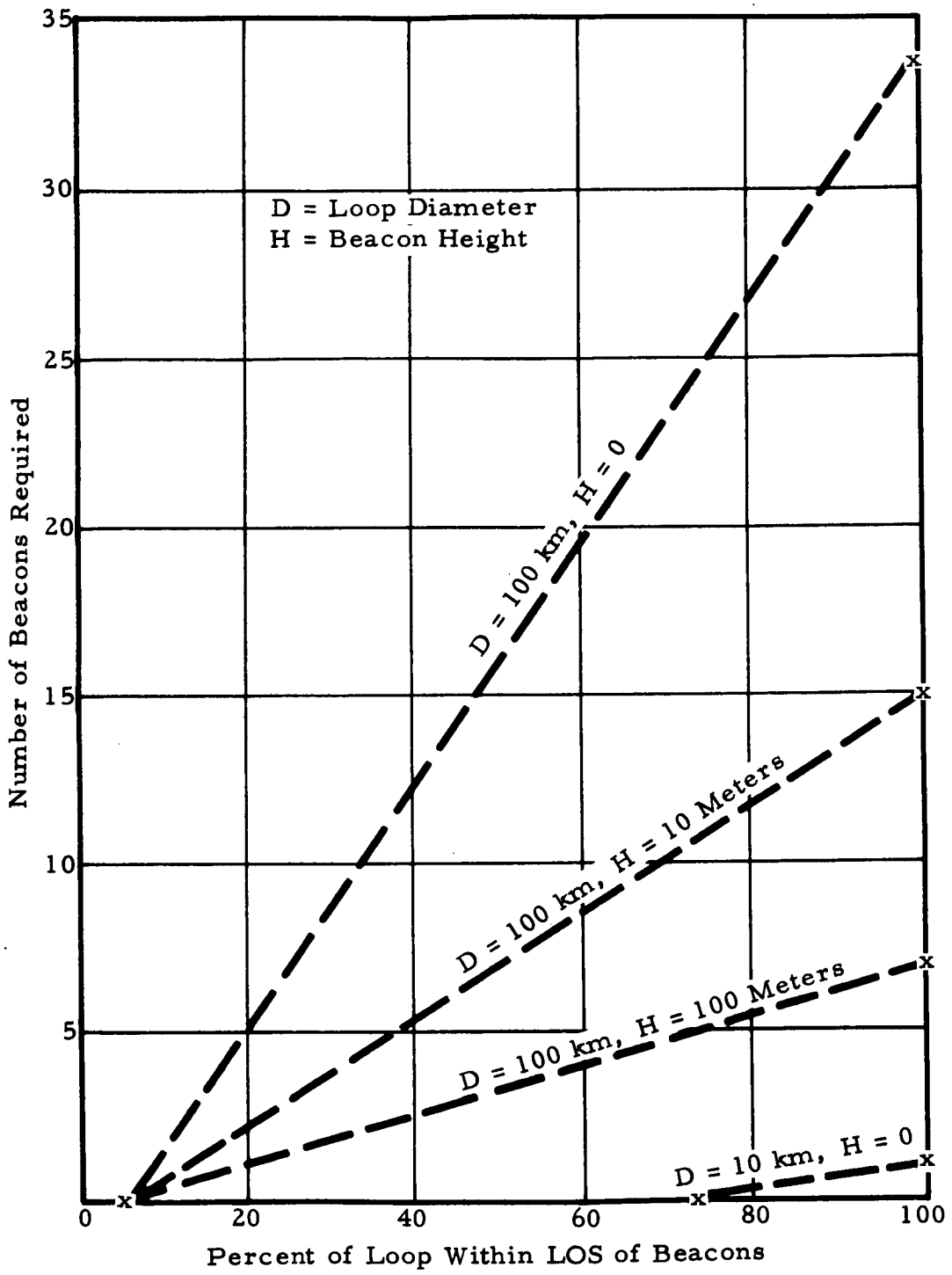
Figure 6-13 Loop Coverage vs Number of Beacons

The curve of L = 100 meters, D = 100 km (Figure 6-13) may also be interpreted as follows: the 100-meter beacon altitude is applicable as well to a beacon mounted at a 100-meter elevation. Thus, seven such elevations would be required during a 100 km diameter loop if surface elevations rather than towers were used. Although the probability of finding seven such elevations within a given lunar area is beyond the scope of the present contract, it would appear that the probability is low.

6.1.3 Dead Reckoning

Some possible techniques in dead-reckoning of the LRV are summarized in Reference 67. A dead-reckoning system consists basically of vertical reference, heading reference, distance or velocity sensor, and position computer. The item of interest here is the distance or velocity sensor. Five techniques are listed in Reference 67.

1. Fifth Wheel

2. Radio Doppler

3. Accelerometers

4. Infrared Chaining

5. Standard Vehicle Odometer.

This report is a state-of-the-art (1960) survey of equipment and techniques and should, therefore, provide a fairly reliable information source.

Odometer systems employing a fifth wheel have accuracies of 1/1000 to 1/3000 but attainment of these accuracies requires frequent position checks, highly skilled operators, or frequent calibration. Thus an accuracy closer to 1/100 might be expected under more realistic conditions.

The survey report did not present data on RF doppler systems.

Systems employing accelerometers exhibit errors which are time-dependent and therefore inherently unsuited for long missions. Hybrid systems, however, employing monitoring by a sensor in which any errors are distance-dependent may well be quite attractive.

Infrared chaining as a technique of distance or velocity sensing is in the development stage. It is postulated[42] that a unit of this type might replace or act as a calibration standard for odometers. The two approaches of infrared chaining are passive and active techniques. The passive system, consisting of two IR detectors and correlation circuitry, determines distance as an integrated velocity measurement. The active unit, consisting of an IR transmitter, detector, and correlation circuitry, measures distance directly. Since uncertainties in terrain thermal conductivities and uncertainties in the terrain directly affect system performance, it is suggested that an odometer might provide back-up sensing capabilities. No accuracy data were reported.

Systems employing a vehicle odometer have accuracies ranging from one part in 100 (1/100) up to 1/1000, although the latter requires ideal conditions.[67] The 1/100 figure is more typical.

During Bendix Systems Division's Phase I study of the Surveyor LRV Program various methods of mechanically measuring distance were considered, including monitoring of the traction drive speed and releasing calibrated lengths of wire. These methods generally suffer from inaccuracy, high complexity, and low reliability. The method selected for direct distance measurement was to use a wheel-type odometer. Positioning of the wheel on the vehicle must take into account the possibility of impeding vehicle motion as well as the accuracy of the wheel in various locations. A noncontacting type of readout is desirable for reliability of the odometer. It was estimated that an accuracy of 2% of the distance traveled could be achieved with the wheel-type odometer. The greatest problem to be dealt with is the reduction of error due to wheel slippage.

Aviation Electric of Montreal produces a land navigation set for military vehicles which incorporates an odometer drive plus a gyro compass for heading. Overall system accuracy of 1% of the distance traveled is claimed based on a compass error of 0.75° (Ref. 110). The exact type of terrain over which this accuracy can be maintained is not stated. Since a lava-flow type of terrain is quite probable for a lunar vehicle and quite improbable for a military vehicle, it is reasonable to assume that the error on lunar terrain would be somewhat above 1%. It might be that an odometer is used only for long flat traverses over smooth terrain. Fixes would be used after travel over rough terrain to redetermine position.

The great majority of the systems surveyed are used in the military area and data presented were in most cases for travel over some undefined type of terrain. Without defining these test course terrains, and possibly conducting further testing, the relation of the expected lunar odometer system accuracy to the above quoted earth odometer system accuracy is uncertain. This may indicate a requirement for periodic calibration of an odometer system or more frequent position fixes.

6.2 NAVIGATION COMPONENTS

6.2.1 Local Vertical Sensors

Sensing of the local vertical must be investigated for both static and dynamic conditions, since techniques suitable for static application may be entirely unsuitable in a dynamic environment.

Indication of the local vertical may be accomplished in several ways, all of which are dependent upon the position of a mass under the influence of the gravity field. The simplest leveling device is the bubble level which allows a quick visual leveling of a single axis. Two levels mounted orthogonally and aligned normal to the gravity vector will serve to indicate the vertical. In its simplest form, the bubble level may be used as a coarse adjustment to the vertical, or may serve as a visual monitor to the proper operation of a more accurate leveling system[124]. Kearfott has employed a pair of electrolytic levels in a two-axis instrument. The device consists of a glass vial partially filled with a conducting fluid. Three electrodes are mounted in a bridge configuration such that in a null position the resistance from the center tap to each leg is equal. Tilting about the sensitive axis increases the resistance in one leg while decreasing it in the other leg. Vertical accuracy of ±3 arc minutes can be achieved with the instrument. The instrument is, however, sensitive to horizontal acceleration and an error of 1 deg of arc exists per 0.018 earth g's of acceleration.

A pendulous device will also serve to indicate the vertical. Humphrey, Inc. produces a pendulous device with potentiometer pickoff for which the following accuracies are quoted for lunar surface:

0.1 deg up to 5 deg tilt

0.2 deg up to 15 deg tilt.

These limits, however, suffer from high cross-axis sensitivity.

The final vertical sensing technique is the use of a pair of orthogonal accelerometers which are leveled by nulling out the components of gravity along their sensitive axes. A floated pendulum accelerometer under development by Minneapolis-Honeywell, when used in pairs for a two-axis inclinometer, will provide a vertical accuracy of ±10 arc seconds. During periods of dynamic operation, the leveling error dead-spot would be increased to ±1.0 degree[124].

The accuracy of these sensing devices, being dependent primarily upon a given null uncertainty of the device, will differ in earth and lunar gravity fields. Generally speaking, disregarding the changes in forces acting within the instrument itself, these instruments will be less accurate on the moon than on earth. The quantity being sensed is $g \sin \theta$ in which θ is the tilt angle from true vertical. The tilt angle required to attain a given gravitational acceleration level will be approximately six times as great on the moon; thus the instrument error will be six times as great.

The particular technique evaluated in any application is, of course, basically dependent upon the vertical accuracy required, both in the static and dynamic modes. It is quite possible that an accurate continuous vertical would not be required. Rather the vertical would be erected accurately only during periods of position fixing in a stationary mode. A gyro system could then serve as reference between fixes. Therefore, the requirements upon local vertical knowledge must be known in both static and dynamic states in considering alternate methods of implementation.

As part of the requirements, it might also be stated not only how accurate the vertical must be known but how reliable the system must be. Thus, both redundancy in identical vertical indicators must be considered, as well as the use of multiple types of indicators as backup to the prime indicators.

The vertical indicator must also be capable of withstanding launch, translunar, lunar landing, and lunar surface environments from the standpoints of vibration, incident radiation, and temperature.

6.2.2 Radar Velocity Sensor

The determination of the ground speed of a moving vehicle using the doppler effect depends upon measuring the frequency difference between

the transmitted signal and the signal returned from scattering objects which lie within the illuminating antenna beam. Doppler difference frequency is proportional to the orientation of the antenna beam(s) relative to the vehicle and to the ground, the wavelength, and the vehicle speed.

Figure 6-14 illustrates the case for an antenna beam central axis directed out in front of a moving vehicle and lying within the vertical plane passing through the vehicle longitudinal axis.
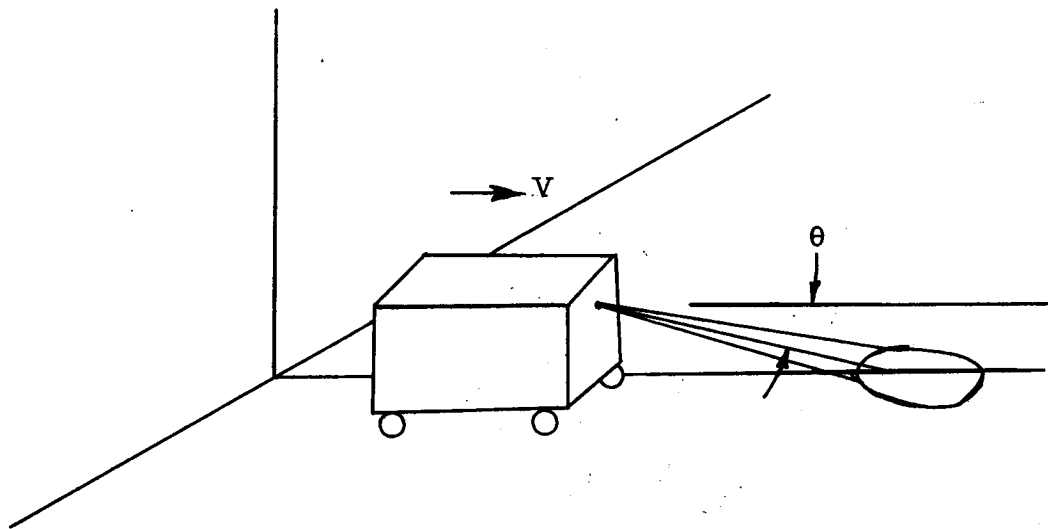
Figure 6-14 Radar Antenna Beam

The frequency of the doppler signal is given by the relationship

$$f_d = \frac{2V}{c} (\cos \theta) f_o$$

where

        V   = velocity of vehicle

        c   = velocity of light

        θ = depression angle

        f_o = carrier frequency.

The quantity f_d, in reality, contains a band of frequencies since the antenna beam is not infinitely narrow.

A sample calculation assuming typical values of

θ = 30 degrees

V   = 5 miles per hour

f_o = 10,000 megacycles/second

yields a doppler frequency of only 127 cycles per second.

Frequencies of this order are measurable using CW heterodyne radars such as those employed by police traffic speed enforcement personnel. In fact, tests have been made using a typical speed trap radar to measure the parent vehicle's own speed. In this mode of operation, the received radar energy is that energy backscattered from the surface of the road as the vehicle is driven down the road. Such tests have been carried out at an automobile manufacturer's proving ground. Information regarding the accuracy obtainable in measuring one's own speed is not immediately available. Police radar equipment housed in a police car and used for the measurement of the speed of other vehicles is ordinarily accurate to 1 mile per hour over the range from 10 mph to 100 mph. The measurement of speeds of less than 10 miles per hour is quite possible using this CW heterodyne technique.

Range capability of such equipment varies from a few hundred feet to 2000 or more feet. This type of equipment operates at 3 centimeter wavelength, 5 degree antenna beamwidth, weighs about 15 to 20 pounds, consumes 20 to 30 watts of power, and occupies less than 1 cubic foot of volume.

Noncoherent detection of the doppler effect, as is used in some groundbased and airborne side-looking moving target indicators, does not seem promising. Airborne side-looking MTI radars illuminating the ground detect the "beat" or phase difference between a moving target and the "stationery" ground clutter and are not ordinarily concerned with measuring platform velocity. The ground clutter appears nearly "stationary" only when observed at right angles to the aircraft ground track.

Ground based MTI radars see all "ground" objects as stationary (neglecting antenna scanning and wind effects) and hence again detect the "beat" between fixed and moving ground targets. In the case of an MTI radar looking forward (or backward) from a moving ground vehicle, all reflecting objects in the antenna pattern are moving at different speeds with respect to both the vehicle and each other. For this reason it is likely that a number of targets would appear to be "moving" and the frequency spectrum is consequently "smeared". This situation would likely cause considerable confusion and does not seem a reasonable approach to determining vehicle ground velocity. Typical airborne doppler navigators do work very well in measuring aircraft speed but the doppler frequencies involved are measured in terms of many kilocycles per second.

An RF doppler velocity measuring system mounted on a ground vehicle is handicapped, in addition to very low speeds, by the antenna side lobe responses. These responses may tend to broaden the envelope of doppler return, especially if large or good reflecting masses exist in the area of the moving ground vehicle. Range and/or velocity gating could be used as an aid to discriminating against some, or most, undesirable reflecting objects. For remote operations, however, it adds another undesirable variable.

Other sources of possible error induced are due to pitch, roll, and yaw of the vehicle while traversing the ground surface. Either the antenna or system data would require stabilization if short time constant readout is required. Stabilization might not be required if relatively long term data smoothing is acceptable.

Velocity can also be deduced by measuring rate of change of range from the vehicle to a certain scatterer (knowing also the antenna pointing angles). This method of obtaining vehicle speed is feasible and likely to work satisfactorily.

Equipment size, weight, and power consumption for a simple radar system capable of ascertaining vehicle speed is estimated at 1/2 cubic foot and 25 pounds, exclusive of the antenna and any space stabilization components.

Power consumption is estimated at but a few watts. The capability of such a radar is limited to a range of a few hundred feet to perhaps a few thousand feet; depending largely upon the target surface backscattering properties.

For reasons of equipment complexity, reliability, size, weight, power consumption, and antenna pointing requirements, the employment of the radar technique for determining vehicle speed is not recommended for use in the forseeable future.

6.2.3 Lunar Marker Materials Survey

A preliminary survey has been made of the materials and techniques which may potentially be employed for creating passive markers on the lunar surface. A literature search has shown that little work has been performed or reported on the lunar environmental effects which may be encountered. In this section several materials are discussed which may be feasible; the relative merits of each are indicated.

6.2.3.1 Discussion

Lunar markers or beacons utilizing radiation in the visible or near-visible portions of the spectrum must be designed specifically to suit the various tasks of interest. Thus, simple path markers, survey tie points, and beacons providing range information all require different optical characteristics. The basic techniques and pertinent materials are tabulated in Table 6-3.

An example of the dependence of marker design on specific task and method is the choice of a specular or diffuse marker. To obtain an omnidirectional capability, a sphere, hemisphere or polyhedron shape is required. The type of optical surface depends on the manner in which the orbiting vehicle (or ground vehicle) approaches the marker. For the same normal albedo, and a single collimated source of illumination (sun or earth), a Lambertian (perfectly diffuse) surface is brighter than a specular surface for certain positions, while the opposite is true for other positions. If the angle of observation, α, is defined as the angle between the source-target line and the observer target line, the ratio of the luminance of a specular sphere to that of a diffuse sphere is given by

$$\frac{B_s}{B_d} = \frac{3\pi}{8} \ \frac{1}{\sin \alpha + (\pi - \alpha) \cos \alpha}$$

assuming they have the same size and total albedo. This is illustrated in Figure 6-15. The significance of this relation is that the brightest target

TABLE 6-3

OPTICAL TECHNIQUES AND MATERIALS FOR LUNAR BEACONS

Basic Technique	Type	Possible Materials	Advantages	Possible Disadvantages
Coatings	Retroreflective	Glass beads Scotchlite	Moderately directive (145) strongly retrodirective	γ-ray discoloration (131) particle, UV degradation (130) polarization effects (129) temperature effects (137)
	Diffuse (146, 147)	$M_g o$	The basic diffuse reflectance standard– highest reflectance (133)	Available only as film, inferior to barite in diffuseness, stability
		$BaSO_4$	highly stable, closer to Lambertian than $M_g o$ (139, 140)	
		$MgCO_{2-3}$	can be prepared in bulk form	
		TiO Porcelain enamel Vibrolite glass		
	Specular (146, 147)	Al	Best broadband reflectance highest of all metals (132, 138) very stable	Has near IR absorption band, 8250° (135, 136) UV degradation (needs protective covering) (134)
		Ag	Highest reflectance in most of visible region (143, 147)	more sensitive than Al, less stable in the atmosphere
		Au Cu Steel		very low reflectance up to $5000\overset{o}{A}$ low reflectance relative to above metals (146, 147)
		Ti	Very stable metal	Little data available, has low overall reflectance, similar to steel (147)
Structures	Retroreflective Elements	Polyhedra with internal corner reflectors	Strongly directive, can be made in variety of sizes and shapes, can control width and off-set of return beam (142)	Polarization effects (129)
	Autocollimator Elements	Individual optical systems	Strongly directive, can control width and off-set of return beam	Adjustment affected by temperature cycling, glass and metal film degradation by UV, γ-ray (130, 131)
Sources	Constant intensity sources	Electroluminescent panels		
	Pulsed sources	Xenon strobe lamp		Requires power (148)
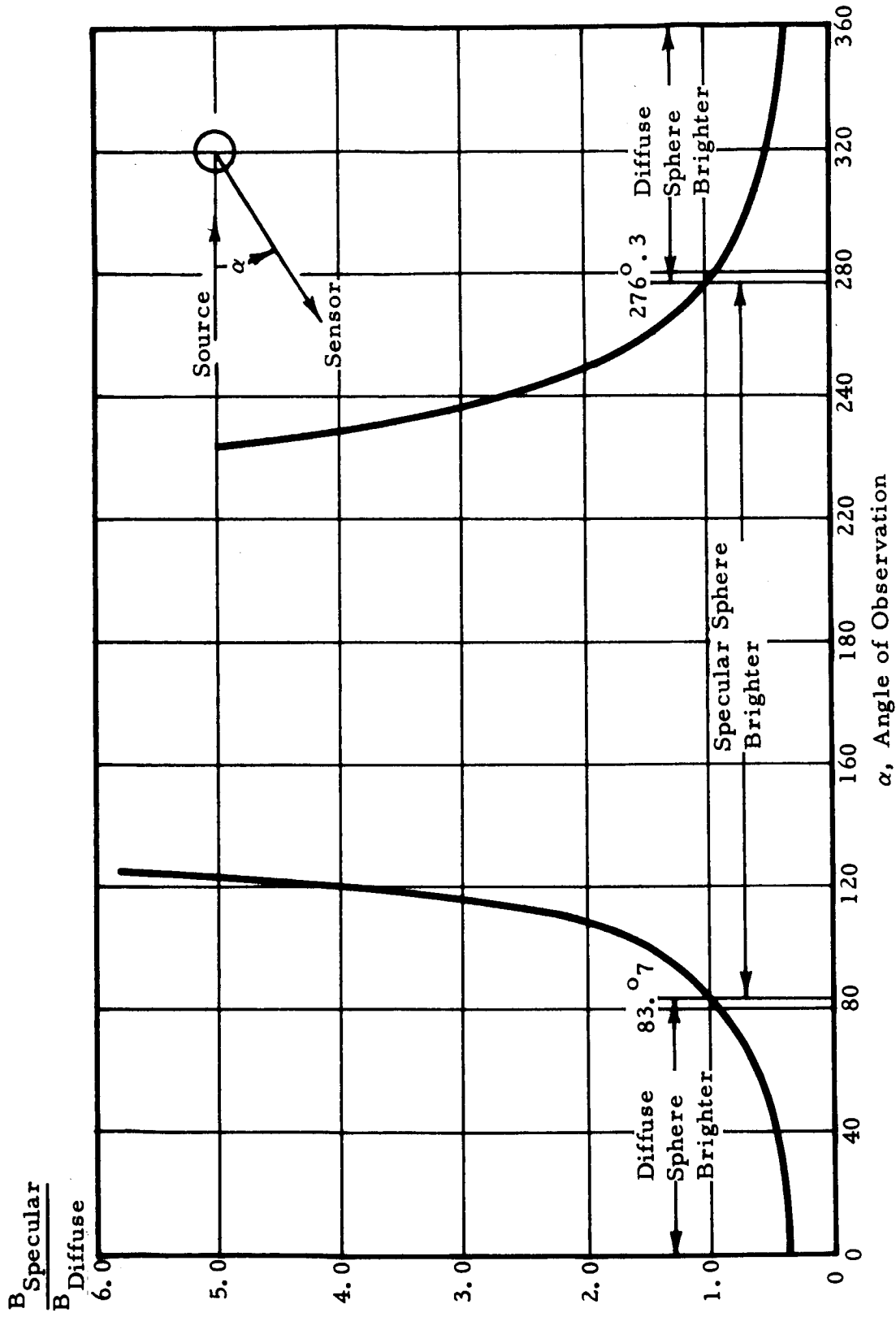
Figure 6-15   Ratio of Luminance of a Specular Sphere to That of a Diffuse Sphere as a Function of Angle of Observation

(with the highest probability of detection) is the diffuse sphere for angles of approach where $|\alpha| \leq 83.7^\circ$, but is the specular sphere for $|\alpha| > 83.7^\circ$. Thus if the mission is such that the vehicle always approaches the marker with the sun behind it, the diffuse sphere will give longer visibility ranges and probability of detection. However, if the vehicle can approach the marker from directions at right angles to the sun direction, or looking into the sun, the specular sphere can produce much higher visibility ranges.

6.2.3.2   Laser Ranging

This technique is feasible for making range measurements on the lunar surface. The best type of target is a retroreflective element (corner reflector or autocollimator) array. The laser ranging technique has been proved feasible for use during the terrestrial day, over paths up to 5 kilometers. Since the general photometric background luminance during terrestrial daytime is even higher than during lunar daytime, this technique can be considered feasible for lunar operation over equivalent path lengths. Portable instruments (presently weighing about 30 kg) have design ranges up to 50 km.

Space-related ranging programs have demonstrated long range capability. The BE-B (Wallops Island) experiment, using an omnidirectional retroreflective array to return a beam from a ground-based laser, has been successful.

6.2.3.3   IR and UV Illumination

The use of IR or UV illumination has some advantages if artificial sources are required. The one major disadvantage of these techniques is that the observer cannot see the beam or the illuminated area without using some type of image converter system. The primary advantage of using UV or IR radiation is that the solar background which peaks at approximately 5000 $\overset{\circ}{A}$ is reduced, which increases the target-to-background contrast. The UV region is superior since the lunar spectral reflectance is lower in the near UV than anywhere else in the IR region, out to 1 micron, which also improves the target-to-background contrast. The near IR has the highest reflectance, but the increase is small, on the order of 10 to 20% over the visible reflectance, so unless this is a critical factor, IR is not ruled out.

6.2.3.4   Factors Affecting Beacon or Marker Performance

   1.   UV, γ-ray and particle irradiation cause degradation of metallic films, glasses and mineral structures. This degradation can involve decreasing the albedo, changing the spectral reflectance, or changing the angular reflectance.

   2.   Temperature cycling can cause degradation of the material. Temperature variations can produce variations in the reflectance of both metals and non-metallic materials. Also structural alterations can occur for a temperature range of 95° K to 400°K.

   3.   High vacuum (10^{-12} atmospheres) may affect performance.

All of these effects may be significant, and there is little experimental data available concerning them.

6.2.3.5   Conclusions

Tentative conclusions are that for path marking or angular position survey purposes, an omnidirectional specular reflecting sphere or hemisphere is best, and for range finding or homing-in purposes, the corner-cube retro-reflector is best. The use of IR or UV illumination enhances the contrast but requires more complex image converter sensors since the unaided eye is not sensitive to these regions of the spectrum.

6.2.4   State-of-the-Art Navigation Component Performance Data

Data received from vendors in response to inquiries on state-of-the-art navigational component performance data are tabulated in Tables 6-4 through 6-12.

The accuracy data, unless specifically stated by the manufacturer, were interpreted as 1 σ and converted to 3 σ. All g parameters are lunar g's.

The range of component accuracy values used in analyzing the performance of the components in the three specified systems is summarized in Table 6-13.

TABLE 6-4

ACCELEROMETER PERFORMANCE DATA

Source	Type (P: Pendulous, A: Axial, VM: Velocity Meter)	Threshold (lunar μg, g ≈ 162 cm/sec²)	Non-Linearity (g ≈ 162 cm/sec²)	Null Stability (lunar μg, g = 162 cm/sec²)	Cross Axis Sensitivity (g/g)	Range (± lunar g, g ≈ 162 cm/sec²)	Weight (Earth pounds)	Status (P-Prod., D-Dev.)
Bell Aero-Systems	P	6	0.0003	900	3×10^{-5}	600	0.77	P
	P	1.2		18	15×10^{-4}	900	0.6	P
	P	6		1800			0.4	P
	P-VM	360	Drift 0.25 μ g/g/Hr	1	30×10^{-6}	900	4.5 (BF) 2.3 (Plat)	P
	P-VM	540	Drift 0.25 μ g/g/Hr	3	30×10^{-6}	900		D (by 1965)
	A-VM	Class.	Class.	Class.	Class.	6×10^{-5} -30 6×10^{-9} -6×10^{-4}	3.0	P
Edcliff	A	1800	0.039		0.015	3.0-300	1.0	P
Eclipse-Pioneer	P-VM	18						P
Fairchild	A	6750	0.015		0.15	600	0.31	P
	P		0.006		0.04	1.5 → 300		P
Giannini	A		0.023			12 → 300	0.63	P
	P		0.08			12 → 150	0.14	P
Kearfott	P	3.6	2.5×10^{-6}/g	540 Long Term 0.0083°	0.0003	60	0.25	P
	P	1.2	2.5×10^{-6}/g	Short Term 0.0017°		360	0.25	P
	VM (Accel. Integ. Gyro)	1.0	10^{-6}	90	0.8×10^{-5} rad/g	120	0.7	D (by 1965)
Litton	P	10.0	2.5×10^{-5}/g			90	0.44	P
Palomar	P	360	0.0006		0.006	1	0.62	P

TABLE 6-5

IR EARTH TRACKER PERFORMANCE DATA

Source	Program	Null Accuracy Deg - 3σ	Scale Factor Accuracy o/o	Suitable Targets E - Earth M - Mars V - Venus	Target Subtense or Range Deg or Km	FOV Deg	Spectral Pass Band μ	Weight Earth Pounds
ATL	Gemini	0.3	5	E, M, V	92 – 3700	1.5 x 1.5	8-18	9.9
	OGO (2 trackers)	0.3	4	E	92 – 406,000	1 x 1	8.5-20	13.2/4.5
	Lunar and Planetary Horizon Sensor (Developmental)	0.3	10	E, M, V (Moon)	$12 – 180^{\circ}$ $6 – 12^{\circ}$			9.5
Barnes	Mariner A	0.3/0.08 (Test) 0.03 (Electronic)		E, M, V	$2 – 52^{\circ}$	0.5 x 0.5 in 70	8-14	
	For JPL, Mariner A Prototype	0.3		E, M, V	$2 – 70^{\circ}$	0.5 x 0.5	10	
GE/MSVD	Advent	0.6 (Des) 1.2 (Test)		E			12-30	
Honeywell/Aero	Proposed	0.3		E			6-20	
	LG 61A	0.75						
JPL	Transit for APL	0.3		E	1110		12	
	Ranger 1 ... 7	0.3	5 (of ang diam)	E				2.6
	Mariner II	0.1 (roll) 0.25 (hinge)	10	E	1.6×10^{6} 60×10^{6}	4 x 10		6.2

TABLE 6-6

GYRO PERFORMANCE DATA

Source	Type	Gyro Drift Rate	Gyro* Accuracy 3σ	Pickoff Accuracy 3σ	Null Accuracy 3σ	Weight	Status
	VG: Vertical Gyro DG: Directional Gyro RIG: Rate Integrating	Deg/hr	1. Random Drift deg/hr 2. Mass Unbalance $^\circ$/Hr/g 3. Anisoelastic $^\circ$/Hr/g^2 (g ≅ 162 cm/sec^2)	Deg	Deg	Earth pounds	P: Production D: Developmental
Aeroflex	VG (with pend V sensors)	15		0.0025 0.10	0.05 0.0083	5.7	P
American Gyro	2 DF Floated Displacement	6.0				8.4	P
	2 DF Floated, Miniature	15-30		0.6		1.8	P
	2 DF Non-Floated Sub-miniature	15				1.2	P
	2 DF Floated	30				4	P
American Bosch-Arma	DG		1: 0.75				P
Eclipse-Pioneer	DG		1: 3.0			7.6	P
	Air Bearing		1: 0.15				P
GE Ordnance	2 Axis Restrained Cryogenic (platform)		1: 0.016 (Present) 1: 0.0003 (Goal)				D (by 1968) (by 1970)
Kearfott	2 DG - DG	30				9.2	P
	VG	30		0.5	0.4	3.5	P
	VG	1.6		0.2	0.37	9.3	P
	VG	18		0.5	0.75	5.5	P
	VG	18		0.5	0.15		P
	RIG - SDF Floated (Platform)		1: V = 0.06 Az = 0.09 2: 0.1 3. 0.0008			0.8	P
	RIG - SDF Floated (Platform)		1: V = 0.015 Az = 0.09 2: 0.1 3: 0.0008			0.8	P
	RIG-SDF Floated (KING)		1: V = 0.009 Az = 0.045 2: 0.075 3: 0.0008			1.0	P
	RIG - SDF Ball Bearing		1: 0.75 1: 1.0			2.8 2.2	P P
Litton	2 DF - Floated		1: 0.03 2: 0.04 3: 0.0032			2	P
Norden	RIG - SDF Floated		1: V = 0.021 Az = 0.06 2: 0.15 3: 0.0016 1: Day to Day V = 0.12 Az = 0.3			.84	P
	RIG - SDF		1: 2.2 3: 0.016			< 1.0	P

*All g sensitive drifts converted to lunar g's

TABLE 6-7

GYRO STABILIZED PLATFORM (ATTITUDE REFERENCE) PERFORMANCE DATA

Source	Type	Gyro Accuracy deg/hr ($g \cong 162\,cm/sec^2$)	Vertical Accuracy Deg - 3 σ	Pickoff Accuracy Deg - 3 σ	Weight Earth Pounds	Life k hr.
Aeroflex	Inertial Vertical Reference		0.15 (Dynamic) 0.075 (Schuler amp)	0.3 or 0.15	22	
American Gyro	2-2 DF Floated or Non-Floated Gyro	36	0.15		16	1
Kearfott	3-Gyro, 2 Mercury Bubble Switches, 4 Gimbal	19	0.3	Az: 0.25 & 0.15 r: 0.25 r: 0.25 P: 0.25 & 0.15	25.5	
Nortronics	3 Gyro	0.15 (Rand) 6/g (Mass) $0.3/g^2$ (Aniso)	0.3 (Align) 0.3 (Caging)	1.2	20	

TABLE 6-8

INCLINOMETER PERFORMANCE DATA

Source	Type	Threshold Deg - Max	Null Repeatability Deg - 3 σ	Range Deg	Life K hr	Weight Earth Pounds
Edcliff	Pendulous - Single Axis	0.3		5-70		0.5
	Pendulous - Dual Axis	0.15		5-45		2
	Pendulous - 2 DF	El: 0.5 Az: 1.0		El: 5-60 Az: 355		3
Kearfott	Pendulous - Dual Axis	0.00028	0.00084	0.05	1	0.2
	Pendulous - Dual Axis	0.0014	0.0011	0.3	1	
	Pendulous - Dual Axis	0.00014	0.00056	0.33	1	
	Pendulous - Dual Axis	0.0020	0.067	0.75 - 1.4	1	
	Pendulous - Dual Axis	0.00084	0.025	0.75 - 1.0		

TABLE 6-9

INERTIAL PLATFORM (GYRO AND ACC) PERFORMANCE DATA

Source	Type G: Gyro A: Accelerometer Gy: Gimbal	Gyro Accuracy - 3σ 1: Random Drift °/Hr 2: Mass Unbalance °/Hr/g 3: Anisoelastic °/Hr/g² (g ≈ 162 cm/sec²)	Accelerometer Accuracy - 3σ 1: Null - lunar g 2: Linearity 3: Scale Factor 4: Range - lunar g (g ≈ 162 cm/sec²)	Pickoff Accuracy - 3σ Deg	Weight Earth Pounds	Life K hrs

Kearfott	Az, & Vert Ref 3G, 2A, 4Gy	1: Az = 2.7
		   P = 1.5
		   r = 1.5
			1: 3.0×10^{-7}
			2: 0.0002
			3: 0.0001
			4: ±48
				0.3	34	

	Az & Vert Ref 3G, 3A, 3Gy	1: 1.0	1: 3.6×10^{-7} 2: 0.8×10^{-6} g/g² 3: 0.0003 4: ±120	Az: 0.15 P: 0.5 r: 0.5	30	

	3G, 3A, 4Gy	1: Az = 0.045
		   P = 0.009
		   r = 0.009
			1: 3.6×10^{-7}
			2: 0.8×10^{-6} g/g²
			3: 0.0003
			4: ±120
				Az: 0.15
				P, r: 0.05 P r <15°
					14	

	Heading & Vert Ref 3G, 2A	1: Az = 0.75
		   P = 1.5
		   r = 1.5
			1: 1.8×10^{-4}
			2: 0.0005
			4: ±6
				Az: 0.15
				P: 0.15, 0.33
				r: 0.15, 0.33
					29	

Litton	*2-2DF Gas G, 3 Pendulous A	1: 0.003 2: 0.005 3: 0.0002	1: 3.6×10^{-5} 4: ±120g		15	10
	2-2DF Floated G	1: 0.03 2: 0.04 3: 0.003	1: 1.8×10^{-4} 2: 5×10^{-5} 3: 5×10^{-5}		30	
Nortronics	3G, 3A, OGy	1: 0.15 2: 0.5 3: 0.003	1: 1.8×10^{-4} 4: ±30	0.3	27	1

*Production in 1965

TABLE 6-10

STAR TRACKER PERFORMANCE DATA

Source	Program or Type	Accuracy Deg - 3σ	Minimum Visual Magnitude m_v	Design Star	FOV i = Inst FOV Deg	Sensor P - Photomult I - Image Dis	Life K hr	Weight Earth Pounds	Status P - Prod Q - Proposed
Aeroneutronic	Narrow and Wide FOV		2.5 (Wide) 5.0 (Nar)		10-0.125 Tr 20-0.5 Acq			5, 7	P
Barnes (JPL Design)	Single-Axis	0.3	+4.5	Canopus	2 x 16 i-0.9 x 10	I		6.3	P
	Single-Axis	0.021	-0.9	Canopus	1 x 20	I	137	8.5	Q
	Two-Axis	0.0083	+1.5		16 x 16 i-1 x 1	I			
Eclipse-Pioneer	OAO Back-Up	0.0025 (Null)	+2.5		0.33	P	12	14.5	
	SOA	0.00056 (Electr) 0.0053 (Total Tracker) 0.0083 (Readout) 0.012 (Total)							
	Single-Axis	0.0075	+3.0		5, 0.5	I			P
Honeywell	Passively Scanned	0.06	+3.0		6 x 6	P	35	20	P
	Quadrant Mult	0.017	-0.9	Canopus	i-2 x 2	P	133	6	P
ITT Fed Lab	OAO	0.0042	+3.0	Canopus					P
	Lunar Orbiter	0.012	-0.9	Canopus					Devel
Kearfott	Miniature (Optical Readout)	0.0025	+2.2		0.25 x 0.5	Photocell			Prototype
Marquardt	Solid State Detector	0.0075	+7.2		2.5	Solid State Grid			Devel
		0.0020 (Goal)			10				Future
Santa Barbara Research Center	Surveyor	0.3	-0.9	Canopus	4 x 5		0.066	4.9	P
	Daylight Tracker	0.0083	2.5						P

TABLE 6-11

SEXTANT PERFORMANCE DATA

Source	Type	Accuracy (deg - 3 σ)	Conditions	Status
Keuffel and Esser	Mark II	0.025	Well defined real horizon	Production
	Mark III	0.010	Real horizon, or artificial horizon of air driven gyro mounted to sextant frame	Prototype - by 1965
Martin	Tri-Sextant	0.05		Prototype
Kollmorgen	Periscopic Theodolite	0.0017 0.012	Body-fixed	Production

TABLE 6-12

TIMER PERFORMANCE DATA

Source	Type	Accuracy hr/hr - 3 σ	Weight Earth Pounds	Note
Bulova	Accutron	0.00005	≈ 0.0015	Significant increases in accuracy are not expected for two years
Eagle Signal Co.	Transistorized-RC	0.005	0.25	
—	Spring-Wound Marine Type Chronometer	0.00003		
—	LORAN, Quartz Crystal Oscillator	3×10^{-10}		
—	Molecular Clock	3×10^{-13} Long Term 3×10^{-9} Short Term		
—	Cesium - "Atom Chronometer" Molecular Clock	3×10^{-11}		

TABLE 6-13

COMPONENT PARAMETERS

Parameter	Suggest Parameter Range (3σ)	Nominal Value	References
Azimuth Ref.	Alignment: 0.1° to 5° Drift: 0.005°/hr to 5°/hr		Component vendors
Odometer Error	0.1% to 10% of distance traveled	1% of distance traveled	Telecon with US Army Mobility Command, Ft. Belvoir, Va.
Vertical Sensor	10 to 160 arc sec	0.01°	102 arc min, 26 June 64 Coordination Meeting at MSFC (12 arc sec feasible in lunar gravity environment with state-of-art accelerometers)
Star Tracker or Periscope Sextant	2 to 120 arc sec	0.01°	"Working Paper" NSL E30-8, June 1964 or Task Order N-21, Vendor data
Timer	0.01 to 10.0 sec	0.1 sec	"Working Paper" NSL E30-8, June 1964 on Task Order N-21 and well within state-of-art
Ephemeris	3 to 120 arc sec	0.01°	"Working Paper" NSL E30-8, June 1964 or Task Order N-21 and "Selenographic Coordinates" Kalensher, JPL #32-41.
Earth Tracker (IR)	1 arc min to 1 deg	0.2°	6 arc min state-of-art from vendors
Earth Tracker (RF)	6 arc min to 2 deg	0.1°	Depends upon correction for earth station location
Platform Null Error	2 arc sec to 10 arc min	0.1°	(Accelerometer state-of-art)
Gyro Drift Rate	0.01°/hr to 1°/hr	0.08°/hr	
Accelerometer Sensitivity	162×10^{-7} cm/sec^2 to 162×10^{-3} cm/sec^2	10^{-6} g	
Accelerometer Linearity	0.01% to .0001%	0.001%	
Computation Errors	Hand Plot: 0.1 min in ele. (6 arc sec) 0.1 deg in az. (360 arc sec) Computer: Ephemeris data accuracy using digital comp.		Bowditch & Dutton "Working Paper" NSL E30-8, June 1964 on Task Order N-21
Doppler Velocity	0.1% to 10%		Bendix estimate
Hand Held Sextant	10 arc sec to 10 min		12 arc sec in 1965 per vendor

SECTION 7

ERROR MODEL DEVELOPMENT

The symbols applied in the error model development are summarized in a terminology list in Section 7.5, p. 7-132.

7.1 GENERAL ERROR MODEL OUTLINE

The purpose of the model is to permit evaluation of component accuracy requirements and evaluation of total concept performance. The depth to which the statistical analysis should be attempted must be determined.

The method of solution selected should be the most effective and expedient, and should use available information regarding equipment parameters. Above all, the results of the model should be expressible in one quantity-position error, regardless of the type of cost functions or assessment criteria.

Three solutions were examined:

1. Error transient response (Ref. 70)

2. Correlation function method (Ref. 65)

3. Covariance method (Ref. 35).

An error model based on determination of the dependent variable (position error) transient response would not be satisfactory. The necessary forcing functions would be step, ramp, and impulse functions of the forcing functions (gyro drift, star tracker pointing error, etc), which are deterministic representations of statistical quantities. This inaccurate representation and the lack of utility of the transient response information precludes the use of the method. Using such an analysis, a 3σ error measure would be difficult to obtain, and the representation of total system errors would be unclear.

A model based on the correlation function technique is hindered by the complexity of deriving the auto-correlation function. Ref. 65 presents an error model for a vehicular navigation system where position error is calculated as a function of odometer error, heading (gyro-compass) error, computation (mechanical analog) error, and selected paths comprised of arcs and incremental line segments. The analysis is performed in a planar coordinate system and represents positional error as an RSS of component error variance and error sensitivity coefficients. The coefficients and variances are dependent upon auto-correlation functions of the components. These functions have as independent variables path length increments, i.e.:

$$\text{Auto correlation} = \Phi_{XX} (S_1, S_2) \text{ where } S_2 = S_1 + \Delta S$$

where S = path length increment. The velocity vector magnitude was assumed constant.

The analysis performed was rigorous and extensive. However, component data in terms of correlation functions are lacking and would require extensive research; therefore a more straightforward technique would be valuable.

The method selected for the error model base is a variation of the covariance technique. It eliminates many unfamiliar variables, maintains statistical continuity, uses available component information and provides a straightforward approach. The technique implicitly includes the correlation and the transient response methods.

7.1.1 Generalized Model

The generalized error model flow diagram is shown in Figure 7-1.

The dependent variable of the total system is position error $(PE)_T$. The forcing functions of the system are component equipment errors $\epsilon_{i,k}$, which are 3σ values, and $\epsilon_{mi,k}$ which are mission dependent inputs which effect model performance. Further, the transformations T_k, T_i represent the implementation of the geometric sensitivity coefficients, and the quan - tities $\epsilon_{i,k}^*$ are 3σ error measures of basic sensor errors $\epsilon_{i,k}$ transformed through T_i, T_k. This is called in particular instances the geometric dilution of precision (GDOP). The error quantity $\epsilon_{i,k}^*$ is termed the transformed error.

7-2
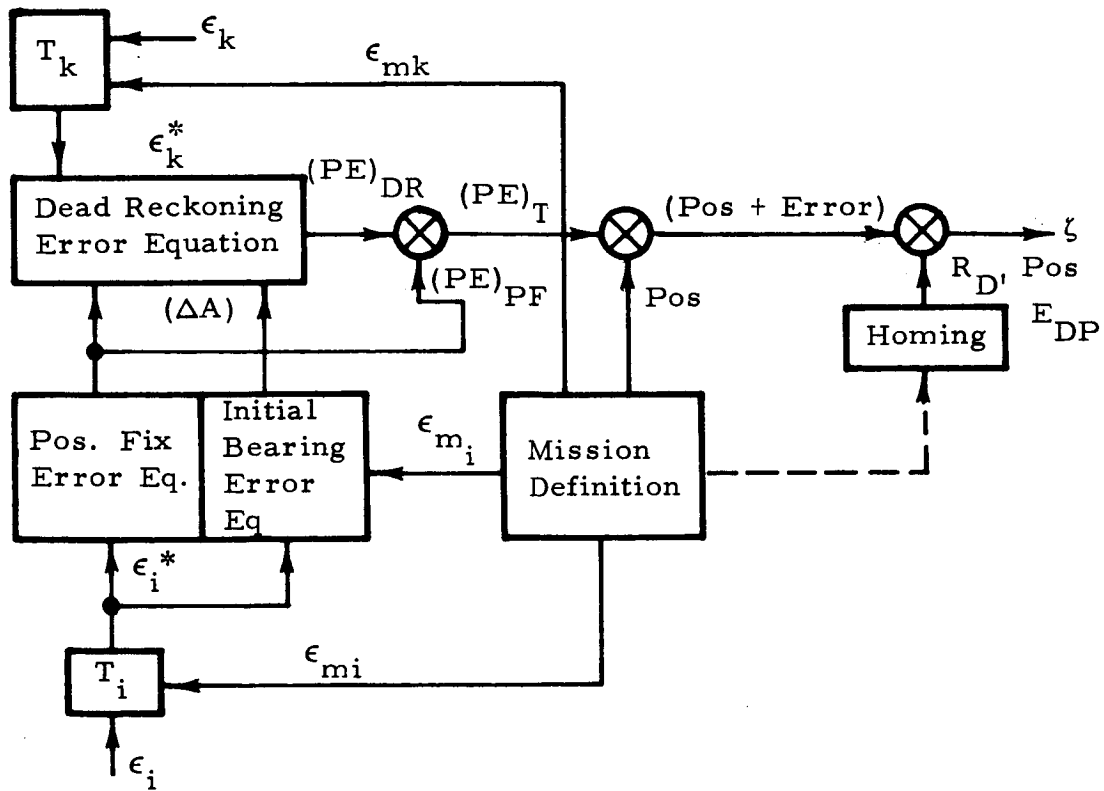
Figure 7-1 Generalized Error Model Flow Diagram

The independent variable is time, t, but not the running time; rather this independent variable is defined quite specifically as an incremental quantity,

$$t = \frac{\text{Distance}}{\left| V_{ave} \right|}$$

where

Distance = incremental distance between mission objectives

V_{ave} = vehicle translational average velocity.

This definition is taken to eliminate transient effects. Actually, the time, t, as defined above is the steady-state value, and the system position error is a function of the steady-state form. The assumption of an average velocity is satisfactory if it is considered that for a particular mission the velocity distribution is gaussian.

The output quantities position fix error $(PE)_{PF}$ and dead-reckoning error $(PE)_{DR}$ are combined to yield a total positional uncertainty $(PE)_T$, an error ellipsoid.

As the vehicle traverses the lunar terrain in a selenographic coordinate system, the vehicle error ellipsoid is translated and rotated accordingly about some mean mission path to the homing coordinates. However, the specific path traveled and the time history in the selenographic coordinates of altitude, latitude, and longitude (R, x, y) are not of explicit importance to the error model. The factors of a particular mission which affect the solution are:

1. Initial coordinates (h_o, x_o, y_o)

2. Final coordinates (h_D, x_D, y_D)

3. Mission distance plus a statistical measure of extra distance traveled for a specific terrain

4. Initial vehicle azimuth plus a statistical measure of the vehicle attitude variation during mission traverse

5. Average vehicle velocity

6. Acceleration distribution caused by vehicle maneuvers and terrain inputs

7. Steady-state variations of vehicle, lunar, and celestial geometry.

The above factors form the mission model.

The homing model is basically a device located at a coordinate position (h_D, x_D, y_D) with some associated detection (rf or optical) range R_D and/or an error in position E_{DR}. These ranges are resolved from the following devices:

1. Passive optical beacon

2. Active optical beacon

3. Lunar landmark detection

4. RF beacon

5. Map indicators.

The values of R_D and E_{DP} are parametric inputs based on a probable range of values.

The comparison of detection range and/or error in destination position with total system position error provides an arbitrary system assessment criteria.

The uncertainties in lunar constants and the relationship to system error are taken into account where the terms appear in the error equations. The nature of the treatment is similar to the equipment error input analysis.

7.1.2 Functional Form

The functional form of the equations and the relationships of the generalized equipment errors are shown in Table 7-1. Equations 1 and 7 are the functional form of the position fix and dead-reckoning model, which

TABLE 7-1

GENERALIZED NAVIGATION EQUATIONS

	Position Fix Error Equation	Application
(1)	$(y_i, x_i) = f(\epsilon_i^*); \; A = \text{Bearing} = g(\epsilon_i^*)$	General
(2)	$(PE)_{PF} = \left[\sum\limits_{i=1}^{n} (C_i \epsilon_i^*)^2 \right]^{1/2}$	
(3)	$C_i = f\left[\left(\dfrac{\partial y_i}{\partial \epsilon_i^*} \right) \; \dfrac{\partial x_i}{\partial \epsilon_i^*} \; \dfrac{\partial A}{\partial \epsilon_i^*} \right]$	
	Position Fix Sensor Transformation	Derived for specific sensor class
(4)	$\epsilon_i^* = f(\epsilon_i, \; C_i)$	
(5)	$\epsilon_i^* = \left[\sum\limits_{i=1}^{n} (\overline{C}_i \epsilon_i)^2 \right]^{1/2} = \left[T_i \right] \left[\epsilon_i^2 \right]$	
(6)	$\overline{C}_i = \dfrac{\partial \epsilon_i^*}{\partial \epsilon_i}$	
	Dead-Reckoning Error Equation	General
(7)	$\left[\Delta h_k, \; \Delta x_k, \; \Delta y_k \right] = f(\epsilon_k^*)$	
(8)	$E_{DR} = \left[\sum\limits_{i=1}^{m} (C_k \epsilon_k^*)^2 \right]^{1/2}$	
(9)	$C_k = f\left[\left(\dfrac{\partial \Delta y_k}{\partial \epsilon_k^*} \right), \; \left(\dfrac{\partial \Delta x_k}{\partial \epsilon_k^*} \right), \; \left(\dfrac{\partial \Delta h_k}{\partial \epsilon_k^*} \right) \right]$	
	Dead-Reckoning Sensor Transformation	Derived for specific sensor class
(10)	$\epsilon_k^* = f(C_k, \; \epsilon_k^*)$	
(11)	$\epsilon_k^* = \left[\sum\limits_{k=1}^{m} (\overline{C}_k \epsilon_k)^2 \right]^{1/2} = \left[T_k \right] \left[\epsilon_k^2 \right]$	
(12)	$\overline{C}_k = \dfrac{\partial \epsilon_k^*}{\partial \epsilon_k}$	

depend on some sensed (transformed) variable $\epsilon^*_{i,k}$. The position errors are given in Equations 2 and 8 as functions of error sensitivity coefficients C_i and C_k. C_i and C_k are formed as shown in Equations 3 and 9.

Equations 4 and 10 are the generalized subsystem equipment or sensor error models. If no transformation exists relating a particular sensed variable, then

$$\epsilon^* = \epsilon.$$

However, where the sensed variable is not equal to the transformed variable, the transformation is made through Equations 5, 6, and 11, 12, respectively.

The application of the generalized Equations 1 through 12 is given in Table 7-1.

Basically the method of error model analysis is the covariance method. The output of the system will be a covariance matrix of the following form.

$$[\overrightarrow{PE}] = \begin{bmatrix} \sigma^2_X & \sigma_{YX} & \sigma_{ZX} \\ \sigma_{XY} & \sigma^2_Y & \sigma_{ZY} \\ \sigma_{XZ} & \sigma_{YZ} & \sigma^2_Z \end{bmatrix} \begin{bmatrix} \overrightarrow{1}_X \\ \overrightarrow{1}_Y \\ \overrightarrow{1}_Z \end{bmatrix}$$

where the elements of the covariance matrix are of the form:

$$\sigma^2_A = \text{variance in direction of unit vector } \overrightarrow{1}_A \text{ etc.}$$

$$\sigma_{AB} = \rho_{AB}\,\sigma_A\,\sigma_B \text{ with } \rho_{AB} \text{ the correlation coefficient of random variables A, B.}$$

The position error $(PE)_T$ will be in the form of an error ellipsoid with directions relative to the orthogonal unit triad $(\overrightarrow{1}_X, \overrightarrow{1}_Y, \overrightarrow{1}_Z)$.

If the correlation coefficients are not equal to zero, the orientation of the ellipsoid major and minor axes relative to the base vectors may be found from the solution of the eigen vectors and values of the covariance matrix. This process of determining the ellipsoid orientation is straight-forward; however, the additional computation necessary for the calculation of the correlation coefficients ρ_{AB} starting with sensed random variables $\epsilon_{i,k}$ would be a lengthy task.

Thus, the direction taken is to assume independence, which then diagonalizes the covariance matrix. In this instance, the positional error ellipsoid will be oriented with the major axis and minor axis directed along the reference triad.

7.2 DERIVATION OF COMPONENT ERROR MODELS

7.2.1 General Dead Reckoning Error Model

The dead reckoning error model was derived in a geometric system of selenocentric coordinates. The analytic system or local reference system which is navigated against is a local vertical, north, east system. The geometric system and analytic system were selected on the basis of com-patibility with the position fix model, convenience in calculations, and wide-spread use.

Neglecting an inertial reference, the basic system in which vehicle position is measured is selenocentric coordinates (R, x, y). Specify an analytic system; local vertical, north, easterly coordinate system at $(R_m + h, x, y)$,

$R_m \equiv$ lunar radius, constant at 1738 km

with the unit vectors directed such that

$\vec{1}_N$ is north along meridian of longitude y

$\vec{1}_E$ is east along parallel of latitude x

$\vec{1}_Z$ is up along radius vector R.

as shown in Figure 7-2.
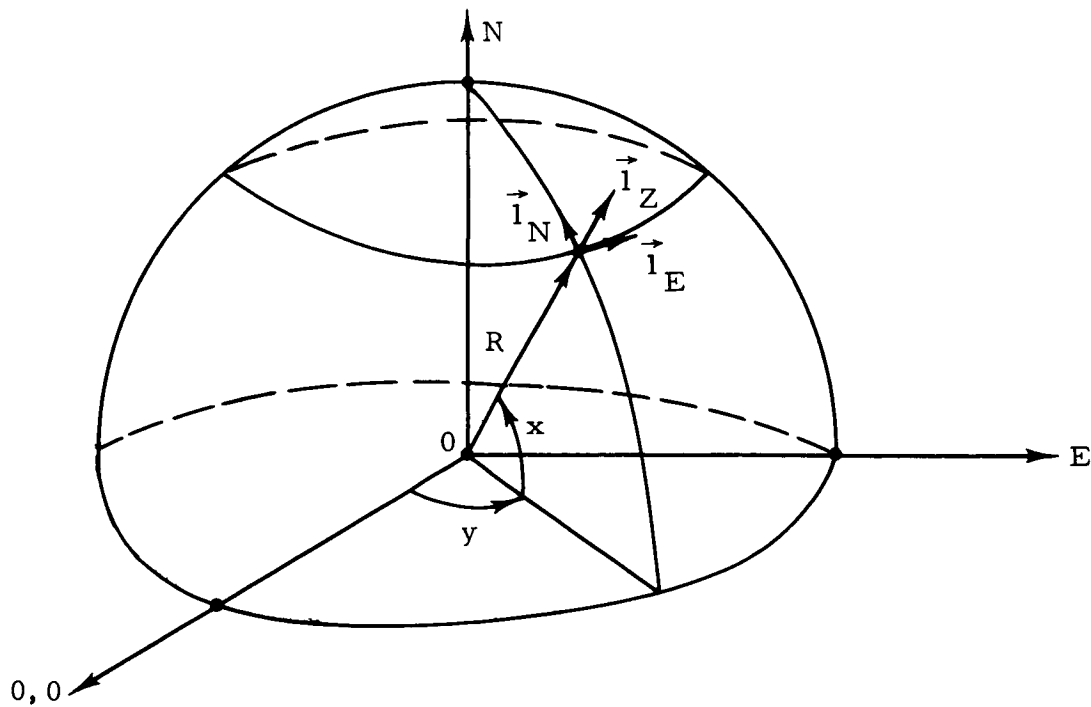
Figure 7-2 Selenocentric Coordinates

Let the analytic system be fixed at the vehicle cg with sensors defining the analytic orientation:

Azimuth sensor referenced to $\vec{1}_N$

Vertical sensor referenced to $-\vec{1}_Z$

$$\vec{1}_E = \vec{1}_N \times \vec{1}_Z \qquad (7-1)$$

Thus, a body-centered coordinate system in the local vertical frame, oriented north, is defined.

Establish the vehicle Euler angles or the angular displacement of the body axis from the local vertical, north, east system. (See Figure 7-3.)

where   A = sensed azimuth angle

P = sensed pitch angle

P = -p
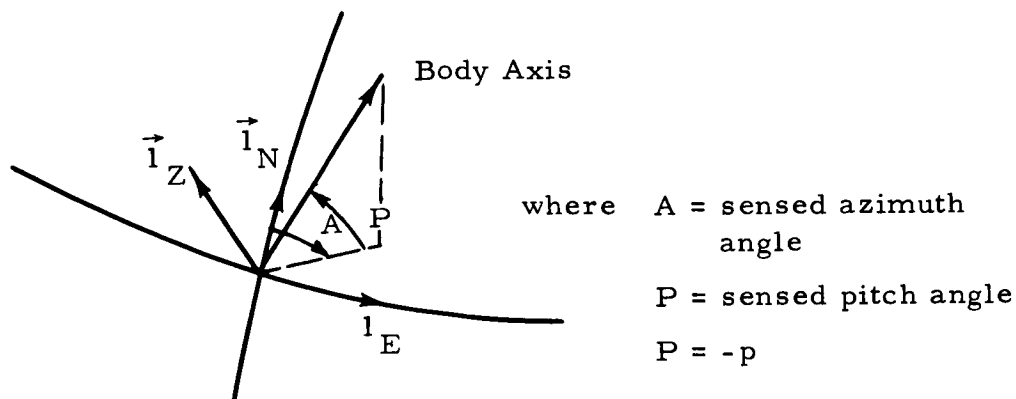
Figure 7-3 Analytic Navigation System Coordinates

Thus, neglecting side slip, angle of attack, etc., the vehicle body axis is the velocity vector direction, and the third measured variable is vehicle speed, V.

The expression $V = \omega R$ defines the tangential component of velocity. The unit vector triad $(\vec{1}_N, \vec{1}_E, \vec{1}_Z)$ is indeed located tangentially to the sphere (moon) at a position defined by (R, x, y).   Then

$$\dot{x} = \frac{V}{R} \cos P \cos A \qquad (7-2)$$

$$\dot{y} = \frac{V \cos P \sin A}{R \cos x} \qquad (7-3)$$

and

$$\dot{h} = V \sin P \qquad (7-4)$$

Solving for x, y, h by direct integration

$$x(t) = \int_{t_o}^{t} \frac{V}{R} \cos P \cos A \, dt + x(t_o) \qquad (7-5)$$

$$y(t) = \int_{t_o}^{t} \frac{V \cos P \sin A \, dt}{R \cos x} + y(t_o) \qquad (7-6)$$

$$h(t) = \int_{t_o}^{t} V \sin P \, dt + h(t_o) \qquad (7-7)$$

where $x(t_o)$, $y(t_o)$, and $h(t_o)$ define initial conditions.

Inspection of Equations 7-5, 7-6, and 7-7 shows that dead reckoning position (R, x, y) is given as a function of the measured variables:

1. speed, V

2. pitch angle, P

3. azimuth angle, A

and V, P, A are all functions of t.

Taking total differentials:

$$dx = \frac{\partial x}{\partial V} dV + \frac{\partial x}{\partial P} dP + \frac{\partial x}{\partial A} dA$$

$$dy = \frac{\partial y}{\partial V} dV + \frac{\partial y}{\partial P} dP + \frac{\partial y}{\partial A} dA$$

$$dh = \frac{\partial h}{\partial V} dV + \frac{\partial h}{\partial P} dP$$

or in matrix form:

$$
\begin{bmatrix} dx \\ dy \\ dh \end{bmatrix} = \begin{bmatrix} \dfrac{\partial x}{\partial V} & \dfrac{\partial x}{\partial P} & \dfrac{\partial x}{\partial A} \\[2ex] \dfrac{\partial y}{\partial V} & \dfrac{\partial y}{\partial P} & \dfrac{\partial y}{\partial A} \\[2ex] \dfrac{\partial h}{\partial V} & \dfrac{\partial h}{\partial P} & O \end{bmatrix} \begin{bmatrix} dV \\ dP \\ dA \end{bmatrix}
$$

The partial derivatives can be evaluated using Leibnitz's rule. However, to facilitate interpretation and computation, the term cos x in the denominator of Equation 7-6 is assumed constant. From Appendix E, which effectively shows the application of the mean value theorem:

$$
\cos x(t) \cong \cos \frac{(x_D + x_o)}{2} \tag{7-8}
$$

then

$$
\frac{\partial x}{\partial V} = \int_{t_o}^{t} \frac{\cos P \cos A \; dt}{R} \tag{7-9}
$$

$$
\frac{\partial x}{\partial P} = -\int_{t_o}^{t} \frac{V \sin P \cos A \; dt}{R} \tag{7-10}
$$

$$
\frac{\partial x}{\partial A} = -\int_{t_o}^{t} \frac{V \cos P \sin A \; dt}{R} \tag{7-11}
$$

$$
\frac{\partial y}{\partial V} = \int_{t_o}^{t} \frac{\cos P \sin A \; dt}{R \cos x} \tag{7-12}
$$

7-12

$$\frac{\partial y}{\partial P} = -\int_{t_o}^{t} \frac{V \sin P \sin A \ dt}{R \cos x} \qquad (7\text{-}13)$$

$$\frac{\partial y}{\partial A} = \int_{t_o}^{t} \frac{V \cos P \cos A \ dt}{R \cos x} \qquad (7\text{-}14)$$

$$\frac{\partial h}{\partial V} = \int_{t_o}^{t} \sin P \ dt \qquad (7\text{-}15)$$

$$\frac{\partial h}{\partial P} = +\int_{t_o}^{t} V \cos P \ dt \qquad (7\text{-}16)$$

If an average speed is assumed, no great loss of generality results. Then referring to Equations 7-5, 7-6, and 7-7, partial derivatives may be written as:

$$\frac{\partial x}{\partial V} = \frac{x(t) - x(t_o)}{V} \qquad (7\text{-}17)$$

$$\frac{\partial x}{\partial P} = -\int_{t_o}^{t} \frac{V \sin P \cos A \ dt}{R} \qquad (7\text{-}18)$$

$$\frac{\partial x}{\partial A} = -\left(y(t) - y(t_o)\right) \cos \frac{x_D + x_o}{2} \qquad (7\text{-}19)$$

$$\frac{\partial y}{\partial V} = \frac{y(t) - y(t_o)}{V} \qquad (7\text{-}20)$$

$$\frac{\partial y}{\partial P} = -\int_{t_o}^{t} \frac{V \sin P \sin A \, dt}{R \cos x} \qquad (7-21)$$

$$\frac{\partial y}{\partial A} = \frac{x(t) - x(t_o)}{\cos \frac{(x_D + x_o)}{2}} \qquad (7-22)$$

$$\frac{\partial h}{\partial V} = \frac{h(t) - h(t_o)}{V} \qquad (7-23)$$

$$\frac{\partial h}{\partial P} = +\int_{t_o}^{t} V \cos P \, dt \qquad (7-24)$$

Now assume for any short traverse, the vehicle maintains constant azimuth (or an average azimuth over an incremental traverse). This assumption reduces a total mission traverse to a series of incremental line segments. It is to be noted that the constant azimuth assumption affects the following partial derivatives, which can be written:

$$\frac{\partial x}{\partial P} = -\frac{(h(t) - h(t_o)) \cos A}{R} \qquad (7-25)$$

$$\frac{\partial y}{\partial P} = -\frac{(h(t) - h(t_o)) \sin A}{R \cos \frac{x_D + x_o}{2}} \qquad (7-26)$$

$$\frac{\partial h}{\partial P} = +\frac{(x(t) - x(t_o)) R}{\cos A} \qquad (7-27)$$

7-14

Referencing the total position increment to the $(\vec{1}_N, \vec{1}_E, \vec{1}_Z)$ system,

$$\vec{\Delta P} = \Delta R_N \vec{1}_N + \Delta R_E \vec{1}_E + \Delta R_Z \vec{1}_Z \qquad (7\text{-}28)$$

or in terms of the latitude, longitude, altitude differential system,

$$\vec{\Delta P} = (R\ dx)\ \vec{1}_N + (R\ dy\ \cos x)\ \vec{1}_E + (dh)\ \vec{1}_Z \qquad (7\text{-}29)$$

Consider the differentials dV, dA, dP as 3σ error quantities or error measures of the uncertainty in sensing speed, pitch, azimuth. The errors in speed, pitch, and azimuth are assumed normally distributed by the central limit theorem. The auto correlation functions of the independent error random variables are assumed independent of incremental path length (or time due to average velocity assumption) and thus are equal to the variance of the random variable.

Hence

$$
\begin{bmatrix}
(\Delta R_N)^2\,_{DR} \\[2ex]
(\Delta R_E)^2\,_{DR} \\[2ex]
(\Delta R_Z)^2\,_{DR}
\end{bmatrix}
=
\begin{bmatrix}
D_1^{\,2} & D_2^{\,2} & D_3^{\,2} \\[2ex]
D_4^{\,2} & D_5^{\,2} & D_6^{\,2} \\[2ex]
D_7^{\,2} & D_8^{\,2} & D_9^{\,2}
\end{bmatrix}
\begin{bmatrix}
\sigma_o^{\,2} \\[2ex]
\sigma_p^{\,*2} \\[2ex]
\sigma_A^{\,*2}
\end{bmatrix}
\qquad (7\text{-}30)
$$

$$
\left.
\begin{aligned}
D_1 &= (x_D - x_o)\,R \\[2ex]
D_2 &= (h_D - h_o)\,\cos A \\[2ex]
D_3 &= (y_D - y_o)\,R\,\cos\left(\frac{x_D + x_o}{2}\right) \\[2ex]
D_4 &= (y_D - y_o)\,R\,\cos(x_D) \\[2ex]
D_5 &= \dfrac{(h_D - h_o)\,\sin A\,\cos(x_D)}{\cos\left(\dfrac{x_D + x_o}{2}\right)}
\end{aligned}
\right\} \qquad (7\text{-}31)
$$

$$D_6 = \frac{(x_D - x_o) \, R \, \cos x_D}{\cos\left(\dfrac{x_D + x_o}{2}\right)}$$

$$D_7 = h_D - h_o$$

$$D_8 = \frac{(x_D - x_o) \, R}{\cos A}$$

$$D_9 = 0$$

Then the position error ellipsoid located at a given point $(R = h_D, \; x_D, \; y_D)$ can be represented with error components in the direction of

$$(\Delta R_N)_{DR} \text{ along } \vec{1}_N$$

$$(\Delta R_E)_{DR} \text{ along } \vec{1}_E$$

and

$$(\Delta R_Z)_{DR} \text{ along } \vec{1}_Z$$

with

$$\sigma_o = \frac{\sigma_V^{\ *}}{V} \qquad\qquad (7\text{-}32)$$

The necessary inputs from the mission model are:

$$h_D, \; h_o, \; x_D, \; x_o, \; y_D, \; y_o, \; V, \; A$$

The azimuth A provides the great circle route from the initial point to the destination point. The above initial points and destination points imply the incremental leg points n + 1, n, and not the mission initial starting coordinates and final destination coordinates.

7.2.2 Celestial Tracker Position Fix Error Model

Generally, vehicle position in latitude and longitude is determined through an iterated solution of the equation:

$$\sin \epsilon_i^* = \sin u_i \sin x + \cos u_i \cos x \cos (w_i - y) \qquad (7-33)$$

where $i = 1, 2$ index designation of observable.

Equation 7-33 is an implicit relation involving the variables ϵ_i^*, u_i, w_i, x, y, and is independent of measured azimuth. Taking total differentials:

$$dx = \frac{\partial x}{\partial \epsilon_1^*} d\epsilon_1^* + \frac{\partial x}{\partial u_1} du_1 + \frac{\partial x}{\partial w_1} dw_1 + \frac{\partial x}{\partial \epsilon_2^*} d\epsilon_2^* + \frac{\partial x}{\partial u_2} du_2 + \frac{\partial x}{\partial w_2} dw_2 \qquad (7-34)$$

$$dy = \frac{\partial y}{\partial \epsilon_1^*} d\epsilon_1^* + \frac{\partial y}{\partial u_1} du_1 + \frac{\partial y}{\partial w_1} dw_1 + \frac{\partial y}{\partial \epsilon_2^*} d\epsilon_2^* + \frac{\partial y}{\partial u_2} du_2 + \frac{\partial y}{\partial w_2} dw_2 \qquad (7-35)$$

Now expressing the differentials as 3σ values of error random variables, assuming independence, and combining in an RSS manner results in the following matrix form:

$$
\begin{bmatrix} \sigma_x^2 \\ \\ \sigma_y^2 \end{bmatrix}
=
\begin{bmatrix} C_1^2 & C_2^2 & C_3^2 & C_4^2 & C_5^2 & C_6^2 \\ \\ C_7^2 & C_8^2 & C_9^2 & C_{10}^2 & C_{11}^2 & C_{12}^2 \end{bmatrix}
\begin{bmatrix} \sigma_{\epsilon_1}^{*2} \\ \\ \sigma_{u_1}^{*2} \\ \\ \sigma_{w_1}^{*2} \\ \\ \sigma_{\epsilon_2}^{*2} \\ \\ \sigma_{u_2}^{*2} \\ \\ \sigma_{w_2}^{*2} \end{bmatrix}
\qquad (7-36)
$$

The partial derivatives are:

$$C_1 = \frac{\partial x}{\partial \epsilon_1^*} = \frac{\cos(\epsilon_1^*)\cos(u_2)\cos(x)\sin(w_2-y)}{D}$$

$$C_2 = \frac{\partial x}{\partial u_1} = \frac{\left(-\cos(u_1)\sin(x)+\sin(u_1)\cos(x)\cos(w_1-y)\right)\cos(u_2)\cos(x)\sin(w_2-y)}{D}$$

$$C_3 = \frac{\partial x}{\partial w_1} = \frac{\cos(u_1)\cos(x)\sin(w_1-y)\cos(u_2)\cos(x)\sin(w_2-y)}{D}$$

$$C_4 = \frac{\partial x}{\partial \epsilon_2^*} = -\frac{\cos(\epsilon_2^*)\cos(u_1)\cos(x)\sin(w_1-y)}{D}$$

$$C_5 = \frac{\partial x}{\partial u_2} = -\frac{\left(-\cos(u_2)\sin(x)+\sin(u_2)\cos(x)\cos(w_2-y)\right)\cos(u_1)\cos(x)\sin(w_1-y)}{D}$$

$$C_6 = \frac{\partial x}{\partial w_2} = -\frac{\cos(u_2)\cos(x)\sin(w_2-y)\cos(u_1)\cos(x)\sin(w_1-y)}{D}$$

$$C_7 = \frac{\partial y}{\partial \epsilon_1^*} = +\frac{\cos(\epsilon_1^*)\left[-\sin(u_2)\cos(x)+\cos(u_2)\sin(x)\cos(w_2-y)\right]}{D}$$

$$C_8 = \frac{\partial y}{\partial u_1} = \frac{1}{D}\left\{\left[-\cos(u_1)\sin(x)+\sin(u_1)\cos(x)\cos(w_1-y)\right]\cdot\right.$$
$$\left.\left[-\sin(u_2)\cos(x)+\cos(u_2)\sin(x)\cos(w_2-y)\right]\right\}$$

7-18

$$C_9 = \frac{\partial y}{\partial w_1} = + \frac{(\cos(u_1)\cos(x)\sin(w_1-y))[-\sin(u_2)\cos(x)+\cos(u_2)\sin(x)\cos(w_2-y)]}{D}$$

$$C_{10} = \frac{\partial y}{\partial \epsilon_2^*} = - \frac{\cos \epsilon_2^* [-\sin(u_1)\cos(x)+\cos(u_1)\sin(x)\cos(w_1-y)]}{D}$$

$$C_{11} = \frac{\partial y}{\partial u_2} = - \frac{1}{D} \left\{ [-\cos(u_2)\sin(x)+\sin(u_2)\cos(x)\cos(w_2-y)] \cdot \right.$$
$$\left. [-\sin(u_1)\cos(x)+\cos(u_1)\sin(x)\cos(w_1-y)] \right\}$$

$$C_{12} = \frac{\partial y}{\partial w_2} = - \frac{[\cos(u_2)\cos(x)\sin(w_2-y)][-\sin(u_1)\cos(x)+\cos(u_1)\sin(x)\cos(w_1-y)]}{D}$$

where

$$D = \cos(u_1)\cos(u_2)\sin(x)\cos(x)[\sin(w_1-y)\cos(w_2-y)-\cos(w_1-y)\sin(w_2-y)]$$
$$+ \left(\sin(u_1)\cos(u_2)\sin(w_2-y)-\cos(u_1)\sin(u_2)\sin(w_1-y)\right) \cos^2 x$$

The position fix model inputs from the mission model are:

x vehicle latitude at fix

y vehicle longitude at fix

$\epsilon_{1,2}^*$ observable true altitude; from Equation 7-33

$u_{1,2}$ observable subpoint latitude

$w_{1,2}$ observable subpoint longitude.

The transformed sensed error inputs are:

$\sigma^{*}_{\epsilon_{1,2}}$ altitude measurement error

$\sigma^{*}_{u_{1,2}}$ observable declination error

$\sigma^{*}_{w_{1,2}}$ observable right ascension error.

The quantity which is of interest is error in position.   Thus,

$$\Delta R_N \vec{1}_N = R \sigma_x \vec{1}_N \qquad (7\text{-}38)$$

$$\Delta R_E \vec{1}_E = R \cos x \, \sigma_y \vec{1}_E. \qquad (7\text{-}39)$$

Then position error due to position fix error is given as

$$(PE)_{PF} = \sqrt{(R \, \sigma_x)^2 + (R \cos(x) \, \sigma_y)^2} \qquad (7\text{-}40)$$

In the instance of Concept 3 where vehicle position is determined from earth-based rf tracking and computation, the position error is treated as a given input with the components (ΔR_N), (ΔR_E). The position error inputs are the result of available data on the capabilities of the DSIF and MSFN.

7.2.3   Initial Azimuth Alignment Error Model

The azimuth alignment error model may be derived from the solution of the astronomical triangle, assuming a lunar based ephemeris.   See Figure 7-4.
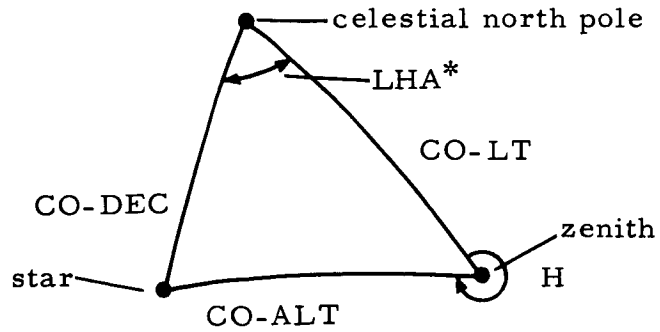
Figure 7-4 Astronomical Triangle

The following definitions apply:

LHA[*] = local hour angle of celestial reference

CO-DEC = co-declination

CO-LT = co-latitude

CO-ALT = co-altitude

H = celestial tracker true azimuth referenced north.

Applying the Law of Sines to the astronomical triangle results in the equation:

$$\sin (360° - H) = \frac{\sin (LHA^*)}{\sin(CO\text{-}ALT)} \sin (CO\text{-}DEC) \qquad (7\text{-}41)$$

Star azimuth is measured relative to the vehicle body axis in the local horizontal plane. Then, from Figure 7-5, the vehicle heading from true north is related by:
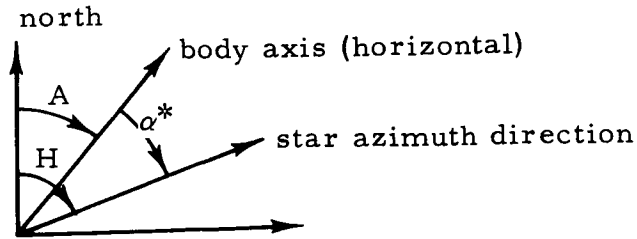
Figure 7-5 Star Azimuth Definition

$$H = A + \alpha^*$$ (7-42)

Substituting the defined nomenclature,

$$LHA^* = y - w$$

$$CO\text{-}DEC = 90^\circ - u$$

$CO\text{-}ALT = 90^\circ - \epsilon^*$, and substituting Equation 7-42 into Equation 7-41,

$$\sin (A + \alpha^*) = \frac{\sin (w - y) \cos u}{\cos \epsilon^*}$$ (7-43)

Now, substituting for ϵ^* and rearranging,

$$\tan (A + \alpha^*) = \frac{\sin (w-y)}{\cos(x) \tan(u) - \sin(x) \cos (w-y)}$$ (7-44)

Equation 7-44 is an implicit relation involving the variables A, w, u, α^*, x, y. Taking total differentials,

$$dA = \frac{\partial A}{\partial x} dx + \frac{\partial A}{\partial \alpha^*} d\alpha^* + \frac{\partial A}{\partial w} dw + \frac{\partial w}{\partial u} du + \frac{\partial A}{\partial y} dy$$ (7-45)

Treating the differentials as 3σ error measures, assuming independence, and combining errors in an RSS manner yields:

$$\sigma_{AO}^{2} = \begin{bmatrix} C_{17}^{2} & C_{18}^{2} & C_{19}^{2} & C_{20}^{2} & C_{21}^{2} \end{bmatrix} \begin{bmatrix} \sigma_{xn}^{2} \\ \sigma_{\alpha i}^{*2} \\ \sigma_{ui}^{*2} \\ \sigma_{wi}^{*2} \\ \sigma_{yn}^{2} \end{bmatrix} \qquad (7\text{-}46)$$

where the coefficients are identified by:

$$C_{17} = \frac{\partial A}{\partial x} - \frac{\sin(w_i - y_n)\left[\sin x_n \tan u_i + \cos x_n \cos(w_i - y_n)\right]}{M} \qquad (7\text{-}47)$$

$$C_{18} = \frac{\partial A}{\partial \alpha^{*}} = -1 \qquad (7\text{-}48)$$

$$C_{19} = \frac{\partial A}{\partial u} - \frac{\sin(w_i - y_n)\sec^2 u_i \cos x_n}{M} \qquad (7\text{-}49)$$

$$C_{20} = \frac{\partial A}{\partial w} = \frac{\cos(w_i - y_n)\cos x_n \tan u_i - \sin x_n}{M} \qquad (7\text{-}50)$$

$$C_{21} = \frac{\partial A}{\partial y} = -C_{20} \qquad (7\text{-}51)$$

$$M = \sin^2(w_i - y_n) + \left[\cos x_n \tan u_i - \sin x_n \cos(w_i - y_n)\right]^2 \qquad (7\text{-}52)$$

Errors in true elevation do not explicity appear but are treated as errors in observable subpoint.

For the following derivation, the required geometry is illustrated in Figure 7-6.
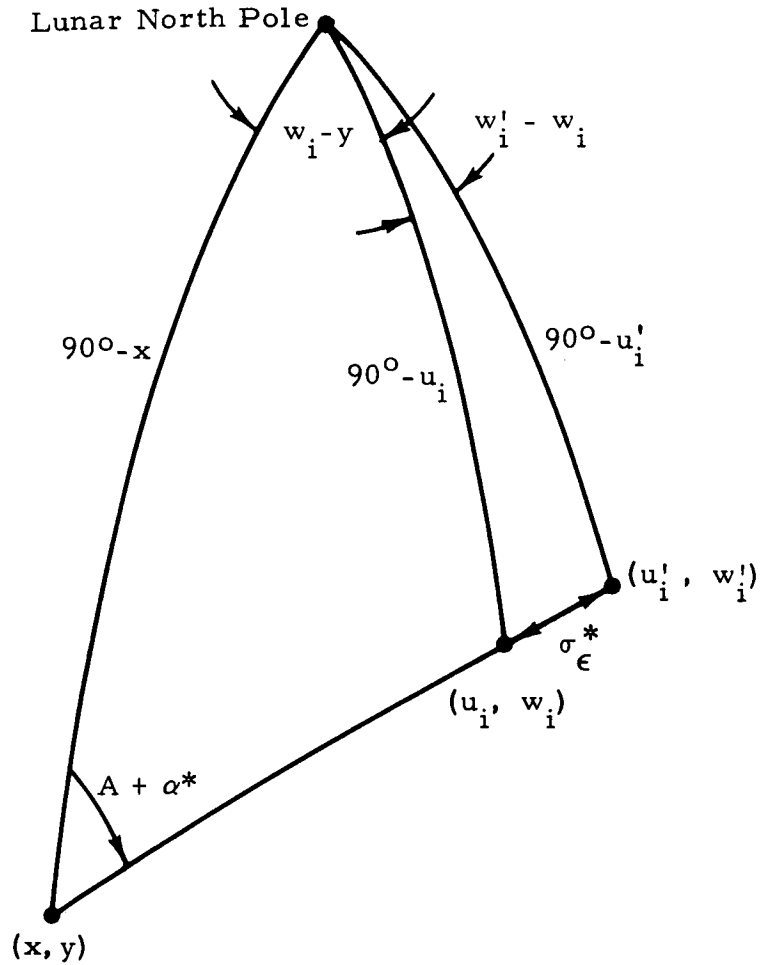
Figure 7-6 Effective Observable Elevation Error

The effective declination error is

$$\bar{\sigma}_{ui} = u_i' - u_i \qquad (7\text{-}53)$$

where

$$u_i' = \sin^{-1}\left[\cos \sigma_{\epsilon_i}^* \sin u_i - \sin \sigma_{\epsilon_i}^* \cos u_i \cos C\right]$$

$$C = \cos^{-1}\left[-\cos (A_{n,\,n+1} + \alpha_i^*) \cos (w_i - y_n)\right.$$

$$\left.+\sin (A_{n,\,n+1} + \alpha_i^*) \sin (w_i - y_n) \sin (x_i)\right]$$

where

$$0 \le C \le 180^{\text{o}}$$

The effective hour angle error is

$$\bar{\sigma}_{w_i} = \sin^{-1}\left[\frac{\sin \sigma_{\epsilon i}^* \sin C}{\cos u_i'}\right] \tag{7-54}$$

The quantities needed from the mission model are:

x_n vehicle latitude

y_n vehicle longitude

u_i observable subpoint latitude

w_i observable subpoint longitude

with error inputs

$$\sigma_\epsilon^*,\ \sigma_\alpha^*,\ \sigma_u^*,\ \sigma_w^*,\ \sigma_{yn},\ \sigma_{xn}.$$

7.2.4 Timer, and Ephemeris Error Model

The necessary error inputs to the position fix error model and initial bearing model, where position and heading are determined from celestial sightings, are the uncertainties in star subpoint positions. Ephemeris errors and timer errors contribute to errors in the celestial subpoint determination in the following manner.

The celestial sphere is assumed to rotate with a negative lunar rate, while the observables retain relative fixed positions on the sphere. The star is located through the angular rotations, hour angle, and declination relative to the prime meridian and celestial equator, respectively. Errors in celestial subpoint are then given in angular measure. Sections 7.2.2 and 7.2.3 present a position fix and initial bearing error model which require error inputs σ_u, σ_w or 3σ values of latitude subpoint error, and 3σ values of longitude subpoint error respectively. Because of timer and ephemeris contributions, these error measures become;

$$(\sigma_u^*)^2 = (\dot{u})^2 (\sigma_t^*)^2 + (\sigma_D)^2 \tag{7-55}$$

$$(\sigma_w^*)^2 = (\dot{w})^2 (\sigma_t^*)^2 + (\sigma_R)^2 \tag{7-56}$$

where

$\dot{u} \equiv$ rate of change of decliniation

$\dot{w} \equiv$ rate of change of hour angle.

The term $\dot{u}$ appears due to lunar physical latitudinal librations. But

$$\dot{w} = \dot{w}_L + \dot{w}_S \tag{7-57}$$

where

$w_L \equiv$ due to longitudinal physical librations

$w_S \equiv$ sidereal rate.

From Reference 12, the following maximum rates have been approximated from 1956 to 1961 libration data. The relative order of magnitude will suffice for future data.

$$\max \dot{w}_L \stackrel{\sim}{=} 6 \times 10^{-11} \text{ rad/sec}$$

$$\max \dot{u} \stackrel{\sim}{=} 3 \times 10^{-11} \text{ rad/sec.}$$

From References 34 and 70, the following sidereal rate was calculated, based on a lunar period of orbital revolution equal to 27.3217 days (known to within $1/10^7$.). Then

$$\dot{w}_S = 2.66 \times 10^{-6} \text{ rad/sec.}$$

The terms $\dot{w}_L$ and $\dot{u}$ will be neglected.

The timer errors are of the form:

$$(\sigma_t^*)^2 = (K_t t)^2 + (\sigma_t)^2 \qquad (7\text{-}58)$$

Equations 7-55 and 7-56 then become:

$$(\sigma_u^*)^2 = (\sigma_D)^2 \qquad (7\text{-}59)$$

$$(\sigma_w^*)^2 = (\dot{w}_S)^2 \left[(K_t t)^2 + (\sigma_t)^2 \right] + (\sigma_R)^2 \qquad (7\text{-}60)$$

The required inputs from the mission model are:

$\dot{w}_S$ = sidereal rate

t = elapsed time.

Error inputs are: K_t, σ_t, σ_D, σ_R.

Note: The angular velocity $\dot{u}$ is actually a function of the star longitude w. Fixing a moon centered coordinate system such that the celestial sphere rotates about the coordinate system with a negative lunar rate, the moon's rotational rate can be expressed as;

$$\vec{\Omega}_m = \omega_1 \vec{1}_x + \omega_2 \vec{1}_E + \omega_3 \vec{1}_N \qquad (7\text{-}61)$$

where

$$\omega_3 = \dot{w}_S + \dot{w}_L$$

$$\omega_2 = - \dot{u}_L \qquad (7\text{-}62)$$

$$\omega_1 = 0.$$

The celestial sphere rotation rate is then

$$\Omega_c = + \overline{\omega}_1 \, \vec{1}_x + \overline{\omega}_2 \, \vec{1}_E + \overline{\omega}_3 \, \vec{1}_N \qquad (7\text{-}63)$$

and

$$\overline{\omega}_3 = - \dot{w}_S - \dot{w}_L$$

$$\overline{\omega}_2 = + u_L \qquad (7\text{-}64)$$

$$\overline{\omega}_1 = 0$$

From Figure 7-7 where $\vec{1} \, w_{Lt}$ defines the direction of the latitudinal rate vector, it can be shown that instantaneous velocities of an observable at a position given by longitude w and latitude u is

$$\dot{w} = - \dot{w}_S - \dot{w}_L \qquad (7\text{-}65)$$

$$\dot{u} = - \dot{u}_L \cos w \text{ which is never greater than } \dot{u}_L.$$
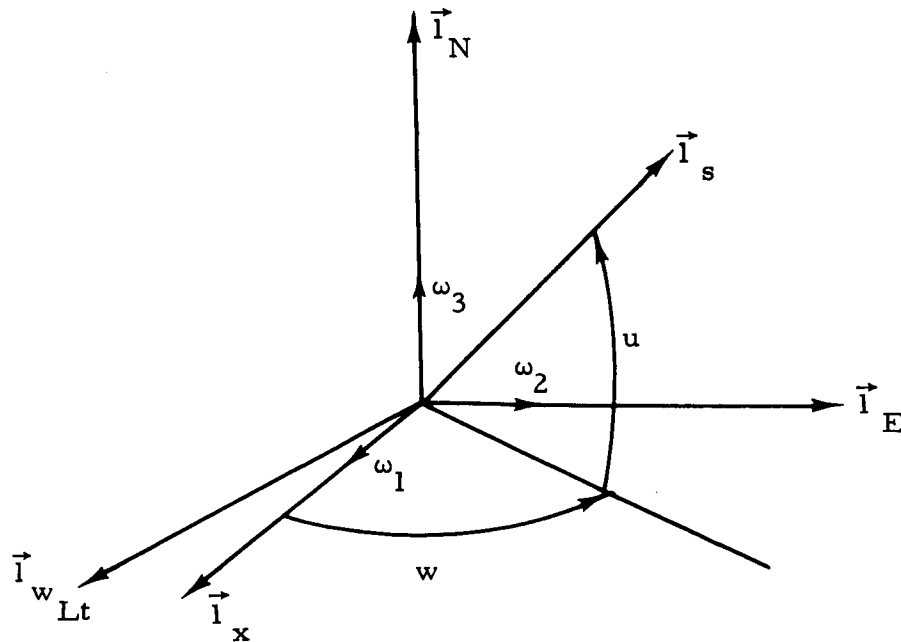
Figure 7-7 Observable Instantaneous Velocity Vector

7.2.5 Celestial Tracker True Elevation, True Azimuth Error Model

To assess the interdependency of vertical sensor errors and tracker pointing angle errors, a model is derived relating the vertical measurement errors to celestial tracker errors, thereby determining the transformed 3σ tracker errors, azimuth σ_α^* and elevation σ_ϵ^*. The quantities, σ_α^* and σ_ϵ^* provide inputs for the position fix and initial bearing error models in Sections 7.2.2 and 7.2.3.

The static geometry is shown in Figure 7-8. The unit vectors $(\vec{1}_x, \vec{1}_y, \vec{1}_z)$ define the basic local vertical reference fixed at the vehicle cg; $\vec{1}_z$ points up along the vertical. The plane of $(\vec{1}_x, \vec{1}_y)$ defines the local tangential plane. If the vehicle body axis is horizontal with roll, pitch, and yaw zero, the body axis points along $\vec{1}_x$.

The vehicle rotations in this derivation are defined as follows:

$(\vec{1}_x, \vec{1}_y, \vec{1}_z)$ rotated with pitch angle p about $\vec{1}_y$ to $(\vec{1}'_x, \vec{1}'_y, \vec{1}'_z)$. Then $(\vec{1}'_x, \vec{1}'_y, \vec{1}'_z)$ rotated with roll angle r about $\vec{1}'_x$ to $(\vec{1}''_x, \vec{1}''_y, \vec{1}''_z)$
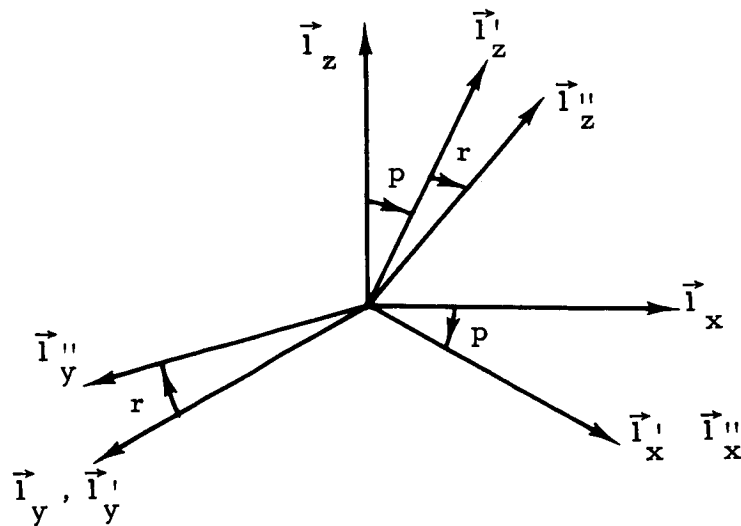
Figure 7-8 Body-Centered Coordinates

The star tracker pointing geometry, elevation ϵ and azimuth α, is shown in Figure 7-9 referenced to the pitched and rolled body axis ($\vec{1}''_x$, $\vec{1}''_y$, $\vec{1}''_z$).
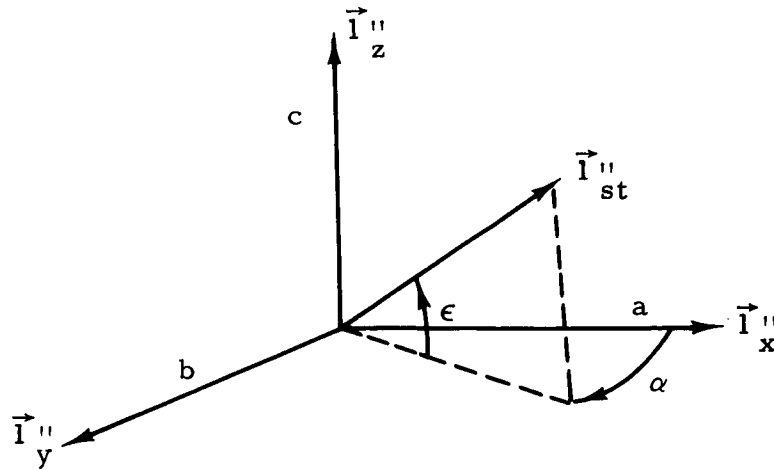
Figure 7-9 Star Tracker Unit Pointing Vector

The orthogonal coordinate transformations are given as

$$
\begin{bmatrix} \vec{1}''_x \\ \vec{1}''_y \\ \vec{1}''_z \end{bmatrix} = \begin{bmatrix} \cos p & 0 & -\sin p \\ \sin r \sin p & \cos r & \sin r \cos p \\ \cos r \sin p & -\sin r & \cos r \cos p \end{bmatrix} \begin{bmatrix} \vec{1}_x \\ \vec{1}_y \\ \vec{1}_z \end{bmatrix} = [\,T_{rp}\,] \begin{bmatrix} \vec{1}_x \\ \vec{1}_y \\ \vec{1}_z \end{bmatrix} \quad (7\text{-}66)
$$

Thus any vector with components in the ($\vec{1}''_x$, $\vec{1}''_y$, $\vec{1}''_z$) space may be related to the local vertical space ($\vec{1}_x$, $\vec{1}_y$, $\vec{1}_z$) by the matrix T_{rp}.

The pitch and roll measurements are made by a two-axis pendulous inclinometer or a two-axis vertical gyro.

These sensors are assumed to have errors of the form:

$$
(\sigma_p^*)^2 = (K_p p)^2 + (\sigma_p)^2 + (\sigma_{pD} t)^2 \quad (7\text{-}67)
$$

$$
(\sigma_r^*)^2 = (K_r r)^2 + (\sigma_r)^2 + (\sigma_{rD} t)^2 \quad (7\text{-}68)
$$

7-30

where

$$\sigma_p^* \qquad = \text{ total } 3\sigma \text{ value of pitch error}$$

$$\sigma_r^* \qquad = \text{ total } 3\sigma \text{ value of roll error}$$

$$K_p p \qquad = 3\sigma \text{ contribution from linearity errors in pitch}$$

$$K_r r \qquad = 3\sigma \text{ contribution from linearity errors in roll}$$

$$\sigma_r, \sigma_p = \text{ basic } 3\sigma \text{ null uncertainties}$$

$$\sigma_{rD}, \sigma_{p_D} = 3\sigma \text{ contribution from drift, where applicable.}$$

There is a dependency upon position fix error and initial bearing error from errors in the local vertical. This development follows:

The necessary inputs to a computer to determine the position fix and initial bearing are star azimuth α^* and elevation ϵ^* relative to the local vertical. But the actual measurements are determined relative to the body axis in $(\vec{1}_x'', \vec{1}_y'', \vec{1}_z'')$ space. Thus the celestial tracker has the point unit shown in Figure 7-9.

$$(\vec{1}_{ST}'') = a\,\vec{1}_x'' + b\,\vec{1}_y'' + c\,\vec{1}_z'' \qquad (7\text{-}69)$$

$$a = \cos \epsilon \cos \alpha \qquad (7\text{-}70)$$

$$b = \cos \epsilon \sin \alpha \qquad (7\text{-}71)$$

$$c = \sin \epsilon \qquad (7\text{-}72)$$

which can be expressed in the local vertical space as:

$$(\vec{1}_{ST}) = \begin{bmatrix} a & b & c \end{bmatrix} \begin{bmatrix} \vec{1}_x'' \\ \vec{1}_y'' \\ \vec{1}_z'' \end{bmatrix} = \begin{bmatrix} a & b & c \end{bmatrix} \begin{bmatrix} \; \\ \; T_{rp} \; \\ \; \end{bmatrix} \begin{bmatrix} \vec{1}_x \\ \vec{1}_y \\ \vec{1}_z \end{bmatrix} \qquad (7\text{-}73)$$

The resulting expression is of the form:

$$\vec{1}_{ST} = A\,\vec{1}_x + B\,\vec{1}_y + C\,\vec{1}_z \qquad (7\text{-}74)$$

where

$$A = A\,(\epsilon,\ \alpha,\ r,\ p)$$

$$B = B\,(\epsilon,\ \alpha,\ r,\ p)$$

$$C = C\,(\epsilon,\ \alpha,\ r,\ p). \quad A,\ B,\ C \text{ are defined below.}$$

Now true elevation ϵ^* and true azimuth α^* can be solved for as:

$$\tan \alpha^* = \frac{B}{A} \qquad (7\text{-}75)$$

$$\tan \epsilon^* = \frac{C}{(A^2 + B^2)^{1/2}} \qquad (7\text{-}76)$$

Equation 7-75 is an implicit relation of the dependent variable α^*, and independent variables $\epsilon,\ \alpha,\ r,\ p$. Taking total differentials

$$d\alpha^* = \frac{\partial \alpha^*}{\partial \epsilon}\,d\epsilon + \frac{\partial \alpha^*}{\partial \alpha}\,d\alpha + \frac{\partial \alpha^*}{\partial r}\,dr + \frac{\partial \alpha^*}{\partial p}\,dp \qquad (7\text{-}77)$$

Similarly from Equation 7-76:

$$d\epsilon^* = \frac{\partial \epsilon^*}{\partial \epsilon}\,d\epsilon + \frac{\partial \epsilon^*}{\partial \alpha}\,d\alpha + \frac{\partial \epsilon^*}{\partial r}\,dr + \frac{\partial \epsilon^*}{\partial p}\,dp \qquad (7\text{-}78)$$

Expressing the differentials as 3σ values of error random variables, assuming independence, and combining in an RSS manner:

$$(\sigma_\alpha^*)^2 = \begin{bmatrix} C_{23}^2 & C_{22}^2 & C_{24}^2 & C_{25}^2 \end{bmatrix} \begin{bmatrix} \sigma_\epsilon^2 \\ \sigma_\alpha^2 \\ \sigma_r^{*\,2} \\ \sigma_p^{*\,2} \end{bmatrix} \qquad (7\text{-}79)$$

7-32

and

$$(\sigma_\epsilon^*)^2 = \begin{bmatrix} C_{14}^2 & C_{13}^2 & C_{15}^2 & C_{16}^2 \end{bmatrix} \begin{bmatrix} \sigma_\epsilon^2 \\ \sigma_\alpha^2 \\ \sigma_r^{*2} \\ \sigma_p^{*2} \end{bmatrix} \qquad (7\text{-}80)$$

where the terms are defined as follows:

Tracker equipment errors:

σ_ϵ = tracker elevation equipment error (includes human readout error if a manual device)

σ_α = tracker azimuth error (includes human readout error if a manual device).

Partial derivative sensitivity coefficients:

$$C_{22} = \alpha_\alpha^* = \frac{B_\alpha A - B A_\alpha}{A^2 \sec^2 \alpha^*}$$

$$C_{23} = \alpha_\epsilon^* = \frac{B_\epsilon A - B A_\epsilon}{A^2 \sec^2 \alpha^*}$$

$$C_{24} = \alpha_r^* = \frac{B_r A - B A_r}{A^2 \sec^2 \alpha^*}$$

$$C_{25} = \alpha_p^* = \frac{B_p A - B A_p}{A^2 \sec^2 \alpha^*}$$

$$C_{13} = \epsilon_\alpha^* = \frac{C_\alpha D^{1/2} - CD^{-1/2}[B B_\alpha + A A_\alpha]}{D \sec^2 \epsilon^*}$$

$$C_{14} = \epsilon_\epsilon^* = \frac{C_\epsilon D^{1/2} - CD^{-1/2} [B B_\epsilon + A A_\epsilon]}{D \sec^2 \epsilon^*}$$

$$C_{15} = \epsilon_r^* = \frac{C_r D^{1/2} - CD^{-1/2} [B B_r + A A_r]}{D \sec^2 \epsilon^*}$$

$$C_{16} = \epsilon_p^* = \frac{C_p D^{1/2} - CD^{-1/2} [B B_p + A A_p]}{D \sec^2 \epsilon^*}$$

(Note: These coefficients must be evaluated for each observable.)

where the A, B, C and D parameters are defined by:

$A = \cos \epsilon \cos \alpha \cos p + \cos \epsilon \sin \alpha \sin r \sin p + \sin \epsilon \cos r \sin p$

$B = \cos \epsilon \sin \alpha \cos r - \sin \epsilon \sin r$

$C = -\cos \epsilon \cos \alpha \sin p + \cos \epsilon \sin \alpha \sin r \cos p + \sin \epsilon \cos r \cos p$

$D = A^2 + B^2$

$A_\alpha = -\cos \epsilon \sin \alpha \cos p + \cos \epsilon \cos \alpha \sin r \sin p$

$A_\epsilon = -\sin \epsilon \cos \alpha \cos p - \sin \epsilon \sin \alpha \sin r \sin p + \cos \epsilon \cos r \sin p$

$A_r = \cos \epsilon \sin \alpha \cos r \sin p - \sin \epsilon \sin r \sin p$

$A_p = -\cos \epsilon \cos \alpha \sin p + \cos \epsilon \sin \alpha \sin r \cos p + \sin \epsilon \cos r \cos p$

$B_\alpha = \cos \epsilon \cos \alpha \cos r$

$B_r = -\cos \epsilon \sin \alpha \sin r - \sin \epsilon \cos r$

$B_\epsilon = -\sin \epsilon \sin \alpha \cos r - \cos \epsilon \sin r$

$B_p = 0$

$$C_\alpha = \cos \epsilon \sin \alpha \sin p + \cos \epsilon \cos \alpha \sin r \cos p$$

$$C_\epsilon = \sin \epsilon \cos \alpha \sin p - \sin \epsilon \sin \alpha \sin r \cos p + \cos \epsilon \cos r \cos p$$

$$C_r = \cos \epsilon \sin \alpha \cos r \cos p - \sin \epsilon \sin r \cos p$$

$$C_p = -\cos \epsilon \cos \alpha \cos p - \cos \epsilon \sin \alpha \sin r \sin p - \sin \epsilon \cos r \sin p$$

(Note: In the above expressions $\alpha \Rightarrow \alpha_i$; $\epsilon \Rightarrow \epsilon_i$; $\alpha^* \Rightarrow \alpha^*_i$; $\epsilon^* \Rightarrow \epsilon^*_i$.)

where p, r, ϵ^*_i and α^*_i are necessary inputs from the mission models.

where ϵ_i and α_i are determined from:

$$\alpha_i = \tan^{-1} \left(\frac{b}{a} \right)$$

$$\epsilon_i = \tan^{-1} \left(\frac{c}{(a^2 + b^2)^{1/2}} \right)$$

$$[a \; b \; c] = [a_o \; b_o \; c_o] \; [T_{rp}]^{-1} \tag{7-81}$$

$$a_o = \cos \epsilon^*_i \cos \alpha^*_i$$

$$b_o = \cos \epsilon^*_i \sin \alpha^*_i$$

$$c_o = \sin \epsilon^*_i \qquad \text{where i indicates the i}^{\text{th}} \text{ observable.}$$

If the tracker is not body fixed, but stabilized in the horizontal plane, the error contributions may be evaluated by setting p = r = o in the partial derivatives.

7.2.6 Vertical Anomaly Error Model

An error model was developed relating the vertical irregularities (anomalies) to position fix and initial bearing errors. The model is applicable to Concepts 1 and 2 (the passive, nongyro and the inertial systems) in which a static mode, position, and initial bearing are determined through celestial measurements.

Assume a body-centered coordinate system $(\vec{1}_x, \vec{1}_y, \vec{1}_z)$ where $-\vec{1}_z$ defines the true vertical and

$$\vec{1}_y \times \vec{1}_x = \vec{1}_z.$$

The vertical anomaly referenced to this coordinate system is defined in Figure 7-10.
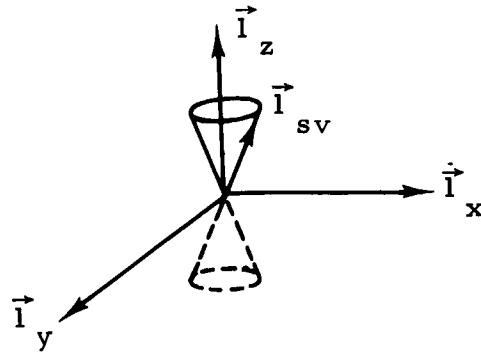
Figure 7-10   Vertical Anomaly Definition

The anomaly considered here is an angular perturbation about the true vertical.   This angular measure is given as the solid angle, γ, which defines an equiprobable cone shown in Figure 7-10.   The general unit vector $-\vec{1}_{sv}$ is the direction sensed by the vertical sensor.   This defines the vertical sensor space.

Figure 7-11 defines the equiprobable anomaly locus in a cylindrical coordinate system; with β arbitrarily selected as measured from the $\vec{1}_x$ axis.
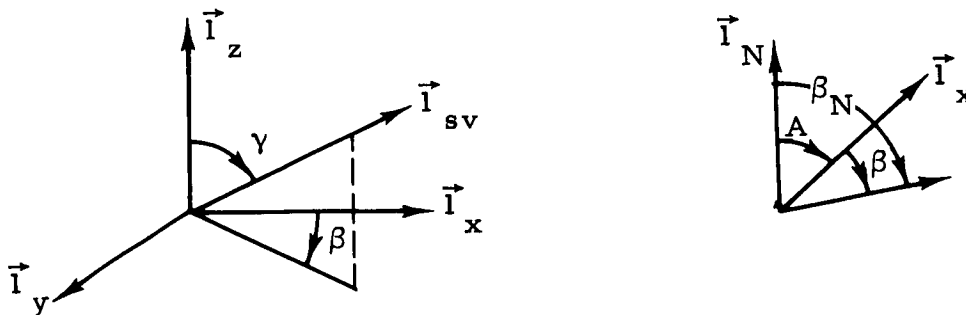
Figure 7-11   Local Vertical Pointing Vector

7-36

At a particular point on the lunar surface, the anomaly will be characterized by a solid angle rotation γ from the true vertical, and an equiprobable angular direction β from the $\vec{1}_x$ axis. The direction of the anomaly as measured by the vertical sensor is given as:

$$\vec{1}_{sv} = \sin \gamma \cos \beta \, \vec{1}_x + \sin \gamma \sin \beta \, \vec{1}_y + \cos \gamma \, \vec{1}_z \qquad (7\text{-}82)$$

If the equiprobable angular rotation β is referenced to true north,

$$\beta = \beta_N - A. \qquad (7\text{-}83)$$

Effectively, the anomalies may be considered as vertical sensor errors. Thus, $\vec{1}_{sv}$ may be defined in terms of roll and pitch errors of a two-axis vertical sensor. With reference to Section 7.2.5,

$$\vec{1}''_z = \vec{1}_{sv} = \cos r_g \sin p_g \, \vec{1}_x - \sin r_g \, \vec{1}_y + \cos r_g \cos p_g \, \vec{1}_z \qquad (7\text{-}84)$$

where r_g, p_g denote roll and pitch angle of anomaly direction with respect to true vertical.

Solving for r_g and p_g in terms of γ, β from Equations 7-82 and 7-83 by equating coefficients

$$r_g = -\sin^{-1} (\sin \gamma \sin \beta) \qquad (7\text{-}85)$$

$$p_g = \cos^{-1} \left(\frac{\cos \gamma}{\cos \left[\sin^{-1} (\sin \gamma \sin \beta) \right]} \right). \qquad (7\text{-}86)$$

Since r_g and p_g are effective instrument errors,

$$r_g = \sigma_{rg} \qquad (7\text{-}87)$$

and

$$p_g = \sigma_{pg} \qquad (7\text{-}88)$$

The inputs from the mission model are

$$\gamma = \sigma_\gamma, \text{ and } \beta_N$$

The vertical anomaly σ_γ has contributions from two sources; selenocentric-selenodetic effect, and gravitational anomalies.

7.2.7   Odometer Error Model

For Concept 1, the passive, nongyro system, the speed (or distance) measuring device is an odometer. The error inputs contributed by an odometer are considered in this section.

For the odometer error contribution, the input is of the form

$$\sigma_o = \left(\frac{\Delta S}{S} \right) \qquad (7\text{-}89)$$

or the dimensionless 3σ error measure expressed as a ratio of distance error to distance traveled.

The sources of odometric error considered are:

1.   Change in effective wheel radius

2.   Angular transducer error

3.   Calibration error

4.   Slippage.

The odometer error is effectively time independent and may be developed as follows:

For any arc length

$$S = R\,\theta \qquad (7\text{-}90)$$

Taking total differentials

$$dS = R\,d\theta + \theta\,dR \qquad (7\text{-}91)$$

or, expressing Equation 7-91 in ratio form,

$$\frac{dS}{S} = \frac{d\theta}{\theta} + \frac{dR}{R}. \qquad (7\text{-}92)$$

7-38

Assuming independence, expressing the effectively normalized terms in Equation 7-92 as 3σ measures of error random variables and combining in an RSS manner,

$$\sigma_o^2 = \sigma_\theta^2 + \sigma_R^2. \tag{7-93}$$

The total error (σ_o^2) is due to rotational and radial contributions.

7.2.7.1 Rotational Errors

Contributions to the rotational error term, σ_θ, are due to the sources of angular transducer error, calibration error, and slippage. The transducer error, (a secondary effect, may be included in the calibration term. Then

$$\sigma_\theta^2 = \sigma_c^2 + \sigma_s^2 \tag{7-94}$$

where

$\sigma_c \equiv 3\sigma$ contribution from calibration error

$\sigma_s \equiv 3\sigma$ contribution from slippage error.

The slippage error is dependent upon such factors as terrain, wheel or track surface, vehicle load and speed, starting and stopping, etc. But with a relatively constant load and continuous mission, the important factors become terrain, wheel surface, and speed. To estimate the effects of slippage due to vehicle speed, and to observe the trend of varying parameters, the equation of motion of a rotating rigid shaft forced by a constant applied torque T_A is written

$$\ddot{\theta}_o I + f \dot{\theta}_o = T_A \tag{7-95}$$

where

I = angular moment of inertia

f = viscous damping.

The effects of slippage may be found by letting the viscous damping f be a piecewise linear function of time. Then the approximate distance recorded during the transient slip stage may be found to be

$$\Delta S \cong V_{SS} \left[\frac{A}{f_2} - \frac{B}{f_2} (f_2 - f_1) \right] \tag{7-96}$$

where

V_{SS} = steady-state vehicle speed

f_1 = initial viscous damping

f_2 = final viscous damping

A, B are constants. The vehicle speed contribution is $K_S V$.

To compensate for odometer slip due to terrain slope variations, the term $(K_{sp} p)$ is added.

$$K_{sp} = K_{sp} \quad p < 0$$

$$K_{sp} = 0 \quad p \geq 0.$$

Nominally $K_{sp} = 0.0021 \deg^{-1}$ for ELMS model and 6500-lb vehicle.

The total slip contribution is

$$\sigma_s = (K_S V)^2 + (K_{sp} p)^2. \tag{7-97}$$

7.2.7.2 Radial Errors

Contributions to the radial term σ_R of Equation 7-93 arise from the changes in effective wheel radius. There are two specific cases, one where the odometer wheel wears uniformly, and the second where the wheel is deflected (see Figures 7-12 and 7-13 respectively).
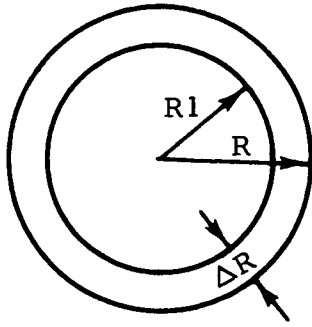
Figure 7-12 Radial Error
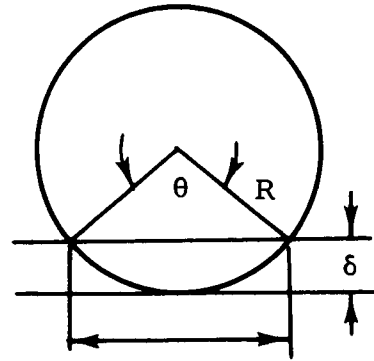
Figure 7-13 Wheel Deflection

It can be found in the first case that

$$\sigma_1 = \frac{\Delta R}{R} = \frac{\Delta S}{S} \qquad (7\text{-}98)$$

In the second case,

$$S_1 = R\theta$$

$$S_2 = \ell = 2R \sin \frac{\theta}{2}$$

$$S_1 - S_2 = R\theta - 2R \sin \frac{\theta}{2}$$

$$\Delta S \cong R\theta - 2R \left[\frac{\theta}{2} - \frac{\theta^3}{8 \cdot 6} \right]$$

$$\cong \frac{R\theta^3}{24}$$

but

$$\delta = R - R \cos \frac{\theta}{2}$$

$$\delta \cong R \left[\frac{\theta^2}{8} - \frac{\theta^4}{16 \cdot 24} \right]$$

$$\delta \cong R \frac{\theta^2}{8}$$

and

$$\frac{\Delta S}{S} = \frac{\delta}{3R} \qquad (7\text{-}99)$$

Now Equation 7-93 becomes

$$\sigma_o^2 = \sigma_c^2 + (K_s V)^2 + \left(\frac{\Delta R}{R}\right)^2 + \left(\frac{\delta}{3R}\right)^2 + \left(K_{sp} \, p\right)^2 \qquad (7\text{-}100)$$

The errors contributed by the dependency of resolving distance components from azimuth and pitch angle information errors is accounted for in the dead reckoning model.

7.2.8 IR, RF Earth Tracker Error Model

The vehicle azimuth sensor of Concept 1, passive, nongyro system, is a body-fixed infrared earth tracker. For Concept 3, RF technology system, the sensor is an RF earth tracker. Vehicle azimuth is obtained through computation. The necessary data inputs are earth ephemerii, time, vehicle position, vehicle attitude, and measured earth altitude and azimuth. The error model follows from the derivation of the initial bearing error model, Section 7.2.3.

The 3σ error in true azimuth is given as:

$$\sigma_A^{*2} = \begin{bmatrix} 1 & C_{17}^2 & C_{18}^2 & C_{19}^2 & C_{20}^2 & C_{21}^2 \end{bmatrix} \begin{bmatrix} \sigma_{AO}^2 \\ \sigma_{x_n}^2 \\ \sigma_{\alpha_i}^{*2} \\ \sigma_{u_E}^{*2} \\ \sigma_{w_E}^{*2} \\ \sigma_{y_n}^2 \end{bmatrix} \qquad (7\text{-}101)$$

where i = E such that

$$u_i \rightarrow u_E$$

$$w_i \rightarrow w_E$$

in the coefficient expressions for $C_{17}, \text{---} C_{21}$ of Section 7.2.3.

$$\sigma_{xn} = \frac{(\Delta R_N)_T}{R} \tag{7-102}$$

$$\sigma_{yn} = \frac{(\Delta R_E)_T}{R \cos x_n} \tag{7-103}$$

$$\sigma_{uE}^{*2} = (B_1 E \sin Et)^2 \left[(K_t t)^2 + \sigma_t^2 \right] + \sigma_{DE}^2 + \bar{\sigma}_{uE}^2 \tag{7-104}$$

$$\sigma_{wE}^{*2} = (B_2 E \cos Et)^2 \left[(K_t t)^2 + \sigma_t^2 \right] + \sigma_{RE}^2 + \bar{\sigma}_{wE}^2 \tag{7-105}$$

σ_{AO} is the initial bearing error from system alignment for Concept 1. For the RF concept, no initial alignment capability exists for the position fix subconcept and here σ_{AO} is equal to zero.

$$\sigma_{\alpha}^{*2} = C_{23}^2 \left(\sigma_e^2 + \sigma_{ce}^2 \right) + C_{22}^2 \left(\sigma_a^2 + \sigma_{ca}^2 \right) + C_{24}^2 \sigma_r^{*2} + C_{25}^2 \sigma_p^{*2}. \tag{7-106}$$

In Equations 7-104 and 7-105 the terms $\bar{\sigma}_{uE}$ and $\bar{\sigma}_{wE}$ are evaluated from Equations 7-53 and 7-54 of Section 7.2.3, respectively, with i = E. Also the term

$$\sigma_{\epsilon}^{*2} = C_{14}^2 \left(\sigma_e^2 + \sigma_{ce}^2 \right) + C_{13}^2 \left(\sigma_a^2 + \sigma_{ca}^2 \right) + C_{15}^2 \sigma_r^{*2} + C_{16}^2 \sigma_p^{*2}. \tag{7-107}$$

is used to evaluate the effective earth subpoint error in the term $\bar{\sigma}_{uE}, \bar{\sigma}_{wE}$.

Since the subpoint varies with time, as the dead reckoning process continues additional errors are contributed due to inaccuracies in time. The motion of the earth subpoint is a complex expression due to physical and optical librations. However, a first order approximation to the motion of the subpoint may be made, and sufficient accuracy results. The position of the earth, in selenographic latitude, u_E, and selenographic longitude, w_E, may be described by the parametric equations of an ellipse:

$$u_E = B_1 \cos Et \qquad (7-108)$$

$$w_E = B_2 \sin (Et + E_1) \qquad (7-109)$$

with the rates

$$\dot{u}_E = -B_1 E \sin Et \qquad (7-110)$$

$$\dot{w}_E = B_2 E \cos (Et + E_1). \qquad (7-111)$$

The parameter E_1, in radians, rotates the major axis of the ellipse. Circular and linear subpoint motion are special cases of this general representation.

7.2.9 Pendulous Vertical Sensor, Vertical Gyro Error Model

The dead reckoning error model requires as inputs errors in the local vertical. These errors depend upon the sensor type and vertical anomalies as discussed in Sections 7.2.5 and 7.2.6. A pendulous vertical sensor is used in Concepts 1 (passive, nongyro) and 3 (RF technology); a vertical gyro is the vertical reference of Concept 2 (inertial).

The expression modeling the sensor's errors are given below:

Pendulous Vertical:

$$\sigma_r^* = \left[(K_r r)^2 + \sigma_r^2 + \sigma_{rg}^2 \right]^{1/2} \qquad (7-112)$$

$$\sigma_p{}^* = \left[(K_p p)^2 + \sigma_p{}^2 + \sigma_{pg}{}^2 \right]^{1/2} \qquad (7\text{-}113)$$

For the static vertical sensor

$$K_r = K_p = K_{rs}$$

$$\sigma_r = \sigma_p = \sigma_{rs}$$

Vertical Gyro:

$$\sigma_r{}^* = \left[(K_r r)^2 + \sigma_r{}^2 + (\sigma_{rD} t)^2 + \sigma_{rg}{}^2 \right]^{1/2} \qquad (7\text{-}114)$$

$$\sigma_p{}^* = \left[(K_p p)^2 + \sigma_p{}^2 + (\sigma_{pD} t)^2 + \sigma_{pg}{}^2 \right]^{1/2} \qquad (7\text{-}115)$$

where the terms represent linearity, null sensitivity, vertical anomalies, and drift errors, respectively.

7.2.10 Directional Gyro and Accelerometer Error Model

The inertial system (system Concept 2) requires a gyro package for vertical and azimuth reference and accelerometers for distance measuring equipment. The output of three accelerometers, which measure the vehicle component accelerations, are doubly integrated to supply distance information. The components may be considered mounted to a stabilized platform or body fixed.

7.2.10.1 Accelerometer Errors

The principal error sources are:

1. Null Sensitivity

   . Insensitivity to threshold accelerations, and/or uncertainty in basic g measurement.

2. Scale Factor

   Linear errors.

3. Cross Coupling

   Errors due to misalignment of sensitive axis and/or instrument errors; e. g. , x-axis acceleration measurements affect y-axis.

4. Vibrational Effects

   a. Vibropendulous Error. — In a pendulous accelerometer a vibropendulous error torque is generated due to linear vibrational forcing functions. The vibrational forcing function generates an average torque and the accelerometer indicates the presence of a ficticious signal. As the frequency of the oscillating input approaches zero, this error source becomes the cross coupling effect.

   b. Size Effects. — Due to physical displacement of the instrument from the vehicle cg, angular accelerations induce instrument errors.

   c. Sculling. — If accelerometers are mounted such that an orthogonal triad is formed, linear vibrational motion on one axis and angular vibrations of the same frequency on the second will produce linear accelerations on an axis perpendicular to the two.

7. 2. 10. 2 Gyro Errors

The principal error sources are

1. Bias

   A non-g-sensitive error source which produces constant drift rate and basic angular measurement uncertainties.

2. Proportional

A g-sensitive error source which induces drift rates when linear acceleration is applied. Gimbal mass unbalance is a typical source.

3. Torquing Error

Drift errors induced by linearity and uncertainty in the torquing signals.

4. Random Drift

The error drift rates which are not compensated.

5. Vibrational Effects

a. Anisoelastic. — In a floated gyro, unequal elasticity along the spin axis and input axis give rise to a steady-state drift rate when linear accelerations are present on both axes simultaneously.

b. Cylindrical Torque. — In a floated gyro, angular accelerations induced upon the output axis give rise to average drift rates if unequal elasticity is present between the spin axis and input axis.

c. Coning. — If the input axis of a SDF floated gyro is displaced such that a cone is swept out, a gyro drift rate will be developed, and the gyro responds to an actual input rate.

d. Anisoinertia. — Simultaneous angular oscillations about the input and spin axes induce gyro drift rates if unequal gimbal inertias exist about these axes.

7.2.10.3 Platform Errors

1. Initial level misalignment

2. Initial azimuth misalignment

3. Drift

4. Component non-orthogonality.

7.2.10.4 Computer Errors

1. Platform

Computation errors would be mainly integrator offset and drift errors if an analog system. If digital, the computation errors are negligible.

2. Body Fixed

In a gimballess system, all coordinate transformations must be made through computations. The errors would arise in truncation, round-off, coordinate transformation matrix commutation, and speed of calculations.

7.2.10.5 Accelerometer Model

The dead reckoning error model is based on a north, east, vertical analytic navigation system. If the system is platform mounted, accelerations will be sensed in the $(\vec{1}_N, \vec{1}_E, \vec{1}_Z)$ system. However, if the accelerometers are mounted to the vehicle structure, a coordinate transformation is required to determine the local vertical, north, east components of acceleration. This transformation is given, with the vehicle sequentially rotated in azimuth A, pitch p, and roll r.

$$
\begin{bmatrix} \vec{1}_x \\ \vec{1}_y \\ \vec{1}_z \end{bmatrix} = \begin{bmatrix} \cos p \cos A & \cos p \sin A & -\sin p \\ -\sin A \cos r + \sin r \sin p \cos A & \cos r \cos A + \sin r \sin p \sin A & \sin r \cos p \\ \sin r \sin A + \sin p \cos A \cos r & -\sin r \cos A + \cos r \sin p \sin A & \cos r \cos p \end{bmatrix} \begin{bmatrix} \vec{1}_N \\ \vec{1}_E \\ \vec{1}_Z \end{bmatrix}
$$

(7-116)

or

$$
\begin{bmatrix} \vec{1}_x \\ \vec{1}_y \\ \vec{1}_z \end{bmatrix} = \begin{bmatrix} T_{Apr} \end{bmatrix} \begin{bmatrix} \vec{1}_N \\ \vec{1}_E \\ \vec{1}_Z \end{bmatrix} \qquad (7\text{-}117)
$$

Thus component accelerations measured in a body-fixed space may be related to the local vertical space by measuring A, p, r, and computing the transformation with the matrix T_{Apr}. Therefore, whether the system is body fixed or stabilized, accelerometer outputs are resolved into the components:

A_N : along $\vec{1}_N$

A_E : along $\vec{1}_E$

A_Z : along $\vec{1}_Z$

Applying vector analysis techniques, the vehicle component accelerations $\dot{V}_N$, $\dot{V}_E$, $\dot{V}_Z$ may be derived:

$$
\dot{V}_N = A_N - \frac{V_N V_Z}{R_m} + \frac{V_E^2}{R_m} \tan x - 2 \dot{w}_s \, V_E \sin x \qquad (7\text{-}118)
$$

$$
\dot{V}_E = A_E + \frac{V_E V_N}{R_m} \tan x - \frac{V_E V_Z}{R_m} + 2 \dot{w}_s \, V_N \sin x + 2 \dot{w}_s \, V_z \cos x \qquad (7\text{-}119)
$$

$$
\dot{V}_Z = A_Z + \frac{V_E^2}{R_m} + \frac{V_N^2}{R_m} + 2 \dot{w}_s \, V_E \cos x - g \qquad (7\text{-}120)
$$

where

$$\left\{ \dot{V}_N, \; V_N, \; \dot{V}_E, \; V_E, \; \dot{V}_Z, \; V_Z \right\} = \text{vehicle accelerations and velocity}$$

in north, east and vertical direction respectively

x = vehicle latitude

$\dot{w}_s$ = lunar sidereal rate (neglect physical librations)

g = lunar gravity.

$A_N, \; A_E, \; A_Z$ = accelerometer outputs.

In the instrumentation of the system, ideally the Coriolis acceleration terms (e.g., $2\dot{w}_s \; V \sin x$, and $V_E V_N / R$) and centripetal accelerations (V^2/R) must be compensated for; however, consideration of the relative magnitude of these terms shows that for purposes of error model derivation, contributions of errors from these apparent force terms will be negligible. For example, allowing an error in velocity of 1 km/hr at 65° latitude

$$\frac{V_E^2}{R_m} \tan x = 1.23 \times 10^{-3} \; \text{km/hr}^2 = 0.604 \times 10^{-9} \; g.$$

To accommodate changes in vehicle path and vehicle velocity, an acceleration model is required. The basic philosophy is again a steady-state approach over extended mission durations to provide compatibility with the error model formulation. The general form of operator applied vehicle accelerations is shown in Figure 7-14.
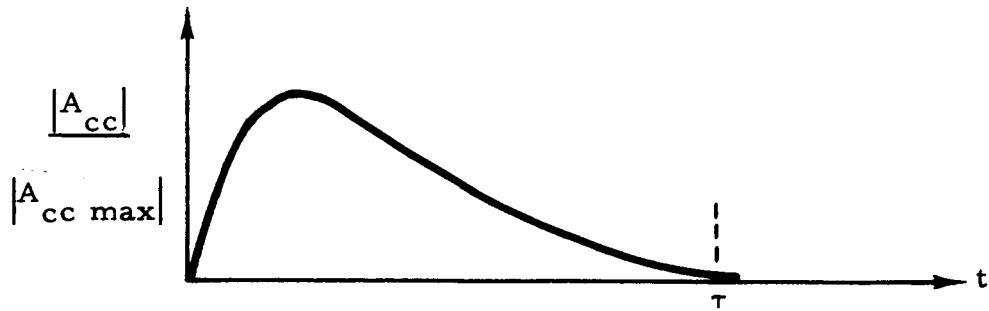
Figure 7-14 Applied Vehicle Accelerations

Because of extensive mission operating times, this can certainly be approximated as shown in Figure 7-15.
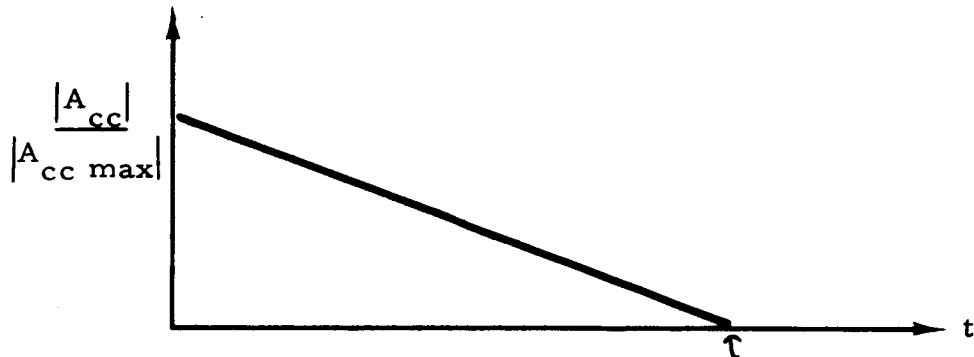
Figure 7-15 Approximate Applied Vehicle Accelerations

Both the body-centered acceleration and analytic system acceleration sensed by on-board accelerometers can be determined from this functional form of the accelerations and actual changes in the vehicle velocity vector.

The maximum vehicle acceleration available, as a function of terrain slope, is constrained to be

$$A_{ccmax} = {}^+K_{A1}P_{n, n+1} {}^+K_{A2} \qquad (7\text{-}121)$$

where K_{A1}, K_{A2} are functions of vehicle path and vehicle type.

Nominally,

$$K_{A1} = 510 \frac{km}{hr^2 \ deg}$$

$$K_{A2} = 10271 \frac{km}{hr^2}$$

With reference to the vehicle analytic coordinate system, the vehicle component velocity change can be calculated from incremental leg to incremental leg:

$$\left| \vec{\Delta V} \right| = \Delta V = \left[\Delta V_N^2 + \Delta V_E^2 + \Delta V_Z^2 \right]^{1/2} \qquad (7\text{-}122)$$

$$\Delta V_N = V_{n,n+1} \cos P_{n,n+1} \cos A_{n,n+1} - V_{n-1,n} \cos P_{n-1,n} \cos A_{n-1,n} \qquad (7\text{-}123)$$

$$\Delta V_E = V_{n,n+1} \cos P_{n,n+1} \sin A_{n,n+1} - V_{n-1,n} \cos P_{n-1,n} \sin A_{n-1,n} \qquad (7\text{-}124a)$$

$$\Delta V_Z = V_{n,n+1} \sin P_{n,n+1} - V_{n-1,n} \sin P_{n-1,n} \qquad (7\text{-}124b)$$

where ΔV_N, ΔV_E, and ΔV_Z now represent the change in steady-state component velocities.

Since the vehicle velocity changes are known, the vehicle accelerations may be derived. The following constraint is imposed upon vehicle accelerations.

$$A_{ccmax} \geqq \left| \vec{A}_{cc} \right| = \left[A_N^2 + A_E^2 + A_Z^2 \right]^{1/2} \qquad (7\text{-}125)$$

where $\left| \vec{A}_{cc} \right|$ is the analytic system sensed acceleration with the components A_N, A_E, A_Z.

Using the functional form of the acceleration shown in Figure 7-15, the steady-state velocity is

$$V_{SS} = \frac{A_{cc} T}{2} \qquad (7\text{-}126)$$

Applying this relation to the inequality constraint, Equation 7-125 yields:

$$\left[\left(\frac{2\Delta V_N}{\tau}\right)^2 + \left(\frac{2\Delta V_E}{\tau}\right)^2 + \left(\frac{2\Delta V_Z}{\tau}\right)^2\right]^{1/2} \leq A_{cc\,max} \quad (7-127)$$

or

$$\tau \leq \frac{2\Delta V}{A_{cc\,max}} \quad (7-128)$$

Now, arbitrarily taking the premise that the vehicle operator will apply one-half the total available acceleration or deceleration during a maneuver, the following results:

$$\tau = \frac{4\Delta V}{A_{cc\,max}} \quad (7-129)$$

The analytic system accelerations may now be solved.

$$A_N = \frac{\Delta V_N}{\Delta V} (1/2\,A_{cc\,max}) \quad (7-130)$$

$$A_E = \frac{\Delta V_E}{\Delta V} (1/2\,A_{cc\,max}) \quad (7-131)$$

$$A_Z = \frac{\Delta V_Z}{\Delta V} (1/2\,A_{cc\,max}) \quad (7-132)$$

If the accelerometers are body fixed, the sensed component accelerations in a body-centered system are:

$$\left[A_x A_y A_z\right] = \left[A_N A_E A_Z\right] \left[T_{Apr}\right]^{-1} \quad (7-133)$$

where

$$[T_{Apr}] \text{ is identified by Equation 7-116.}$$

An analysis was performed to relate errors in the $(\vec{1}_x, \vec{1}_y, \vec{1}_z)$ coordinate system to output errors in the $(\vec{1}_N, \vec{1}_E, \vec{1}_Z)$ reference. After extensive manipulation, the result was

Body Fixed:

$$\sigma_{A_{c'c}}{}^2 = \sigma_{Ax}{}^2 + \sigma_{Ay}{}^2 + \sigma_{Az}{}^2 + C_{26}{}^2 \sigma_p^{*2} + C_{27}{}^2 \sigma_r^{*2} + C_{28}{}^2 \sigma_A^{*2}$$

(7-134)

$$+ \left(K_{A3} \right)^2 \left(A_x{}^2 + A_y{}^2 + A_z{}^2 \right)$$

$$C_{26}{}^2 = A_x{}^2 + (\sin r A_y)^2 + (A_z \cos r)^2 + 2 \cos r \sin r A_z A_y \qquad (7-135)$$

$$C_{27}{}^2 = A_y{}^2 + A_z{}^2 \qquad (7-136)$$

$$C_{28}{}^2 = (A_x \cos p)^2 + A_y{}^2 (\cos^2 r + \sin^2 r \sin^2 p) + A_z{}^2 (\sin^2 r + \cos^2 r \sin^2 p)$$

(7-137)

$$+ 2 A_x A_y (\cos p \sin r \sin p) + 2 A_x A_z (\cos p \cos r \sin p)$$

where

$(A_x, A_y, A_z) =$ sensed accelerations along $\vec{1}_x, \vec{1}_y, \vec{1}_z$

$\sigma_p^*, \sigma_r^*, \sigma_A^* =$ pitch, roll, and azimuth sensing equipment or alignment errors

$C_{26}, C_{27}, C_{28} =$ partial derivative error sensitivity coefficients

$K_{A3} =$ linearity error of accelerometers.

For a stabilized platform, the quantities r and p of Equations 7-135, 7-136, and 7-137 are equal to zero.

The accelerometer input to the dead reckoning error model is in the following normalized form

$$\sigma_o = \frac{\left[\sigma_{A_x}^2 + \sigma_{A_y}^2 + \sigma_{A_z}^2\right]^{1/2}\left[t_{n+1}^2 - t_n^2\right]}{2 D_{n,\,n+1}}$$

(7-138)

$$+ \frac{\left[(C_{26}\sigma_p^*)^2 + (C_{27}\sigma_r^*)^2 + (C_{28}\sigma_A^*)^2 + K_{A3}^2(A_x^2 + A_y^2 + A_z^2)\right]^{1/2}(\tau)(t_{n+1}-t_n)}{2 D_{n,\,n+1}}$$

7.2.10.6 Directional Gyro Model

The directional gyro error model has the form

$$\sigma_A^{*2} = \sigma_{AO}^2 + (\sigma_{gD}t)^2 + (\sigma_{GA})^2$$

where

σ_{AO} = initial alignment error (Section 7.2.3)

σ_{GA} = uncertainty in angular measurement

σ_{gD} = drift error.

The degradation of gyro performance due to torquing errors, random drift, proportional and vibrational effects, is collected in the drift term.

All vibrational errors have been combined in the drift term since preliminary data indicate vehicle suspension natural frequencies are much lower than 5 cps. The vibrational effects such as anisoelastic error and cylindrical torque depend upon the frequency of oscillation, but

material resonances occur at frequencies of about 1 kc to 3 kc at which these effects peak. This is far in excess of an assumed vehicle bandpass of 5 cps. Thus the vehicle suspension system acts as a lowpass filter upon noise inputs from wheels or tracks traversing the terrain. The result is that vibrational amplitudes will be significantly attenuated and the accelerometer and gyros mounted in a satisfactory environment. High frequency vibrational pick-up from within the vehicle (power supply hum or drive motor inputs) are combined in the drift term as previously stated.

7.2.11 Doppler Radar Error Model

The distance error input, σ_o, required as an input to the dead reckoning model is:

$$\sigma_o = \frac{\sigma_V^* (t_{n+1} - t_n)}{D_{n,\,n+1}} \qquad (7\text{-}139)$$

where

$$\sigma_V^* = 3 \text{ sigma error measure of sensed vehicle speed.}$$

The error equations are derived for a single beam CW (or pulsed) doppler radar. The radar is body mounted and aligned in the plane of the vehicle longitudinal axis. Components of the vehicle velocity are obtained through resolution of speed data by pitch and azimuth sensor data. It is shown below that the vehicle speed error σ_V^* is

$$\sigma_V^* = \left[(C_{29}\sigma_f)^2 + (C_{30}\sigma_\delta^*)^2 + (\sigma_b)^2 \right]^{1/2} \qquad (7\text{-}140$$

where

$$C_{29} = \frac{\lambda_S}{2} \sec \delta \qquad (7\text{-}141)$$

$$C_{30} = K_1 V \tan \delta \qquad (7\text{-}142)$$

$$\sigma_f = \frac{3}{2} \sqrt{\frac{V \cos \delta}{\lambda_S T}} \qquad (7\text{-}143)$$

$$\sigma_\delta^* = \left[\sigma_\delta^2 + \sigma_p^{*2} \right]^{1/2} \qquad (7\text{-}144)$$

where

σ_b = 3 sigma bias error.

Derivation:

The generalized doppler equation is given as

$$f_o = \frac{f_S \left[c + \dfrac{\vec{\rho} \cdot \vec{V}_R}{|\vec{\rho}|} \right]}{c + \dfrac{\vec{\rho} \cdot \vec{V}_S}{|\vec{\rho}|}} \qquad (7\text{-}145)$$

where

f_o = frequency at receiver

f_S = frequency at transmitter (carrier)

c = velocity of light

$\vec{D}$ = position vector from transmitter to receiver

$\vec{V}_R$ = velocity vector of receiver

$\vec{V}_S$ = velocity vector of transmitter

For transmitter and receiver aboard the same vehicle,

$$f_o = f_S \frac{\left[1 + \dfrac{V}{C} \cos \delta \right]}{1 - \dfrac{V}{C} \cos \delta} \qquad (7\text{-}146)$$

The geometry is defined in Figure 7-16, where $(\vec{1}_x, \vec{1}_y, \vec{1}_z)$ is fixed to the vehicle body axis; δ is the antenna pitch angle.
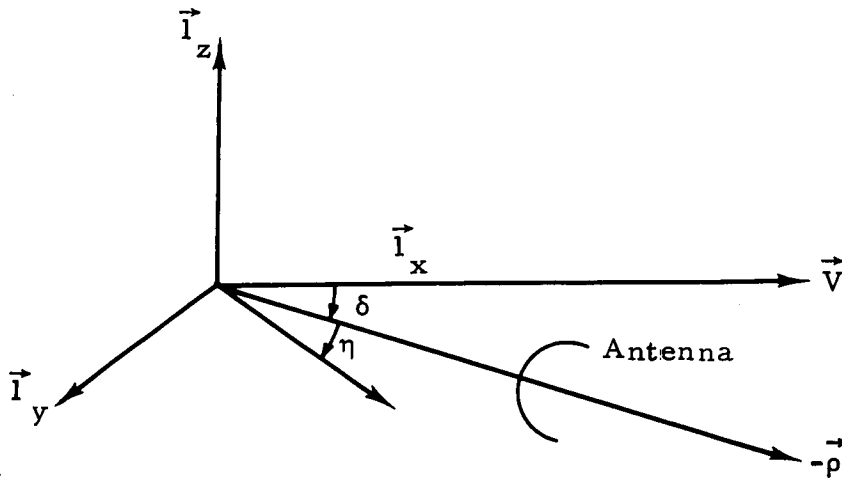
Figure 7-16 Doppler Antenna Pointing Angle

Now, dividing the denominator into the numerator, the following expansion results,

$$f_o = f_S \left[1 + \frac{2V}{c} \cos \delta + 2 \left(\frac{V}{c} \right)^2 \cos^2 \delta + \dots \right] \qquad (7-147)$$

Neglecting second order and higher terms,

$$f_o \cong f_S \left[1 + \frac{2V}{c} \cos \delta \right] \qquad (7-148)$$

or the doppler shift is

$$f_o - f_S = \frac{2f_S V}{c} \cos \delta \qquad (7-149)$$

then

$$f_m = \frac{2V}{\lambda_S} \cos \delta = \text{modulation frequency} \qquad (7-150)$$

Solving for V

$$V = \frac{f_m \lambda_S}{2} \sec \delta \qquad (7\text{-}151)$$

If a misalignment exists, and the antenna axis is perturbed in yaw, η, about the vehicle $\vec{1}_z$ axis (Figure 7-16)

$$V = \frac{f_m \lambda_S}{2} \sec \delta \sec \eta \qquad (7\text{-}152)$$

Hence

$$V = f(f_m, \lambda_S, \delta, \eta)$$

and

$$dV = \frac{\partial V}{\partial f_m} df_m + \frac{\partial V}{\partial \lambda_S} d\lambda_S + \frac{\partial V}{\partial \delta} d\delta + \frac{\partial V}{\partial \eta} d\eta \qquad (7\text{-}153)$$

Evaluation of the partial derivatives yields

$$dV = \frac{\lambda_S}{2} \sec \delta \sec \eta \, df_m + \frac{f_m}{2} \sec \delta \sec \eta \, d\lambda_S$$

$$+ \frac{\lambda_S f_m}{2} \sec \delta \sec \eta \tan \delta \, d\delta \qquad (7\text{-}154)$$

$$+ \frac{\lambda_S f_m}{2} \sec \delta \sec \eta \tan \eta \, d\eta$$

but nominally

$$\eta = 0 \text{ and } d\lambda_S \cong 0, \text{ then}$$

$$dV = \frac{\lambda_S}{2} \sec \gamma \, df_m + \frac{\lambda_S f_m}{2} \sec \delta \tan \delta \, d\delta \qquad (7\text{-}155)$$

Expressing the differentials as 3 sigma values and taking the root-sum-square:

$$\sigma_V = \left[\left(\frac{\lambda_S}{2} \sec \gamma \right)^2 \sigma_f^2 + \left(V \tan \delta \right)^2 \sigma_\delta^{*2} \right]^{1/2} \qquad (7\text{-}156)$$

An expression for the uncertainty in the modulation frequency is given (Ref. 13) as

$$\sigma_f = \frac{3 f_m}{2 \sqrt{N}} \qquad (7\text{-}157)$$

where N is the number of samples taken by the frequency determining device in time T. But to fully characterize a band-limited signal, from sampling theory, the number of samples taken per second should be $2 f_m$. Hence

$$\sigma_f = 3 \sqrt{\frac{f_m}{8T}} \qquad (7\text{-}158)$$

and substituting for f_m from Equation 7-148

$$\sigma_f = \frac{3}{2} \sqrt{\frac{V \cos \delta}{\lambda_S T}} \qquad (7\text{-}159)$$

A bias error, σ_b, is added to compensate for errors in data read out.

Nominal values are:

$$\delta = 30^\circ$$

$$T = 0.0014 \text{ hours}$$

$$\lambda_S = 0.00003 \text{ km}$$

$$f_o = 10^{10} \text{ cps.}$$

7.2.12   CSM Reference Error Model

Error models are derived for the CSM reference concepts given in Table 7-2.

TABLE 7-2

CSM REFERENCE CONCEPTS

Function	Technique/ Sensed Variables	On-Board LRV Equipment	LRV Status/ Number of Data Points	Required CSM Position Data
Heading Reference	Angular CSM elevation CSM azimuth	Antenna Tracking Optical Tracking	Static One	Radius Latitude Longitude
Position Reference	Angular CSM elevation CSM azimuth	Antenna Tracking Optical Tracking	Static Two	Radius Latitude Longitude
	Ranging CSM range	RF Tracking (CW or Pulse)	Static Three	Radius Latitude Longitude

CSM Orbit:

The error models are based upon the assumption that:

1.   CSM is in a circular orbit

2.   CSM position known in a selenocentric spherical coordinate system.

A requirement of the error model is that the position of the CSM in the circular orbit be known as a function of time. For convenience the selected coordinate system defining the CSM position is a spherical latitude, longitude, altitude selenocentric system. This choice assures compatibility with previously derived models. The geometry is shown in Figure 7-17.
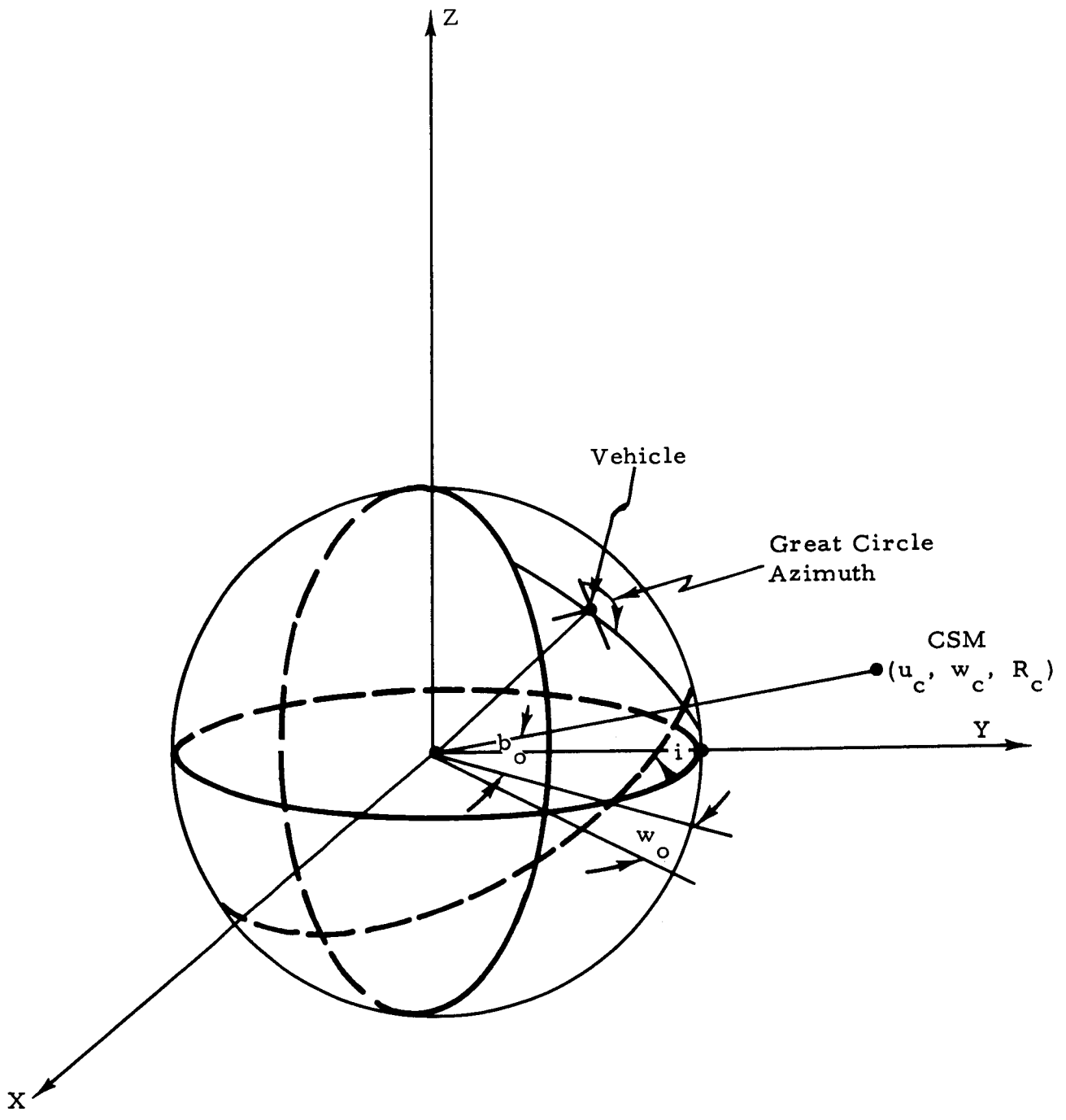
Figure 7-17 CSM Orbital Geometry

For a circular orbit, the CSM position is specified by

u_c = CSM latitude

w_c = CSM longitude

R_c = CSM orbit radius.

With the application of spherical trigonometry to the geometry of Figure 7-17 the following can be derived:

$$u_c(t) = \sin^{-1} \left[\sin \left(\frac{V_c t}{R_c} + b_o \right) \sin i \right] \tag{7-160}$$

$$w_c(t) = \sin^{-1} \left[\frac{\sin \left(\dfrac{V_c t}{R_c} + b_o \right) \cos i}{\cos u_c} \right] - \dot{w}_s t + w_o \tag{7-161}$$

where

w_o = initial longitude of equator - orbit intersection

b_o = initial solid angle rotation along the CSM orbit from w_o

i = orbit inclination from equator

V_c = CSM tangential velocity

$\dot{w}_s$ = lunar sidereal rate

t = time.

7.2.12.1   CSM Position Reference Error Model

Angular Technique

Position of the vehicle may be determined if the CSM is treated as a celestial observable and elevation and azimuth measurements are

made from the vehicle to the CSM. Two independent measurements and a knowledge of the CSM position at the instant of data acquisition are necessary. (It is assumed that the ambiguities in the locus of vehicle position can be resolved.)

Figure 7-18 shows the instantaneous geometry of the great circle azimuthal plane of the vehicle intersecting the CSM orbit.

The following expressions can be written

$$\cos E_i = \sin u_{c_i} \sin x_n + \cos u_{c_i} \cos x_n \cos (w_{c_i} - y_n) \quad (7\text{-}162)$$

$$E_i = 180^\circ - F_i - G \quad (7\text{-}163)$$

$$F_i = 90 + \epsilon_i^* \quad (7\text{-}164)$$

$$G_i = \sin^{-1} \left[\frac{R_n \sin F_i}{R_c} \right] \quad (7\text{-}165)$$

$$E_i = 90 - \epsilon_i^* - \sin^{-1} \left[\frac{R_n \cos \epsilon_i^*}{R_c} \right] \quad (7\text{-}166)$$

$$R_n = R_m + h_n \quad (7\text{-}167)$$

$\{x_n, y_n, h_n\} \equiv$ vehicle latitude, longitude, altitude at point n.

$\epsilon_i^* \equiv$ true elevation angle of CSM.

Equation 7-162 is of the same form from which the position fix error model using celestial sighting was derived. For that model, E_i is the measured true co-altitude to the observable. However, for the CSM model, E_i is not the measured co-altitude due to the relatively low altitude of the CSM (as compared to the "infinite" radius of the celestial sphere)

Geometry of ith Instantaneous Point:
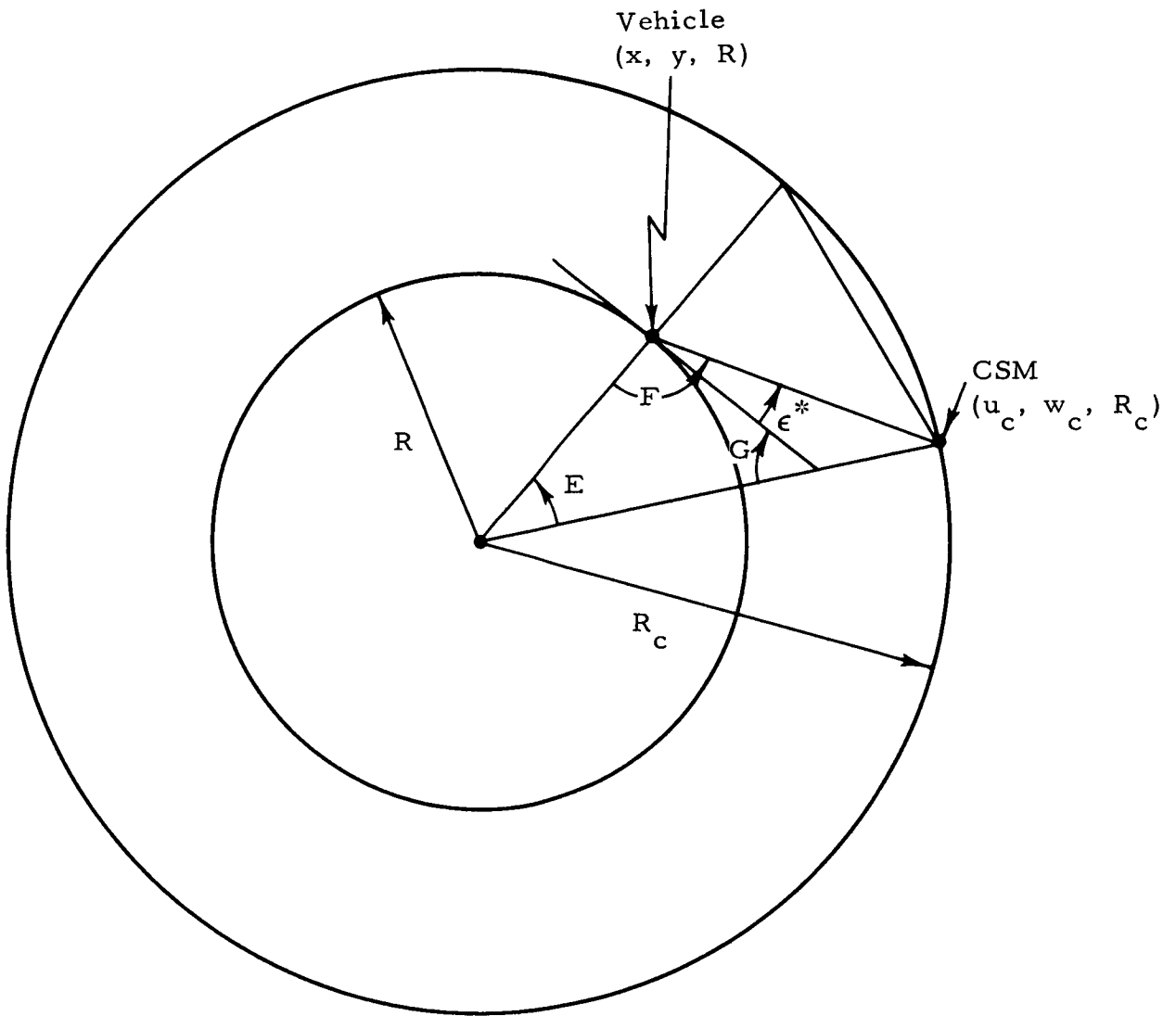
Figure 7-18 Great Circle Plane Intersecting Vehicle and CSM

but rather the lunar central angle between the CSM and the observer. The same model is applicable however, with one alteration. The total differential of E_i must be evaluated. Thus, $E = f(\epsilon, R_n, R_c)$ from Equation 7-166,

$$dE = \frac{\partial E}{\partial \epsilon} \, d\epsilon + \frac{\partial E}{\partial R_n} \, dR_n + \frac{\partial E}{\partial R_c} \, dR_c \qquad (7\text{-}168)$$

and putting the total differentials equal to 3 σ error measures and summing in a RSS fashion.

$$\sigma_{E_i}^{*\,2} = C_{31}^2 \, \sigma_{\epsilon_i}^{*\,2} + C_{32}^2 \, \sigma_{h_n}^2 + C_{33}^2 \, \sigma_{h_c}^2$$

where:

σ_{h_n} $\equiv$ Vehicle altitude or lunar attitude error

σ_{h_c} $\equiv$ CSM altitude error

$\sigma_{\epsilon_i}^{*}$ $\equiv$ CSM tracker elevation error.

$$C_{31} = \frac{\partial E}{\partial \epsilon_i^{*}} = \frac{\sin \epsilon_i^{*}}{\sqrt{\left(\dfrac{R_c}{R_n}\right)^2 - \cos^2 \epsilon_i^{*}}} - 1 \qquad (7\text{-}169)$$

$$C_{32} = \frac{\partial E}{\partial R_n} = - \frac{\cos \epsilon_i^{*}}{\sqrt{R_c^2 - R_n^2 \cos^2 \epsilon_i^{*}}} \qquad (7\text{-}170)$$

$$C_{33} = \frac{\partial E}{\partial R_c} = \frac{\cos \epsilon_i^{*}}{R_c \sqrt{\left(\dfrac{R_c}{R_n}\right)^2 - \cos^2 \epsilon_i^{*}}} \qquad (7\text{-}171)$$

Since the term representing the transformed CSM tracker elevation measurement error is now available, the position fix model can be generated in the same manner as the position fix model of the celestial tracking technique. Referring to Section 7.2.2, the position fix error model is:

$$
\begin{bmatrix} \sigma_x^2 \\ \\ \sigma_y^2 \end{bmatrix} = \begin{bmatrix} C_1^2 & C_2^2 & C_3^2 & C_4^2 & C_5^2 & C_6^2 \\ \\ C_7^2 & C_8^2 & C_9^2 & C_{10}^2 & C_{11}^2 & C_{12}^2 \end{bmatrix} \begin{bmatrix} \sigma_{E_1}^{*\,2} \\ \\ \sigma_{u_{c_1}}^{*\,2} \\ \\ \sigma_{w_{c_1}}^{*\,2} \\ \\ \sigma_{E_2}^{*\,2} \\ \\ \sigma_{u_{c_2}}^{*\,2} \\ \\ \sigma_{w_{c_2}}^{*\,2} \end{bmatrix}
\tag{7-172}
$$

where

$C_1 \ldots C_{12}$ are derived in Section 7.2.2

$i = 1 = > $ 1st observation of the CSM

$i = 2 = > $ 2nd observation of the CSM

$$
\sigma_{u_{c_i}}^{*} = \frac{\overline{\Delta R}_N}{R_c} K_2
\tag{7-173}
$$

$$\sigma^*_{w_{c_i}} = K_2 \frac{\overline{\Delta R}_E}{R_c \cos u_{c_i}} \qquad (7\text{-}174)$$

$$K_2 = 57.296 \text{ deg/rad}$$

$$\overline{\Delta R}_N, \ \overline{\Delta R}_E = \text{CSM positional uncertainty, km.}$$

Ranging Technique

Vehicle position may be determined by taking three independent range measurements of the CSM. Ranging techniques using pulse or CW phase shifting techniques such as used in SECOR apply to the derived error model. Also laser ranging techniques apply to the error model philosophy. Range rate techniques such as used in the Transit program are discredited because of the slow lunar sidereal rate which gives rise to position ambiguities[4].

The instantaneous geometry of the ranging technique is shown in Figure 7-19.

It can be seen that:

$$R_{nc_i}^2 = R_n^2 + R_c^2 - 2 R_n R_c \cos E_i \qquad (7\text{-}175)$$

$$R_{nc} = \text{vehicle to CSM range, km}$$

and, as before,

$$\cos E_i = \sin u_{c_i} \sin x_n + \cos u_{c_i} \cos x_n \cos (w_{c_i} - y_n) \qquad (7\text{-}176)$$

Equations 7-175 and 7-176 are implicit relations of the dependent variables R_n, x_n, y_n. Three independent measurements of the range R_{nc} and knowledge of the CSM latitude u_c, and longitude w_c, will fix the vehicle position. Taking the total differentials, treating the differentials as 3σ error measures, and summing in an RSS manner, yields:
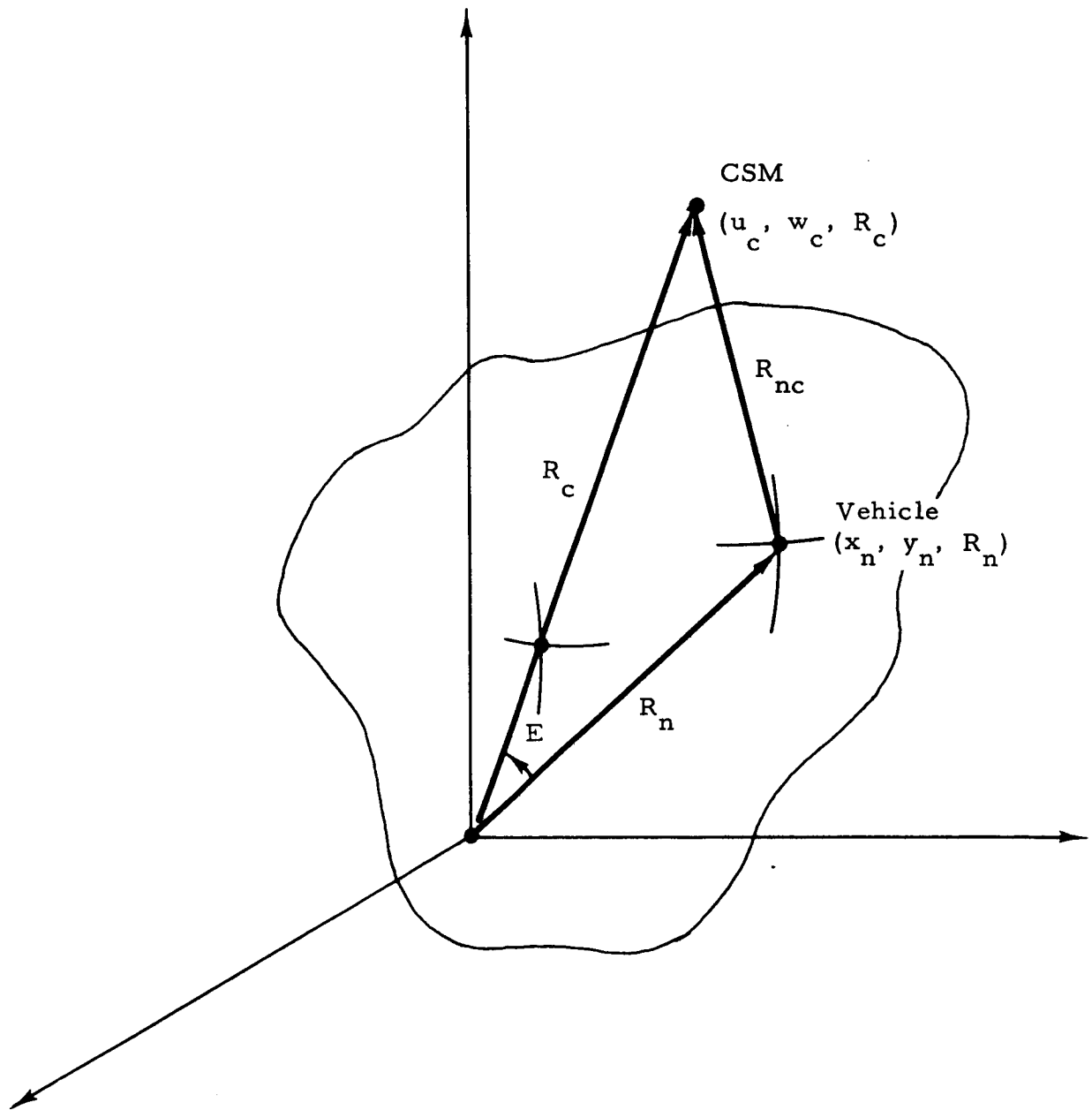
Figure 7-19 Ranging Instantaneous Geometry

$$
\begin{bmatrix} \sigma_{h_n}^2 \\[6pt] \sigma_{x_n}^2 \\[6pt] \sigma_{y_n}^2 \end{bmatrix}
=
\begin{bmatrix}
J_1^2 & J_2^2 & J_3^2 & J_4^2 & J_5^2 & J_6^2 & J_7^2 & J_8^2 & J_9^2 & J_{10}^2 \\[6pt]
J_{11}^2 & J_{12}^2 & J_{13}^2 & J_{14}^2 & J_{15}^2 & J_{16}^2 & J_{17}^2 & J_{18}^2 & J_{19}^2 & J_{20}^2 \\[6pt]
J_{21}^2 & J_{22}^2 & J_{23}^2 & J_{24}^2 & J_{25}^2 & J_{26}^2 & J_{27}^2 & J_{28}^2 & J_{29}^2 & J_{30}^2
\end{bmatrix}
\begin{bmatrix}
\sigma_{R_{nc_1}}^2 \\[6pt]
\sigma_{R_{nc_2}}^2 \\[6pt]
\sigma_{R_{nc_3}}^2 \\[6pt]
\sigma^*_{u_{c_1}}{}^2 \\[6pt]
\sigma^*_{u_{c_2}}{}^2 \\[6pt]
\sigma^*_{u_{c_3}}{}^2 \\[6pt]
\sigma^*_{w_{c_1}}{}^2 \\[6pt]
\sigma^*_{w_{c_2}}{}^2 \\[6pt]
\sigma^*_{w_{c_3}}{}^2 \\[6pt]
\sigma_{R_c}^2
\end{bmatrix}
\qquad (7\text{-}177)
$$

where

J_K for $K = 1 \ldots 30$ are partial derivative error sensitivity coefficients and are listed below.

$\sigma_{R_{nc_i}}$ = 3σ equipment errors in making the range measurements

$\sigma_{u_{c_i}}^{*}$ = CSM latitude error (Equation 7-173)

$\sigma_{w_{c_i}}$ = CSM longitudinal error (Equation 7-174)

σ_{R_c} = 3σ orbit radius uncertainty

usually

$$\sigma_{R_{nc_1}} = \sigma_{R_{nc_2}} = \sigma_{R_{nc_3}}$$

$$\sigma_{u_{c_1}}^{*} = \sigma_{u_{c_2}}^{*} = \sigma_{u_{c_3}}^{*}$$

Following is a listing of the error sensitivity coefficients; however, the following changes in nomenclature were used:

$$b_i = R_{nc_i}$$

$$r = R_n$$

$$c = R_c$$

$$u_i = u_{c_i}$$

$$w_i = w_{c_i}$$

$$\cos E_i = \sin u_i \sin x + \cos u_i \cos x \cos (w_i - y)$$

$$F = b_1^2 + r^2 + c^2 - 2 \, rc \, (\sin u_1 \sin x + \cos u_1 \cos x \cos (w_1 - y))$$

$$G = - b_2^2 + r^2 + c^2 - 2 \, rc \, (\sin u_2 \sin x + \cos u_2 \cos x \cos (w_2 - y))$$

$$H = - b_3^2 + r^2 + c^2 - 2 \, rc \, (\sin u_3 \sin x + \cos u_3 \cos x \cos (w_3 - y))$$

$$F_x = -2 \, rc \, (\cos x \sin u_1 - \cos u_1 \sin x \cos (w_1 - y))$$

$$G_x = -2 \, rc \, (\cos x \sin u_2 - \cos u_2 \sin x \cos (w_2 - y))$$

$$H_x = -2 \, rc \, (\cos x \sin u_3 - \cos u_3 \sin x \cos (w_3 - y))$$

$$F_y = -2 \, rc \cos u_1 \cos x \sin (w_1 - y)$$

$$G_y = -2 \, rc \cos u_2 \cos x \sin (w_2 - y)$$

$$H_y = -2 \, rc \cos u_3 \cos x \sin (w_3 - y)$$

$$F_r = 2r - 2c \cos E_1$$

$$G_r = 2r - 2c \cos E_2$$

$$H_r = 2r - 2c \cos E_3$$

$$D = F_x (G_y H_r - G_r H_y) - F_y (G_x H_r - H_x G_r) + F_r (G_x H_y - G_y H_x)$$

$$F_{b_1} = -2b_1$$

$$G_{b_1} = 0$$

$$H_{b_1} = 0$$

$$F_{b_2} = o$$

$$G_{b_2} = -2b_2$$

$$H_{b_2} = 0$$

$$F_{b_3} = 0$$

$$G_{b_3} = 0$$

$$H_{b_3} = -2b_3$$

$$F_c = -2c - r \cos E_1$$

$$G_c = 2c - r \cos E_2$$

$$H_c = 2c - r \cos E_3$$

$$F_{u_1} = -2 \, rc \, (\cos u_1 \, \sin x - \sin u_1 \, \cos x \, \cos (w_1 - y))$$

$$G_{u_1} = 0$$

$$H_{u_1} = 0$$

$$F_{u_2} = 0$$

$$G_{u_2} = -2 \, rc \, (\cos u_2 \, \sin x - \sin u_2 \, \cos x \, \cos (w_2 - y))$$

$$H_{u_2} = 0$$

$$F_{u_3} = 0$$

$$G_{u_3} = 0$$

$$H_{u_3} = -2\ rc\ (\cos u_3\ \sin x - \sin u_3\ \cos x\ \cos (w_3 - y))$$

$$F_{w_1} = 2\ rc\ \cos u_1\ \cos x\ \sin (w_1 - y)$$

$$G_{w_1} = 0$$

$$H_{w_1} = 0$$

$$F_{w_2} = 0$$

$$G_{w_2} = 2\ rc\ \cos u_2\ \cos x\ \sin (w_2 - y)$$

$$H_{w_2} = 0$$

$$F_{w_3} = 0$$

$$G_{w_3} = 0$$

$$H_{w_3} = 2\ rc\ \cos u_3\ \cos x\ \sin (w_3 - y)$$

$$J_1 = \frac{\partial r}{\partial b_1} = -\ \frac{F_{b_1}\ (G_x\ H_y - G_y\ H_x)}{D}$$

$$J_2 = \frac{\partial r}{\partial b_2} = +\ \frac{G_{b_2}\ (F_x\ H_y - F_y\ H_x)}{D}$$

$$J_3 = \frac{\partial r}{\partial b_3} = -\frac{H_{b_3}(F_x G_y - F_y G_x)}{D}$$

$$J_4 = \frac{\partial r}{\partial u_1} = -\frac{F_{u_1}(G_x H_y - G_y H_x)}{D}$$

$$J_5 = \frac{\partial r}{\partial u_2} = +\frac{G_{u_2}(F_x H_y - F_y H_x)}{D}$$

$$J_6 = \frac{\partial r}{\partial u_3} = -\frac{H_{u_3}(F_x G_y - F_y G_x)}{D}$$

$$J_7 = \frac{\partial r}{\partial w_1} = -\frac{F_{w_1}(G_x H_y - G_y H_x)}{D}$$

$$J_8 = \frac{\partial r}{\partial w_2} = +\frac{G_{w_2}(F_x H_y - F_y H_x)}{D}$$

$$J_9 = \frac{\partial r}{\partial w_3} = -\frac{H_{w_3}(F_x G_y - F_y G_x)}{D}$$

$$J_{10} = \frac{\partial r}{\partial c} = -\frac{F_c(G_x H_y - G_y H_x) - G_c(F_x H_y - F_y H_x) + H_c(F_x G_y - F_y G_x)}{D}$$

$$J_{11} = \frac{\partial x}{\partial b_1} = -\frac{F_{b_1}(G_y H_r - G_r H_y)}{D}$$

$$J_{12} = \frac{\partial x}{\partial b_2} = + \frac{G_{b_2}(F_y H_r - F_r H_y)}{D}$$

$$J_{13} = \frac{\partial x}{\partial b_3} = - \frac{H_{b_3}(F_y G_r - F_r G_y)}{D}$$

$$J_{14} = \frac{\partial x}{\partial u_1} = - \frac{F_{u_1}(G_y H_r - G_r H_y)}{D}$$

$$J_{15} = \frac{\partial x}{\partial u_2} = + \frac{G_{u_2}(F_y H_r - F_r H_y)}{D}$$

$$J_{16} = \frac{\partial x}{\partial u_3} = - \frac{H_{u_3}(F_y G_r - F_r G_y)}{D}$$

$$J_{17} = \frac{\partial x}{\partial w_1} = - \frac{F_{w_1}(G_y H_r - G_r H_y)}{D}$$

$$J_{18} = \frac{\partial x}{\partial w_2} = + \frac{G_{w_2}(F_y H_r - F_r H_y)}{D}$$

$$J_{19} = \frac{\partial x}{\partial w_3} = - \frac{H_{w_3}(F_y G_r - F_r G_y)}{D}$$

$$J_{20} = \frac{\partial x}{\partial c} = - \frac{F_c(G_y H_r - G_r H_y) - G_c(F_y H_r - F_r H_y) + H_c(F_y G_r - F_r G_y)}{D}$$

$$J_{21} = \frac{\partial y}{\partial b_1} = + \frac{F_{b_1}(G_x H_r - G_r H_x)}{D}$$

$$J_{22} = \frac{\partial y}{\partial b_2} = - \frac{G_{b_2}(F_x H_r - F_r H_x)}{D}$$

$$J_{23} = \frac{\partial y}{\partial b_3} = + \frac{H_{b_3}(F_x G_r - F_r G_x)}{D}$$

$$J_{24} = \frac{\partial y}{\partial u_1} = + \frac{F_{u_1}(G_x H_r - G_r H_x)}{D}$$

$$J_{25} = \frac{\partial y}{\partial u_2} = - \frac{G_{u_2}(F_x H_r - F_r H_x)}{D}$$

$$J_{26} = \frac{\partial y}{\partial u_3} = + \frac{H_{u_3}(F_x G_r - F_r G_x)}{D}$$

$$J_{27} = \frac{\partial y}{\partial w_1} = + \frac{F_{w_1}(G_x H_r - G_r H_x)}{D}$$

$$J_{28} = \frac{\partial y}{\partial w_2} = - \frac{G_{w_2}(F_x H_r - F_r H_x)}{D}$$

$$J_{29} = \frac{\partial y}{\partial w_3} = + \frac{H_{w_3}(F_x G_r - F_r G_x)}{D}$$

$$J_{30} = \frac{\partial y}{\partial c} = - \frac{-F_c(G_x H_r - G_r H_x) + G_c(F_x H_r - F_r H_x) - H_c(F_x G_r - F_r G_x)}{D}$$

7.2.12.2 CSM Heading Reference

If the vehicle position is known, an initial heading alignment may be made by measuring the CSM azimuth and elevation. Again the constraint of CSM position information is required. Figures 7-7 and 7-18 show the instantaneous geometry relating vehicle azimuth to CSM position. The expression can be written,

$$\tan A_{nc} = \frac{\sin (w_c - y_n)}{\cos x_n \tan u_c - \sin x_n \cos (w_c - y_n)} \qquad (7-178)$$

$$A_{nc} = A_{n,\,n+1} + \alpha_c^* \qquad (7-179)$$

where

A_{nc} = true CSM azimuth referenced to true north from vehicle

$A_{n,n+1}$ = true vehicle heading, referenced north

α_c^* = true CSM tracker azimuth angle referenced to vehicle horizontal body axis.

Equation 7-178 is identical to Equation 7-44, of Section 7.2.3. This latter equation forms the basis of the celestial tracker initial bearing error model and the earth tracker error models. The results are applicable with a slight modification. Rather than considering only errors in observable elevation angle ϵ^*, propagation of errors from the solid angle E must be considered due to the relatively low CSM altitude; hence $E = f(\epsilon, R_n, R_c)$.

The initial azimuth alignment error is expressed (Section 7.2.3) as:

$$\sigma_{A0}^2 = \begin{bmatrix} C_{17}^2 & C_{18}^2 & C_{19}^2 & C_{20}^2 & C_{21}^2 \end{bmatrix} \begin{bmatrix} \sigma_{x_n}^2 \\[6pt] \sigma_{\alpha_c}^{*\,2} \\[6pt] \overline{\sigma_{u_c}^{*}}^{\,2} \\[6pt] \overline{\sigma_{w_c}^{*}}^{\,2} \\[6pt] \sigma_{y_n}^2 \end{bmatrix} \qquad (7\text{-}180)$$

where

$$\left\{ C_{17} \ldots C_{21} \right\} \equiv \text{Section 7. 2. 3 with } i = c$$

$\sigma_{\alpha_c}^{*}$ = Equation 7-79 (Section 7. 2. 5)

σ_{x_n} = Latitudinal position error due to position fix errors.

σ_{y_n} = Longitudinal position error due to position fix errors.

As in Section 7. 2. 3, to account for errors in elevation measurement:

$$\overline{\sigma_{u_c}^{*}}^{\,2} = \sigma_{u_c}^{2} + \sigma_{u_c}^{*\,2} \qquad (7\text{-}181)$$

where

$\sigma_{u_c}^{*}$ = Equation 7-173

and

$$\sigma_{u_c} = u'_c - u_c \qquad (7\text{-}182)$$

where

$$u'_c = \sin^{-1}\left[\cos\sigma_E^* \sin u_c - \sin\sigma_E^* \cos u_c \cos C\right] \qquad (7\text{-}183)$$

where

$$C = \cos^{-1}\left[-\cos(A_{nc})\cos(w_c - y_n) + \sin A_{nc}\sin(w_c - y_n)\sin x_n\right] \qquad (7\text{-}184)$$

$$0 \le C \le 180$$

and

$$\sigma_E^{*2} = C_{31}^2\,\sigma_\epsilon^{*2} + C_{32}^2\,\sigma_{h_n}^2 + C_{33}^2\,\sigma_{h_c}^2 \qquad (7\text{-}185)$$

where σ_ϵ^* = Equation 7-80 (Section 7.2.5).

Also

$$\overline{\sigma_{w_c}^*}^2 = \sigma_{w_c}^2 + \sigma_{w_c}^{*2} \qquad (7\text{-}186)$$

where

$$\sigma_{w_c}^* = \text{Equation 7-174}$$

and

$$\sigma_{w_c} = \sin^{-1}\left[\frac{\sin\sigma_E^* \sin C}{\sin u'_c}\right] \qquad (7\text{-}187)$$

7-80

For convenience, in the digital program the CSM azimuth angle, A_{nc}, was calculated as follows:

$$a_1 = 90° - u_c \qquad (7-188)$$

$$c_1 = 90° - x_n \qquad (7-189)$$

$$s = \frac{1}{2} \left[a_1 + c_1 + E \right] \qquad (7-190)$$

$$k^2 = \frac{\sin(s-a)\ \sin(s-b)\ \sin(s-c)}{\sin s} \qquad (7-191)$$

$$A_{nc} = 2 \tan^{-1} \left[\frac{k}{\sin(s-a)} \right] \qquad (7-192)$$

with E calculated from Equation 3-162 and u_c and w_c from Equations 7-160 and 7-161, respectively.

The calculation of CSM true elevation angle, ϵ^*, proceeded as follows:

$$A_2 = \frac{180° - E}{2} \qquad (7-193)$$

$$c_2 = 2 R_c \sin \frac{E}{2} \qquad (7-194)$$

$$b_2 = R_c - R \qquad (7-195)$$

$$a_2 \overset{\Delta}{=} \left[b_2^2 + c_2^2 - 2 b_2 c_2 \cos A_2 \right]^{1/2} \qquad (7-196)$$

$$s = \frac{1}{2} \left[a_2 + b_2 + c_2 \right] \qquad (7-197)$$

$$C_2 = 2 \sin^{-1} \left[\frac{(s - a_2)(s - b_2)}{a_2 b_2} \right] \qquad (7-198)$$

$$\epsilon^* = 90° - C_2 \qquad (7-199)$$

7.3 DERIVATION OF CONCEPT MODELS

Previous sections treat the derivation of the lunar surface navigation error models in component or modular form. For each sensor of the three navigation concepts, an error model is derived and described without reference to the functioning of the total system. This section emphasizes total concept functioning and summarizes the digital computer program of the Lunar Surface Navigation Error Models.

7.3.1 General Formulation

To maintain continuity in the analysis of three quite distinct hybrid land navigation systems, a generalized format was required. An investigation into total land navigation concept functioning leads to the general flow diagram shown in Figure 7-20. The error inputs or forcing functions (σ_{PF}, σ_{DR}, σ_{FP}, and σ_{FD}) originate from position fix sensors, dead reckoning sensors, and physical uncertainties. The errors are 3 σ quantities and are inputs to the generalized position fix/initial azimuth and dead reckoning models. The formulation of the error models is basically the covariance technique, where 3 σ error inputs are related to vehicle position errors by partial derivative error sensitivity coefficients. To evaluate the partial derivatives, the necessary variables POS are supplied by the mission model, which basically consists of the calculations which model the varying vehicle, lunar, and celestial geometries during a position fix operation or a dead reckoning traverse. The homing model is a range of terminal requirements (T_R) located at particular destination coordinates. When the vehicle true position is within the terminal range, which is specified by the assessment function J, the dead reckoning function ceases as a guidance technique and the vehicle enters a homing or pilotage mode.

The functional output of the error models is a diagonalized covariance matrix. When related to the analytic navigational system, the model output is a 3 σ error ellipsoid located at a set of true vehicle coordinates (see Figure 7-21).

The origin of the ellipsoid is located at the set of coordinates, P_o, of the geometric navigational system. The σ_{x_i}'s are the magnitudes of the vehicle position errors with reference to the navigational analytic
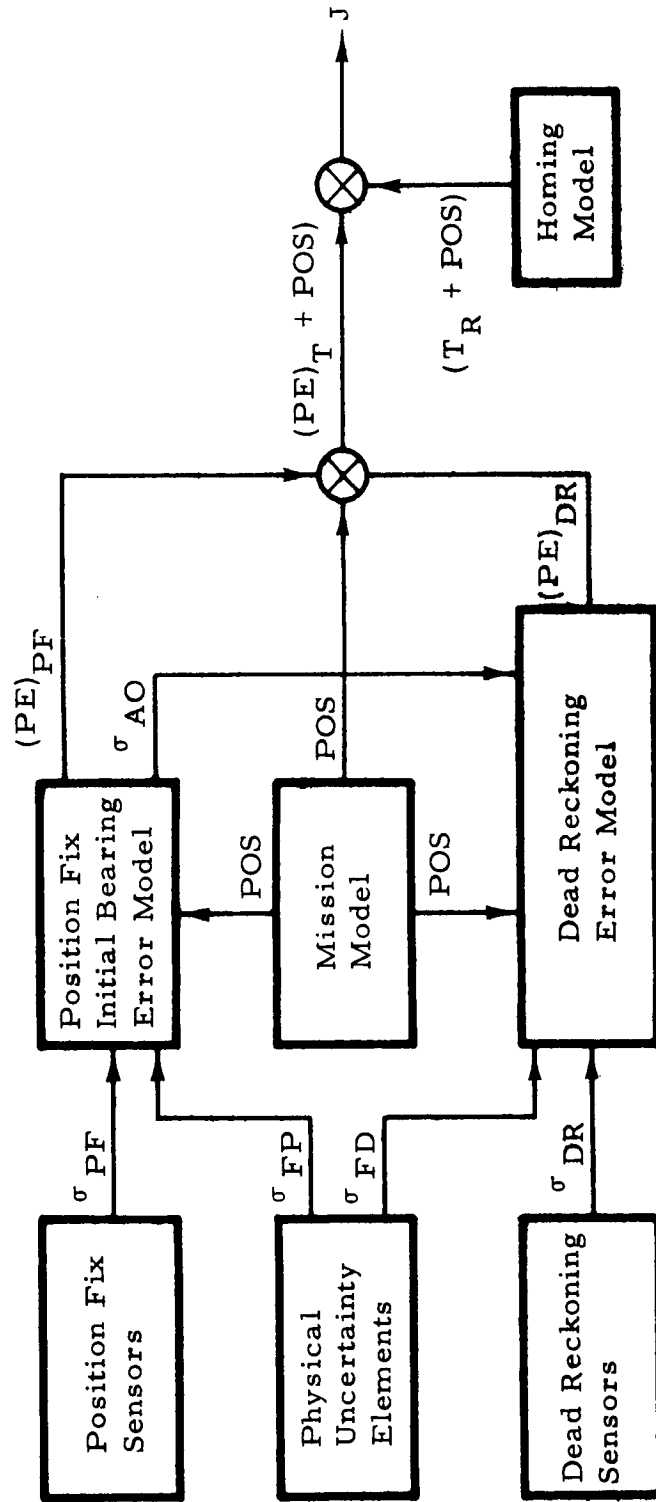
Figure 7-20 Concept Error Model Flow Diagram
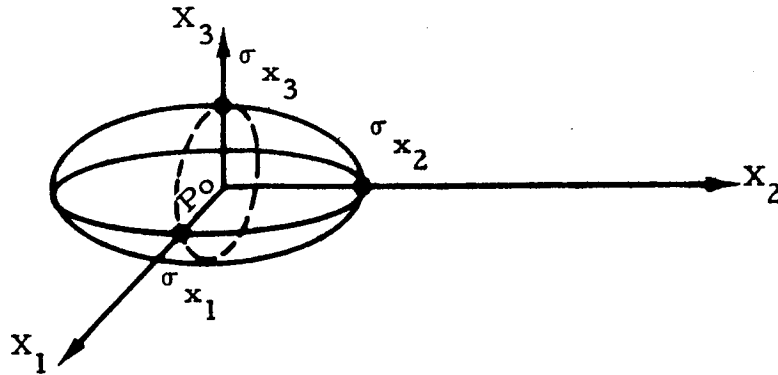
Figure 7-21   Vehicle Error Ellipsoid

system $\overline{X}_i$.   The vehicle traverses the lunar surface in the geometric sys-
tem and the navigational sensors make measurements in the analytic sys-
tem.   As the vehicle traverses the set of true geometric coordinates, the
error ellipsoid grows and is translated and rotated accordingly about the
true path to the set of homing coordinates.

7.3.2   Coordinate Systems

The general nature of the three lunar surface navigation concepts
and the associated error models requires a common base of coordinates.
Six specific coordinate systems are defined and applied.

Lunar-Based Celestial Sphere

This reference frame, shown in Figure 7-22, defines the lunar-
based ephemeris.   Angles of right ascension, RA, and declination, DEC,
define the celestial observable position.   The lunar-based celestial sphere
rotates with a negative lunar rate with respect to a fixed moon, and with
knowledge of the lunar ephemeris, the equivalent celestial observable sub-
point longitude w and latitude u can be calculated.
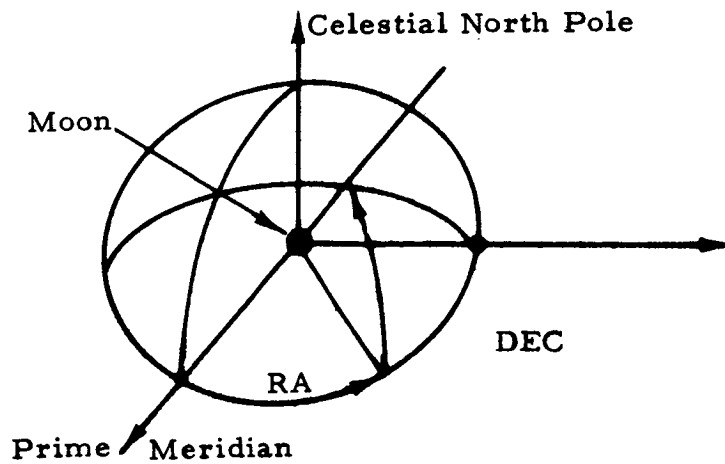
Figure 7-22   Lunar Based Celestial Sphere

Geometric System

The geometric system is a selenocentric system of latitude (x), longitude (y), and altitude (R) which defines vehicle position. See Figure 7-23.
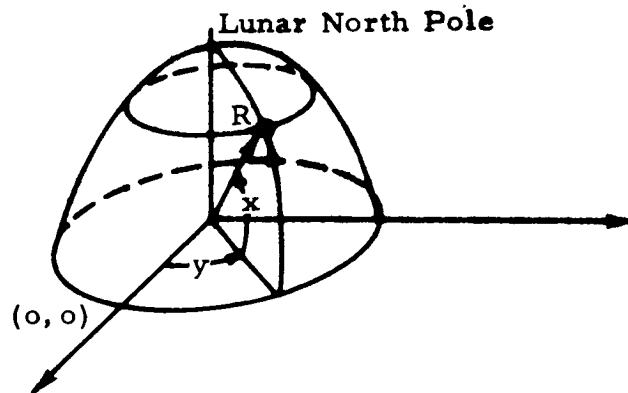
Figure 7-23   Geometric Navigational System

Analytic System

The analytic coordinate system, shown in Figure 7-24, is a local vertical, north, and east system with origin defined at a point (x, y, R) of the geometric system.   The navigational sensors perform measurements relative to the orthogonal unit triad $(\vec{1}_N, \vec{1}_E, \vec{1}_Z)$ defining this system.

The unit vector $\vec{1}_N$ is directed north along a meridian of longitude; $\vec{1}_E$ is directed east along a parallel of latitude; and $\vec{1}_Z$ the vertical direction up along R ($\vec{1}_Z = \vec{1}_E \times \vec{1}_N$).
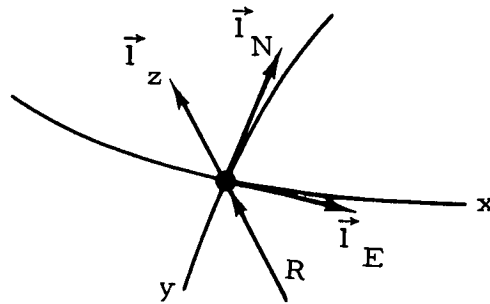
Figure 7-24 Analytic Navigational System

Vehicle System

The body-centered vehicle system, shown in Figure 7-25, is defined by the unit triad ($\vec{1}_x$, $\vec{1}_y$, $\vec{1}_z$). The vehicle longitudinal axis is along $\vec{1}_x$, the lateral axis along $\vec{1}_y$, and $\vec{1}_z = \vec{1}_y \times \vec{1}_x$. The origin of the body centered system is the vehicle cg, and is fixed at the origin of the analytic system. The vehicle azimuth, A, and vehicle Euler angles pitch, p, and roll, r, are defined relative to the analytic system.
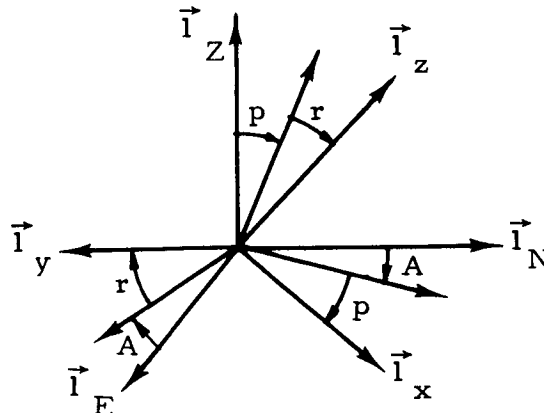
Figure 7-25 Body Centered System

Local Vertical Space

The local vertical space, shown in Figure 7-26, which is required to analyze vertical anomalies, defines the vertical anomaly unit pointing vector relative to true vertical. The solid angle γ represents the deviation of the vertical from the true vertical, while the equiprobable angle β_N defines the direction of the anomaly relative to the analytic system. Projection of the vehicle longitudinal axis $\vec{1}_x$ into the true horizontal plane then defines the anomaly direction β relative to the body-centered system.

$$\vec{1}_Z \qquad \gamma \qquad \beta_N \qquad A \qquad \vec{1}_N \qquad \vec{1}_E \qquad \beta \qquad \vec{1}_x$$
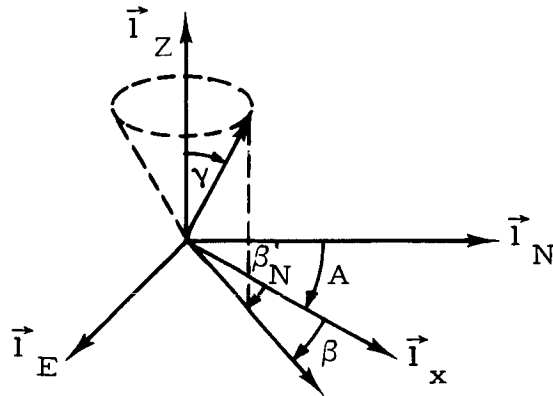
Figure 7-26 Local Vertical Space

Celestial Tracker Space

Definition of the celestial tracker unit pointing vector, $\vec{1}_{ST}$, is shown in Figure 7-27. Azimuth, α, and elevation, ϵ, define the unit pointing vector relative to the body-centered system. Resolution of this pointing vector into the analytic system defines the true azimuth, α^*, relative to the projected vehicle longitudinal axis in the local horizontal plane and true elevation, ϵ^*.

7.3.3 Vehicle Trajectories

The error analysis of a land vehicle navigation system is hampered due to difficulty in the description of vehicle equations of motion or vehicle state. Typical analyses in other fields evaluate system performance for vehicle motion on a ballistic trajectory, straight line flight path, an elliptical orbit, etc. However, the analysis of a land vehicle is not as convenient and is restricted since no closed form exists for the vehicle
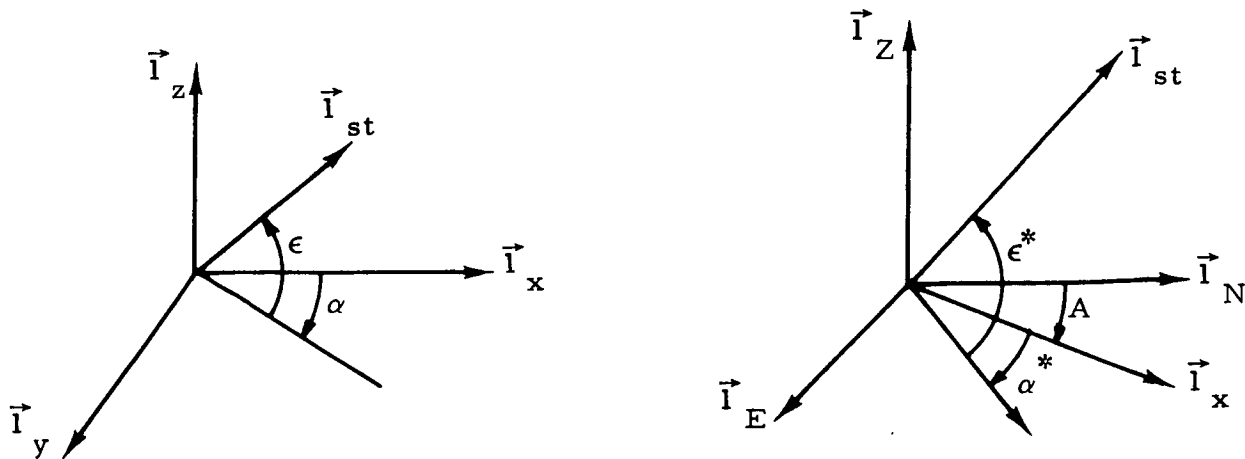
Figure 7-27 Celestial Tracker Space

equations of motion. But this difficulty in vehicle path description is sur-
mounted by the application of a Monte Carlo technique. Random number
generator routines are applied and the steady-state vehicle path and vehicle
attitude are calculated. When knowledge of the true vehicle path and true
vehicle attitude is acquired, the dead reckoning partial derivative error
sensitivity coefficients can be evaluated.

If it is desired to dead reckon from a given initial point ($P_o = x_o$,
y_o, h_o) to a given destination point ($P_D = x_D$, y_D, h_D), the ideal traverse
would be a straight line or great circle route with initial azimuth, A_{OD}.
This is seldom the case in land navigation, and the true path is actually
statistical in nature. The vehicle path may be constructed in incremental
steady-state form if the philosophy of land vehicle guidance is interpreted
in a navigation function. Taking the premise:

> if present and destination coordinates are known, the navigator
> tends to travel in an azimuthal direction that provides desti-
> nation intersection

then the following guidance philosophy is effected. During a traverse,
when confronted with a terrain obstacle, the operator will perform a
maneuver which makes the vehicle veer from the homing azimuth. (1) The
maneuver entails the selection of an azimuthal course such that the devia-
tion from homing azimuth is minimal but still allows obstacle avoidance.

(2) Upon passing the obstacle, the operator steers to a new homing azimuth defined by vehicle present position and final destination coordinates.

The above premise and corollaries 1 and 2 imply the following mathematical interpretation: For given initial and final destination coordinates, the planar path in latitude, longitude coordinates may be constructed by comparatively short incremental line segments. The azimuth of the line segment is randomly selected from a gaussian density function with mean centered on the homing azimuth and standard deviation corresponding to obstacle densities of various terrain types.

Altitude variations are treated in a similar manner, with increment leg end points being selected randomly from a gaussian density with mean centered on the altitude variation which provides the gradient to reach final destination altitude from vehicle present position. The standard deviation is a measure of the altitude variation occurring in the distance of the incremental line segment and also infers a terrain type.

In this manner, the vehicle path or trajectory can be defined and the steady-state variations in vehicle attitude obtained. The following steps illustrate the iterative procedure required:

1. Given initial and final coordinates:

$$P_o = (x_o, y_o, h_o)$$

$$P_D = (x_D, y_D, h_D)$$

The points are separated by a distance

$$D_{TO} \cong \left(\left[h_D - h_o \right]^2 + D_{oD}^2 \right)^{1/2}$$

with the final coordinates at a bearing, measured from true north, of A_{oD}. See Figure 7-28.
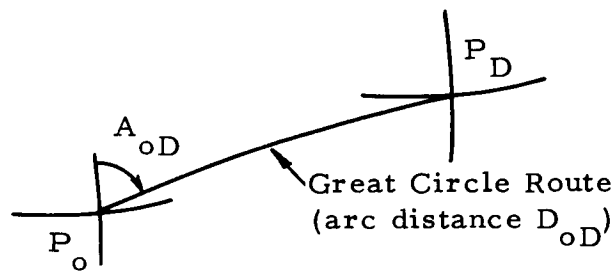
Figure 7-28   Initial Path Geometry

2.   Select a small incremental leg distance

$$D_j$$

$$D_j \ll D_{oD}$$

At constant altitude, the locus of the vehicle coordinates
after traversing a straight line course is a circle,
with radius D_j centered on P_o.

The specific point P_1 can be determined if A_{01} and h_1 are
known.   Randomly determine A_{01} and h_1 from the probability
density functions in Figure 7-29.   Then the geometry in
Figure 7-30 is fixed.
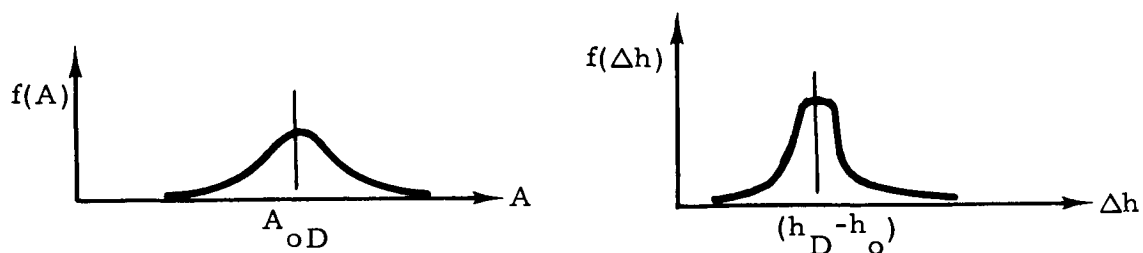
Figure 7-29   Path Density Functions
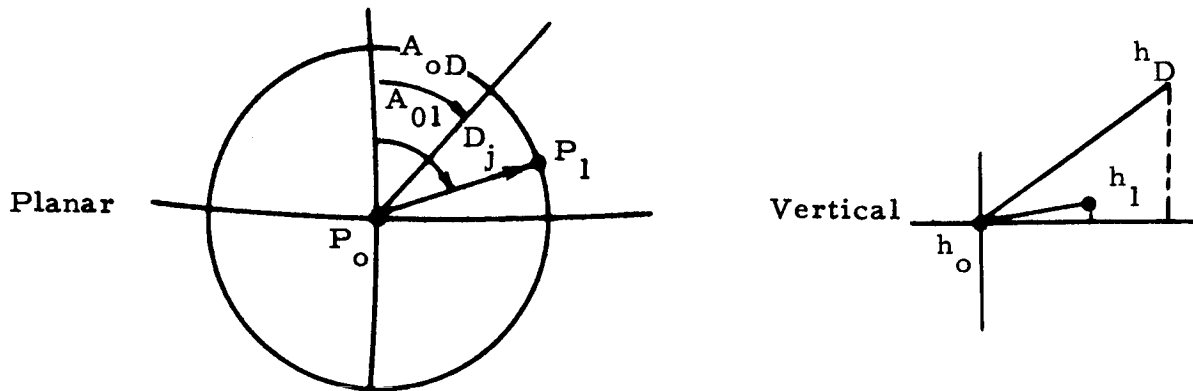
Figure 7-30 Incremental Leg Loci

3.   Calculate the coordinates of P_1

$$P_1 = (x_1, \ y_1, \ h_1)$$

4.   At P_1, determine the required homing azimuth A_{1D} and homing slope $(h_D - h_1)$.

5.   The locus of point P_2 will be a circle with radius D_j, centered on point P_1. P_2 may be specifically fixed if A_{12} and h_2 are known. See Figure 7-31.
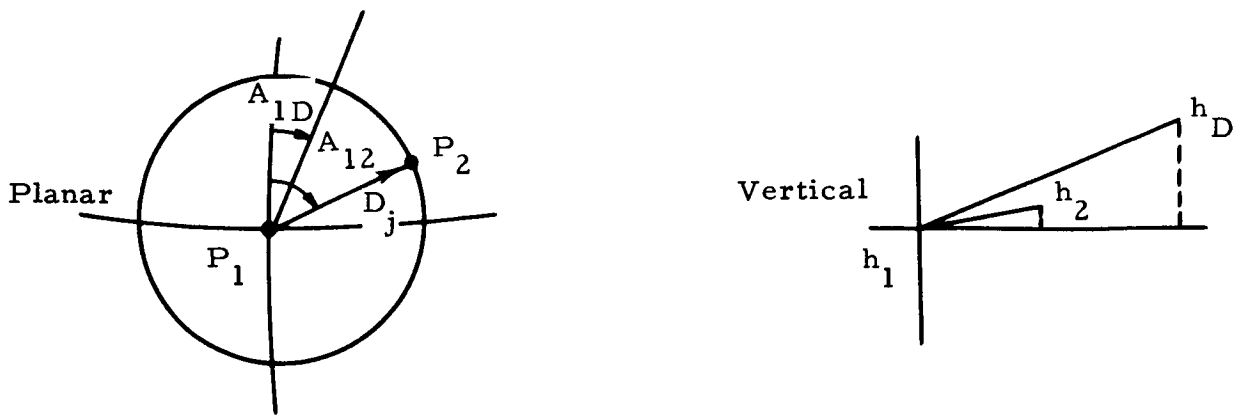
Figure 7-31   Incremental Leg Loci

The azimuth A_{12}, and altitude h_2 may be determined as in step 2 above by simply changing the means of the gaussian density functions to A_{1D} and $(h_D - h_1)$ respectively.

6. This process may now be repeated and the points P_n may be determined. Figure 7-32 shows the general nomenclature.
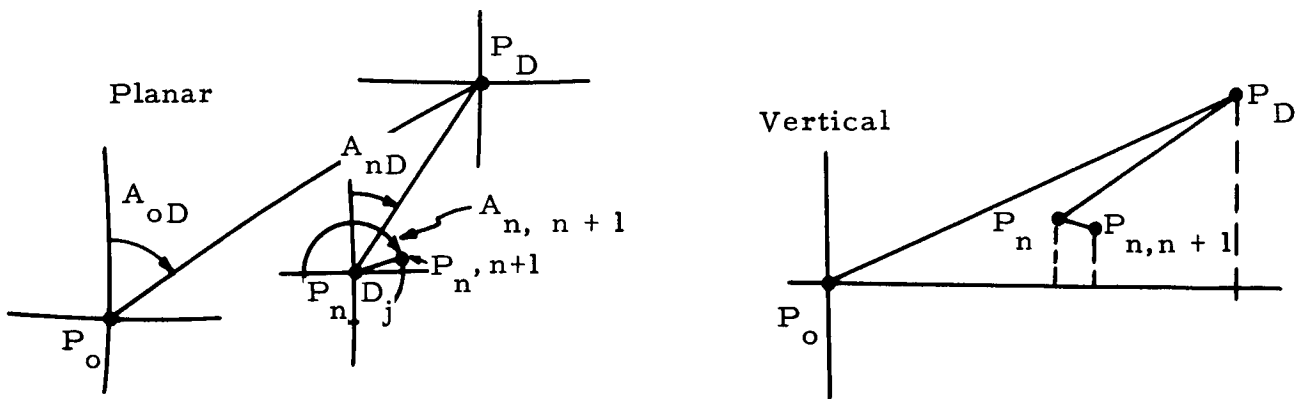
Figure 7-32   General Path Definitions

Thus the path of the vehicle, in short incremental line segments, may be randomly determined in terms of endpoints, and as long as $D_j \ll D_{oD}$ the path approximates a curvilinear vehicle traverse. The azimuthal and altitude variations are determined from gaussian density functions. Since

the density functions are assumed normal, two quantities are necessary to characterize the distributions: the mean, μ, and standard deviation, σ. The mean value, μ, is known or can be calculated. Thus the standard normal curve ($\mu = 0$, $\sigma = 1$), Figure 7-33, can be used to select the value of the random variable; this allows the use of conventional digital computation random number routines. Figure 7-34 is a plot of the frequency distribution generated by the gaussian random number routine. In the digital computation, the density functions are truncated at the 3σ value.
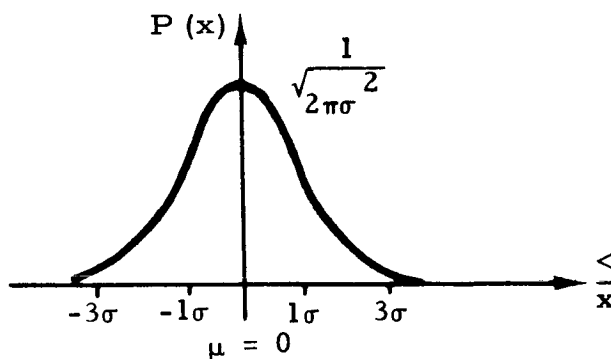
Figure 7-33 Standard Normal

To fully characterize vehicle attitude variation, vehicle roll angle must be considered in addition to azimuth and pitch variations. A similar treatment is given vehicle roll angle. On each incremental leg of the path model, the vehicle roll angle is determined from a normal density function with zero mean, and a standard deviation less than or equal to the standard deviation of the vehicle pitch (terrain slope) variation. The roll standard deviation is less than or equal to the standard deviation of the pitch variation since the operator, while maneuvering on a mission path, allows greater variations in vehicle pitch angle than in vehicle roll angle. Theoretically, the 3σ limit of terrain slope is independent of path. That is, if the vehicle initiates a traverse in homogeneous terrain, vehicle pitch variation due to terrain slope will be statistically independent of vehicle heading. Hence, randomly selected vehicle pitch and roll angle from terrain slope could be selected from density functions with identical variance. But when the operator characteristics enter the analysis, the decision abilities of the operator filter or attenuate the 3σ limit of terrain slope effect on vehicle roll angle.
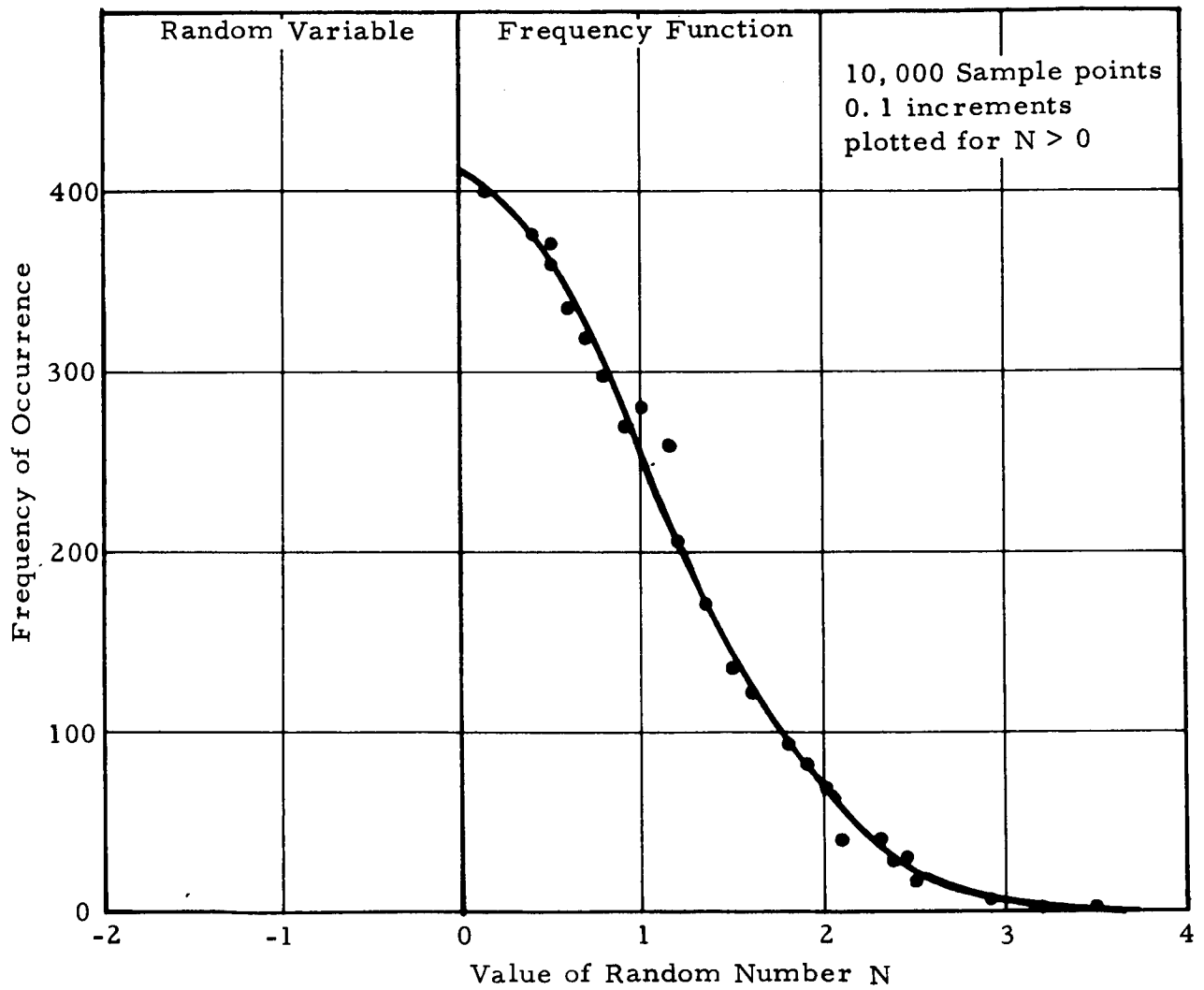
Figure 7-34 Random Variable Frequency Function

An additional variable treated in a random fashion is the direction of the vertical anomalies. For each incremental leg, the anomaly direction is selected from a normal density function with mean centered on an initial reference direction and a given standard deviation.

This path philosophy is easily instrumented on a digital computer. The programmed equations written for the nth path leg follow. To evaluate the entire path, n is indexed from zero to n.

Inputs:

$$P_n = (x_n, y_n, h_n) \qquad n = 0$$

$$P_D = (x_D, y_D, h_D)$$

$$\Delta A_{max}$$

$$\Delta h_{max}$$

$$\Delta r_{max}$$

$$V$$

$$D_j$$

$$R_m$$

$$K_{vp}$$

$$K_{vr}$$

$$\beta_n$$

Figure 7-35 shows the trigonometry used in the path derivations.
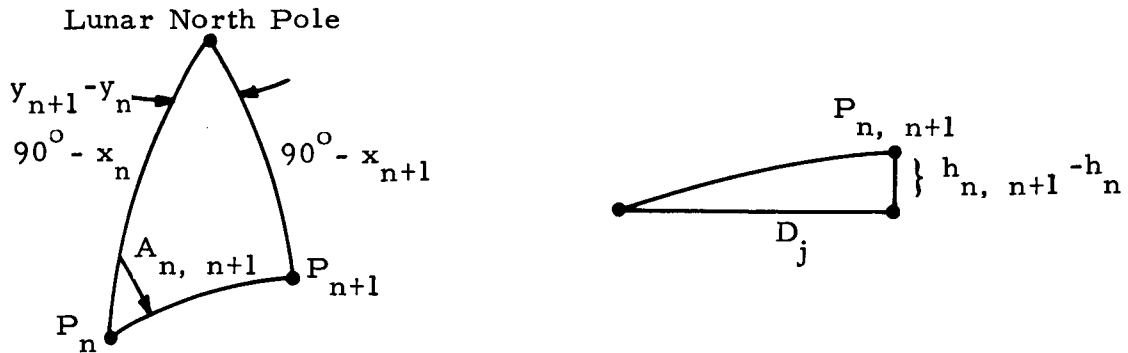
Figure 7-35 Path Geometry

Homing Azimuth:

$$A_{nD} = \sin^{-1} \left[\frac{\cos (x_D) \sin (y_D - y_n)}{\sin b} \right] \qquad (7\text{-}200)$$

with $b = \cos^{-1} \left[\sin (x_D) \sin (x_n) + \cos (x_n) \cos (x_D) \cos (y_D - y_n) \right]$ $\quad$ (7-201)

An equivalent digital computation procedure which is used to facilitate quadrant determination is

If $0 \le (y_D - y_n) \le 180^\circ$, then $A_{nD} = + |A|$

If $180 \le (y_D - y_n) \le 360^\circ$, then $A_{nD} = 360^\circ - |A|$

where $|A| = 2 \tan^{-1} \dfrac{K}{\sin (s-a)}$.

$$K^2 = \frac{\sin (s-a) \sin (s-b) \sin (s-c)}{\sin s} \qquad (7\text{-}202)$$

where

$$s = (a + b + c)/2$$

where

$$a = 90^\circ - x_D$$

$$c = 90^\circ - x_n$$

Total Straight Path Distance

$$D_{TN} = \left[(h_D - h_n)^2 + D_{nD}^2\right]^{1/2} \qquad (7\text{-}203)$$

Great Circle Distance:

$$D_{nD} = b\,R \qquad (7\text{-}204)$$

where

$$R = R_m + h_n \qquad (7\text{-}205)$$

Incremental Leg Azimuth

$$A_{n,\,n+1} = A_{nD} + A_s \qquad (7\text{-}206)$$

where

A_s = Determined randomly from normal density function with:

mean = A_{nD}

3σ value = ΔA_{max}

Incremental Leg End Point Coordinates:

Latitude:

$$x_{n+1} = \sin^{-1}\left[\cos(d)\sin(x_n) + \sin(d)\cos(x_n)\cos(A_{n,\,n+1})\right] \qquad (7\text{-}207)$$

where

$$d = \frac{D_j}{R}$$

Longitude:

$$y_{n+1} = \sin^{-1}\left[\frac{\sin(d)\,\sin(A_{n,\,n+1})}{\cos(x_{n+1})}\right] + y_n \qquad (7\text{-}208)$$

Altitude:

$$h_{n+1} = h_n + h_s \qquad (7\text{-}209)$$

where

h_s = Determined randomly from normal density function with:

mean = $\Delta h_{n,\,n+1}$

3σ value = Δh_{max}

$$\Delta h_{n,\,n+1} = (h_D - h_n)\,\frac{D_j}{D_{Tn}} \qquad (7\text{-}210)$$

Incremental Leg Distance:

$$D_{n,\,n+1} = \left[(h_{n,\,n+1} - h_n)^2 + D_j^{\,2}\right]^{1/2} \qquad (7\text{-}211)$$

Vehicle Attitude on Incremental Leg:

Azimuth:

$$A_{n,\,n+1} = (\text{Equation } 7\text{-}206) \qquad (7\text{-}212)$$

Pitch:

$$P_{n,\,n+1} = \tan^{-1}\left[\frac{h_n - h_{n,\,n+1}}{D_j}\right] \qquad (7\text{-}213)$$

Roll:

$$r_{n,\,n+1} = r_s \qquad (7\text{-}214)$$

where

$r_s \equiv$ Determined randomly from normal density function with:

mean = 0

3σ value = Δr_{max}

Vertical Anomaly Direction on Incremental Leg:

$$\beta_{n,\,n+1} = \beta_N - A_{n,\,n+1} - \beta_s \qquad (7\text{-}215)$$

where

$\beta_s \equiv$ Determined randomly from normal density functions with:

mean = β_N

3σ value = $\Delta\beta_{max}$

Vehicle Speed on Incremental Leg:

$$V_{n,\,n+1} = V - \Delta V_{n,\,n+1} \qquad (7\text{-}216)$$

where

$$\Delta V_{n,\,n+1} = -K_{vp}\,P_{n,\,n+1} + K_{vr}\left|r_{n,\,n+1}\right|$$

$$K_{vr} = 0 \text{ if } \left|r_{n,\,n+1}\right| < 6^{\circ}$$

K_{vp}, K_{vr} are constants for a particular vehicle and operator type.

Accumulated Steady State Time:

$$t = \sum_{K=0}^{n} \left(\frac{D_{K,\,K-1}}{V_{K,\,K+1}} \right) \tag{7-217}$$

Path Termination:

To terminate the dead reckoning process, point P_n must lie within the terminal requirement T_R locus of P_D. In Figure 7-36 it is observed that the following condition must be satisfied:

$$D_{T_n} \leq T_R. \tag{7-218}$$
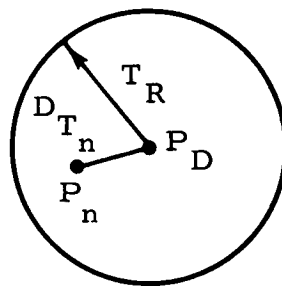
Figure 7-36   Terminal Conditions for Dead Reckoning

A second method of path termination is

$$n > 2 \frac{D_{TO}}{D_j}. \tag{7-219}$$

This arbitrary condition prevents an excessive number of points from being calculated if the statistically chosen points for a particular run cannot satisfy the terminal requirement constraint.

The above sequential steps allow the vehicle path to be constructed. This path is analogous to the purpose of a ballistic trajectory in the perturbation error analysis of a ballistic missile. The path and the calculated

vehicle variables permit the evaluation of the partial derivative error sensitivity coefficients of the dead-reckoning model. The path is the traverse followed by an errorless navigation system. As the vehicle traverses the lunar terrain, the error models are evaluated on this path and an error ellipsoid calculated at each point of the incremental leg.

Various lunar surfaces may be simulated by properly selecting ΔA_{max}, Δh_{max}, Δr_{max}, $\Delta \beta_{max}$, the 3σ values of the normal density functions. These 3σ values infer terrain characterization properties which directly correspond to the difficulty of traversing a given terrain. For example, in Figure 7-37 representative density functions of three terrain types are shown.
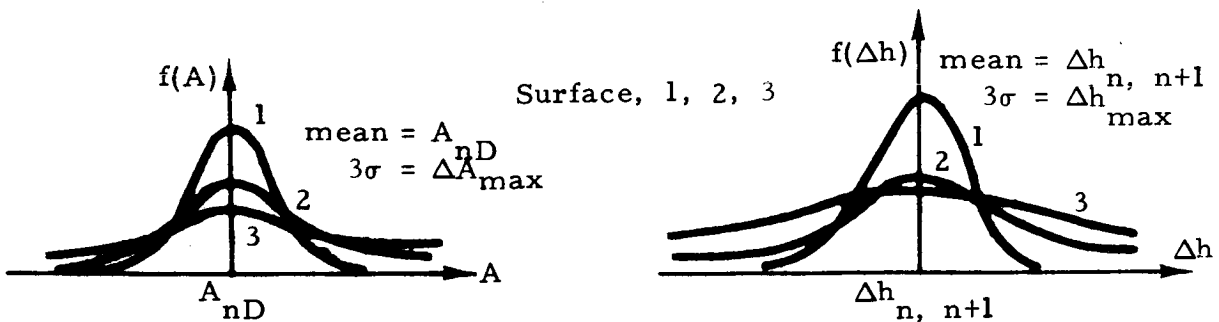
Figure 7-37 Path Density Functions

In the instance when

$$A_{max_1} < A_{max_2}$$

larger variations will occur in traversing the second surface. Hence, the implication is that Surface 2 is a more severe surface. This is analogous to a marial traverse with fewer obstacles, versus a pitted region with many obstructions and, therefore, more required vehicle maneuvers. Similarly the other 3σ limits and a measure of extra distance traveled between the initial and final destination points complete the terrain characterization. The extra distance traveled from P_o to P_D due to surface obstructions and contours is

$$EDT = \sum_{K=0}^{n} \left(D_{K, K+1} \right) + D_{Tn} - D_{TO}. \qquad (7\text{-}220)$$

Per cent EDT is

$$\%EDT = \frac{EDT}{D_{T0}} \times 100 \qquad (7\text{-}221)$$

7.3.4 Error Model Flow Diagrams

7.3.4.1 Nongyro Concept

The error model functional flow diagram of the position fix and initial azimuth alignment portions of the nongyro concept is shown in Figure 7-38. The inputs of equipment errors and physical uncertainties form the model forcing functions. The T_i's represent transformations upon the input error variables. The transformations are both functional in form and matrices of partial derivative error sensitivity coefficients. All summer notation implies an RSS combination. The output of the model is vehicle position error in latitude, σ_x, and longitude, σ_y, and initial azimuth alignment, σ_{AO}. The input variables associated with each transformation and sensor are required to evaluate the respective transformations or sensor error outputs.

The data inputs are labeled as mission inputs, and the program calculations are:

Vehicle True Heading:

$A = A_{OD} \doteq$ The homing azimuth from the initial point, Equation 7-200, with n = 0.

Anomaly Direction:

$$\beta = \beta_N - A_{OD} \qquad (7\text{-}222)$$

For i = 1 (star 1), i = 2 (star 2)
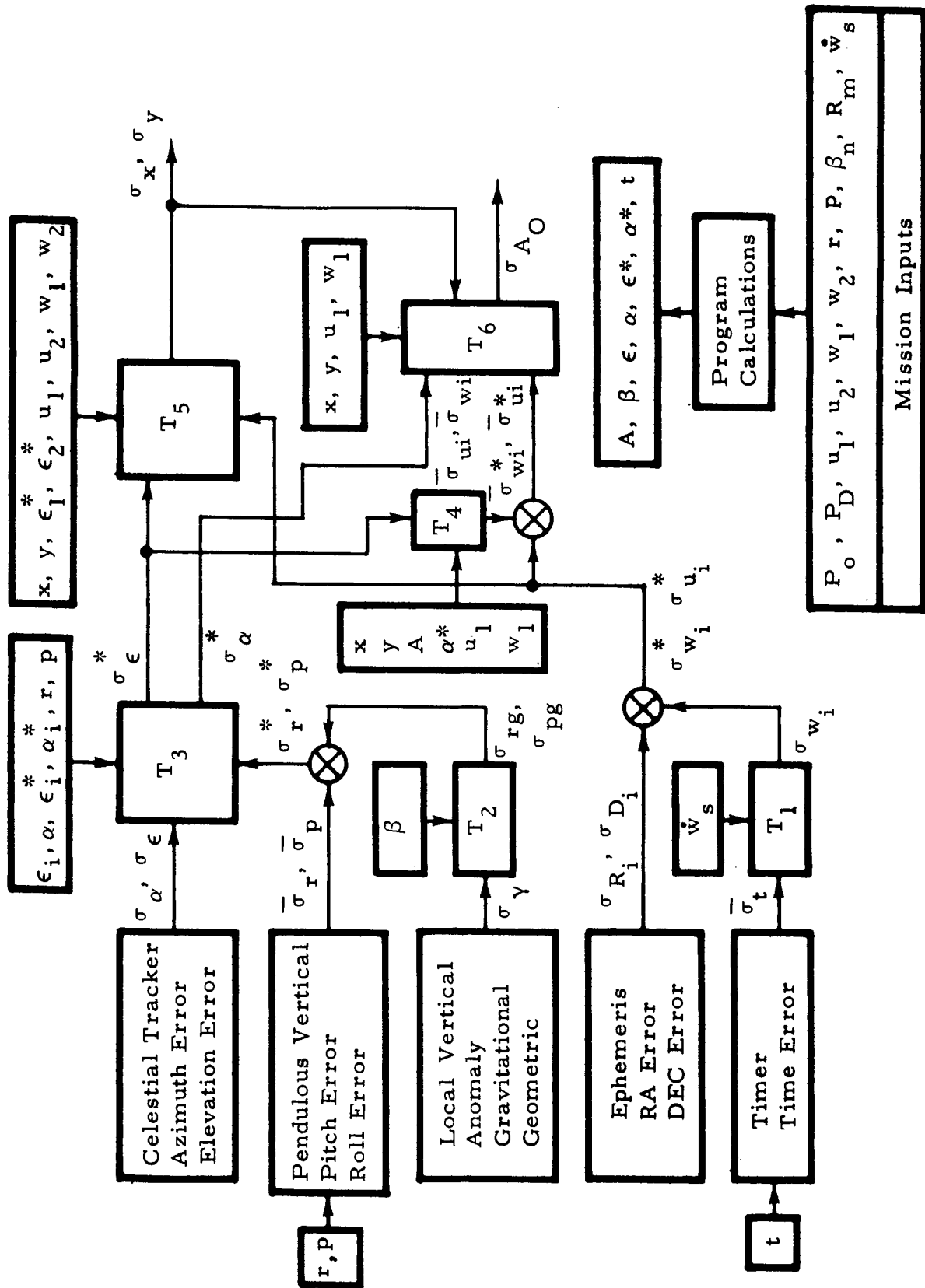
Figure 7-38 Concept 1 Error Model Flow Diagram, Position Fix, Initial Azimuth Alignment

Observable True Altitude:

$$\epsilon_i^* = \sin^{-1} \left[\sin(u_i) \sin(x_o) + \cos(u_i) \cos(x_o) \cos(w_i - y_o) \right] \qquad (7\text{-}223)$$

Observable True Relative Azimuth:

$$\alpha_i^* = \sin^{-1} \left[\frac{\sin(w_i - y_o) \cos(u_i)}{\cos(\epsilon_i^*)} \right] - A_{OD} \qquad (7\text{-}224)$$

(An equivalent procedure to calculate α_i^*, and one that facilitates digital computation, is given by Equation 7-202 with $u_i = x_D$, $w_i = y_D$.)

Observable Elevation:

$$\epsilon_i = \tan^{-1} \left[\frac{c_i}{[a_i^2 + b_i^2]^{1/2}} \right] \qquad (7\text{-}225)$$

Observable Azimuth:

$$\alpha = \tan^{-1} \left[\frac{b_i}{a_i} \right] \qquad (7\text{-}226)$$

with

$$[a_i \; b_i \; c_i] = [a_{oi} \; b_{oi} \; c_{oi}] \begin{bmatrix} \cos p & \sin r \sin p & \cos r \sin p \\ o & \cos r & -\sin r \\ -\sin p & \sin r \cos p & \cos r \cos p \end{bmatrix} \qquad (7\text{-}227)$$

where

$$a_{oi} = \cos \epsilon_i^* \; \cos \alpha_i^* \qquad (7\text{-}228)$$

$$b_{oi} = \cos \epsilon_i^* \; \sin \alpha_i^* \qquad (7\text{-}229)$$

$$c_{oi} = \sin \epsilon_i^* \qquad (7\text{-}230)$$

Error Transformations:

T_1 :   A functional transformation relating timer error to an effective observable subpoint error

$$\sigma_{w_i} = \dot{w}_s \left[(K_t t)^2 + \sigma_t^2 \right]^{1/2} \qquad i = 1, 2 \qquad (7\text{-}231)$$

T_2 :   A functional transformation relating vertical anomalies to effective vertical equipment errors.

$$\sigma_{rg} = -\sin^{-1} \left[\sin(\sigma_\gamma) \sin(\beta) \right] \qquad (7\text{-}232)$$

$$\sigma_{pg} = \cos^{-1} \left(\frac{\cos(\sigma_\gamma)}{\cos\left[\sin^{-1}(\sin\sigma_\gamma \sin\beta) \right]} \right) \qquad (7\text{-}233)$$

T_3 :   A matrix of partial derivative error sensitivity coefficients relating vertical errors and celestial tracker equipment errors to true elevation and true azimuth errors.

$$
\begin{bmatrix} \sigma_{\epsilon i}^{*2} \\ \\ \sigma_{\alpha i}^{*2} \end{bmatrix}
=
\begin{bmatrix} C_{13}^2 & C_{14}^2 & C_{15}^2 & C_{16}^2 \\ \\ C_{22}^2 & C_{23}^2 & C_{24}^2 & C_{25}^2 \end{bmatrix}
\begin{bmatrix} \sigma_\alpha^2 \\ \sigma_\epsilon^2 \\ \sigma_r^{*2} \\ \sigma_p^{*2} \end{bmatrix}
\quad ; i = 1, 2
\qquad (7\text{-}234)
$$

T_4 :   A functional transformation relating celestial tracker elevation error to effective observable subpoint error.

$$\bar{\sigma}_{ui} = u_i' - u_i \qquad (7\text{-}235)$$

where

$$u_i' = \sin^{-1}\left[\cos(\sigma^*_{\epsilon i})\sin(u_i) - \sin(\sigma^*_{\epsilon i})\cos(u_i)\cos C\right] \quad (7\text{-}236)$$

and

$$\bar{\sigma}_{wi} = \sin^{-1}\left[\frac{\sin(\sigma^*_{\epsilon i})\sin(C)}{\cos(u_i')}\right] \quad (7\text{-}237)$$

where

$$C = \cos^{-1}\left[-\cos(A_{OD} + \alpha_i^*)\cos(w_i - y_o)\right.$$

$$\left. + \sin(A_{OD} + \alpha_i^*)\sin(w_i - y_o)\sin(x_o)\right] \quad (7\text{-}238)$$

T_5 : A matrix of partial derivative error sensitivity coefficients relating transformed error inputs to vehicle position error.

$$\begin{bmatrix} \sigma_x^2 \\[2mm] \sigma_y^2 \end{bmatrix} = \begin{bmatrix} C_1^2 & C_2^2 & C_3^2 & C_4^2 & C_5^2 & C_6^2 \\[2mm] C_7^2 & C_8^2 & C_9^2 & C_{10}^2 & C_{11}^2 & C_{12}^2 \end{bmatrix} \begin{bmatrix} \sigma_{\epsilon 1}^{*2} \\[2mm] \sigma_{u1}^{*2} \\[2mm] \sigma_{w1}^{*2} \\[2mm] \sigma_{\epsilon 2}^{*2} \\[2mm] \sigma_{u2}^{*2} \\[2mm] \sigma_{w2}^{*2} \end{bmatrix} \quad (7\text{-}239)$$

T_6 : A row vector of partial derivative error sensitivity coefficients relating transformed error inputs to vehicle initial azimuth error.

$$\sigma_{AO}^2 = \begin{bmatrix} C_{17}^2 & C_{18}^2 & C_{19}^2 & C_{20}^2 & C_{21}^2 \end{bmatrix} \begin{bmatrix} \sigma_x^2 \\ \sigma_{\alpha}^{*2} \\ \sigma_{u_1}^{*2} \\ \sigma_{w_1}^{*2} \\ \sigma_y^2 \end{bmatrix} \tag{7-240}$$

The output of the passive, nongyro concept position fix error model is the vehicle 3σ position error ellipse. The magnitude of the ellipse major and minor axis in the analytic north, east system located at a point P_o on the lunar surface is

$$\Delta R_N = R\sigma_x \tag{7-241}$$

and

$$\Delta R_E = R\cos(x)\,\sigma_y \tag{7-242}$$

The total vehicle position error due to the position fix system error is:

$$(PE)_{PF} = \left[(\Delta R_N)^2 + (\Delta R_E)^2 \right]^{1/2} \tag{7-243}$$

The vehicle position error and the associated error ellipse components together with initial vehicle azimuth error impose error initial conditions on the dead reckoning subconcept.

The dead reckoning portion of the passive, nongyro concept error model flow diagram is shown in Figure 7-39. The error model is effectively
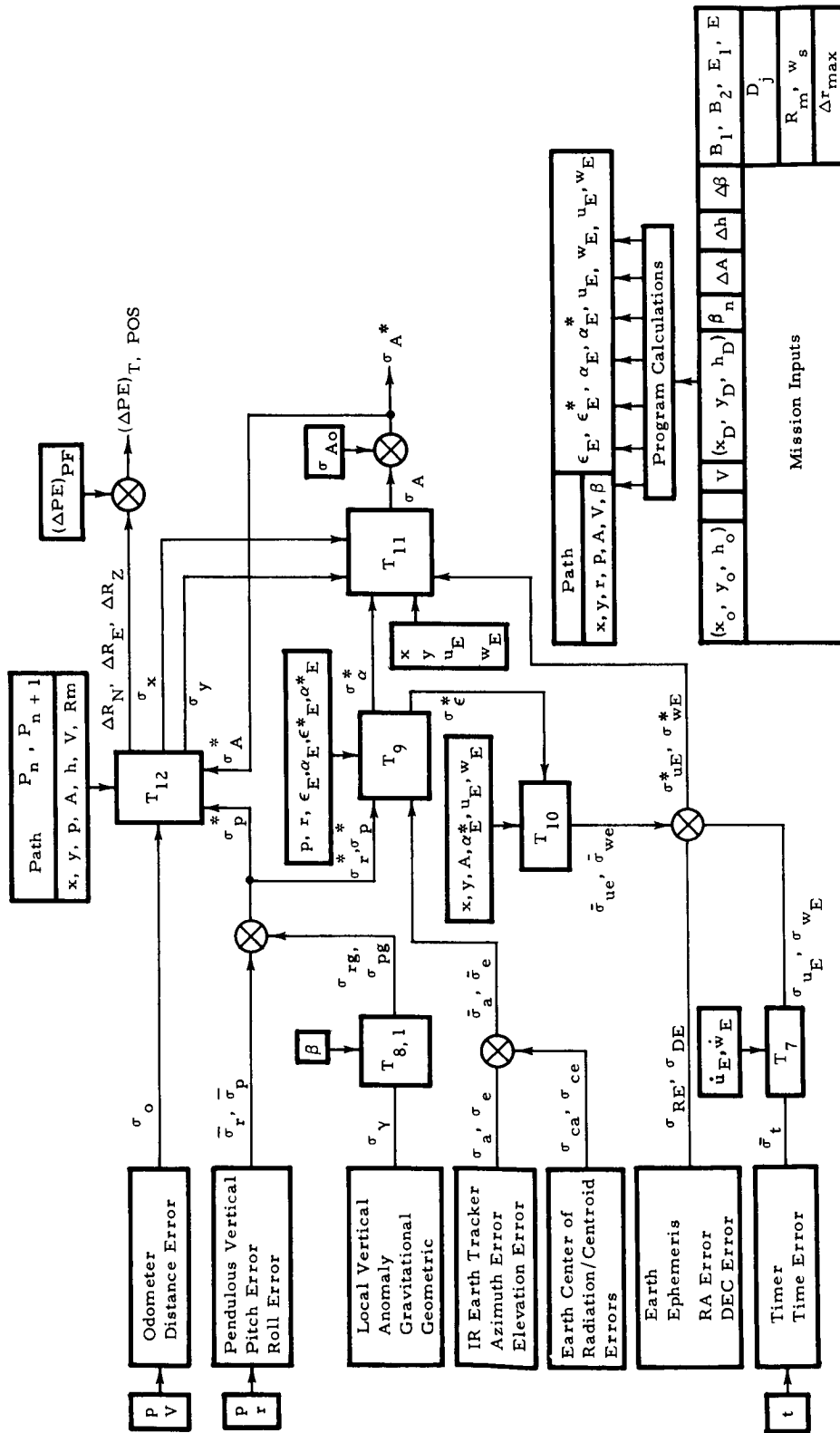
Figure 7-39 Concept 1 Error Model Flow Diagram, Dead Reckoning

a transfer function relating sensor and physical errors to vehicle position and azimuth error as the vehicle traverses the path calculated from the mission inputs. On each incremental leg of the path model, the error is calculated and, as the vehicle advances along the path, the 3σ error ellipsoid is computed. Thus, located at the end of each incremental leg of the true vehicle path is a vehicle error ellipsoid. The components of this ellipsoid together with the azimuth error are the output of the model.

The program calculations performed on the mission inputs follow:

True Vehicle Path:

The path variables are calculated as discussed above.

Earth Subpoint Position:

$$u_E = B_1 \cos Et \qquad (7\text{-}244)$$

and

$$w_E = B_2 \sin (Et + E_1) \qquad (7\text{-}245)$$

Earth Subpoint Motion:

$$\dot{u}_E = -B_1 E \sin Et \qquad (7\text{-}246)$$

and

$$\dot{w}_E = B_2 E \cos (Et + E_1) \qquad (7\text{-}247)$$

Earth True Altitude:

$$\epsilon_E^* = \sin^{-1}\left[\sin (u_E) \sin (x_n) + \cos (u_E) \cos (x_n) \cos (w_E - y_n) \right] \qquad (7\text{-}248)$$

Earth True Azimuth:

$$\alpha_E^* = \sin^{-1}\left[\frac{\sin (w_E - y_n) \cos u_E}{\cos (\epsilon_E^*)} \right] - A_{n, n+1} \qquad (7\text{-}249)$$

The earth elevation angle, ϵ_E, and azimuth angle, α_E, are calculated as in the position fix case for the observable elevation and azimuth, but with

$$r = r_n \qquad\qquad (7-250)$$

and

$$p = p_n. \qquad\qquad (7-251)$$

Error Transformations:

T_7 : A functional transformation relating timer error to earth subpoint errors.

$$\sigma_{uE} = \dot{u}_E \left[(K_t t)^2 + \sigma_t^2 \right]^{1/2} \qquad\qquad (7-252)$$

and

$$\sigma_{wE} = \dot{w}_E \left[(K_t t)^2 + \sigma_t^2 \right]^{1/2} \qquad\qquad (7-253)$$

T_8 : Identical to T_2 but sensitivity coefficients are evaluated with earth variables and updated vehicle position on path.

T_9 : Identical to T_3 but evaluated with path variables.

T_{10}: Identical to T_4 but sensitivity coefficients evaluated along vehicle path.

T_{11}: Identical to T_6 but sensitivity coefficients evaluated along vehicle path.

T_{12}: The matrix of error sensitivity coefficients representing the general dead reckoning error model which relates transformed dead reckoning sensor errors to vehicle position errors. At each point P_n of the vehicle path,

$$
\begin{bmatrix} (\Delta R_N)^2_{DR} \\\\ (\Delta R_E)^2_{DR} \\\\ (\Delta R_Z)^2_{DR} \end{bmatrix} = \begin{bmatrix} D_1^2 & D_2^2 & D_3^2 \\\\ D_4^2 & D_5^2 & D_6^2 \\\\ D_7^2 & D_8^2 & D_9^2 \end{bmatrix} \begin{bmatrix} \sigma_o^2 \\\\ \sigma_p^{*2} \\\\ \sigma_A^{*2} \end{bmatrix}
\tag{7-254}
$$

The sequence of points P_n represent the vehicle path of an <u>errorless</u> dead reckoning navigation system. These points are the true points. However, due to the navigation system errors, there is located at each true point an uncertainty in position. Thus at each P_n, a position error ellipsoid is calculated, with components in a northerly, easterly, and altitude direction. The dead reckoning ellipsoid components calculated for the entire traverse are:

$$
(\Delta R_N)_{DR} = \left[\left[\sum_{K=1}^{n} (|D_1| \sigma_o)_K \right]^2 + \left[\sum_{K=1}^{n} (|D_2| \sigma_p^*)_K \right]^2 + \left[\sum_{K=1}^{n} (|D_3| \sigma_A^*)_K \right]^2 \right]^{1/2}
\tag{7-255}
$$

$$
(\Delta R_E)_{DR} = \left[\left[\sum_{K=1}^{n} (|D_4| \sigma_o)_K \right]^2 + \left[\sum_{K=1}^{n} (|D_5| \sigma_p^*)_K \right]^2 + \left[\sum_{K=1}^{n} (|D_6| \sigma_A^*)_K \right]^2 \right]^{1/2}
\tag{7-256}
$$

$$
(\Delta R_Z)_{DR} = \left[\left[\sum_{K=1}^{n} (|D_7| \sigma_o)_K \right]^2 + \left[\sum_{K=1}^{n} (|D_8| \sigma_p^*)_K \right]^2 + \left[\sum_{K=1}^{n} (|D_9| \sigma_A^*)_K \right]^2 \right]^{1/2}
\tag{7-257}
$$

The total error ellipsoid components of system error are:

$$
(\Delta R_N)_T = \left[(\Delta R_N)^2_{DR} + (\Delta R_N)^2_{PF} \right]^{1/2}
\tag{7-258}
$$

$$(\Delta R_E)_T = \left[(\Delta R_E)^2_{DR} + (\Delta R_E)^2_{PF} \right]^{1/2} \qquad (7\text{-}259)$$

$$(\Delta R_Z)_T = (\Delta R_Z)_{DR} . \qquad (7\text{-}260)$$

And the total vehicle position error at a point P_n is

$$(PE)_T = \left[(\Delta R_N)^2_T + (\Delta R_E)^2_T \right]^{1/2} \qquad (7\text{-}261)$$

The derivations and coefficients of the passive nongyro concept transformations $T_1 \cdots T_{12}$ may be found in the indicated sections.

T_1 : Section 7.2.4	T_7 : Section 7.2.4
T_2 : Section 7.2.6	T_8 : Section 7.2.6
T_3 : Section 7.2.5	T_9 : Section 7.2.5
T_4 : Section 7.2.3	T_{10} : Section 7.2.3
T_5 : Section 7.2.2	T_{11} : Section 7.2.3
T_6 : Section 7.2.3	T_{12} : Section 7.2.1

7.3.4.2 Inertial Concept

The position fix portion of the inertial concept is identical to the position fix portion of the passive nongyro concept with the exception that a vertical gyro is utilized as the local vertical reference. Therefore the error model flow diagram of the two concepts is identical with the vertical gyro model replacing the pendulous vertical model. Figure 7-40 shows this elemental substitution:
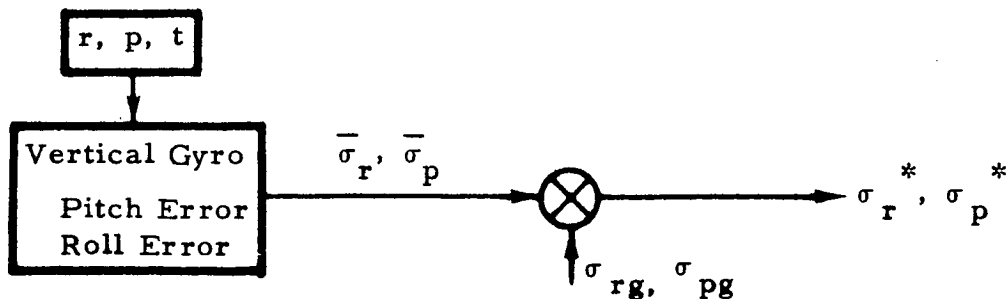
Figure 7-40 Vertical Errors, Inertial Concept

The remainder of the error transformations and error outputs are identical.

The error model program during the position fix calculations will substitute a static inclinometer error input rather than a vertical gyro error input if the conditional designating K_{rs} and σ_{rs} is set. Then the vertical error output has the form.

$$\sigma_r = \left[(K_{rs}r)^2 + (\sigma_{rs})^2 \right]^{1/2} \tag{7-262}$$

$$\sigma_p = \left[(K_{rs}p)^2 + (\sigma_{rs})^2 \right]^{1/2} \tag{7-263}$$

The inertial concept dead reckoning error model flow diagram is shown in Figure 7-41.

The transformations T_8 and T_{12} are identical to the transforms T_8 and T_{12} of the passive nongyro concept. Also the computation of the vehicle dead reckoning error is performed as in the passive nongyro concept.

The transformation T_{13} relates accelerometer null, linearity, and alignment errors to a normalized distance error.
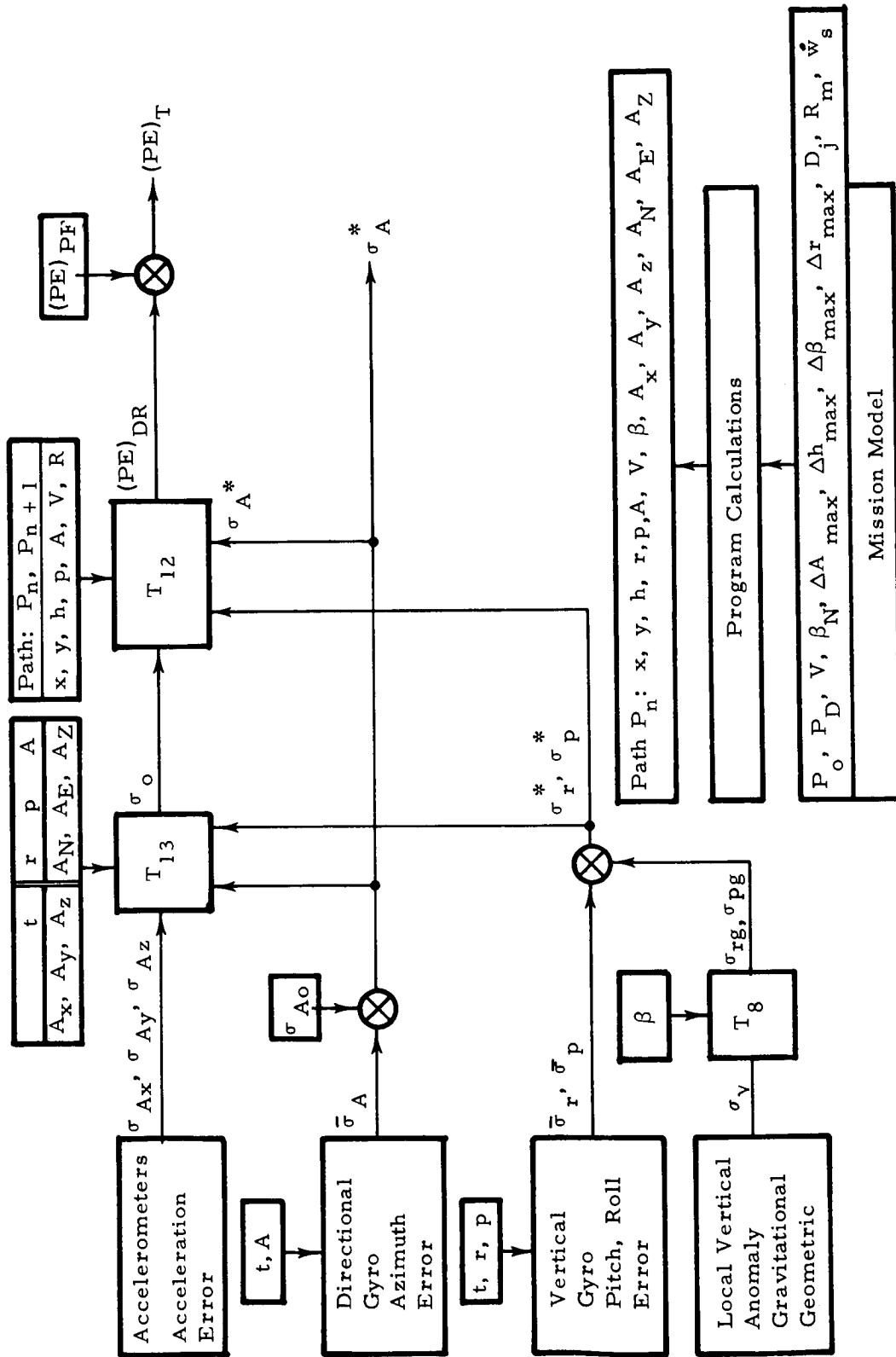
Figure 7-41 Concept 2 Error Model Flow Diagram, Dead Reckoning

T_{13} : A functional transformation relating acceleration errors to vehicle distance error.

$$\sigma_o = \frac{\left[\sigma_{A_x}^2 + \sigma_{A_y}^2 + \sigma_{A_z}^2 \right]^{1/2}}{2 D_{n,\, n+1}} \; (t_{(n+1)}^2 - t_n^2)$$

$$+ \frac{\left[(C_{26}\sigma_p^{*2}) + (C_{27}\sigma_r^{*2}) + (C_{28}\sigma_A^{*2}) + K_{A3}^2 (A_x^2 + A_y^2 + A_z^2) \right]^{1/2}}{2 D_{n,\, n+1}} \cdot$$

$$\tau \; (t_{(n+1)} - t_n) \tag{7-264}$$

The program computes the mission path from the input data as presented above. The additional computation to approximate vehicle accelerations during vehicle maneuvers, so that accelerometer non-linearity errors can be assessed, result in both body-fixed accelerations (A_x, A_y, A_z) and analytic system accelerations (A_N, A_E, A_Z).

$$[A_x \; A_y \; A_z] = [A_N \; A_E \; A_Z] \left[T_{Apr} \right]^{-1} \tag{7-265}$$

The transformation, T_{13}, the body-fixed accelerations, and the equations of $[T_{Apr}]$, C_{26}, C_{27}, C_{28} are found in Section 7.2.10.

7.3.4.3 RF Technology Concept

The position fix model of the RF technology concept entails only the input of the vehicle position error ellipse on the lunar surface as the result of earth-based rf tracking. Figure 7-42 shows the input form.

Earth-Based
RF Tracking and
Computation
Position Error $\longrightarrow (\Delta R_N)_{PF}, \; (\Delta R_E)_{PF}$
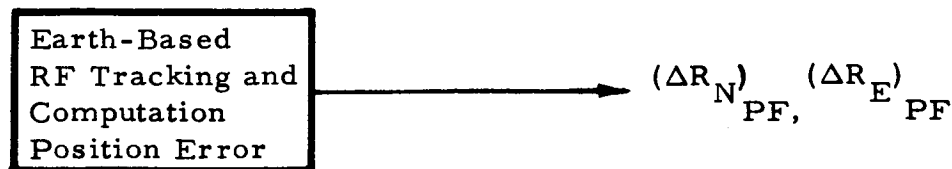
Figure 7-42 Position Fix Subconcept

The only program calculations required are a resolution of the above position errors into latitude and longitude errors at a true point of the vehicle location.

$$\sigma_x = \frac{(\Delta R_N)_{PF}}{R} \qquad\qquad (7\text{-}266)$$

$$\sigma_y = \frac{(\Delta R_E)_{PF}}{R \cos x} \qquad\qquad (7\text{-}267)$$

The error model functional form of the RF technology dead reckoning is identical to that of the passive nongyro concept with the exceptions that vehicle distance is measured with a doppler radar, vehicle azimuth with an RF earth tracker. Also no initial azimuth alignment error is available due to RF position fixing. Therefore, the flow diagram is identical to the flow diagram of the passive nongyro concept with the elemental substitutions shown in Figure 7-43.
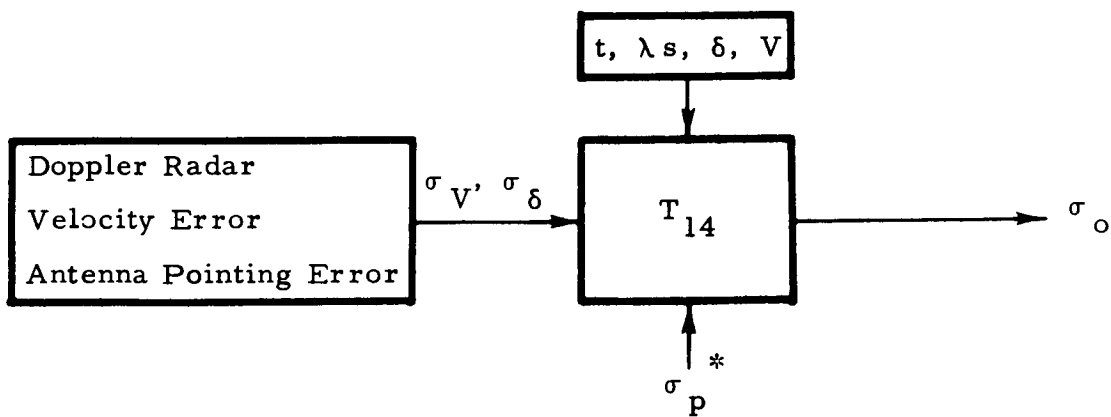
Figure 7-43 Doppler Radar Flow Diagram

T_{14} : A functional transformation relating velocity errors to normalized vehicle distance errors:

$$\sigma_o = \frac{\sigma_V^* (t_{n+1} - t_n)}{D_{n, n+1}} \qquad (7\text{-}268)$$

$$\sigma_V^* = \left[(C_{29} \sigma_f)^2 + (C_{30} \sigma_\delta^*) + (\sigma_b)^2 \right]^{1/2} \qquad (7\text{-}269)$$

The doppler model and T_{14} are derived in Section 7.2.11.

The functioning of the total RF technology system model and the program calculations is as described for the passive nongyro and inertial concept error models.

7.3.4.4 Alternate Position Fix Error Models

7.3.4.4.1 CSM Angular Tracking Technique

The position fix and initial azimuth error model flow diagram, using the CSM as a position fix reference and performing angular tracking of the satellite, is shown in Figure 7-44.

The basic error model is similar to the position fix celestial tracker error model and most calculations are identical. The primary differences are the calculation of the CSM position, and the transformations T_{14}, T_{15}.

CSM Position:

$$u_{c_i} = \sin^{-1} \left[\sin\left(\frac{V_c t}{R_c} + b_o \right) \sin i \right] \qquad (7\text{-}270)$$

and

$$w_{ci} = \sin^{-1} \left[\frac{\sin \left[\frac{V_c t}{R_c} + b_o \right] \cos i}{\cos u_{ci}} \right] - \dot{w}_s t + w_o \qquad (7\text{-}271)$$
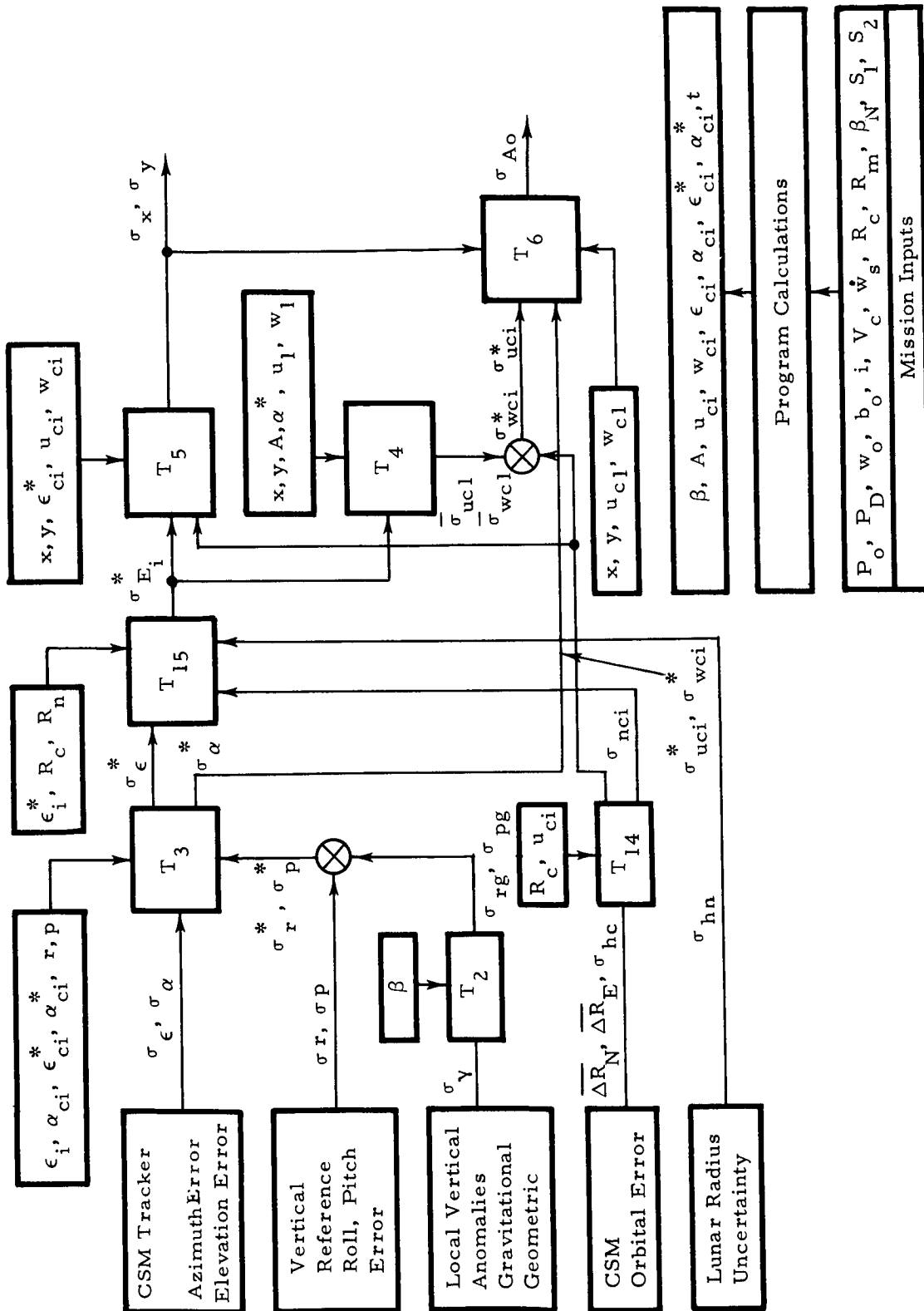
Figure 7-44 CSM Position Fix, Initial Azimuth Alignment, Angular Tracking

Time t in the above equation is incremented by:

$$t = k \Delta t$$

where

Δt is a program input

k is an integer sequence.

The program then calculates the points where the CSM is visible from the vehicle. If the total time, $K \Delta T$, is defined as the period of CSM visibility, then the CSM sightings are made at the times:

Sighting 1: $t_1 = S_1 K \Delta t$

Sighting 2: $t_2 = S_2 K \Delta t$ where S_1, $S_2 \leq 1$ are program inputs.

Hence, the geometry existing at the time of Sightings 1 and 2 presents the necessary variables for model evaluation.

CSM True Azimuth:

$$\overset{*}{\alpha}_{c_i} = A_{nci} - A_{OD} \qquad (7\text{-}272)$$

where

$$A_{nci} = 2 \tan^{-1} \left[\frac{K}{\sin (s-a)} \right]$$

where

$$K^2 = \frac{\sin (s-a_1) \, \sin (s-E_i) \, \sin (s-c_1)}{\sin s} \qquad (7\text{-}273)$$

where

$$s = 1/2 \left[a_1 + c_1 + E_i \right]$$

$$a_1 = 90^\circ - u_{ci}$$

$$c_1 = 90^\circ - x_o$$

$$E_i = \cos^{-1} \left[\sin (u_{ci}) \sin (x_o) + \cos (u_{ci}) \cos (x_o) \cos (w_{ci} - y_o) \right]$$

CSM True Elevation:

$$\epsilon_{ci}^* = 90^\circ - C \qquad (7\text{-}274)$$

where

$$C = 2 \sin^{-1} \left[\frac{(s-a_2)(s-b_2)}{a_2 b_2} \right]^{1/2}$$

$$s = (a_2 + b_2 + c_2)/2$$

$$a_2 = \left[b_2^2 + c_2^2 - 2 b_2 c_2 \cos A_2 \right]^{1/2}$$

$$b_2 = R_c - R$$

$$c_2 = 2 R_c \sin \frac{E_i}{2}$$

$$A_2 = \frac{180^\circ - E_i}{2}$$

All remaining program calculations are identical to the celestial tracker position fix model with the substitutions of u_{ci}, w_{ci}, ϵ_{ci}^*, α_{ci}^*.

Error Transformations:

T_{14} : A functional transformation relating position errors of the CSM to latitude, longitude errors

$$\sigma_{u_{c_i}}^* = \frac{\overline{\Delta R_N}}{R_{ci}} \qquad (7\text{-}275)$$

$$\sigma^*_{wci} = \frac{\overline{\Delta R_E}}{R_{ci} \cos (u_{ci})} \tag{7-276}$$

T_{15} : A functional transformation relating transformed tracker elevation errors and physical uncertainties to an equivalent great circle error of CSM position.

$$\sigma^{2*}_{Ei} = \begin{bmatrix} C^2_{31} & C^2_{32} & C^2_{33} \end{bmatrix} \begin{bmatrix} \sigma^{*2}_{\epsilon i} \\ \sigma^{2}_{hn} \\ \sigma^{2}_{hc} \end{bmatrix} \tag{7-277}$$

where the coefficients are evaluated for the ith sighting geometry.

The above transformations are derived in Section 7.2.12.1.

7.3.4.4.2 CSM Ranging Technique

Figure 7-45 shows the error model for vehicle position determination by range measurements on the CSM.
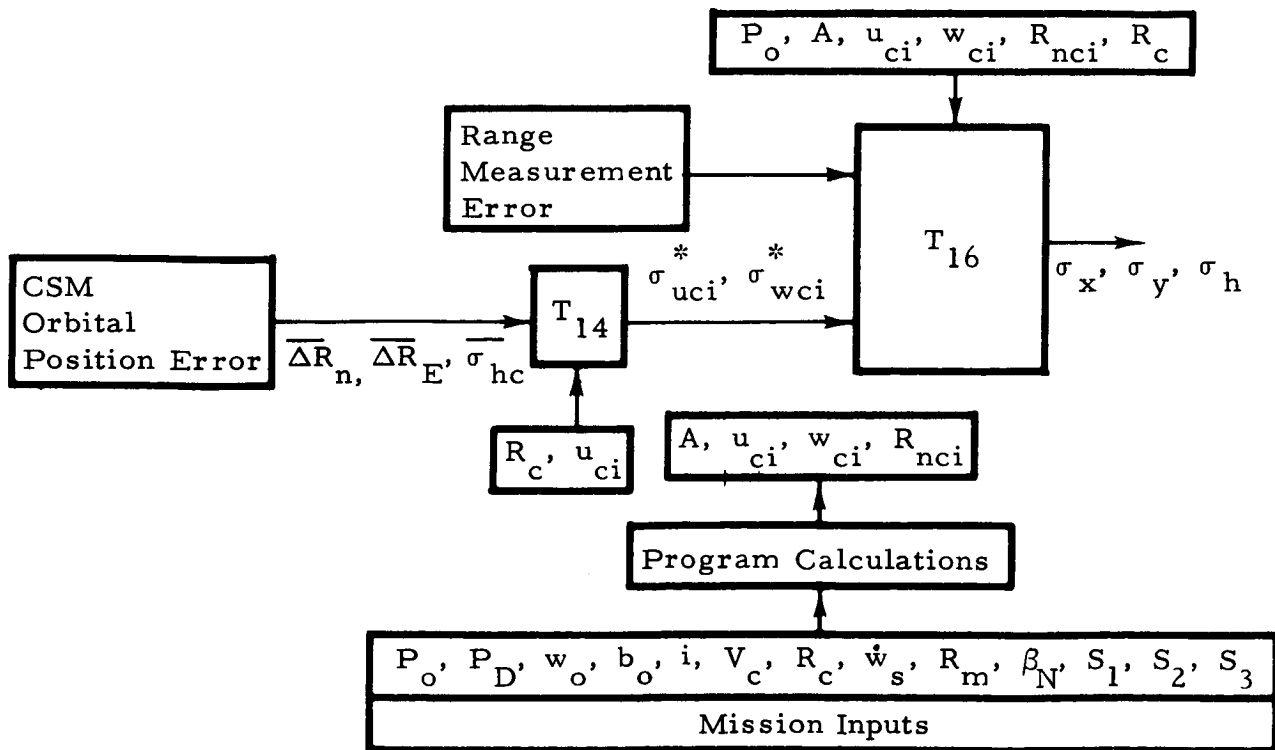
Figure 7-45 CSM PF Error Model Ranging

The output is a vehicle position error ellipsoid located at point P_o on the lunar surface. Program calculations to achieve the input variables are performed as in the previous section, with these exceptions: one additional sighting required, and the vehicle to CSM range calculation.

Vehicle to CSM Range

$$R_{nci} = R_n{}^2 + R_c{}^2 - 2R_n R_c \cos E_i \qquad (7-278)$$

where

$i \quad = 1, 2, 3$

$i \quad = 1 \Longrightarrow$ Sighting 1, defined at S_1 KΔT

$i \quad = 2 \Longrightarrow$ Sighting 2, defined at S_2 KΔT

$i \quad = 3 \Longrightarrow$ Sighting 3, defined at S_3 KΔT

Error Transformations:

T_{16} : A matrix of partial derivative error sensitivity coefficients relating range measurement errors and CSM orbital position errors to vehicle position errors.

$$
\begin{bmatrix} \sigma^2_{h_n} \\[6pt] \sigma^2_x \\[6pt] \sigma^2_y \end{bmatrix}
=
\begin{bmatrix} J_1^2 & J_2^2 & J_3^2 & J_4^2 & J_5^2 & \cdots & J_{10}^2 \\[6pt] J_{11}^2 & \cdots\cdots\cdots\cdots & J_{20}^2 \\[6pt] J_{21}^2 & \cdots\cdots\cdots\cdots & J_{30}^2 \end{bmatrix}
\begin{bmatrix} \sigma^2_{R_{nc1}} \\[4pt] \sigma^2_{R_{nc2}} \\[4pt] \sigma^2_{R_{nc3}} \\[4pt] \sigma^{*2}_{uc_1} \\[4pt] \sigma^{*2}_{uc_2} \\[4pt] \sigma^{*2}_{uc_3} \\[4pt] \sigma^{*2}_{wc_1} \\[4pt] \sigma^{*2}_{wc_2} \\[4pt] \sigma^{*2}_{wc_3} \\[4pt] \sigma^2_{hc} \end{bmatrix}
\qquad (7-279)
$$

T_{16} is derived in Section 7.2.12.1

7-122

7.3.5 Updating Dead Reckoning System Errors

Navigation system errors may be reduced by taking position fixes. Essentially this results in updating the dead reckoning navigation subsystem. The treatment of determining the minimum number of position fixes follows.

Defining a system cost function:

$$J \overset{\Delta}{=} 1 - \frac{(T_R)^2 - (P_E)^2}{(T_R)^2} \qquad (7-280)$$

where

J = Accuracy cost function

T_R = Homing range-circle of detection

P_E = System error

The theory of the J assessment criteria is based on the inequality that

$$(P_E)^2 \leq (T_R)^2 \qquad (7-281)$$

for target detection, and termination of the pursuit problem.

An examination of the J function shows four specific cases:

1. Optimal

    $\min J = 0 \Rightarrow P_E = 0$

2. Minimal

    $\min J = 1 \Rightarrow P_E = T_R$

3. Acceptable

$$0 \leq \min J \leq 1 \implies (P_E{}^2) \leq (T_R{}^2)$$

4. Unacceptable

$$\min J > 1 \implies (P_E{}^2) \geq (T_R)^2$$

and min $J \overset{\Delta}{=}$ minimum cost function

The class definitions A, B, C, D define the system as an optimal, minimal, acceptable, or unacceptable system, depending upon the value of J.

Applying the defined J function, the following iterative procedure is required by the computer program to update the dead reckoning errors.

A position fix is taken initially at P_O. Then the vehicle dead reckons to the point P_N (the true position not containing system errors) which lies within the homing radius T_R of the destination point P_D.

Let N = max n.

Then if

$$J > 1 \text{ at } P_N$$

return the vehicle to point P_K

where

$$K = \frac{N}{2} \text{ (K, the nearest integer)}$$

take a position fix and dead reckon to P_D. If J > 1 again, return to point P_K

where

$$K = \frac{3N}{4}$$

take position fix, and dead reckon to P_D. If $J > 1$ again, return to point P_K

where

$$K = \frac{7N}{8}$$

and dead reckon to point P_D. Thus the number of position fixes required to achieve $J < 1$ can be determined.

A constraint is that the position fix error is less than the destination detection distance T_R; i.e., $\{(PE)_{PF} < T_R\}$.

Figure 7-46 shows the schematic representation of this homing, updating model.
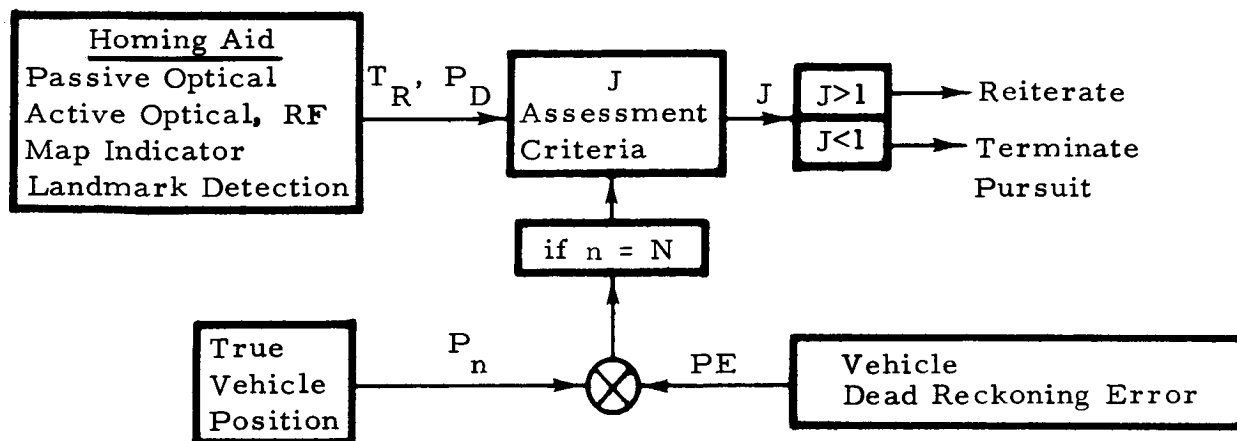
Figure 7-46 Dead Reckoning Updating Procedure

7.4 DEFINITION OF REQUIRED INPUTS

In the analysis of three designated lunar navigation concepts, the important factors which require assessment are the effect of component errors together with the dependence of total concept functioning on parameterized missions. A summary of the component errors and physical uncertainties considered in the model development and required for error model evaluation is tabulated in the succeeding sections. The parameterized missions and the corresponding descriptors are also listed and the connotation of these variables together with the error inputs facilitate computer application and interpretation.

7.4.1 Error Inputs

Table 7-3 summarizes the variables, parameters, and error inputs of the passive nongyro concept error model. Tables 7-4 and 7-5 summarize the inertial and RF technology concepts respectively; Table 7-6 presents the CSM summary.

7.4.2 Mission and Environmental Parameters

The parameters and variables in Table 7-7 are used as computer inputs to describe, simulate, and evaluate the lunar surface missions and environment as applicable to the surface navigation problem.

TABLE 7-3

PASSIVE, NONGYRO CONCEPT

Concept Subsystem	Function	Sensor or Aid	Sensed Variable	Equipment Errors	Physical Uncertainties
Position Fix	Position, Initial Bearing	Celestial Tracker	Observable altitude, azimuth ϵ, α	Null, readout σ_ϵ, σ_α	
		Pendulous Vertical	Local Vertical roll, pitch r, p	Linearity, null K_r, σ_r, K_p, σ_p	Vertical Anomalies σ_γ
		Timer	Elapsed Time t	Linearity, null K_t, σ_t	
		Ephemeris	Observable Position u, w		Right Ascension, Declination σ_R σ_D
Dead Reckoning	Azimuth	IR Earth Tracker	Earth altitude, azimuth ϵ_E, α_E	Null, readout σ_e, σ_a	Center of Radiation/ Centroid σ_{ca} σ_{ce}
		Timer	Elapsed Time t	Linearity, null K_t, σ_t	
		Ephemeris	Observable Position u_E, w_E		Right Ascension Declination σ_{RE} σ_{DE}
	Pitch	Pendulous Vertical	Local Vertical roll pitch r, p	Linearity, null K_r, σ_r, K_p, σ_p	Vertical Anomalies σ_γ
	Distance	Odometer	Distance traveled D_K	Slip, calibration K_s, K_{sp}, σ_s, σ_c	

TABLE 7-4

INERTIAL CONCEPT

Concept Subsystem	Function	Sensor or Aid	Sensed Variable	Equipment Errors	Physical Uncertainties
Position Fix	Position, Initial Bearing	Celestial Tracker	Observable altitude ε, azimuth α	Null, read-out σ_ϵ σ_α	
		Vertical Gyro or Static Vertical	Local Vertical roll r, pitch p	Linearity, null drift $K_r, \sigma_r, \sigma_{rD}$ $K_p, \sigma_p, \sigma_{pD}$ K_{rs}	Vertical Anomalies σ_γ
		Timer	Elapsed Time t	Linearity null K_t, σ_t	
		Ephemeris	Observable Position u, w		Right Ascension, Declination σ_R σ_D
Dead Reckoning	Azimuth	Directional Gyro	Azimuth A	Alignment null, drift σ_{GA}, σ_{gD}	
	Pitch	Vertical Gyro	Local Vertical roll r, pitch p	Linearity, null, drift $K_r, \sigma_r, \sigma_{rD}$ $K_p, \sigma_p, \sigma_{pD}$	Vertical Anomalies σ_γ
	Distance	Accelerometer	Acceleration Acc	Linearity null, random vibration, alignment K_{A3}, σ_{Ax} σ_{Ay}, σ_{Az}	

TABLE 7-5

RF TECHNOLOGY CONCEPT

Concept Subsystem	Function	Sensor or Aid	Sensed Variable	Equipment Errors	Physical Uncertainty
Position Fix	Position	Earth Based Tracking of Active RF Beacon			
Dead Reckoning	Azimuth	RF Earth Tracker	Earth altitude ϵ_E azimuth α_E	Null, read-out σ_e σ_a	Center of Radiation/Centroid σ_{ce} σ_{ca}
		Ephemeris	Earth Position u_E w_E		Right Ascension σ_{RE} Declination σ_{DE}
		Timer	Elapsed Time t		
	Pitch	Pendulous Vertical	Local Vertical roll r pitch p	Linearity, null K_r, σ_r K_p, σ_p	Vertical Anomalies σ_γ
	Distance	Doppler Radar	Velocity V	Linearity, null, calibration, Antenna pointing σ_b σ_δ	Noise, Back scatter σ_f

TABLE 7-6

CSM NAVIGATIONAL SATELLITE CONCEPT

Concept Subsystem	Function	Sensor/ Technique	Sensed Variable	Equipment Errors	Physical Uncertainties
Position Fix	Position, Initial Bearing	Angular Tracking			
		RF, Optical	CSM elevation, azimuth ϵ_c α_c	Pointing angle $\sigma_{\epsilon c}$ $\sigma_{\alpha c}$	
		Vertical Sensor	Local Vertical roll r pitch p	Linearity, null K_r, σ_r K_p, σ_p	Vertical Anomalies σ_γ
		"CSM Ephemeris"	CSM Position u_c w_c R_c		Orbital Position $\overline{\Delta R_N}$, $\overline{\Delta R_E}$ σ_{hc}
Position Fix	Position	Ranging			
		RF, Laser Ranging	CSM Range R_{nc}	Range measurement σR_{nc}	
		"CSM Ephemeris"	CSM Position u_c w_c R_c		Orbital Position $\overline{\Delta R_N}$, $\overline{\Delta R_E}$ σ_{hc}

TABLE 7-7

MISSION AND ENVIRONMENT PARAMETERS

Inputs	Descriptors (Implied Traverse Parameter)
$H_R = T_R$	Homing Range (Concept/Component Accuracy Req.)
$(x_o, y_o, h_o), (x_D, y_D, h_D)$	Selenographic Location/Region (Traverse Range, Bearing)
$\Delta h_{max}, \Delta A_{max}, \Delta \beta_{max}, \Delta r_{max}, D_j$	Terrain Characterization (Traverse/Terrain Degree of Difficulty)
$V, K_{vp}, K_{vr}, K_{A1}, K_{A2}$	Vehicle Constraints (Traverse Duration)
$u_1, u_2, w_1, w_2, R_m, \dot{w}_s, B_1, B_2, E, E_1$	Associated Celestial Geometry (Auxiliary Traverse Constraints)

7.5 TERMINOLOGY LIST

7.5.1 Symbol Identification

Symbol	Units	Definition
A	deg	Vehicle azimuth angle referenced north
A_{cc}	km/hr^2	Magnitude of vehicle acceleration vector
A_{nc}	deg	True CSM azimuth angle referenced north from vehicle
$A_{n, n+1}$	deg	Great circle azimuth from P_n to P_{n+1}
A_{nD}	deg	Great circle azimuth from P_n to destination P_D
A_N, A_E, A_Z	km/hr^2	Analytic system accelerometer outputs; north, east, and altitude respectively
A_{oD}	deg	Great circle azimuth from initial point P_o to destination P_D
A_x, A_y, A_z	km/hr^2	Body fixed system accelerometer outputs
b_o	deg	Initial solid angle rotation along the CSM orbit from w_o
B_1	deg	Maximum latitude subpoint of earth
B_2	deg	Maximum longitude subpoint of earth
D_j	km	Distance along an incremental leg
$D_{n, n+1}$	km	Distance between P_n and P_{n+1}
D_{oD}	km	Great circle distance between P_o and P_D
D_{Tn}	km	Total distance between P_n and P_D
D_{To}	km	Total distance between P_o and P_D
f_m	cps	Doppler modulated frequency
E	deg/hr	Rate of rotation of earth subpoint
E_1	deg	Parameter which rotates major axis of earth subpoint ellipse

Units	Symbol	Definition
h	km	Altitude reference to R_m
h_D	km	Destination altitude
h_n	km	Altitude at point P_n
h_o	km	Initial vehicle altitude
i	deg	CSM orbit inclination at equator
K_{A1}	$\frac{km}{hr^2} deg^{-1}$	Vehicle available acceleration coefficient; terrain slope function
K_{A2}	$\frac{km}{hr^2}$	Vehicle available acceleration with terrain slope zero
K_{A3}	—	Accelerometer nonlinearity coefficient
K_p	—	Pitch sensor nonlinearity coefficient
K_r	—	Roll sensor nonlinearity coefficient
K_{rs}	—	Static inclinometer nonlinearity coefficient
K_s	$\frac{hr}{km}$	Odometer slip coefficient, velocity contribution
K_{sp}	deg^{-1}	Odometer slip coefficient, pitch contribution
K_t	—	Timer nonlinearity coefficient
K_{vp}	$\frac{km}{hr} deg^{-1}$	Vehicle speed variation coefficient, pitch contribution
K_{vr}	$\frac{km}{hr} deg^{-1}$	Vehicle speed variation coefficient, roll contribution
Lg	deg	Longitude
Lt	deg	Latitude
p	deg	Vehicle pitch angle

Symbol	Units	Definition
P_D	—	Destination coordinates (x_D, y_D, h_D)
P_g	deg	Pitch component of vertical anomaly
P_n	—	Vehicle coordinates at nth point (x_n, y_n, h_n)
$P_{n,n+1}$	deg	Vehicle pitch angle between points P_n and P_{n+1}
P_o	—	Initial vehicle coordinates (x_o, y_o, h_o)
PE	km	Position error
r	deg	Vehicle roll angle
r_g	deg	Roll component of vertical anomaly
R	km	Altitude referenced to lunar center
R_c	km	Radius of CSM orbit
R_{nc}	km	Vehicle to CSM range
R_m	km	Lunar radius
t	hr	Time
T	hr	Doppler data smoothing time
u	deg	Latitude subpoint of celestial observable
u_c	deg	CSM latitude
u_E	deg	Latitude subpoint of earth
u_i	deg	Latitude subpoint of ith observable
V	km/hr	Vehicle speed
V_c	km/hr	CSM tangential velocity
V_N, V_E, V_Z	km/hr	Vehicle analytic system velocity components; north, east, altitude

Symbol	Units	Definition
w	deg	Longitude subpoint of celestial observable
w_c	deg	CSM longitude
w_E	deg	Longitude subpoint of earth
w_i	deg	Longitude subpoint of ith observable
w_o	deg	Initial longitude of CSM orbit-lunar equator intersection
$\dot{w}_s$	deg/hr	Moon sidereal rate of rotation
x	deg	Vehicle latitude
x_D	deg	Vehicle destination latitude
x_n	deg	Vehicle latitude at n^{th} point
x_o	deg	Initial vehicle latitude
y	deg	Vehicle longitude
y_D	deg	Vehicle destination longitude
y_n	deg	Vehicle longitude at n^{th} point
y_o	deg	Initial vehicle longitude
α_E	deg	Earth azimuth angle, measured relative to the vehicle body-centered system
α_E^*	deg	Earth true azimuth angle, referenced to vehicle longitudinal axis
α_c	deg	CSM azimuth angle, relative to vehicle body-centered system

Symbol	Units	Definition
α_c^*	deg	CSM true azimuth angle, referenced to vehicle longitudinal axis
α_i	deg	Azimuth angle, i^{th} observable, referenced to vehicle body-centered system
α_i^*	deg	True azimuth angle, i^{th} observable, referenced to vehicle longitudinal axis
β	deg	Vertical anomaly direction, referenced to vehicle longitudinal axis
β_N	deg	Vertical anomaly direction referenced to true north
δ	deg	Doppler radar antenna pointing angle
ΔA_{max}	deg	3σ value of the azimuth density function used in vehicle path construction
Δh_{max}	km	3σ value of the altitude density function used in vehicle path construction
Δr_{max}	deg	3σ value of the vehicle roll density function used in vehicle path construction
$\Delta \beta_{max}$	deg	3σ value of the vertical anomaly density function used in vehicle path construction
ΔR_N	km	Northerly component of vehicle position error. Subscripted DR implies dead-reckoning contribution, PF implies position fix, and T implies total
ΔR_E	km	Easterly component of vehicle position error
ΔR_Z	km	Altitude component of vehicle position error
ϵ_E	deg	Earth elevation angle, relative to vehicle body-centered system

Symbol	Units	Definition
ϵ_E^*	deg	Earth true elevation angle
ϵ_c	deg	CSM elevation angle; relative to vehicle body-centered system
ϵ_c^*	deg	CSM true elevation angle
ϵ_i	deg	Elevation angle, i^{th} observable
ϵ_i^*	deg	True elevation angle, i^{th} observable
λ_S	km	Doppler radar carrier wave length

7.5.2 3σ Error Terms—Equipment Errors

Symbol	Units	Description
σ_a	deg	Earth tracker azimuth null error
$\sigma_{A_x}, \sigma_{A_y}, \sigma_{A_z}$	km/hr^2	Accelerometer null error
σ_α	deg	Celestial tracker, CSM tracker azimuth null error
σ_b	km/hr	Doppler radar velocity calibration error
σ_c, σ_s		Odometer calibration/slip error
σ_δ	deg	Doppler radar antenna pointing error
σ_e	deg	Earth tracker elevation null error
σ_ϵ	deg	Celestial tracker, CSM tracker elevation null error
σ_f	hr^{-1}	Doppler frequency detection error
σ_{GA}	deg	Directional gyro null error and/or alignment error
σ_{gD}	deg/hr	Directional gyro drift error
σ_p	deg	Pendulous vertical, vertical gyro pitch null error
σ_{pD}	deg/hr	Vertical gyro pitch component drift error
σ_r	deg	Pendulous vertical, vertical gyro roll null error
σ_{rD}	deg/hr	Vertical gyro roll component drift error
σ_{rs}	deg	Static pendulous inclinometer roll, pitch null error

Symbol	Units	Description
σ_{Rnc_i}	km	Vehicle to CSM range measurement error i^{th} data point
σ_t	hr	Timer null error
K_{A_3}	—	Accelerometer non-linearity coefficient
K_p	—	Pendulous vertical, vertical gyro non-linearity pitch coefficient
K_r	—	Pendulous vertical, vertical gyro non-linearity roll coefficient
K_{rs}	—	Static inclinometer non-linearity pitch, roll coefficient
K_s	hr/km	Odometer slip coefficient, velocity contribution
K_{sp}	deg^{-1}	Odometer slip coefficient, pitch contribution
K_t	—	Timer non-linearity coefficient
$\left(\dfrac{\Delta R}{R}\right)$	—	Odometer coefficient, radial error contribution
$\left(\dfrac{\delta}{3R}\right)$	—	Odometer coefficient, deflection error contribution
$(\Delta R_N)_{PF}$, $(\Delta R_E)_{PF}$, $(\Delta h)_{PF}$	km	Earth-based RF tracking vehicle position error; northerly, easterly, and altitude components respectively

7.5.3 3σ Error Terms—Physical Uncertainties

Symbol	Units	Description
σ_{ca}	deg	Earth center of radiation—centroid error, azimuth component
σ_{ce}	deg	Earth center of radiation—centroid error, elevation component
σ_{D_E}	deg	Earth declination error
σ_{D_i}	deg	Ephemeris declination error, i^{th} observable
σ_{h_c}	km	CSM altitude error
σ_{γ}	deg	Vertical anomaly
σ_{pg}	deg	Vertical anomaly, pitch component
σ_{rg}	deg	Vertical anomaly, roll component
σ_{R_E}	deg	Earth right ascension error
σ_{R_i}	deg	Ephemeris right ascension error, i^{th} observable
$\overline{\Delta R_N}$	km	CSM northerly position error
$\overline{\Delta R_E}$	km	CSM easterly position error

7.5.4 3σ Error Terms—Calculated Errors

Symbols	Units	Description
σ_A^*	deg	Vehicle azimuth error.
σ_{AO}	deg	Initial vehicle azimuth error.
σ_o		Dimensionless distance error.

Symbol	Units	Description
σ_p^*	deg	Vehicle pitch error.
σ_r^*	deg	Vehicle roll error.
$\sigma_{u_{c_i}}$	deg	CSM latitude error at i^{th} sighting.
$\sigma_{u_E}^*$	deg	Latitude subpoint error, earth.
$\sigma_{u_i}^*$	deg	Latitude subpoint error, i^{th} observable.
σ_V	km/hr	Vehicle speed error.
$\sigma_{w_{c_i}}$	deg	CSM longitudinal error, i^{th} sighting.
$\sigma_{w_E}^*$	deg	Longitudinal subpoint error, earth.
$\sigma_{w_i}^*$	deg	Longitudinal subpoint error, i^{th} observable.
σ_x	deg	Vehicle latitude error.
σ_y	deg	Vehicle longitude error.

In the derivation of the error models, terminology denoted with an asterisk frequently appears, e.g.,

$$\sigma_\alpha^* , \ \sigma_A^* \ \cdot \ \cdot \ \cdot \ \cdot$$

In all instances when error terms are discussed, this starred notation designates a matrix or functional transformation upon a given input error variable and the resultant term is an effective or transformed error quantity.

7.5.5 Error Sensitivity Coefficients

Coefficients	Partial Derivative Definition	Sensitivity Relationship—Sensitivity of:
C_1	$\dfrac{\partial x}{\partial \epsilon_1^*}$	Vehicle latitude error to true elevation error
C_2	$\dfrac{\partial x}{\partial u_1}$	Vehicle latitude error to latitude subpoint error
C_3	$\dfrac{\partial x}{\partial w_1}$	Vehicle latitude error to longitude subpoint error
C_4	$\dfrac{\partial x}{\partial \epsilon_2^*}$	Vehicle latitude error to true elevation error
C_5	$\dfrac{\partial x}{\partial u_2}$	Vehicle latitude error to latitude subpoint error
C_6	$\dfrac{\partial x}{\partial w_2}$	Vehicle latitude error to longitude subpoint error
C_7	$\dfrac{\partial y}{\partial \epsilon_1^*}$	Vehicle longitude error to true elevation error
C_8	$\dfrac{\partial y}{\partial u_1}$	Vehicle longitude error to latitude subpoint error
C_9	$\dfrac{\partial y}{\partial w_1}$	Vehicle longitude error to longitude subpoint error
C_{10}	$\dfrac{\partial y}{\partial \epsilon_2^*}$	Vehicle longitude error to true elevation error
C_{11}	$\dfrac{\partial y}{\partial u_2}$	Vehicle longitude error to latitude subpoint error
C_{12}	$\dfrac{\partial y}{\partial w_2}$	Vehicle longitude error to longitude subpoint error
C_{13}	$\dfrac{\partial \epsilon^*}{\partial \alpha}$	True elevation error to azimuth error

Coefficients	Partial Derivative Definition	Sensitivity Relationship—Sensitivity of:
C_{14}	$\dfrac{\partial \epsilon^*}{\partial \epsilon}$	True elevation error to elevation error
C_{15}	$\dfrac{\partial \epsilon^*}{\partial r}$	True elevation error to roll error
C_{16}	$\dfrac{\partial \epsilon^*}{\partial p}$	True elevation error to pitch error
C_{17}	$\dfrac{\partial A}{\partial x}$	Vehicle azimuth error to vehicle latitude error
C_{18}	$\dfrac{\partial A}{\partial \alpha^*}$	Vehicle azimuth error to true azimuth error
C_{19}	$\dfrac{\partial A}{\partial u}$	Vehicle azimuth error to latitude subpoint error
C_{20}	$\dfrac{\partial A}{\partial w}$	Vehicle azimuth error to longitude sub-point error
C_{21}	$\dfrac{\partial A}{\partial y}$	Vehicle azimuth error to vehicle longitude error
C_{22}	$\dfrac{\partial \alpha^*}{\partial \alpha}$	True azimuth error to azimuth error
C_{23}	$\dfrac{\partial \alpha^*}{\partial \epsilon}$	True azimuth error to elevation error
C_{24}	$\dfrac{\partial \alpha^*}{\partial r}$	True azimuth error to roll error
C_{25}	$\dfrac{\partial \alpha^*}{\partial p}$	True azimuth error to pitch error
C_{26}	$\dfrac{\partial A_{cc}}{\partial p}$	Vehicle acceleration error to pitch error
C_{27}	$\dfrac{\partial A_{cc}}{\partial r}$	Vehicle acceleration error to roll error

Coefficients	Partial Derivative Definition	Sensitivity Relationship—Sensitivity of:
C_{28}	$\dfrac{\partial A_{cc}}{\partial A}$	Vehicle acceleration error to azimuth error
C_{29}	$\dfrac{\partial V}{\partial f_m}$	Vehicle velocity error to doppler frequency error
C_{30}	$\dfrac{\partial V}{\partial \delta}$	Vehicle velocity error to doppler antenna pointing error
C_{31}	$\dfrac{\partial E_c}{\partial \epsilon *}$	CSM true co-altitude error to true elevation error
C_{32}	$\dfrac{\partial E_c}{\partial R}$	CSM true co-altitude error to vehicle altitude error
C_{33}	$\dfrac{\partial E_c}{\partial R_c}$	CSM true co-altitude error to CSM orbit radius error
D_1	$\dfrac{\partial R_N}{\partial V}$	Vehicle northerly position error to vehicle speed error.
D_2	$\dfrac{\partial R_N}{\partial p}$	Vehicle northerly position error to vehicle pitch error.
D_3	$\dfrac{\partial R_N}{\partial A}$	Vehicle northerly position error to vehicle azimuth error.
D_4	$\dfrac{\partial R_E}{\partial V}$	Vehicle easterly position error to vehicle speed error.
D_5	$\dfrac{\partial R_E}{\partial p}$	Vehicle easterly position error to vehicle pitch error.
D_6	$\dfrac{\partial R_E}{\partial A}$	Vehicle easterly position error to vehicle azimuth error.

Coefficients	Partial Derivative Definition	Sensitivity Relationship—Sensitivity of:
D_7	$\dfrac{\partial h}{\partial V}$	Vehicle altitude error to vehicle speed error.
D_8	$\dfrac{\partial h}{\partial p}$	Vehicle altitude error to vehicle pitch error.
$J_1 J_2 J_3$	$\dfrac{\partial R}{\partial R_{nc_i}}$ $i = 1, 2, 3$	Vehicle altitude error to vehicle-CSM range measurement error.
$J_4 J_5 J_6$	$\dfrac{\partial R}{\partial u_{c_i}}$	Vehicle altitude error to CSM latitude error.
$J_7 J_8 J_9$	$\dfrac{\partial R}{\partial w_{c_i}}$	Vehicle altitude error to CSM longitude error.
J_{10}	$\dfrac{\partial R}{\partial R_c}$	Vehicle altitude error to CSM altitude error.
$J_{11} J_{12} J_{13}$	$\dfrac{\partial x}{\partial R_{nc_i}}$ $i = 1, 2, 3$	Vehicle latitude error to vehicle-CSM range measurement error
$J_{14} J_{15} J_{16}$	$\dfrac{\partial x}{\partial u_{c_i}}$	Vehicle latitude error to CSM latitude error.
$J_{17} J_{18} J_{19}$	$\dfrac{\partial x}{\partial w_{c_i}}$	Vehicle latitude error to CSM longtidue error.
J_{20}	$\dfrac{\partial x}{\partial R_c}$	Vehicle latitude error to CSM altitude error.
$J_{21} J_{22} J_{23}$	$\dfrac{\partial y}{\partial R_{nc_i}}$	Vehicle longitude error to vehicle-CSM range measurement error.

Coefficients	Partial Derivative Definition	Sensitivity Relationship—Sensitivity of:
$J_{24} J_{25} J_{26}$	$\dfrac{\partial y}{\partial u_{c_i}}$	Vehicle longitude error to CSM latitude error.
$J_{27} J_{28} J_{29}$	$\dfrac{\partial y}{\partial w_{c_i}}$	Vehicle longitude error to CSM longitude error.
J_{30}	$\dfrac{\partial y}{\partial R_c}$	Vehicle longitude error to CSM altitude error.